Investigation of the role of MYC as a stress responsive protein

Untersuchung der Rolle von Myc als stress-reguliertes Protein

Doctoral thesis

for a doctoral degree

at the Graduate School of Life Sciences,

Julius-Maximilians-Universität Würzburg,

Section Biomedicine

submitted by

Francesca Romana Dejure

From Trani

Würzburg 2017

Members of the Thesis Committee

Chairperson: Prof. Alexander Buchberger

Primary Supervisor: Prof. Martin Eilers
Supervisor (Second): Prof. Thomas Rudel
Supervisor (Third): Prof. Antje Gohla

Submitted on:

Date of Public Defence:

Date of Receipt of Certificate:

Table of content

Summary **1**

Zusammenfassung **2**

1 Introduction **4**

1.1 The oncogenic transcription factor c-MYC 4

1.2 Metabolic requirements in normal and cancer cells 15

1.3 Role of MYC in metabolic reprogramming 20

1.4 Aim of the thesis 30

2 Materials **31**

2.1 Cell lines and bacteria strains 31

2.2 Culture media and supplements 31

2.3 Bacteria culture media and supplements 34

2.4 Solutions, and buffers 35

2.5 Standards, enzymes and kit 41

2.6 Nucleic acids 43

2.7 Antibodies 49

2.8 Consumables 50

2.9 Equipment and membranes 50

2.10 Software and online programs 52

3 Methods **54**

3.1 Cell biology methods 54

3.2 Molecular biology methods 61

3.3 Biochemical methods 69

3.4 Next-generation sequencing 75

4 Results **80**

4.1 Comparison between effects mediated by glutamine and glucose 80

4.2 Identification of mechanisms responsible for the glutamine-mediated regulation of MYC 84

4.3 Investigation of post-transcriptional mechanisms of MYC regulation 94

4.4 Dissection of the glutamine-derived stimulus sensed by the 3´-UTR 101
4.5 Evaluation of biological downstream MYC downregulation 106
4.6 Transcriptional consequences associated with the glutamine-mediated regulation of MYC: evaluation of gene expression 108
4.7 Transcriptional consequences associated with the glutamine-mediated regulation of MYC: evaluation of RNA Polymerase II function 119

5 Discussion 131
5.1 MYC is regulated in a glutamine-dependent way 131
5.2 Glutamine regulates MYC protein levels through the 3´-UTR 134
5.3 Molecular players involved in the glutamine-mediated regulation of MYC: current investigations and future directions 142
5.4 The 3´-UTR of *MYC* responds to glutamine-derived adenosine 145
5.5 Links between the 3´-UTR and MYC-induced apoptosis: unifying opposite observations 149
5.6 The 3´-UTR of *MYC* as a link between the cellular metabolic status and the transcriptional output 153
5.7 The glutamine-induced downregulation of MYC prevents apoptosis due to accumulation of transcriptional stress 162
5.8 Glutamine-mediated regulation of MYC: revisiting old concepts in the light of new findings 164

6 Bibliography 167

7 Appendix 190
7.1 Abbreviations 190
7.2 Acknowledgments 196
7.3 Publications 197
7.4 Curriculum Vitae 198
7.5 Affidavit 199

Summary

The transcription factor MYC is deregulated in over 70% of all human tumors and, in its oncogenic form, plays a major role in the cancer metabolic reprogramming, promoting the uptake of nutrients in order to sustain the biosynthetic needs of cancer cells.

The research presented in this work aimed to understand if MYC itself is regulated by nutrient availability, focusing on the two major fuels of cancer cells: glucose and glutamine.

Initial observations showed that endogenous MYC protein levels strongly depend on the availability of glutamine, but not of glucose. Subsequent analysis highlighted that the mechanism which accounts for the glutamine-mediated regulation of MYC is dependent on the 3´-untranslated region (3´-UTR) of *MYC*. Enhanced glutamine utilization by tumors has been shown to be directly linked to MYC oncogenic activity and MYC-dependent apoptosis has been observed under glutamine starvation. Such effect has been described in experimental systems which are mainly based on the use of *MYC* transgenes that do not contain the 3´-UTR. It was observed in the present study that cells are able to survive under glutamine starvation, which leads to cell cycle arrest and not apoptosis, as previously reported. However, enforced expression of a *MYC* transgene, which lacks the 3´-UTR, strongly increases the percentage of apoptotic cells upon starvation. Evaluation of glutamine-derived metabolites allowed to identify adenosine nucleotides as the specific stimulus responsible for the glutamine-mediated regulation of MYC, in a 3´-UTR-dependent way. Finally, glutamine-dependent MYC-mediated effects on RNA Polymerase II (RNAPII) function were evaluated, since MYC is involved in different steps of global transcriptional regulation. A global loss of RNAPII recruitment at the transcriptional start site results upon glutamine withdrawal. Such effect is overcome by enforced MYC expression under the same condition.

This study shows that the 3´UTR of *MYC* acts as metabolic sensor and that MYC globally regulates the RNAPII function according to the availability of glutamine. The observations presented in this work underline the importance of considering stress-induced mechanisms impinging on the 3´UTR of *MYC*.

Zusammenfassung

In über 70% aller Krebserkrankungen ist der Transkriptionsfaktor MYC dereguliert. Dabei spielt onkogenes MYC unter anderem eine wichtige Rolle bei der Umprogrammierung metabolischer Prozesse indem es z.B. die Aufnahme von Nährstoffen wie Glutamin oder Glukose fördert, um den veränderten Bedürfnissen an den Stoffwechsel der Krebszellen Rechnung zu tragen.

Die im Rahmen dieser Arbeit erzielten Ergebnisse zeigen, dass auch das MYC-Protein selbst durch die Verfügbarkeit von Nährstoffen in der Zelle reguliert werden kann.

Erste Beobachtungen zeigten, dass die endogenen MYC Proteinlevel stark von der Verfügbarkeit von Glutamin, jedoch nicht von Glucose, abhängen. Weiterführende Experimente ergaben außerdem, dass der Mechanismus, der der Glutamin vermittelten Regulation von MYC zugrunde liegt, abhängig von der 3´-untranslatierten Region (3´-UTR) der *MYC*-mRNA ist.

Es konnte bereits gezeigt werden, dass in Tumoren die verstärkte Nutzung von Glutamin in direktem Zusammenhang mit der onkogenen Aktivität von MYC steht und Zellen unter Glutaminentzug MYC-abhängig Apoptose einleiten. Diese Effekte wurden in experimentellen Systemen beschrieben, die auf einer Überexpression eines *MYC*-Transgenes basierten, welches keine 3´-UTR enthält. In dieser Arbeit konnte jedoch beobachtet werden, dass Zellen, die ohne Glutamin kultiviert wurden, in der Lage waren zu überleben, da entgegen den Resultaten vorausgegangener Studien, ein Arrest des Zellzyklus und nicht Apoptose eingeleitet wurde. Die verstärkte Expression eines *MYC*-Transgenes ohne 3´-UTR, erhöhte jedoch auch unter diesen Bedingungen die Anzahl apoptotischer Zellen.

Weiterhin war es möglich Adenosin, für dessen Biosynthese Glutamin notwendig ist, als Stimulus zu identifizieren, der für die 3´-UTR abhängige Regulation von *MYC* verantwortlich ist.

Da MYC in verschiedene Schritte der globalen Regulation der Transkription eingebunden ist, wurden abschließend die durch MYC vermittelten Glutamin-abhängigen Effekte auf die RNA-Polymerase II (RNAPII) untersucht. Dabei zeigte sich, dass es nach Glutaminentzug zu einem globalen Verlust der Rekrutierung von RNAPII

zu den Transkriptionsstartstellen kommt, was durch eine verstärkte MYC-Expression wieder aufgehoben werden kann.

Zusammenfassend konnte in dieser Arbeit gezeigt werden, dass die 3´-UTR von *MYC* als metabolischer Sensor fungiert und dass MYC in Abhängigkeit der Verfügbarkeit von Glutamin global die RNAPII Funktion reguliert. Diese Studie hebt weiterhin die Bedeutung der 3´-UTR von *MYC* für die Vermittlung stressinduzierter Feedback-Mechanismen hervor.

1 Introduction

1.1 The oncogenic transcription factor c-MYC

C-MYC (or MYC) is a basic-region/helix-loop-helix/leucine zipper transcription factor belonging to the MYC protein family, which is also comprised of N-MYC and L-MYC. MYC binds consensus sequences called E-boxes (CACGTG) with the binding protein MAX in a heterodimeric form (Adhikary and Eilers, 2005). MYC plays a central role in regulating cell proliferation by coordinating several pathways (Dang 2012). The importance of its role is highlighted by the fact that MYC levels are deregulated in the majority of human cancers (Vita and Henriksson, 2006).

1.1.1 Transcriptional functions of MYC

1.1.1.1 Mechanisms of MYC-mediated control of transcription

As central regulator of cell growth and proliferation, MYC can control transcription mediated by RNA Polymerase (RNAP) I, II and III; Thus, controlling the expression of both coding RNA, such as messenger RNAs (mRNAs), and non-coding RNA, such as ribosomal RNAs (rRNAs) or transfer RNA (tRNA) (van Riggelen et al, 2010). Although these processes share similarities, an explanation on how specifically MYC controls RNAPII-dependent transcription is summarized in the next part of this section. Transcription is a controlled multistep process depending on the activity of hundreds of proteins, including the enzyme RNA Polymerase II (RNAPII), general transcription factors part of the pre-initiation complex, specific transcription factors, such as MYC, which modulate the transcription process and cofactors.

In the classical model of MYC-mediated transcription initiation, MYC first binds to open chromatin sequences, i.e. not packed into the nucleosome structure and accessible to transcription factors and other components of the transcription machinery. Sequence recognition (e.g. E-boxes) by the MYC/MAX heterodimers occurs subsequently. MYC binds to both conserved and non-conserved E-boxes and the presence of MAX is an

essential requirement for ensuring proper MYC folding and DNA binding. When bound to the DNA, MYC can recruit a plethora of cofactors, for example histone acetyltransferases, which further open the chromatin structure, chromatin-remodeling complexes and positive regulators of transcription, such as p-TEFb. Recruitment of these proteins facilitates the transcription processes (Sabo and Amati, 2014). Probably the best characterized function of MYC in regulating transcription steps is represented by its positive role in promoting RNAPII pause-release, i.e. promoting elongation of RNAPII molecules paused shortly downstream the transcription start site (Rahl et al, 2010). Changes in RNAPII function are dictated by post-translational modifications, such as phosphorylation, on its carboxy-terminal domain (CTD), which contains 52 heptapeptide repeats. Through pTEFb recruitment, MYC mediates the phosphorylation of the RNAPII on the serine residue in position 2 of the CTD repeats. This modification allows RNAPII to initiate a productive elongation (Jonkers and Lis, 2015). Control of RNAPII pause-release has been described as one of the major mechanisms through which MYC influences transcription (Rahl et al, 2010; Lin et al, 2012), implying that MYC functions in a setting in which RNAPII is already loaded onto promoters. However, MYC can also dictate the recruitment of RNAPII at promoter sites, as shown by the direct correlation between MYC and RNAPII occupancy, i.e. increased binding of RNAPII at promoter regions when MYC protein levels increased (Walz et al, 2014). Thus, MYC promotes both transcriptional initiation and elongation. This latter function has been demonstrated to be specifically dependent upon MYC turnover, since MYC degradation allows the transfer of pro-elongating factors onto RNAPII (Jaenicke et al, 2016).

1.1.1.2 Transcriptional regulation: specifier *versus* amplifier model

Since MYC discovery and characterization many efforts have been invested into identifying MYC target genes and the cellular processes driven by MYC activation. A broad spectrum of genes has been identified as direct MYC targets. Although showing a cell specific profile, MYC target genes have been systematically shown to be involved in essential cellular processes, such as regulation of cell cycle (e.g. genes encoding for cyclins), metabolism (e.g. *LDH-A*, *ODC*, see 1.3), protein synthesis and cell growth

(e.g. rRNA), etc. A growing number of MYC target genes have emerged over time consistent with technological advantages, such as genome-wide techniques (e.g. RNA-sequencing; Chromatin-immunoprecipitation (ChIP)-sequencing). Rather than a unified model of MYC´s regulation over transcription, the vast amount of data obtained from large-scale experiments only lead to further questions. It is therefore worth mentioning the latest and most relevant findings, which are continuing to fuel a debate in the MYC´s research field. After decades of investigation on MYC target genes, two papers in 2012 proposed a new model to explain MYC´s function: the global amplifier model (Lin et al, 2012; Nie et al, 2012). According to such model, MYC´s function does not result in the activation of a specific set of target genes, but rather amplifies the pre-existing transcriptional program of a cell, which is dictated by the chromatin context, i.e. open and accessible chromatin where RNAPII is loaded. Due to the fact that the basic landscape of epigenetic modifications is cell-type specific (Barrero et al, 2010), MYC-driven transcriptional changes depend on the cell identity, rather than on the MYC-mediated transcriptional specifications. Thus, this model suggests that the magnitude of MYC occupancy (i.e., the amount of MYC molecules bound to specific regions of DNA, such as promoters) distinguishes cells expressing low or high levels of MYC. Accordingly, high MYC levels result in the invasion of enhancers and the increase of the amount of total RNA, i.e. the more MYC is bound, the more RNA is transcribed. Notably, the amplification occurs in a non-linear way, i.e. higher MYC levels result in a higher expression and amplification of the gene. Enhanced global RNAPII pause-release is the proposed mechanism leading to transcriptional amplification.

Further studies have attempted to clarify this model, although some of them have provided contradicting evidence against some elements (Walz et al, 2014; Sabò et al, 2014). One study highlighted that the global changes associated with increased MYC levels, such as increased amount of mRNAs and increased cell size, are indirect and secondary and are the result of MYC-mediated activation of specific transcriptional programs (Sabò et al, 2014). Other studies have demonstrated that the strength of MYC binding is dictated by different promoter affinities, which in turn define differences between low and high levels of MYC. Particularly, at low, or physiological levels, MYC binds to high affinity sites, like those containing canonical E-boxes, while at high,

or oncogenic levels, these sites are saturated and MYC binds to low affinity sites until enhancer invasion, potentially behaving as a general amplifier (Walz et al, 2014; Lorenzin et al, 2016). In general, all these studies highlight the potential of MYC to bind to every genomic site, if in the proper chromatin context. This knowledge can therefore suggest an implicit redefinition of the concept of a MYC target gene. Further research into the complexity of MYC function remains to be explored, for example the interaction or competition with other factors, the cell-type specificity, and how such changes occur in a cancer context (Wolf et al, 2015).

1.1.1.3 Physiological *versus* oncogenic MYC: levels matter

The existence of mechanisms able to regulate MYC in multiple cellular processes, from transcription to protein degradation, highlights the importance of keeping MYC levels under control. Physiologically, MYC plays a key role in proliferating cells and is not expressed in differentiated cells (Eilers and Eisenman, 2008). An increase in MYC levels up to a few thousand molecules per cell is sufficient to induce cell proliferation (Waters et al, 1991). Under these physiological conditions, mRNA expression and protein activity are dependent upon mitogenic stimulation and the removal of mitogens leads to the downregulation of MYC levels (Waters et al, 1991). In contrast, the number of MYC molecules in tumor cell lines has been calculated to range between one hundred thousand and three million (Lorenzin et al, 2016). Although, as mentioned above, exact ways to define MYC-dependent transcriptional signatures in a cancer context are still under discussion, it has been continually demonstrated that even small differences in MYC levels have a deep impact on cellular behavior (Shichiri et al, 1993). High MYC levels in tumors are associated with genomic instability, increased S-phase entry, angiogenesis and metastasis (Adhikary and Eilers, 2005). Deregulated MYC is essential for both tumor initiation and progression. Moreover, blocking MYC activity in established tumors led to their regression, indicating that cancers generally need to maintain high MYC levels (MYC-addiction) (Jain et al, 2002). High MYC levels can also induce apoptosis, a fail-safe mechanism that cells use to avoid transformation (Adhikary and Eilers, 2005). The ectopic expression of MYC sensitizes a variety of cells to apoptosis through nutrients deprivation or DNA damage (Shim et al,

1998; Yuneva et al, 2007; Wiese et al, 2015). It has been proposed that tumor initiation is promoted by a small deregulation of MYC levels; however, these levels are still far from the threshold needed to activate an apoptotic response. Progressive accumulation of genetic lesions, e.g. loss of the tumor suppressors ARF or p53, engaged in MYC-dependent apoptosis, contributes to increase MYC levels during tumor progression (Murphy et al, 2008).

1.1.2 Mechanisms of MYC regulation between physiology and cancer

While MAX expression is constitutive and not limiting for MYC function, MYC levels are tightly controlled through several mechanisms during normal cell cycle progression (Blackwood et al, 1992). Increased MYC levels result mainly from the loss or alteration of regulatory mechanisms impinging on MYC and acting at different steps. In addition to these mechanisms, which are further analyzed in the next sections, higher MYC levels can also result from genetic events which lead to increased mRNA production. Gene amplification (Beroukhim et al, 2010) and chromosomal translocation are common events involving the *MYC* locus. The best-characterized rearrangement is the translocation of the *MYC* locus on chromosome 8 under the control of the immunoglobulin heavy or light chain enhancer on chromosome 14, 22 or 2. This translocation leads to very high levels of MYC expression and occurs in all cases of Burkitt's lymphomas (Dalla-Favera et al, 1982).

1.1.2.1 Transcriptional regulation

Physiologically, *MYC* is expressed at very low levels in quiescent cells and its expression can increase up to 40 folds in proliferating cells (Kelly et al, 1983). *MYC* is defined as an 'immediate early gene', which can be rapidly (within one and three hours) activated following growth factors stimulations (Kelly et al, 1983). This process leads to the controlled activation of an intracellular cascade of events ending with *MYC* expression. Four *MYC* promoters have been identified: P0, P1, P2 and P3. The *MYC* mRNA contains three exons; the majority of transcripts are produced from the weak P1 and the stronger P2 promoters, located in the 5′ region of exon one (Levens, 2010). *MYC* transcription is also subject to negative auto-regulation, as demonstrated by the

fact that introducing an ectopic MYC constructs downregulates the endogenous mRNA. Thus, this mechanism represents a form of homeostatic regulation aimed to restraining MYC levels (Penn et al, 1990). Regulation of MYC transcription has yet to be fully understood. Multiple, some of which are redundant, transcription factor binding sequences have been identified as far as kilobases from the *MYC* genomic locus, making it difficult to disentangle the physiological and oncogenic contribution of single factors or single sequences to *MYC* transcription (Levens, 2013). Importantly, the main regulatory mechanism of *MYC* transcription is the release of paused RNAPII (Eick and Bornkamm, 1986), i.e. RNAPII that has accumulated near the transcriptional start site (TSS) and that is ready to elongate following proper stimulation (Brannan and Bentley, 2012). This mechanism is consistent with the rapid upregulation of *MYC* following external stimulation.

Several transcription factors that can activate *MYC* expression have been identified and their deregulation has been shown to contribute to the genesis of specific tumors. Activation of the transcription factors T-cell factor/lymphoid enhancer factor (TCF/LEF) downstream of the Wnt signaling pathway represents an illustrative model in colorectal cancer (Fig. 1.1). The Wnt/β-catenin pathway is physiologically important for maintaining intestinal proliferative homeostasis and is activated in the stem cell compartment of the intestinal crypts (Reya and Clevers, 2005). Mutations in different components of the pathway are found in around 90% of colorectal cancers (CRCs) and often result in the production of a nonfunctional adenomatous polyposis coli protein (APC) (Ahmed et al, 2013). The effect of these mutations is to enhance the TCF-mediated transcription of Wnt targets, such as *MYC* (He et al, 1998). Deregulated MYC levels play a pivotal role in CRC pathogenesis (Myant and Sansom, 2011). TCF-binding sites, referred to as WRE (Wnt Responsive Elements), have been mapped in both the proximal region of the *MYC* locus (5′and 3′WRE) and in the distal region, ca. 335 kb upstream from the *MYC* TSS (He et al, 1998; Yochum et al, 2008; Tuupanen et al, 2009). An enhancer sequence has been identified in the distal WRE (Tuupanen et al, 2009). Interestingly, a single nucleotide polymorphism (SNP) found in this region is strongly associated with an increased TCF binding strength and CRC incidence (Tomlinson et al, 2007). Binding of TCF/β-catenin to the WRE implies the formation of

chromatin loops to place distant genomic regions in contact with each other (Yochum et al, 2010; Jaeger et al, 2015).

Increased *MYC* transcription is further potentiated by the presence of a super-enhancer, which is located approximately 50 kb upstream from *MYC* TSS and which can form additional looping structures (Hnisz et al, 2013). A super-enhancer is defined as a large cluster of enhancers characterized by increased binding and occupancy of transcription factors, chromatin regulators and cofactors. Most importantly, in addition to their function in untransformed cells, they are associated with cell type-specific genes and oncogene-associated super-enhancers have been found to be selectively acquired in cancer cells (Hnisz et al, 2013; Loven et al, 2013).

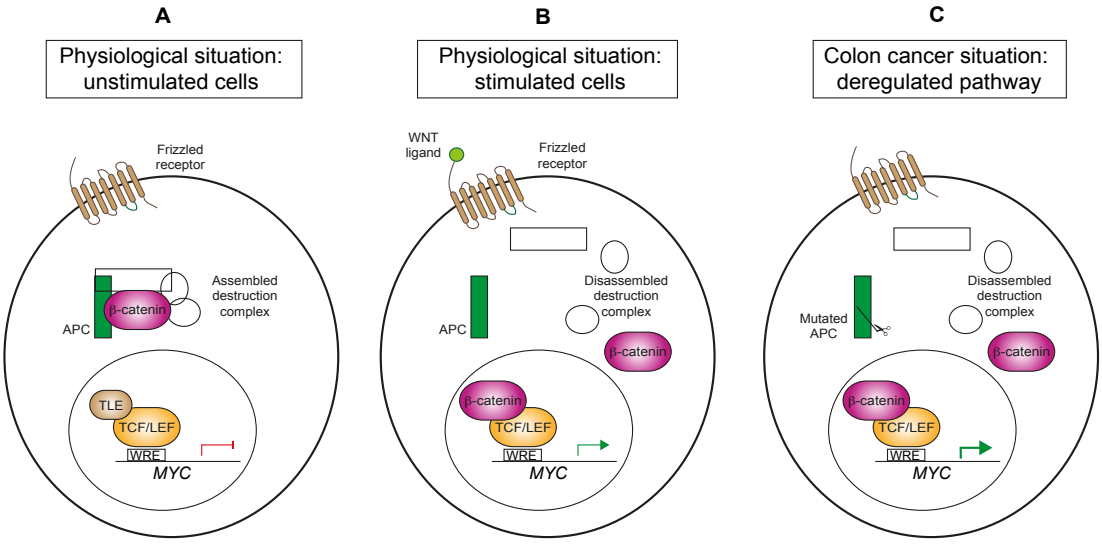

Figure 1.1: Schematic overview of the Wnt pathway

A) In quiescent cells the Frizzled receptor is not bound by its ligand Wnt. The transcriptional co-activator β-catenin undergoes proteasomal degradation in the cytosol following the formation of the destruction complex comprising of the scaffold proteins APC and AXIN, the glycogen synthase kinase 3 (GSK3) and the casein kinase 1 (CK1). Phosphorylation of β-catenin triggers its ubiquitination, mediated by beta-transducin repeat containing E3 ubiquitin protein ligase (β-TrCP), and subsequent degradation. Under these conditions, TCF transcription factors bind to transcriptional co-repressors, e.g. transducin-like enhancer protein (TLE).

B) Following ligand stimulation in the intestinal crypt (the stem cells compartment), the destruction complex is disassembled and inactivated. This event allows for cytosolic β-catenin accumulation followed by its nuclear translocation. In the nucleus β-catenin displaces TLE and activates a TCF-mediated transcription of target genes, which are involved in the regulation of cell cycle.

C) Mutations in components of the Wnt signaling pathway uncouple the ligand binding and the intracellular response due to the constitutive inactivation of the destruction complex. β-catenin is therefore constitutively localized in the nucleus where it drives deregulated expression of target genes, such as *MYC*, *CCND1* (encoding Cyclin D1), etc. (Rennol and Yochum, 2015).

1.1.2.2 Post-transcriptional and translational regulation

The most abundant and best-characterized form of MYC is the protein p64, which contains 439 amino acids and is translated from the ATG (Met) codon present in the second exon. Two less abundant isoforms, which differ in the N-terminus, have also been identified, although their function is less known and less characterized. A longer MYC isoform (p67) containing 454 amino acids is translated from a non-canonical CTG (Leu) codon present in the first exon (Hahn et al, 1988); a shorter isoform (MYCS) contains 339 amino acids and its translation is initiated from an internal AUG codon (Spotts et al, 1997).

A schematic overview of the most abundant *MYC* mRNA form (transcribed from the promoter P2) is shown in Fig. 1.2.

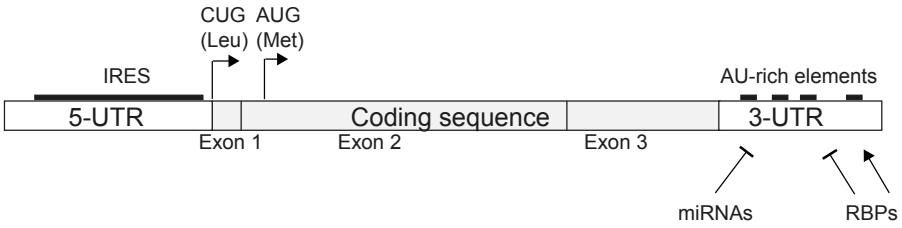

Figure 1.2: Structure of *MYC* mRNA

The length of the 5′-UTR, coding sequence (CDS) and 3′-UTR is 525, 1365 and 476 bases (b), respectively.
The 5′-UTR has a complex tridimensional structure, characterized by the presence of loops and pseudo-knots. A 396b long internal ribosomal entry site (IRES) is present (black bold line) and allows CAP-independent translation, which mainly occurs under stress.
The 3′-UTR contains interspersed AU-rich elements (black squares) in a U-rich context. It is target of miRNAs, which block mRNA translation, and RNA binding proteins (RBPs), which can have either a positive or negative effect on *MYC* transcript stability. The tridimensional conformation assumed by the 3′-UTR can undergo changes following protein binding, exposing miRNAs binding sites otherwise not accessible, see for example Kim et al, 2007.
MYC has three exons, whose length is 30, 772 and 563 bases, respectively. A non-canonical CUG starting site is present in the first exon and its use leads to translation of MYC 1 or p67, i.e. the longer MYC isoform. Translation usually starts from the AUG site, located 15 bases after the beginning of exon 2. Therefore, the CDS relative to the major MYC isoform (MYC 2 or p64) is 1320 bases long and contains two exons (Source: UCSC genome browser; Kent et al, 2002)

Post-transcriptional regulation can occur at many levels and *MYC* mRNA regulation can also occur at the level of processing or cytoplasmic export. Mechanisms influencing *MYC* mRNA stability will be described in more detail in this section. *MYC* mRNA is

short lived (Dani et al, 1984); its half-life is approximately 15-30 minutes and is dictated by the presence of specific sequences, mainly in the 3′-UTR. This region contains determinants of mRNA stability called adenosine-uridine (AU) rich elements (AREs). AREs are commonly found in the 3′-UTR of mRNAs coding for proto-oncogenes or cytokines and are bound by RNA-binding proteins. *MYC* AREs are constituted by four pentamers (AUUUA) placed in a uridine-rich context (Brewer, 1991). Different AU-binding proteins (AUBPs) have been identified and characterized for their ability to either increase or decrease *MYC* stability (Table 1.1). Importantly, expression of AUBPs or signaling pathways controlling their activity can be deregulated in cancer, thereby impacting the stability of target mRNAs (Audic and Hartley, 2004).

Table 1.1: List of main *MYC* AUBPs and their role in controlling *MYC* stability

Name	Function	Mechanism	Reference
Human antigen R (HuR)	Destabilizer	3′-UTR conformational change induced by HuR binding allows binding of miRNA let-7 and repression of translation.	Kim et al, 2009; Gunzburg et al, 2015
		HuR cleavage product (HuR-CP1) associates with *MYC* 3′-UTR, blocking its translation after prolonged hypoxia.	Talwar et al, 2011
	Stabilizer	HuR protects *MYC* mRNA from degradation in presence of polyamines.	Liu et al, 2009; Liu et al, 2015
Tristetraprolin (TTP)	Destabilizer	Mediates mRNA decay following rapamycin treatment.	Marderosian et al, 2006
TIA-1 related protein (TIAR)	Destabilizer	Represses *MYC* translation following UV-C irradiation; Antagonizes AUF-1.	Mazan-Mamczarz et al, 2006; Liao et al, 2007
ARE/poly(U)-binding/degradation factor 1 (AUF-1)	Stabilizer	Promotes MYC translation by antagonizing TIAR and likely by interacting with translation initiating factors.	Liao et al, 2007

MYC 3′-UTR is the preferential binding site of miRNAs. miRNAs are short non-coding RNAs able to block translation of target mRNAs by binding complementary sequences on their 3′-UTR (Bartel, 2009). Similar to AUBPs, also miRNAs usually recognize multiple targets whose function is potentially linked. Therefore, they can act according to a coordinated program, for example by blocking cell proliferation, and their expression can be regulated under specific conditions, such as cellular stress (Bartel, 2009). miRNAs belonging to the miR-34 family (miR-34a, b and c) are among the best characterized miRNAs targeting *MYC* (Hermeking, 2010). Their expression is controlled by p53 and is activated in response to DNA damage. This is consistent with their role in suppressing cell proliferation, i.e. protecting cells from transformation (He et al, 2007). Mechanisms of p53-independent induction of miR-34 components have also been described (Christoffersen et al, 2010; Cannell et al, 2010; Kress et al, 2011). miRNAs are usually part of the regulatory circuits that are often lost in cancer, for example due to the inactivation of an upstream regulator (e.g. p53), or silencing or repression of miRNA expression (Jackstadt and Hermeking, 2015; see 1.3.3).

MYC can regulate its own stability through coding sequences (CDS), more specifically through coding region instability determinant (CRD) elements (Wisdom and Lee, 1991). The insulin-like growth factor-2 mRNA-binding protein-1 (IGF2BP1) binds to the CRD and confers stability to *MYC* mRNA, protecting it from endonucleolytic cleavage (Bernstein et al, 1992). This process is normally regulated during translation; however, overexpression of IGF2BP1 and subsequent increase MYC stability has been observed in human cancers (Doyle et al, 2000; Ross et al, 2001; Gutschner et al, 2014). *MYC* 5′-UTR also influences *MYC* translation. The canonical *MYC* transcript (from promoters P1 and P2) includes a long (more than 500 bases) and structured 5′UTR, which, under physiological conditions, ensures to maintain a basal MYC translation (Koromilas et al, 1992; Svitkin et al, 2001). This process is coordinated with the controlled expression of rate-limiting components involved in translation initiation, such as the cap-interacting protein eIF4E and the RNA helicase eIF4A (Pelletier et al, 2015) (see 1.3.2). An interesting structural feature of *MYC* 5′-UTR is represented by the presence of G-quadruplexes. These complex tridimensional structures are made of stacked layers of four guanine bases (Mendoza et al, 2016). The translation of mRNAs containing G-quadruplexes in their 5′-UTR, including *MYC*, has been shown to be

dependent upon the helicase eIF4A, which can unwind these complex structures (Wolfe et al, 2014). Rather than mutations affecting the structure of *MYC* 5′-UTR and potentially facilitating *MYC* translation, upregulation of components of the translational machinery represents a common mechanism leading to increased *MYC* translation. Evidence of the oncogenic role of both eIF4E (see 1.3.2) and eIF4A (Abdelhaleem, 2004) have been provided and these proteins are considered good therapeutic targets (Pelletier et al, 2015; Wolfe et al, 2014). Characteristic of *MYC* 5-′UTR is also the presence of an internal ribosomal entry site (IRES), which mediates cap-independent translation, a process that typically does not require eIF4E (Stoneley, 2000). IRES-mediated *MYC* translation occurs predominantly during the M/G1 transition when cap-dependent translation is inactive (Kim et al, 2003). Stress conditions also result in blocking cap-dependent translation and subsequently enhancing cap-independent mechanisms (Merrick, 2004). Thus, IRES-dependent *MYC* translation has been observed in apoptotic cells, following DNA damage or drug treatment (Stoneley, 2000; Subkhankulova et al. 2001; Shi et al, 2013). The only known mutation in this region has been observed in patients with multiple myeloma. It consists in a single nucleotide mutation associated with increased IRES-mediated *MYC* translation (Chappell et al, 2000).

1.1.2.3 Protein stability and post-translational regulation

Like *MYC* mRNA, the MYC protein is characterized by a short half-life. In addition to several post-translational modifications influencing different aspects of MYC function (Vervoorts et al, 2006), two sequential phosphorylation events affect MYC stability and lead to its proteasomal degradation in a growth factor-dependent way. Activation of RAS following mitogenic stimulation results in the activation of both the ERK and the Phosphatidylinositol-4,5-bisphosphate 3-kinase (PI3K)/protein kinase B (PKB or AKT) pathways. The first kinase phosphorylates a specific residue of MYC (Serine 62), located in the N-terminus of the protein and the second kinase phosphorylates and inhibits GSK-3β. Phosphorylation on Ser62 stabilizes MYC. Growth factor stimulation also increases *MYC* transcription; thus, leading to a general, but controlled, increase of MYC levels, which is important for driving the cells towards the cell cycle. The

subsequent decrease in stimulation weakens RAS signaling and results in the activation of GSK-3β. This kinase phosphorylates MYC on Threonine 58, but only when MYC is primed by phosphorylation on Ser62. This ordered sequence of events ensures coordination between the MYC activity and the cell cycle entrance, followed by a controlled decline in MYC levels, which occurs in late G1 (Sears et al, 2000). The E3 ubiquitin ligase F-box/WD repeat domain-containing 7 (FBW7) mediates MYC degradation. It recognizes phosphorylated MYC and stimulates its ubiquitination and subsequent proteasomal degradation (Welcker et al, 2004). Increased MYC stability is a common event in cancer, due to mutations either in the MYC sequence or in the components of the pathway, which comprises more players than those described. A frequent mutation found in lymphomas occurs on Thr58 (mutated to the non-phosphorylatable residue Alanine), which results in increased MYC stability during the cell cycle (Bahram et al, 2000). Inactivating mutations of FBW7 also occur at different frequencies across a broad spectrum of tumors (Akhoondi et al, 2007).

1.2 Metabolic requirements in normal and cancer cells

1.2.1 Balanced metabolic processes in proliferating cells

Proliferation is a tightly controlled process in normal cells. It occurs following the stimulation of external growth factors and the induction of intracellular pathways that coordinate events necessary for ensuring proper cell division. Availability of biosynthetic building blocks is a necessary requirement to sustain the needs of proliferative cells. Nutrients enter metabolic pathways and are subsequently used for the production of macromolecules, such as nucleotides for the biosynthesis of DNA or RNA, amino acids for proteins and lipids for new membranes formation, etc. (Vander Heiden, 2009). The activation of metabolic pathways is regulated by a growth factor-induced signal transduction, which allows cells to couple external nutrient availability with cell cycle progression (DeBerardinis et al, 2008).

Increased expression of many of the enzymes involved in metabolic reactions occurs between G1- and S-phase, according to the increased cellular demand for

macromolecules (Kaplon et al, 2015). Glucose and glutamine represent the main fuels for proliferating cells (Locasale and Cantley, 2011). Although the activation of specific metabolic pathways is highly cell type-dependent, quiescent cells typically use nutrients to produce energy, in the form of ATP, through the glycolysis and the tricarboxylic acid (TCA) cycle. On the other hand, proliferating cells tend to use these pathways for shunting metabolites towards catabolic reactions (Ward and Thompson, 2012), (Fig. 1.3). The metabolic pathways are closely connected with one another. A clear example of this is provided by the mitochondrial TCA cycle, whose intermediates can be diverted to biosynthetic pathways (e.g. lipid or protein biosynthesis), a process referred to as cataplerosis, and can be continuously replenished, a process referred to as anaplerosis (Owen et al, 2002). Thus, the complexity of metabolic networks helps to underline the importance of balancing several pathways by coordinating the activity of intracellular effectors designed to orchestrate these responses. It is worth to mention, therefore, that cells have evolved mechanisms of nutrients sensing in order to integrate external stimuli with the cellular response (see 1.3.3).

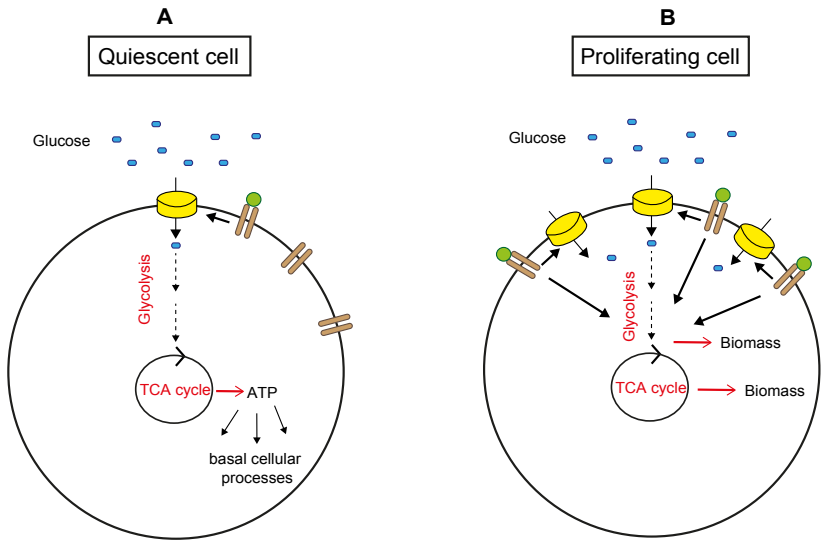

Figure 1.3: Metabolism in quiescent and proliferating cells

A) Basal levels of signaling ensure entrance of glucose into quiescent cells. Glucose is usually completely oxidized in the TCA cycle, leading to the production of 36 molecules of ATP, used for maintaining essential cellular processes (e.g. basal transcription, translation).
B) Growth factor stimulation allows for the entrance and the use of external nutrients, by increasing expression of transporters on the cell membrane and enzymes. Metabolites are mainly used for biosynthetic purposes, in order to support cell proliferation.

1.2.2 Metabolism in cancer cells

From a metabolic point of view, tumor cells can be viewed as proliferating cells. However, cancer cells display metabolic features that distinguish them from their healthy counterpart and allow them to sustain biosynthetic programs in a way that is uncoupled from growth factor stimulation. The complex change in metabolism that cancer cells undergo is termed metabolic reprogramming and represents a hallmark of cancer (Hanahan and Weinberg, 2011). Overall, the metabolic reprogramming is the result of the crosstalk between cell-extrinsic and -intrinsic mechanisms that allow tumor cells to overcome the selective pressure imposed during cancer progression and, consequently, to survive under unfavorable conditions, e.g. hypoxia (Pavlova and Thompson, 2016). Cell-extrinsic mechanisms are dictated by the tumor microenvironment. For example, nutrient and oxygen availability depends on the tumor-supportive blood vessels, which are usually irregularly distributed. This irregularity promotes the formation of perfused or hypoxic areas (Nakazawa et al, 2016). Cell-intrinsic metabolic changes are instead driven by the activity of deregulated oncogenes and by the inactivation of tumor suppressors (Chen and Russo, 2012). Common genetic lesions occurring in tumors lead to increased nutrient uptake and utilization. In general, upregulation of key-rate limiting enzymes involved in many metabolic pathways has been demonstrated in different kinds of tumors, resulting in both an increased uptake of glucose and glutamine and in the use of alternative energetic sources, e.g. acetate (Comerford et al, 2014) and lipids (Kamphorst et al, 2013). Moreover, in order to survive under unfavorable conditions, tumors can activate additional mechanisms to obtain nutrients, for example scavenging extracellular proteins through macro pinocytosis (Comisso et al, 2013) or recycling intracellular components through autophagy (Jin and White, 2007).

Another point to consider is that, although tumors rewire their metabolism to support growth and proliferation, they still need to keep these processes balanced to avoid a metabolic catastrophe, such as an unsustainable depletion of ATP, especially when experiencing nutrients starvation (Qiu and Simon, 2015). The AMP-activated protein kinase (AMPK) represents an example of a mechanism that aids tumors in the maintenance of cellular homeostasis. AMPK is a sensor of the cellular energetic status

and is activated by increased AMP/ATP ratio (Hardie et al, 2007). AMPK activation blocks energy-consuming processes, e.g. protein synthesis, and activates catabolic pathways, e.g. fatty acids oxidation and autophagy, in order to allow cells to cope with stress (Jeon and Chandel, 2012; Chaube et al, 2015). Maintaining a high rate of protein synthesis under stress conditions leads cells to die following the exhaustion of energy and substrates (Leprivier, 2013). Importantly, supporting biosynthetic requirements or activation of homeostatic mechanisms often imply the differential use of enzymes or the hijacked expression of proteins in a cancer-specific way. This concept poses the rational for identifying cancer-associated metabolic liabilities to be used as therapeutic targets (Martinez-Outschoorn et al, 2016).

1.2.2.1 Glucose metabolism in cancer

A typical feature of cancer cell metabolism is the Warburg effect or aerobic glycolysis, according to which tumors avidly consume glucose and metabolize it through the glycolytic pathway even in presence of oxygen (Vander Heiden, 2009). Glucose enters the cell through the transporter GLUT1, is oxidized to pyruvate in the glycolytic pathway and secreted as lactate through the transporter MCL1. Both transporters are upregulated in cancer cells. The activity of two rate-limiting glycolytic enzymes is often increased or altered in cancer cells. The Hexokinase 2 (HK2) is the enzyme that catalyzes the conversion of glucose to glucose-6-phosphate. Addition of a phosphate group allows glucose to be trapped into the cells; thus, driving the glycolytic process. The pyruvate kinase (PK) M2 (PKM2) is an embryonic specific isoform of the enzyme PK, is reactivated in cancer and has been identified to be responsible for the Warburg effect. The low PKM2 activity indeed changes the flux of glycolytic intermediates, promoting their accumulation and consequent channeling into biosynthetic pathways, such as the pentose phosphate pathway, which provides cells with carbon-derived metabolites and reducing equivalents (NADPH) necessary for supporting biosynthesis. Lactate production from pyruvate is increased through Lactate Dehydrogenase A (LDH-A) upregulation. This reaction helps to maintain the glycolytic flux by re-generating the co-factor NAD^+ (Fig. 1.4).

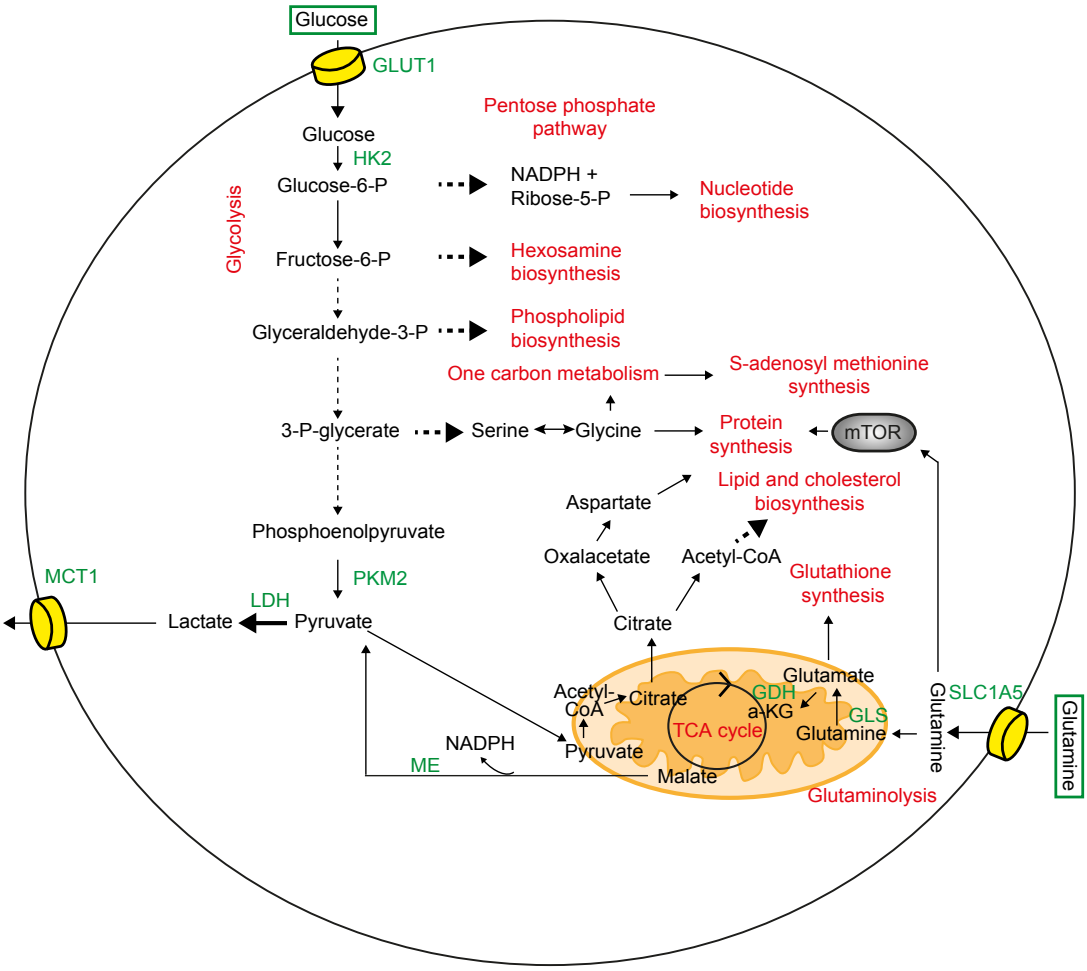

Figure 1.4: Schematic overview of metabolic pathways active in cancer cells

Glucose and glutamine are the major nutrients for cancer cells, although other fuels are used, especially under stress conditions (not shown in this figure). The intracellular routes of these two metabolites are dictated by increased expression and activation of enzymes, due to deregulated oncogene activity, e.g. MYC, AKT, PI3K or loss of tumor suppressor, e.g. p53.
The main pathways are indicated in red. Enzymes belonging to these pathways are often upregulated in cancer. Hexosamines are amino sugars used in post-translational modifications; phospholipids, lipids and cholesterol are used for membrane production; S-adenosyl methionine is necessary for methylation reactions, included those driving epigenetic changes. Although not shown for simplicity, these pathways and their intermediates are interconnected between each other, e.g. glutamine also enters the nucleotides biosynthetic pathway. Full arrows show direct reactions, dashed ones indicate the presence of metabolic intermediates (not shown). (Pavlova and Thompson, 2016).

1.2.2.2 Glutamine metabolism in cancer

In addition to glucose, another main metabolite for cancer cells is represented by glutamine (Locasale and Cantley, 2011). Glutamine enters the cells through specific

transporters, e.g. SLC1A5, which are often overexpressed in cancer. The main route for metabolizing glutamine is the glutaminolysis pathway. Glutamine is converted to glutamate through the mitochondrial glutaminase (GLS) and glutamate is in turn converted to α-ketoglutarate through the glutamate dehydrogenase (GDH). In this form, glutamine can enter the TCA cycle (anaplerosis) to replenish intermediates used for biosynthetic reactions, e.g. citrate, used for synthetizing lipids. Glutamine-derived malate can be converted to pyruvate through the malic enzyme (ME). Similarly to glycolysis, glutaminolysis can contribute to the production of lactate from pyruvate. This reaction also contributes to maintaining the pool of NADPH, which provides reducing power necessary for sustaining anabolic reactions. Glutamine also assumes a fundamental role as a donor of nitrogen groups necessary for the biosynthesis of nucleotides and contributes to the biosynthesis of glutathione, which serves as a scavenger of reactive oxygen species (ROS) (Fig. 1.4). Glutathione is a tripeptide constituted of glutamate, cysteine and glycine. Glutamine-derived glutamate is not only directly incorporated into the GSH, but is also exchanged with cystine through the X_c^- antiporter. Cystine, in turn, is reduced to cysteine (DeBerardinis and Cheng, 2010).

1.3 Role of MYC in metabolic reprogramming

Metabolic reprogramming is the result of the concerted deregulated activity of pathways able to drive biomass accumulation and cell proliferation in a manner independent from extracellular stimuli. The ability of MYC to control the expression of several targets involved in metabolism and to coordinate different pathways makes it a key factor in orchestrating the metabolic reprogramming. Although this classical view of MYC´s function in the metabolic context may be reconsidered in light of the recent amplifier model and of its implications (see 1.1.1.2), there is much empirical evidence suggesting MYC´s involvement in metabolic reprogramming.

1.3.1 Mechanisms supporting MYC-driven metabolic reprogramming

MYC levels are tightly controlled in normal proliferating cells (see 1.1.2). This, in turn, is reflected in the controlled activation of target genes. E-box sequences have been

identified in several genes whose products are involved in metabolism, for example genes whose products control glycolysis (Osthus et al, 2000) or genes encoding for enzymes in the nucleotide biosynthetic pathway (Liu et al, 2008) (Fig. 1.5).

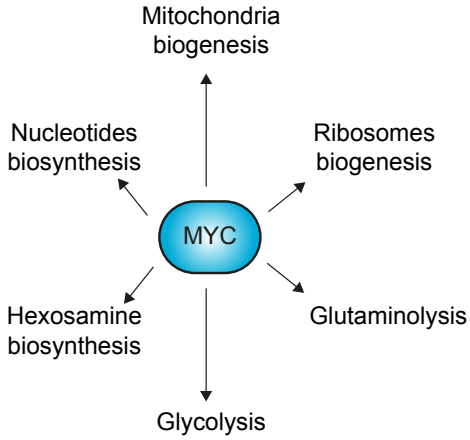

Figure 1.5: Metabolic pathways driven by MYC

MYC controls the expression of genes encoding for enzymes involved in many metabolic processes. These pathways are interconnected between each other, allowing MYC to orchestrate a coordinated response. For example, increased mitochondrial function is necessary for glutamine-dependent anaplerosis; coordinated protein synthesis and DNA replication occurs following increased nucleotide biosynthesis and ribosome biogenesis.

Examples of MYC target genes involved in several metabolic pathways are presented in Table 1.2.

The same spectrum of MYC targets involved in metabolic pathways is activated both during physiological cell proliferation and in transformed cells. However, in its oncogenic form, MYC is able to rewire cancer cell metabolism through different mechanisms. Since MYC activity in cancer cells is uncoupled from growth factor control and from the regulated uptake of nutrients, MYC continuously stimulates expression of target genes; thus, inducing an increased uptake of nutrients and their metabolism (Fig. 1.6).

Table 1.2: MYC targets involved in metabolic processes

Pathway	Target	Function & notes	Reference
Glycolysis	GLUT1	glucose transporter	Osthus et al, 2000
	HK2 (Hexokinase)	Glu-6-P synthesis rate limiting enzyme	
	PFK (Phosphofructo kinase)	Fru-6-P to Fru-1,6-BP conversion rate limiting enzyme	
	PKM2 (Pyruvate kinase M2)	low activity isoform of PK splicing process driven by MYC	David et al, 2010
	LDH-A (Lactate dehydrogenase-A)	lactate production from both Glc- and glutamine-derived pyruvate	Osthus et al, 2000 Wise et al, 2010
	MCT1 (Monocarbolylate transporter 1)	lactate transporter secretion of lactate	Doherty et al, 2014
Glutaminolysis	SLC1A5	glutamine transporter	Wise et al, 2010
	GLS2 (Glutaminase)	regulated in both a transcriptional and post-transcriptional way	Gao et al, 2009 Wise et al, 2010
Nucleotide biosynthesis (purines)	PRPS2 (Phosphoribosyl pyrophosphate synthetase 2)	activation of ribose to PRPP; shown to be both direct MYC target and indirectly increased through eIF4E (see 1.3.2)	Mannava et al, 2008 Cunningham et al, 2014
	PPAT (phosphoribosyl pyrophosphate amidotransferase)	first step in purine biosynthesis; needs glutamine as nitrogen donor	Liu et al, 2008 Mannava et al, 2008
	IMPDH2	IMP synthesis; rate limiting enzyme	
Nucleotide biosynthesis	RRM2 (Ribo nucleotide reductase small subunit)	subunit of ribonucleotide reductase which catalyze formation of deoxyribonucleotides	
Nucleotide biosynthesis (pyrimidines)	CAD (carbamoyl-phosphate synthetase 2, aspartate transcarbamylase, and dihydroorotase)	encodes for the tri-functional rate limiting enzyme catalyzing the first three steps; one of the first genes identified as MYC target	Miltenberger et al, 1995
	DHODH (dihydroorotate	respiratory chain-coupled mitochondrial enzyme	Liu et al, 2008

	dehydrogenase)		
	TYMS (thymidylate synthetase)	dUMP to dTMP conversion; rate limiting enzyme needs THF from folate cycle	Mannava et al, 2008
Serine biosynthesis	PHGDH (phospho glycerate dehydrog.)	3-PG to 3-P-pyruvate conversion	Vazquez et al, 2011 Vazquez et al, 2013
	PSAT (phosphoserine aminotransferase)	3-PP to phosphoserine conversion	
	SHMT2 (serine hydroxymethyl transferase)	serine to glycine conversion; reaction needed in the folate cycle, necessary for nucleotide synthesis	
Mitochondria biogenesis	TFAM (mitochondrial transcription factor A)	nuclear-encoded mitochondrial protein; induces also mitochondrial DNA replication	Li et al, 2005
	NDUFS1 (NADH-ubiquinone oxidoreductase 75 kDa subunit)	subunit of the respiratory chain complex I	

Two effects have been linked with deregulated MYC activity. Firstly, MYC overexpressing-cells become dependent on a continued influx of nutrients, such as glucose or glutamine, in order to sustain biosynthetic processes (Shim et al, 1998; Yuneva et al, 2007). Secondly, high MYC levels change the fluxing rate of metabolites, impacting the production of substrates (Murphy et al, 2013). Flux distribution analysis in a human B-cell line expressing high or low levels of MYC demonstrated an increased flux of glucose through glycolysis and an increased mitochondrial activity and oxygen consumption induced by high MYC levels (Murphy et al, 2013).

Although MYC induces characteristic metabolic changes, the tumor context, i.e. the tissue of origin, is likely to play a role in determining the metabolic features. For example, MYC-induced mouse liver tumors consume glutamine, while MYC-driven lung tumors produce it. This effect has been linked to the differential expression of enzymes, e.g. glutamine synthetase expressed in lung, rather than in liver tumors (Yuneva et al, 2012). A similar effect has been demonstrated in lung or pancreatic

tumors induced by K-RAS. Those tumors are able to differentially use and catabolize branched-chain amino acids, according to the expression of specific enzymes (Mayers et al, 2016). These observations could support the role of MYC as a transcriptional amplifier, i.e. MYC amplifies a pre-existing transcriptional program of proliferating cells (Stine et al, 2015). This could explain both the increased expression of metabolic genes and the tissue specificity.

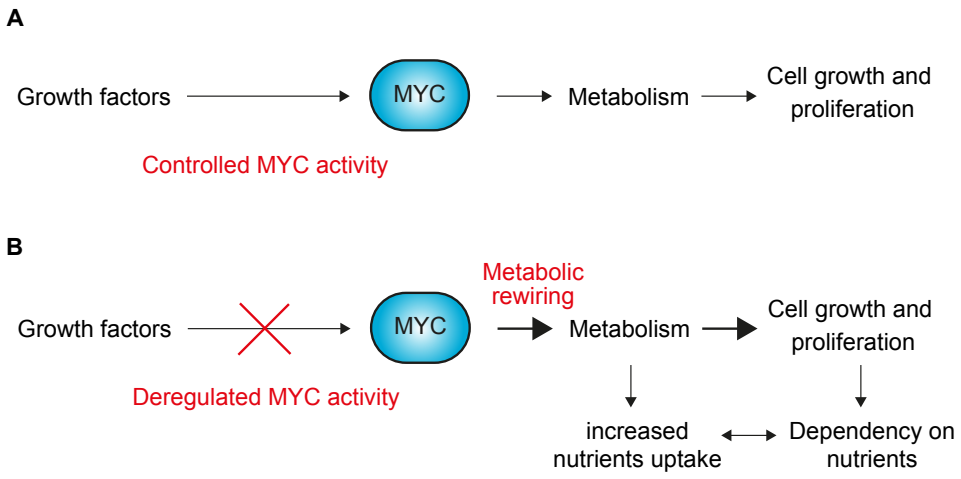

Figure 1.6: Impact of deregulated MYC on cancer cell metabolism

A) In healthy proliferating cells, MYC activity is regulated by external growth factor stimulation, which leads to a controlled response able to adapt metabolism to the needs of proliferating cells.
B) In cancer cells MYC´s activity is uncoupled from growth factor stimulation. Deregulated MYC induces metabolic reprogramming, which allows cells to acquire a proliferative advantage over their normal counterpart. In order to drive biosynthetic processes, MYC increases the uptake of nutrients, mainly glucose and glutamine, whose continue influx became essential for sustaining cellular growth and proliferation.

1.3.2. MYC is a central regulator of cell growth

Cell growth implies the biosynthesis of macromolecules and allows for cell proliferation. The Serine/Threonine kinase mechanistic target of rapamycin (mTOR), in the complex one (mTORC1), is a master regulator of cell growth by promoting protein synthesis. mTOR is hyperactivated in many human cancers, for example following the loss of upstream negative regulators (Laplante and Sabatini, 2012). It is worth to emphasize that oncogenic translation implies not only a global but also a selective upregulation of the synthesis of proteins necessary for cancer progression and the use of

translation factors that can be dispensable in untransformed cells (Truitt and Ruggero, 2016). Among selectively translated products are antiapoptotic proteins (such as induced myeloid leukemia cell differentiation protein (MCL-1) or B-cell lymphoma 2 (BCL2)), oncogenes (such as MYC), proteins involved in metabolic processes (such as mitochondria components) and ribosomal proteins, according to specific characteristic of their 5'-UTR (Pelletier et al, 2015).

Translation is a demanding, energy-consuming process, which requires not only proper assembly of molecular machines, i.e. the ribosomes, but also availability of amino acids to synthetize proteins. MYC plays a key role in protein synthesis, since it is able to sustain the activity of mTOR and of many additional translation factors (Fig. 1.7). The cross talk between MYC and mTOR has been well documented and components of the mTORC1 axis have been demonstrated to be essential for MYC-driven tumors. MYC drives energy production and the uptake of nutrients, including amino acids. Amino acids are not only essential for synthetizing proteins, but are also needed for mTOR activation, especially leucine and glutamine (Duran et al, 2012; Nicklin et al, 2013). Deregulated MYC enhances the expression of the eukaryotic translation initiation factor 4E (eIF4E), the limiting factor of the initiation complex eIF4F, whose activity is also promoted by mTOR-mediated phosphorylation of its inhibitor 4E-binding protein 1 (4EBP1) (Lin et al, 2008). eIF4E is required for cancer growth and is necessary for development of MYC-driven lymphomas (Pourdehnad, 2013). Even a modest upregulation of eIF4E is sufficient to enhance translation. Another mechanism highlighting the connection between mTOR and MYC function in coordinating cell growth can be found in the specific upregulation of *PRPS2*, encoding for the rate-limiting enzyme in the nucleotide biosynthesis phosphoribosyl-pyrophosphate synthetase 2 (Cunningham et al, 2014). This process, which is driven by deregulated eIF4E and is dependent upon MYC levels (i.e. is enhanced during lymphoma progression), represents an example of coordination between the metabolic input and output in terms of protein and nucleotide biosynthesis.

In addition to its function as a transcription factor, MYC has also been shown to be able to increase the capping of nascent transcripts, thereby promoting their translation, through a mechanism dependent upon high MYC levels (Lombardi et al, 2016). MYC has been also identified as a coordinator between increased rates of transcription and

translation, further demonstrating its key role in controlling essential cellular processes (Elkon et al, 2015). MYC is also able to activate both the RNA Polymerase I-dependent transcription of ribosomal RNA (rRNA) and the RNA Polymerase III-dependent transcription of 5S rRNA and tRNA, in addition to genes encoding for ribosomal proteins (van Riggelen et al, 2010).

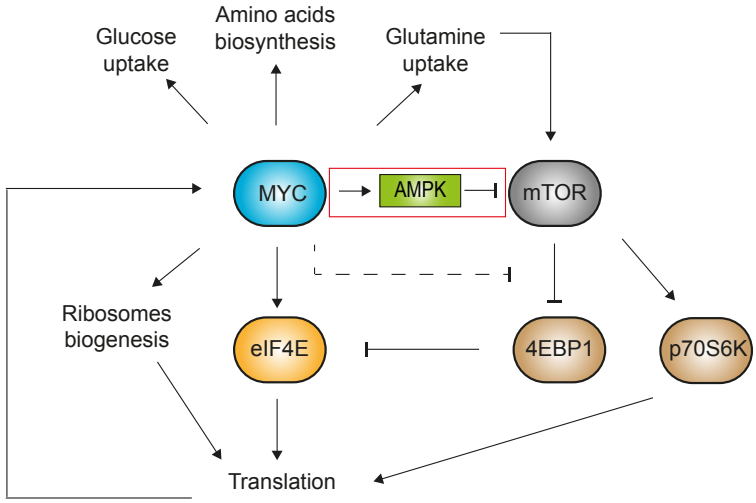

Figure 1.7: The cross talk between MYC and mTOR sustains cell growth

Scheme showing how MYC cooperates with mTOR (see text for description).
The dashed arrow indicates that the mechanism through which MYC stimulates the mTOR-mediated phosphorylation of 4EBP1 has not been yet elucidated. 4EBP1 and p70S6 kinase (p70S6K) are the two major mTORC1 targets, respectively inactivated and activated by phosphorylation. p70S6K activity contributes to ribosomal assembly and initiation of translation, while 4EBP1 inactivation allows the release of bound eIF4E and its interaction with initiation factors.

As mentioned above (1.2.2), although cancer cells increase their metabolism, they also need to maintain homeostatic mechanisms to protect themselves from undergoing metabolic catastrophe following excessive nutrients consumption. The mTOR-MYC cooperation represents a good example of a pathway-triggering activation of homeostatic mechanisms. Sustained anabolic metabolism and processes, such as protein synthesis, lead to energy depletion and AMPK activation in a MYC-dependent way, as shown in different experimental systems (Liu et al, 2012; von Eyss et al, 2015; Edmunds et al, 2015). In turn, AMPK inhibits mTORC1 activity and, thereby, restrains protein synthesis (Hardie, 2007), (red square in Fig. 1.7).

1.3.3 Links between MYC levels and the cellular metabolic status

The central role of MYC in coordinating metabolism and driving cell proliferation could be confirmed by the fact that cells have developed mechanisms able to restrain its activity. MYC expression is not only physiologically tightly controlled by mitogenic stimuli, but also by several mechanisms of control that impinge on MYC. These mechanisms can be potentially linked with the cellular nutrient status. An example is provided by the interplay between MYC and FOXO transcription factors (Fig. 1.8). FOXOs are homeostatic regulators, whose function is particularly important during stress (Eijkelenboom and Burgering, 2013). Energetic and oxidative stresses represent two main activating stimuli of FOXO proteins, which, in turn, are able to antagonize MYC function. FOXO3 have been shown to respond to oxidative stress or hypoxia and subsequently inhibits mitochondrial biogenesis (Jensen et al, 2011; Ferber et al, 2012). This process is driven by MYC and is important for sustaining cell proliferation, in both a physiological and, especially, in a cancer context. FOXO3A can limit MYC levels, thereby inducing the expression of miR-34b/c, which is then able to target the 3´-UTR of *MYC*, thereby inhibiting its translation. This mechanism is positively controlled by the MAP kinase-activated protein kinase 5 (MK5), although the activating stimulus has yet to be identified (Kress et al, 2011). This mechanism is also negatively controlled by mTORC2, which is physiologically activated by growth factors stimulation (Masui et al, 2013).

In general, mechanisms restraining MYC activity can be lost in a cancer setting, resulting in increased MYC levels and, among many other effects, subsequent increased metabolic demand. Common lesions in cancer are represented by the hyperactivation of PI3K, which acts upstream of mTORC2, or AKT (Yuan and Cantley, 2008). In both cases, this results in the inhibition of FOXO activity and subsequent MYC activation, as described in glioblastoma (Masui et al, 2013). Moreover, Kress *et al*. could demonstrate that the feedback mechanism established by MYC, MK5 and miR-34b/c is disrupted during colon cancer progression, through the silencing of miR-34 b/c expression (Kress et al, 2011). These observations help to highlight the heterogenic features that cancer cells develop during progression, i.e. the loss of feedback mechanisms in advanced

tumor stages. The role of FOXO factors can also be contextualized during tumor progression. Like AMPK, FOXOs can suppress tumor formation in stress-exposed cells, help to maintain homeostasis and adapt to adverse conditions during tumor progression (Faubert et al, 2013; Eijkelenboom and Burgering, 2013). However, expression of FOXO3 has been shown to be decreased during colorectal cancer progression, compared to healthy tissues (Bullock et al, 2013). This observation suggests for a tumor suppressive role of FOXO3 in this context and provides another indication of disruption of a mechanism negatively regulating MYC levels. The transcription factor p53 is another important metabolic sensor. It can be activated by different stimuli, including energy and nutrient depletion, and is in turn able to control cellular metabolism (Kruiswijk et al, 2015). p53 is also a negative regulator of MYC levels and function. The best-characterized role of p53 is the MYC-dependent induction of apoptosis, i.e. as a failsafe mechanism associated with MYC overexpression (Hoffman and Liebermann, 2008) or to restrain MYC levels by activating negative feedback mechanisms, e.g. through miRNAs (Feng et al, 2011). MYC-induced DNA damage and genotoxic stress have been described as major stimuli that lead to p53 activation. Metabolic stress can potentially regulate MYC levels in a p53-dependent way, although experimental evidence supporting this model has yet to be provided.

As already discussed, activation or deregulation of these pathways can differentially occur according to the tumor status and to conditions dictated by the microenvironment, that the tumor has to adapt to. MYC-involving mechanisms of response to environmental cues have been described. Specifically, MYC is downregulated following hypoxia, due to increased degradation (Wong et al, 2013). Glucose starvation can further potentiate this response either through proteasomal degradation (Okuyama et al, 2010), or through the induction of a calpain-mediated cleavage of MYC and subsequent formation of MYC-nick (Conacci-Sorell et al, 2014). Myc-nick comprises the N-terminal region of Myc and has transcriptional independent functions because it lacks the nuclear localization signal and the DNA binding domain (Conacci-Sorrell, 2010). Particularly, it has been shown to promote autophagy, thereby protecting cells from stress-induced apoptosis. These mechanisms have been described to help cancer cells survival under unfavorable conditions and could be either conserved, and therefore

used in untransformed cells, or evolved to support the selective pressure cancer cells are exposed to.

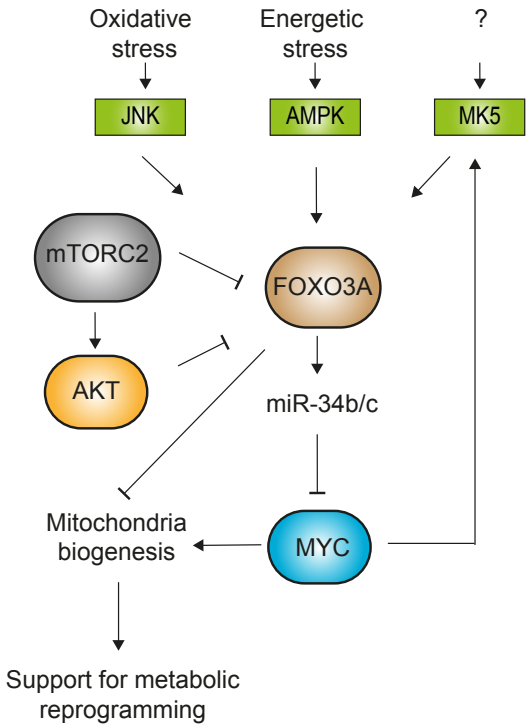

Figure 1.8: The interplay between MYC and FOXO

Schematic illustrating how FOXO transcription factors, specifically FOXO3A, are activated following stress and negatively regulate MYC. FOXO3A activity is positively or negatively regulated by post-translational modifications. AMPK, c-Jun N-terminal kinases (JNK) or MK5-mediated phosphorylation induce its nuclear translocation and allow it to work as transcription factor. mTORC2 promotes FOXO acetylation, inhibiting its function.

1.4 Aim of the thesis

The role of MYC in driving metabolic reprogramming during carcinogenesis has been widely studied and characterized while little is known regarding MYC regulation under nutrient stress conditions. The aim of this project was to evaluate if and how MYC is regulated under metabolic stress conditions using as stress paradigm the starvation of glucose and glutamine, which are the major metabolic fuels for cancer cells. In order to acquire a complete view of mechanisms regulating MYC, the majority of experiments have been planned to analyze effects on the endogenous transcript or protein. Thus, the colorectal cancer cell line HCT116 has been used as experimental system. Colorectal cancer is a well-established MYC-driven tumor, suitable therefore for studying MYC biology. These cells show high levels of endogenous MYC, because of increased gene expression, due to mutations in the upstream WNT signaling pathway.

2 Materials

2.1 Cell lines and bacteria strains

2.1.1 Human cell lines

Cell lines were validated using STR analysis and routinely tested for mycoplasma contamination

HEK293T	human embryonic kidney cell line (ATCC)
HCT116	human colon carcinoma cell line (ATCC), wildtype (*p53*$^{+/+}$) or *p53*-deficient (*p53*$^{-/-}$) (Bunz et al, 1998)

2.1.2 Bacteria strains

DH5α	*Escherichia coli*, genotype F– Φ80lacZΔM15 Δ (lacZYA-argF) U169 recA1 endA1 hsdR17 (rK–,mK+) phoA supE44 λ– thi-1 gyrA96 relA1; used for plasmid amplification
XL1 blue	*Escherichia coli*, genotype recA1 endA1 gyrA96 thi-1hsdR17 supE44 relA1 lac [F′ proAB lacIqZΔM15 Tn10 (Tetr)]; used for plasmid amplification

2.2 Culture media and supplements

2.2.1 Cell culture media

Reconstituted media (#3 and #4) were sterile filtered with 0,45 µm, 250 ml vacuum filter immediately after preparation;

All media and solutions were stored at 4°C.

Name	Use	Supplements
DMEM D6429 (Sigma)	Cell lines propagation/infection	10% FBS (Biochrom, heat inactivated at 56°C for 30 min before use) 1% Penicillin/Streptomycin (Sigma)
DMEM D6429 (Sigma)	Cell transfection	2% FBS (Biochrom)
DMEM D5030 (Sigma) dissolved in ddH_20	All described experiments	3.7 g/l Sodium Bicarbonate (Roth) 10% dialyzed FBS (Sigma, heat inactivated at 56°C for 30 min before use) 1% Penicillin/Streptomycin (Sigma) 2.5 g/l glucose (Sigma) 2 mM glutamine (Sigma)
DMEM without methionine, leucine and glutamine, prepared in Earle's balanced salt solution (Sigma)	Experiment described in Fig. 4.9	MEM Vitamin solution (Life Technologies) 2.5 g/l glucose 10% dialyzed FBS 0.0001 g/l $Fe(NO^3)^3$ • 9H2O (Sigma) all remaining amino acids (Sigma), according to the DMEM composition
DMEM D0422 (Sigma), without methionine, cysteine, glutamine	Metabolic labeling	10% dialyzed FBS 2 mM glutamine 500 μCi ^{35}S labeled L-Cystein, L-Methionin (Hartmann analytics)
Freezing medium	Cell line storage	90% FBS (Biochrom, heat inactivated at 56°C for 30 min before use) 10% DMSO (Sigma)

2.2.2 Supplements

All reagents were obtained from Sigma, unless otherwise indicated

	Stock concentration	Final concentration
4-hydroxytamoxyfen	10 mM, in ethanol (EtOH) stored at -20°C	100 nM; 20 nM, as specified
Cycloheximide	100 mg/ml, in EtOH; prepared freshly before use	100 μg/ml
Dymethyl-α-ketoglutarate	6.7 M	10 mM
Dimethyl succinate	8 M	20 mM
Doxycycline	1 mg/ml in EtOH; stored at -20°C	1 μg/ml
EmbryoMax Nucleosides mix (Merck)	100 x	5 x
Glutathione reduced ethyl ester	200 mM, in H_2O; stored at -20°C	5 mM
Glutamate	200 mM, in H_2O (see 2.4)	1.35 mM
MG132 (Calbiochem/Millipore)	20 mM, in DMSO; stored at -20°C	20 μM
N-acetyl-L-Cysteine solution	1 M, in H_2O (see 2.4)	5 mM
OSI-027 (Active biochemical)	10 mM, in DMSO; stored at -20°C	20 μM
Puromycin (Invivogen)	10 mg/ml; stored at -20°C	2 μg/ml

Rapamycin (LCLabs)	100 µM, in DMSO; stored at -20°C	20 nM
Single nucleosides and deoxynucleosides	10 mM, in in H_2O or DMSO (see 2.4)	150 µM each, if not otherwise specified; 50 µM thymidine
Sodium Pyruvate	100 mM; stored at 4°C	2 mM

2.3 Bacteria culture media and supplements

2.3.1 Culture media

Name	Components and preparation
LB medium	10% (w/v) Bacto tryptone (Roth) 0.5% (w/v) yeast extract (Roth) 1% (w/v) NaCl (Roth) autoclaved immediately after preparation
LB agar	LB-medium with 1.2% (w/v) agar-agar (Roth) autoclaved, heated in a microwave oven, cooled down to 50°C; antibiotics were added the medium poured into 10 cm dishes

2.3.2 Antibiotics

All powder formulations were obtained from Roth. Stock solutions were prepared in ddH_2O and sterile filtered before use.

Ampicillin	100 µg/ml final concentration
Kanamycin	30 µg/ml final concentration
Chloramphenicol	25 µg/ml final concentration

2.4 Solutions, and buffers

All solutions and buffers were prepared using dd H_2O, unless otherwise indicated.
All solutions were stored at RT, unless otherwise specified.
All chemicals were purchased from Sigma and Roth.

Ammonium persulfate (10%)	5 g ammonium persulfate (APS) dissolved in 50 ml ddH_2O; aliquots stored at -20°C
Ampicillin stock solution	10 g ampicillin solubilized in 100 ml ddH_2O and sterile filtered; aliquots stored at -20°C
Annexin V binding buffer	10 mM HEPES, pH 7.4 140 mM NaCl 2.5 mM $CaCl_2$
Blocking solution for PVDF membrane	5% (w/v) skim milk powder in TBS-T 5% (w/v) BSA in TBS-T
Blocking solution for ChIP	5 mg/ml BSA in PBS; sterile filtered with 0,45 µm, 250 ml vacuum filter immediately after preparation; stored at 4°C
Bis-Tris (3.5 x)	1.25 M Bis-Tris
Bis-Tris stacking gel	4% (v/v) acrylamide / bisacrylamide 1 x Bis-Tris 0.03% (v/v) APS 0.05% (v/v) TEMED
Bis-Tris separation gel	8-15% (v/v) acrylamide / bisacrylamide 1 x Bis-Tris 0.03% (v/v) APS 0.05% (v/v) TEMED

Bradford reagent	0.01% (w/v) Coomassie Brilliant Blue G250 8.5% phosphoric acid 4.75% ethanol; filtrated through a paper filter and stored at 4°C in the dark
Crystal violet solution	0.1% (w/v) crystal violet 20% (v/v) ethanol
ChIP elution buffer	50 mM Tris, pH 8.0 1 mM EDTA 1% SDS 50 mM $NaHCO_3$; prepared immediately before use
ChIP swelling buffer	5 mM PIPES, pH 8 85 mM KCl 0.5% NP-40; stored at 4°C; 0.5 mM PMSF, 1:1000 protease and phosphatase inhibitors added freshly before use
ChIP wash buffer I	20 mM TRIS/HCl, pH 8 150 mM NaCl 2 mM EDTA 0.1% SDS 1% Triton X-100; stored at 4°C
ChIP wash buffer II	20 mM TRIS/HCl, pH 8 500 mM NaCl 2 mM EDTA 0.1% SDS 1% Triton X-100; stored at 4°C

ChIP wash buffer III	10 mM TRIS/HCl, pH 8 250 mM LiCl 1 mM EDTA 1% NP-40 1% deoxycholic acid sodium salt; stored at 4°C
Deoxynucleotide triphosphate (dNTP) mix stock (10 mM)	50 µl each dNTP (100 mM) mixed with 300 µl ddH_2O to 500 µl final volume; aliquoted and stored at -20°C
DNA loading buffer (6 x)	10 mM EDTA, pH 8.0 0.2% (w/v) Orange G 40% (w/v) sucrose; stored at -20°C
D-PBS	PBS with 100 mg/l $CaCl_2$ and 100 mg/l $MgCl_2$
Gel fixing solution	70 ml ddH_2O 20 ml Methanol 10 ml acetic acid
Glucose stock solution (250 mg/ml)	12.5 g in 50 ml ddH_2O; sterile filtered with 0.2 µM syringe filter; stored at 4°C
Glutamate stock solution (200 mM)	1.48 g glutamate in 50 ml ddH_2O; sterile filtered with 0.2 µM syringe filter; stored at 4°C
Glycine stock solution (1M)	15 g glycine dissolved in 200 ml ddH_2O; sterile filtered with 0,45 µm, 250 ml vacuum filter immediately after preparation; stored at 4°C
Kanamycin stock solution	1 g kanamycin solubilized in 100 ml ddH_2O and sterile filtered; aliquots stored at -20°C
Miniprep lysis	0.2 M NaOH

buffer	1% SDS
Miniprep neutralization buffer	3 M NaOAc pH 4.8
Miniprep resuspension buffer	1:1000 RNAse in TE buffer; stored at 4°C
N-Acetyl L-cysteine buffered stock solution (1M)	5 g dissolved in 20 ml ddH_2O; pH carefully adjusted to 7.2/7.4 with HCl; volume adjusted to 30,6 ml total; sterile filtered with 0.2 µM syringe filter; aliquoted and stored at -20°C
NuPAGE transfer buffer (20 x)	25 mM Bis-Tris 25 mM Bicine 1 mM EDTA; stored at 4°C
NuPAGE transfer buffer 1x (ready to use)	NuPAGE transfer buffer with 20% methanol, 0.001% sodium bisulfite 1M; stored at 4°C
MOPS running buffer (5 x)	250 mM MOPS 250 mM Tris base 5 mM EDTA 0.5% SDS; stored at 4°C and warm up before use
MOPS running buffer 1x (ready to use)	MOPS running buffer with 5 mM sodium bisulfite; stored at 4°C
PBS (1 x)	137 mM NaCl 2.7 mM KCl 10.1 mM Na_2HPO_4 1.76 mM KH_2PO_4; autoclaved after preparation

Phenol-chloroform	25 ml phenol 24 ml chloroform 1 ml isoamyl alcohol prepare at least one day before using, stored at 4°C
Phenylmethyl sulfonylfluorid (PMSF)	150 mM in isopropanol
Phosphatase inhibitor	Ser/Thr phosphatase inhibitor (Sigma, P0044), Tyr phosphatase inhibitor (Sigma, P5726); used 1:1000; stored at -20°C
Polybrene stock solution (4mg/ml)	200 mg dissolved in 50 ml H_2O; sterile filtered with 0.2 µM syringe filter; aliquoted and stored at -20°C
Polyethylenimin (PEI)	450 µl PEI (10%, MW 25,000 g/mol, Sigma) 150 µl HCl (2 N) 49.5 ml ddH_2O
Propidium Iodide (PI) stock solution	1 mg/ml in PBS
Protease inhibitor	protease inhibitor cocktail (Sigma, P8340), aliquoted and stored at -20°C; used 1:1000
Proteinase K	10 mg/ml in ddH_2O; stored at -20 °C
RIPA lysis buffer	50 mM HEPES, pH 7.9 140 mM NaCl 1 mM EDTA 1% Triton X-100 0.1% Na-deoxycholate 0.1% SDS; stored at 4°C; 1 mM PMSF; 1:1000 protease and phosphatase inhibitors

	added freshly before use
RNase A (10 mg/ml)	100 mg RNase A (Roth) in 27 µl 3 M sodium acetate, pH 5.2 9 ml ddH_2O; aliquoted in 450 µl, boiled for 30 min at 100°C to inactivate DNases; 50 µl 1M Tris, pH 7.4 added per aliquot; stored at -20°C
Sample buffer (6 x)	1.2 g SDS pellet 6 mg bromphenol blue 4.7 ml 100% glycerol 1.2 ml 0.5 M Tris, pH 6.8 2.1 ml ddH_2O heated up, then dissolved 0.93 g DTT; aliquoted and frozen at -20°C
Single nucleosides (adenosine, guanosine, cytidine, uridine, thymidine, deoxyadenosine, deoxycytidine, deoxyguanosine) stock solutions (0.1 M)	0.1 M stock solutions prepared according to specific molecular weights in PBS or DMSO (guanosine; adenosine); sterile filtered with 0.2 µM syringe filter; stored at -20°C
Single nucleosides solutions	0.1 M stocks diluted 1:10 to 10 mM in DMEM D5030 reconstituted without glutamine; aliquoted and stored at 4°C
Stripping buffer (10 x)	2 M glycin, pH 2.5 2% Tween-20
TAE (50 x)	2 M Tris, pH 8.0 5.7% acetic acid

	50 mM EDTA
TBE (5 x)	54 g TRIS base 27.5 g boric acid 20 ml 0.5 M EDTA, pH 8 in 1 l ddH_2O
TBE polyacrylamide gel	19.9 ml acrylamide/bis-acrylamide 29:1 59.3 ml ddH_2O 20.0 ml TBE 5 x 0.71 ml APS 10% 35 µl TEMED
TBS (20 x)	500 mM Tris base 2.8 M NaCl; adjusted to pH 7.4 with concentrated HCl
TBS-T	1 x TBS 0.2% Tween-20
TE	10 mM Tris, pH 7.4 1 mM EDTA, pH 8.0

2.5 Standards, enzymes and kit

2.5.1 Standards

DNA marker	Gene Ruler 1 kb Plus DNA ladder (Thermo Scientific)
Protein marker	PageRuler Prestained Protein Ladder (Thermo Scientific)
Protein marker	HiMark Prestained High molecular weight Standard (Life Technologies)

2.5.2 Enzymes

Gateway BP clonase II	Life Technologies
Gateway LR clonase II	Life Technologies
M-MLV Reverse Transcriptase	Promega
Phusion HF DNA polymerase	Thermo Scientific
Restriction endonuclease	Thermo Scientific, New England Biolabs (NEB)
RNase-free DNase	Qiagen
SYBR Green qPCR Master Mix	Thermo Scientific
T4 DNA ligase	Thermo Scientific

2.5.3 Kits

ATP lite 300 assay kit	Perkin Elmer
CM-H2DCFDA (General Oxidative Stress Indicator)	Life Technologies
Dual Luciferase reporter assay	Promega
Experion DNA 1K analysis kit	Bio-Rad
Experion RNA StdSense Analysis Kit	Bio-Rad
GeneJET Gel Extraction Kit	Thermo Scientific
Immobilon Western HRP Substrate	Millipore
MiniElute PCR Purification Kit	Qiagen
miRNeasy MiniKit	Qiagen
NEBNext ChIP-Seq Library Prep Master Mix Set for Illumina	NEB
NEBNext Multiplex Oligos for Illumina (Index Primer 1-12)	NEB
NEBNext Multiplex Oligos for Illumina (Dual Index Primers Set 1)	NEB

NEBNext Poly (A) mRNA Magnetic Isolation Module	NEB
NEBNext Small RNA Library Prep Set for Illumina	NEB
NEBNext Ultra RNA Library Prep Kit for Illumina	NEB
PureLink HiPure Plasmid Maxiprep Kit	Invitrogen
QIAquick Gel Extraction Kit	Qiagen
QIAquick PCR Purification Kit	Qiagen
Quant-iT PicoGreen dsDNA Assay Kit	Life Technologies
RNeasy Mini Kit	Qiagen

2.6 Nucleic acids

2.6.1 Primers

All oligos were synthetized by and obtained from Sigma.

All oligos were synthetized at 0.025 μmole scale and purified by desalting (DST), unless otherwise indicated.

Each primer was resuspended in Ampuwa H_2O to 100 μM and used at 10 μM final concentration, unless otherwise specified. Stock and diluted primers were stored at -20°C.

Primers for cloning

Primers were designed manually, according to standard required parameters.

Oligos longer than 50 bases were purified by HPLC.

For = forward (5´-3´)

Rev = reverse (5´-3´)

OL = overlapping

attB1 5utr for	GGGGACAAGTTTGTACAAAAAAGCAGGCTTCGACCCCCGA GCTGTGCTGCTCGCGG
MYC HA attB2 rev	GGGGACCACTTTGTACAAGAAAGCTGGGTCTTAGGCGTAA TCTGGAACATCGTATGGGTACGCACAAGAGTTCCGTAGCTG

MYC 3utr OL rev	TAGAAGGAATCGTTTTCCTTACTTTTCCTTAAGCGTAATCTGGAACATCGTATGGGTACGCACAAGAGTTCCGT
HA MYC OL 3utr for	GTGCGTACCCATACGATGTTCCAGATTACGCTTAAGGAAAAGTAAGGAAAACGATTCCTTCTAACAGAAATGTCCTGAGC
3utr attB2 rev	GGGGACCACTTTGTACAAGAAAGCTGGGTCTTAAGATTTGGCTCAATGATATATTTGCCAG
attB1 MYC for	GGGGACAAGTTTGTACAAAAAAGCAGGCTTCACCATGCCCCTCAACGTTAGCTT
3utr XhoI for	TAAGCACTCGAGGGAAAAGTAAGGAAAACGATTCCTTCTAAC
3utr NotI rev	TGCTTAGCGGCCGCTTAAGATTTGGCTCAATGATATATTTGCCA
3utr Del1 (Δ 1997-2366) attB2 rev	GGGGACCACTTTGTACAAGAAAGCTGGGTCACTCAGCCAAGGTTGTGAGGTTGCATTTGAT
3utr Del2 (Δ 2025–2366) attB2 rev	GGGGACCACTTTGTACAAGAAAGCTGGGTCCATTATGGCTAAATCTTTCAGTCTCAAG
3utr Del3 (Δ 2127–2366) attB2 rev	GGGGACCACTTTGTACAAGAAAGCTGGGTCTTTTTAAAAACAATTCTTAAATACAAAT
3utr Del4 (Δ 2262–2366) attB2 rev	GGGGACCACTTTGTACAAGAAAGCTGGGTCAGGGTTTATAGTACCTATAATACTAGGTACT
MYC SalI for	TAAGCAACCGGTATGCCCCTCAACGTTAGCTTCA
ER OL 3utr rev	TGCTTAACTAGTTTAAGATTTGGCTCAATGATATATTTGCCA
3utr OL ER for	TAAGCAACCGGTATGCCCCTCAACGTTAGCTTCA
3utr SalI rev	TGCTTAACTAGTTTAAGATTTGGCTCAATGATATATTTGCCA

MYC AgeI for	TAAGCAACCGGTATGCCCCTCAACGTTAGCTTCA
3utr SpeI rev	TGCTTAACTAGTTTAAGATTTGGCTCAATGATATATTTGCCA

Primers for mutagenesis

Primers were designed manually, according to the parameters indicated in the instruction manual of the QuikChange II XL site-directed mutagenesis kit.

Oligos were purified by HPLC.

Each primer was resuspended in Ampuwa H_2O to 1 µg/µl and used at 0.125 µg/µl final concentration.

MYC I codon Mut for	CCTTGCAGCTGCTTAGACGTAGGATTTTTTTCGGGTAGTGG
MYC I codon Mut rev	CCACTACCCGAAAAAAATCCTACGTCTAAGCAGCTGCAAGG

Primers for qPCR

Exon-exon spanning primers were designed with Primer 3, according to default parameters. Specificity of alignment was verified by nucleotide Blast alignment. Specific product amplification after qPCR was evaluated from the melting curve.

Target	Forward sequence (5´-3´)	Reverse sequence (5´-3´)
B2MG	ttctggcctggaggctatc	tcaggaaatttgactttccattc
HA (exogenous *MYC*)	aagaggacttgttgcggaaa (*MYC*)	Agcgtaatctggaacatcgt (HA)
MYC	caccagcagcgactctga	gatccagactctgacctttgc

Primers for ChIP-qPCR

Primers were manually designed according to the intensity of the visualized ChIP peak on the Integrated Genome Browser, based on ChIP-sequencing data generated in this study or on collected data (from Encode database).

Specificity of alignment was verified by nucleotide Blast alignment.

Specific product amplification after qPCR was evaluated from the melting curve.

Target	Forward sequence (5´-3´)	Reverse sequence (5´-3´)
ACTB TES	ccagggcttacctgtacactg	tggcctcatttttaaggtgtg
ACTB TSS	cgttccgaaagttgcctttt	gccgctgggttttataggg
Control Region	ttttctcacattgcccctgt	tcaatgctgtaccaggcaaa
GNL3 TES	gttatggtatgcatgagctgtg	ctacttccactcacaatgagatg
GNL3 TSS	gtgacgctcgtcagtgg	catattggctgtagaaggaagc
NCL TES	agccttcatccaggtgagaa	ggccacacggcatatagact
NCL TSS	tactgggcaggctcagtctt	gaagatcccggagcacgta
TKT GB (P3)	ttccctgttcacaacccctt	ttcgagactagggacaaggc
TKT P1	acattctgtgaggacccagg	agccttctgtgaggtctgtc
TKT P2	ggcaggttcttgctttgtca	tgcatcactgggctacttga
TKT P4	agtgctgcttctggatgagt	ccccttttgtggagaaagcc
TKT TES (P5)	gattccagaaaccgacgctc	atgttctgctgtgctgttcc
TKT TSS	agccgctatctctgtgtgtc	gttggccgtgtccttcaag

2.6.2 antimiRNAs

AntimiRNAs were purchased from Dharmacon. Each oligo was resuspended in siRNA resuspension buffer 1x, according to the manufacturer´s instructions, to 20 μM and used at 50 nM final concentration.

AntimiRNA	Catalog number
miRIDIAN microRNA Human hsa-let-7a-5p	IH-300474-05-0005
miRIDIAN microRNA Human hsa-let-7f-5p	IH-300481-07-0005
miRIDIAN microRNA Human hsa-let-7g-5p	IH-300583-06-0005
miRIDIAN microRNA Human hsa-miR-20a-5p	IH-300491-05-0005
miRIDIAN microRNA Human hsa-miR-21-5p	IH-300492-05-0005
miRIDIAN microRNA Human hsa-miR-24-3p	IH-300497-05-0005
miRIDIAN microRNA Human hsa-miR-26a-5p	IH-300499-06-0005

miRIDIAN microRNA Human hsa-miR-34a-5p	IH-300551-08-0005
miRIDIAN microRNA Human hsa-miR-98-5p	IH-300515-07-0005
miRIDIAN microRNA Human hsa-miR-148a-3p	IH-300540-07-0005
miRIDIAN microRNA Human hsa-miR-429	IH-300722-07-0005
miRIDIAN microRNA Hairpin Inhibitor Negative Control #1	IN-001005-01-05

2.6.3 Plasmids

All sequences cloned into the vectors refer to human sequences.

All constructs were verified by Sanger sequencing, which was carried out by LCG Genomics.

Empty vectors

pBabe-puro	retroviral expression vector with a SV40-promoter and puromycin resistance (Morgenstern and Land, 1990)
pDONR221	vector for generating entry clones for Gateway cloning
pInducer21	doxycycline-inducible cDNA expression vector with IRES GFP (Meerbrey et al, 2011)
pRRL-SFFV-IRES-puro	lentiviral expression vector with SFFV-promoter and puromycin resistance (Wiese et al, 2015)
psiCheck2	dual luciferase vector for transient expression. Firefly luciferase used as internal control for signal normalization (Promega)

Packaging vectors for lentiviral production

pMD2.G	plasmid encoding for virion envelope
psPAX.2	plasmid encoding for virion packaging system

Plasmids available in the laboratory of Prof. Eilers

pBabe-puro-MYC-ER	expression vector with *MYC* coding sequence (CDS) and estrogen receptor (ER). Generated by D. Murphy
pBabe-puro 5′-UTR-MYC CDS	expression vector with 5′-UTR and *MYC* CDS (Kress et al, 2011)
pBabe-puro MYC-CDS-3′-UTR	expression vector with *MYC* CDS and 3′-UTR (Kress et al, 2011)
pInducer21-MYC-HA	expression vector with *MYC* CDS and C-terminal HA-tag (Jaenicke et al, 2016)
pRRL-SFFV-MYC-ER-IRES-puro	expression vector with *MYC* CDS and ER (Wiese et al, 2015)

Plasmids generated in this study

pBabe-puro-MYC-ER-3′-UTR	expression vector with *MYC* CDS, human ER and *MYC* 3′-UTR
pInducer21-5′-UTR-MYC-HA	expression vector with 5′-UTR, *MYC* CDS and C-terminal HA-tag
pInducer21-MYC-HA-3′-UTR	expression vector with *MYC* CDS, C-terminal HA-tag and *MYC* 3′-UTR
pInducer21-MYC-HA-3′-UTR (Δ 2262-2366) Del.4	expression vector with *MYC* CDS, C-terminal HA-tag and deleted *MYC* 3′-UTR
pInducer21-MYC-HA-3′-UTR (Δ 2127-2366) Del.3	expression vector with *MYC* CDS, C-terminal HA-tag and deleted *MYC* 3′-UTR
pInducer21-MYC-HA-3′-UTR (Δ 2025-2366) Del.2	expression vector with *MYC* CDS, C-terminal HA-tag and deleted *MYC* 3′-UTR
pInducer21-MYC-HA-3′-UTR	expression vector with *MYC* CDS, C-terminal HA-tag and deleted *MYC* 3′-UTR

(Δ 1997-2366) Del.1	
pInducer21-5´-UTR-MYC-HA-3´-UTR	expression vector with 5´-UTR, *MYC* CDS, C-terminal HA-tag and 3´-UTR
pInducer21-Mut-5´-UTR-MYC-HA	expression vector with mutated 5´-UTR (CTG → TAG in first exon), *MYC* CDS and C-terminal HA-tag
pRRL-SFFV-MYC-ER-3´-UTR-IRES-puro	expression vector with *MYC* CDS, ER and *MYC* 3´-UTR
psiCheck2-3´-UTR	reporter vector with the 3´-UTR of *MYC* cloned downstream the *Renilla firefly luciferase* gene

2.7 Antibodies

Primary antibodies

(IB: immunoblotting; IP: immunoprecipitation; ChIP: Chromatin immunoprecipitation)

Target	Company	Order number	Use
4E-BP1	Cell Signaling	#9452	IB
AKT	Cell Signaling	#9272	IB
AMPKα	Cell Signaling	#2532	IB
c-JUN	Cell Signaling	#9165	IB
CYCLIN-E	Santa Cruz	sc-247	IB
HA	Abcam	ab9110	IB
IgG from rabbit serum	Sigma-Aldrich	I5006	ChIP/ChIP-seq
MCL-1	Santa Cruz	sc-819	IB
MYC	Abcam	ab32072	IB/IP
MYC	Santa Cruz	sc-764X	ChIP-seq
P53	EDM Millipore	Ab-2/OP09	IB
p70 S6 Kinase	Cell Signaling	#2708	IB
Phospho-4E-BP1 (Thr70)	Cell Signaling	#9455	IB
Phospho-AKT (Ser473)	Cell Signaling	#9271	IB
Phospho-AMPKα (Thr172)	Cell Signaling	#2535	IB

Phospho-p53 (Ser15)	Cell Signaling	#9284	IB
Phospho-p70 S6 Kinase (Thr389)	Cell Signaling	#9234	IB
Phospho-RNAPII (Ser2)	Abcam	ab5095	ChIP/ChIP-seq/IB
RNA Polymerase II	Santa Cruz	sc-899X	ChIP/ChIP-seq
RNA Polymerase II	BioLegend	MMS-126R	IB
Vinculin	Sigma-Aldrich	V9131	IB

Secondary antibodies

Target	Company	Order number	Use
anti-mouse IgG-HRP	Santa Cruz	sc-2314	IB
anti-rabbit IgG-HRP	Santa Cruz	sc-2313	IB
FITC mouse anti-BrdU	BioLegend	364104	FACS

2.8 Consumables

Consumables were purchased from the companies Eppendorf, Greiner, Nunc, Sarstedt and VWR and included disposable plastic items such as cell culture dishes, reaction tubes, cryotubes, syringes, cuvettes, pipettes.

2.9 Equipment and membranes

Automated Electrophoresis	Experion Automated Electrophoresis System (Bio-Rad)
Chemiluminescence imaging	LAS-4000 mini (Fujifim)
Cell culture incubator	BBD 6220 (Heraeus)
Cell Counter	Casy cell counter (Innovatis)
Centrifuges	Avanti J-26 XP (Backman Coulter)

	Eppendorf 5417 R (Eppendorf) Eppendorf 5425 (Eppendorf) Eppendorf 5430 (Eppendorf) Galaxy MiniStar (VWR) Multifuge 1S-R (Heraeus)
Deep-sequencer	Illumina GAIIx sequencer (Illumina) NextSeq 500 (Illumina)
Flow cytometer	BD FACS Canto II (BD Biosciences) BD FACS Aria III (BD Biosciences)
Gel dryer	Slab dryer model 483 (Bio-Rad)
Heating block	Dry Bath System (Starlab) Thermomixer® comfort (Eppendorf)
Immunoblot transfer chamber	PerfectBlue Tank Electro Blotter Web S (Peqlab)
Luminometer	GloMax 96 Microplate Luminometer (Promega)
Microscopes	Axiovert 40CFL (Zeiss) TCS SP5 (Leica)
PCR thermal cycler	C1000 Thermal cycler (Bio-Rad)
Phosphorimager cassette	Storage Phosphor Screen BAS-IP (GE Healthcare)
Phosphorimaging	Typhoon FLA 7000 scanner (GE Healthcare)
Photometer	Multiscan Ascent (Thermo Labsystems) UltrospecTM 3100 pro UV/Visible (Amersham Biosciences) Spectrofluorometer NanoDrop 1000 (Thermo Scientific)
Power supply	Power Pac (Bio-Rad)

	Consort EV231/EV243 (Roth)
PVDF transfer membrane	Immobilon-P transfer membrane (Millipore)
Quantitative RT-PCR machine	StepOne plus (Applied Biosystem)
SDS-PAGE system	Minigel (Bio-Rad) Mini-PROTEAN Tetra Cell (Bio-Rad)
Sterile bench	HeraSafe (Heraeus)
Ultrasonifier	Digital Sonifier W-250 D (Branson)
UV fluorescent table	Maxi UV fluorescent table (Peqlab)
Vortex mixer	Vortex-Genie 2 (Scientific Industries)
Water bath	Julabo ED-5M water bath (Julabo) Memmert waterbath (Memmert)
Whatman filter paper	Gel Blotting Paper (Schleicher and Schuell)

2.10 Software and online programs

ApE plasmid editor	by M. Wayne Davis
BD FACSDiva v6.1.2	BD Biosciences
BedTools v2.26	Quinlan and Hall, 2010
Bowtie v1.1.2	Langmead et al, 2009
EndNote X7	Clarivate Analytics
Fast QC	Babraham Bioinformatics
FlowJo v8.8.6	FlowJo, LLC
FlyCapture 2 Camera Selection v2.7.3.18	Flir
Illustrator, Photoshop, Acrobat	Adobe Inc.
Image J	by Wayne Rasband
Integrated Genome Browser	Nicol et al, 2009

Mac OS X	Apple Inc.
MACS v1.4.2	Zhang et al, 2008
MSigDB v3.1	Subramanian et al, 2005
Multi Gauge	Fujifilm
ngs.plot v2.61	Shen et al, 2014
Office 2011 Mac	Microsoft Inc.
Prism4	GraphPad Software Inc.
R version v3.1.0	R core team
R samtools v1.16.0	
EdgeR v3.6.2	
TreeView v1.6.6	Bio-soft net
SeqMiner v1.3.3	Ye et al, 2011
Stepone software v2.3	Applied Biosystem
UCSC Genome Bioinformatics	http://genome.ucsc.edu

3 Methods

3.1 Cell biology methods

3.1.1 Cultivation of eukaryotic cell lines

Cell lines were cultivated in a cell incubator at 37°C, 5% CO_2 and a relative humidity of 95%.

3.1.1.1 Cell passaging

Cells were passaged every two to three days and never allowed to become over confluent. After medium removal, cells were washed twice with PBS and trypsinized to detach them from the cell culture dish. Once detached, serum-containing medium was added to the trypsin, in a ratio 3:1, in order to stop the enzymatic activity of the trypsin. The cells were collected into a 15 ml tube and centrifuged at 1500 rpm for 3 min. Supernatant was removed, the cell pellet resuspended in the cell culture medium and a fraction of the cell suspension was plated on a new cell culture dish with fresh medium. For plating cells at a specific cell number, the cell number of a suspension was determined with the CASY automated cell counter.

3.1.1.2 Cell freezing

Cells were harvested by trypsinization, as described above. After centrifugation, the cell pellet was resuspended in the appropriate volume of freezing medium, e.g. 1 ml for cells collected from an 80% confluent 10 cm dish. Cell suspension was transferred to a cryotubes and immediately transferred into a freezing container filled with isopropanol and placed overnight at -80°C. Afterwards, cryotubes were transferred to storage boxes in liquid nitrogen tanks.

3.1.1.2 Cell thawing

Cryotubes were placed for few min in a water bath at 37°C. The cell suspension was transferred to a 15 ml falcon tube containing 5 ml fresh medium and centrifuged at 1500 rpm for 3 min. This step helped removing the DMSO present in the freezing medium. After centrifugation the supernatant was removed, the cell pellet resuspended in 1 ml fresh culture medium and plated on a new cell culture dish with fresh medium. Thawed cells were passaged at least 2 times before performing experiments.

3.1.1.3 Cell starvation

In order to perform starvation experiments, a specific number of cells was plated, as described in 3.1.1.1. Twenty-four h later cells were washed twice with PBS and the medium was changed to the reconstituted DMEM (D5030), lacking glucose or glutamine, as indicated. When glutamine starvation was performed for more than 24 h, cells were plated in a 3:1 ratio compared to those grown in complete medium, in order to account for the arrested proliferation. The same procedure was used for performing single amino acid starvation (Methionine, Leucine, Glutamine), using the medium described in 2.2.1.

3.1.2 Cell transfection

3.1.2.1 Transfection by Polyethylenimine (PEI)

This method was used for lentiviral production (3.1.3). Cells were washed twice with PBS and medium was changed to transfection medium. In one 1.5 ml reaction tube 250 µl Opti-MEM (Gibco) were mixed with 24 µl PEI and incubated 5 min at RT; in a second 1.5 ml reaction tube 250 µl Opti-MEM were mixed with the appropriate amount of plasmid DNA. The reactions were mixed and incubated 20 min at RT. The mix was added dropwise to the cells.

3.1.2.2 Transfection by Lipofectamine 2000

This method was used for performing the luciferase assay (3.1.5). The amount of each reagent refers to a single well of a 24-well dish. Cells were washed twice with PBS and medium was changed to transfection medium. In one 1.5 ml reaction tube 25 µl Opti-MEM were mixed with 1.2 µl Lipofectamine 2000 (Invitrogen) and incubated 5 min at RT; in a second 1.5 ml reaction tube 25 µl Opti-MEM were mixed with 10 ng plasmid DNA. The reactions were mixed and incubated 20 min at RT. The mix was added dropwise to the cells.

3.1.2.3 Transfection by RNAi Maxx

This method was used for transfecting anti-miRNAs (anti-miRs) (3.1.6). The amount of each reagent refers to a single well of a 6-well dish. Cells were washed twice with PBS and medium was changed to transfection medium. In one 1.5 ml reaction tube 500 µl Opti-MEM were mixed with 10 µl RNAi Maxx (Invitrogen) and incubated 5 min at RT; in a second 1.5 ml reaction tube 500 µl Opti-MEM were mixed with each antimiRNA at a final concentration of 50 nM (7.5 µl from 20 µM stock). The reactions were mixed and incubated 20 min at RT. The mix was added dropwise to the cells.

3.1.3 Production of lentiviruses

Five million HEK293T cells were plated in 10 cm dish. After 24 h cells were transfected by PEI, using 8 µg lentiviral expression plasmid, 5 µg psPAX.2 plasmid and 1.25 µg pMD2.G. Cells were incubated in a biosafety level-2 (BSL-2) incubator and the following steps were performed in a BSL-2 environment. After 24 h transfection medium was replaced by 5 ml DMEM containing FBS and antibiotics. Viral sups were harvested for 3 times every 12 h, collected into a 15 ml falcon tube and stored at 4°C. After the last harvesting the viral sup was filtered using a 0.44 µm syringe-filter, aliquoted in cryotubes and stored at -80°C.

3.1.4 Cell infection with lentiviruses

One million HCT116 cells were plated in a 10 cm dish. The infections were performed in a BSL-2 environment after 24 h. The viral sups were thawed in a water bath at 37°C and 0.5 to 1 ml viral sup were used for each infection. Viral sups were mixed with 5 ml fresh medium and polybrenene was added to a final concentration of 6 μg/ml. After 24 h the procedure was repeated. After 48 h from the first infection cells infected with pRRL-SFFV plasmids were selected with puromycin and cells infected with pInducer21 plasmids were sorted according to the highest GFP signal.

3.1.5 Luciferase assay

HCT116 cells were plated in 24-well dishes (50,000 cells/well), in triplicate per each condition. After 24 h cells were transfected by Lipofectamine 2000, using the following plasmids: psiCheck2 and psiCheck2-3´-UTR. After 24 h transfection medium was replaced by 0.5 ml DMEM containing FBS and antibiotics. After 72 h cells were washed twice with PBS and medium was replaced by DMEM reconstituted with or without glutamine for 6 h.

Cells were washed with PBS and lysed in passive lysis buffer 1 X (Promega). Renilla and firefly luciferase activity was measured using Dual-Luciferase reporter assay system, according to manufacturer´s instruction. Renilla luciferase activity was normalized to firefly activity.

3.1.6 Measurement of intracellular ATP levels

Cells were treated according to the experimental protocol, e.g. starved for glucose or glutamine. Cells were harvested by trypsinization and counted using a CASY cell counter. An equal number of viable cells was taken for measuring ATP using ATPlite assay kit (Perkin Elmer), according to manufacturer´s instructions. Luminescence was measured using the Glomax 96 Microplate Luminometer.

3.1.7 Anti-miRs selection and activity evaluation

3.1.7.1 Anti-miRs selection

miRNAs targeted by anti-miRs were selected applying the following criteria: first, the highest expressed miRNAs in HCT116 (+Q) were filtered, according to available miRNAs sequencing data (see 3.4.1). Normalized read count, fold change regulation -Q/+Q and adjusted p-values are shown in Table 4.1. Second, eleven miRNAs targeting *MYC* were selected, according to data available on http://mirtarbase.mbc.nctu.edu.tw. miRNAs binding site on *MYC* 3´-UTR was predicted using http://www.microrna.org and are shown in Table 4.1. Numbers refers to the annotated MYC sequence NM_002467.4.

3.1.7.2 Anti-miRs transfection and evaluation of the effect on MYC protein levels

HCT116 cells were plated in 6-well dishes (300,000 cells/well). After 24 h cells were transfected by RNAi Maxx, using each selected anti-miR and a negative control. After 10 h transfection medium was replaced by 3 ml DMEM containing FBS and antibiotics. After 24 h, per each well cells were split on a 1:6 ratio and plated in 2 wells of a new 6-well dish. After 72 h cells were washed twice with PBS and medium was replaced by DMEM reconstituted with or without glutamine for 2 h. Cells were harvested and MYC protein levels detected by immunoblot (see 3.3.3 and 3.3.4).

3.1.8 Crystal violet staining and quantification

Cells were fixed for 15 min with 3.7% formaldehyde, incubated for 1 hour with crystal violet solution, washed under tap water and air-dried. The color intensity was quantified by destaining the cells with 10% w/v acetic acid solution. An aliquot of destained solution was diluted 1:4 with water and the absorbance at 550 nm was read with a microplate reader.

3.1.9 FACS analyses

FACS was performed using BD FACSCanto II and results were analyzed using FlowJo software.

3.1.9.1 Annexin V/PI FACS analysis

Cell supernatants were collected in 15 ml falcon tubes. Cells were washed with ice-cold PBS, which was poured into the falcon tubes. Cells were trypsinized long enough to allow complete cell detachment and trypsin was inactivated using the supernatant. Cells were collected in each falcon tube and centrifuged at 1500 rpm for 5 min at 4°C. The cell pellet was resuspended in 100 µl Annexin V binding buffer and incubated with 20 µl Pacific Blue-conjugated Annexin V (25 µg/ml) for 15 min in the dark, in ice. Three hundred µl Annexin V binding buffer were added to each sample and volumes were transferred to FACS tubes containing 5 µl PI. Tubes were kept in ice until being analyzed by FACS. The following parameters were considered: PI-2A; Pacific blue; SSC-A; FSC-A.

3.1.9.2 PI FACS

Cells were collected as above. Cell pellets were washed with ice-cold PBS. Washed pellets were resuspended in 1 ml ice-cold PBS and dropwise added into 4 ml ice-cold 100% EtOH in 15 ml polystyrene tubes, while vortexing. Tubes were incubated overnight at -20°C, in order to fix the cells in EtOH. Afterwards, cells were centrifuge at 1500 rpm for 10 min at 4°C. Pellets were washed with ice cold PBS, resuspended in 38 mM sodium citrate, 54 µM PI, 24 µg/ml RNase A, incubated 30 min in the dark at 37°C. The mix was transferred to FACS tubes and kept in ice until being analyzed by FACS. The following parameters were considered: PI-2A; PI-2W; SSC-A; FSC-A. The Sub-G1 population of cells was considered to assess the number of apoptotic cells.

3.1.9.3 BrdU/PI FACS

Cells were labeled for 1 hour with 10 µM 5-Bromo-2'-deoxyuridine (BrdU). A negative control was included for subsequent FACS analysis, i.e. a non-labeled sample. Cells were harvested and fixed in EtOH, as described above. After fixation, Cells were washed with ice cold PBS and incubated in 2 M HCl/0.5% Triton-X-100 for 30 min at RT, mixing every 10 min, in order to denaturate the DNA. Cells were centrifuged at 1500 rpm for 5 min at 4°C. Pellets were resuspended in 100 µl 1% BSA-PBS-T with 5 ul FITC anti-BrdU antibody and incubated 30 min in the dark at RT. Cells were centrifuged at 1500 rpm for 5 min at 4°C, washed with 200 µl 1% BSA-PBS-T and spun down again. Pellets were resuspended in 38 mM sodium citrate, 54 µM PI, 24 µg/ml RNase A, incubated 30 min in the dark at 37°C. The mix was transferred to FACS tubes and kept in ice until being analyzed by FACS. The following parameters were considered: PI-2A; PI-2W; FITC; SSC-A; FSC-A.

3.1.9.4 GFP FACS for oxidative stress measurement

CM-H2DCFDA, General Oxidative Stress Indicator kit (Invitrogen) was used to detect ROS. CM-H2DCFDA is an indicator of intracellular ROS levels. It passively diffuses into cells, where it reacts intracellular glutathione and other thiols (i.e. molecules that have been oxidated by ROS). Subsequent oxidation leads to a fluorescent adduct that can be monitored by FACS.

Cells were washed once with DPBS (PBS with 100 mg/l $CaCl_2$ and 100 mg/l $MgCl_2$), incubated in DPBS with freshly prepared DCFDA solution (in DMSO, final concentration 1.6 µM) for 30 minutes at 37°C, in the dark. Cells were washed once with PBS, harvested by trypsinization and pellets washed once with PBS and once with ice cold PBS. Cells were resuspendend in PBS, kept in ice and analyzed by FACS using the Alexa Fluor 488 channel for green emission. PI was added immediately before analyzing cells and used to exclude dead cells. Unstained cells and H_2O_2-treated cells were used as negative and positive controls, respectively.

3.2 Molecular biology methods

3.2.1 Transformation of competent cells with plasmid DNA and plasmid amplification

Chemically competent bacteria were thawed on ice and 90 µl were mixed with the plasmid DNA. The bacteria were incubated on ice for 30 min, followed by a heat shock for 30 sec at 42 °C. The reactions were shortly placed on ice for 2 min. Two hundred fifty µl of pre-warmed LB medium were added and the mix was incubated for 1 h at 37°C on a shaker. The mix was plated on pre-warmed LB-agar plate containing the appropriate antibiotic for selection. LB agar plates were incubated at 37°C over night.

3.2.2 Analytical preparation of plasmid-DNA from bacteria (Miniprep)

A bacteria overnight culture was transferred to a 1.5 ml tube and the rest was stored at 4°C. The bacteria were spun down for 5 min at RT and the culturing medium was completely removed. The bacteria pellet was resuspended in 150 µl miniprep resuspension buffer, followed by the addition of 150 µl miniprep lysis buffer. The mix was inverted 5 times and incubated for 5 min at RT. Afterwards, 150 µl miniprep neutralization buffer were added to stop the reaction of lysis. The samples were spun down for 5 min at 4°C and the supernatant was transferred into a new 1.5 ml tube. Eight hundred µl isopropanol were added and each sample was briefly vortexed and spun down for 30 min at 4°C. The supernatant was carefully removed, the pellets were washed with 500 µl 70 % EtOH and spun down for 10 min at 4°C. The supernatant was removed, the pellets were air-dried and resuspended in 20-40 µl of TE buffer. The samples were stored at -20°C.

3.2.3 Preparative isolation of plasmid DNA (Maxiprep)

Two hundred ml overnight culture was processed according to the manufacturer's protocol (PureLink HiPure Plasmid Maxiprep Kit, Life Technologies). The purified plasmid DNA was solubilized in TE and adjusted to a concentration of 1 µg/µl.

3.2.4 Restriction analysis of DNA

Restriction endonucleases from Fermentas and New England Biolabs were used following the manufacturer's protocol, i.e. the recommended restriction buffers and enzyme amounts. Analytical digestion was set up as follows:

0.5-1 µg DNA
0.5 µl restriction endonuclease (or 0.2 µl each, if two different enzymes were used)
2 µl 10x reaction buffer
up to 20 µl ddH_2O

Preparative digestion was set up as follows:

5 µg DNA
2.5 µl restriction endonuclease (or 1 µl each, if two different enzymes were used)
5 µl 10x reaction buffer
up to 50 µl ddH_2O

3.2.5 Gel electrophoretic separation of DNA fragments

Gels were prepared according to the expected size of the DNA fragments. The appropriate amount of agarose was boiled in TAE, briefly cooled down, supplemented with 0.4 µg/ml ethidium bromide and poured into a gel chamber with combs. The samples were mixed with DNA loading buffer and loaded into each well of the gel. A DNA ladder was loaded. The separation was performed at 120 V for one h and the DNA fragments were visualized on a UV transilluminator.

3.2.6 Extraction and purification of DNA fragments and PCR products

The DNA fragment was cut out of the agarose gel and extracted with the gel extraction kit according to the manufacturer's protocol (GeneJET Gel Extraction Kit, Thermo Scientific). Purification of PCR products was performed according to the manufacturer's protocol (QIAquick PCR Purification Kit, Qiagen).

3.2.7 Ligation of DNA fragments

The DNA fragment (insert) was used in 3x molar excess to the linearized vector.
A control reaction without insert was included as negative control
Ligation was set up as follows:
100 ng linearized vector
X ng fragment
1 µl T4 DNA ligase
2 µl 10x ligation buffer
up to 20 µl ddH_2O
The ligation mix was incubated for 2 h at RT und transformed into competent bacteria.

3.2.8 Gateway cloning

To clone cDNA into the pINDUCER21 vector, the Gateway® cloning technology from Life technologies was used. The DNA fragment containing attB1 and attB2 sequences inserted by PCR was first cloned into pDORN 221 vector using the BP clonase enzyme, according to the manufacture's protocol. After bacteria transformation and analytical preparation of plasmid DNA, the presence of the fragment into the plasmid was verified by quantitative reverse transcriptase PCR reaction (see 3.2.12.2) using specific primers. The positive entry clones were then ligated into pInducer 21 using the LR clonase enzyme, according to the manufacture's protocol.

3.2.9 Nucleic acid quantification

3.2.9.1 Nanodrop

DNA and RNA concentration was determined with the NanoDrop 1000, unless specifically indicated. The absorbance was measured at 260 nm. To assess the purity of the nuclei acid solution, the ratio of absorbance at 260 and 280 nm was determined. A ratio of 1.8 for DNA and 2 for RNA indicate a pure preparation, i.e. without protein contaminants.

3.2.9.2 PicoGreen

Quantification of immune-precipitated chromatin samples for ChIP-sequencing experiments was performed with the QuantiTTM PicoGreen dsDNA reagent (Invitrogen), according to the manufacturer's protocol.

3.2.9.3 Bioanalyzer

RNA, which was used for library preparation for RNA-Sequencing, as well as the prepared
DNA-libraries, were quantified with the Experion Automated Electrophoresis System from Bio-Rad, following the manufacturer's protocol.

3.2.10 Nucleic acid isolation

3.2.10.1 RNA isolation with TriFAST

Total RNA was isolated with peqGOLD TriFast (Peqlab), unless otherwise specified. Cells plated on a tissue culture dish were washed two times with PBS, lysed directly on the plate with 1 ml Trifast and transferred into a 1.5 ml reaction tube. The mix was incubated for 5 min at RT. Two hundred µl chloroform was added and the suspension was vortexed for 30 s. The reactions were centrifuged for 15 min at 14,000 rpm, at 4 C°.

The upper aqueous phase containing the RNA (c.ca 500 µl) was transferred into a new reaction tube. To precipitate the RNA, 500 µl isopropanol and 1 µl GlycoBlue coprecipitant (15 mg/ml stock solution, Fermentas) were added. The samples were incubated on ice for 15 min followed by centrifugation for 15 min at 14,000 rpm, at 4 C°. The supernatant was carefully discarded and the RNA pellet washed twice with 70% EtOH. The pellet was air-dried and solubilized in 50 µl RNAse free ddH_2O. The RNA was stored at -80°C.

3.2.10.2 RNA isolation with miRNeasy Mini Kit

RNA used for miRNA-Sequencing (see 3.4.1), isolation was performed with the miRNeasy Mini Kit (Qiagen), according to manufacturer's protocol.

3.2.10.3 RNA isolation with the RNeasy Mini

RNA used for RNA-Sequencing (see 3.4.2), isolation was performed with the RNeasy Mini Kit and additional DNase I digestion according to manufacturer's protocol.

3.2.10.4 DNA isolation with phenol-chloroform

DNA used for chromatin immunoprecipitation (see 3.3.8) and ChIP-seq (see 3.4.3). One volume of phenol-chloroform-isoamyl alcohol solution was added to the decrosslinked chromatin and the mix was vortexed for 30 sec. Samples were centrifuged for at 14,000 rpm for 10 min at RT and the upper phase containing the DNA was transferred to a new reaction tube. Nine hundred µl 100% EtOH, 38 µl Na-acetate pH 5.2 and 3 µl Glyco blue were added to the mix. The samples were briefly vortexed and incubated at -80°C for 40 min. Afterwards, samples were centrifuged at 14,000 rpm for 30 min at 4°C. The DNA pellet was washed with 80% EtOH, air-dried and resuspended in TE buffer or ddH_2O.

3.2.11 cDNA synthesis

In order to perform the quantitative reverse transcriptase PCR reaction (see 3.2.12.2), the extracted total RNA was reverse transcribed into complementary DNA (cDNA). RNA samples were diluted to 0.25 µg/µl final concentration with RNAse free ddH_2O.
Reactions were set up as follows:
10 µl RNA
2 µl random hexanucleotide primers (2 µg/ml Stock, Roche)
The mix was incubated for 3 min at 65°C on a thermo-block.
The following reagents were added:
10 µl 5x First strand reaction buffer (Promega)
5 µl dNTP 10 mM stock
0.2 µl RiboLock RNase Inhibitor (40 U/µl, Fermentas)
1 µl M-MLV reverse transcriptase (200 U/µl, Promega)
up to 50 µl ddH_2O

A reaction without M-MLV reverse transcriptase was included as used as negative control for the following quantitative reverse transcriptase PCR reaction.
The samples were incubated in a PCR thermal cycler as follows,
10 min 22°C
50 min 37°C
15 min 70°C
The cDNA was stored at -20°C.

3.2.12 Polymerase chain reaction (PCR)

3.2.12.1 PCR to amplify cDNA for cloning

Specific primers were used according to the purpose, i.e. mutagenesis, insertion of attB1 and attB2 sequences for Gateway cloning, insertion of restriction sites, overlapping PCR.

Reactions were set up as follows:

10 ng cDNA template

5 µl 5x Phusion High-Fidelity (HF) reaction buffer

1 µl dNTPs (10 mM Stock, Roth)

1µl forward primer (10 µM Stock)

1µl reverse primer (10 µM Stock)

1 µl Phusion HF DNA polymerase (2.5 U/ µl, Fermentas)

up to 50 µl nuclease-free H_2O

The reaction was performed in a PCR thermal cycler as follows,

Segment	Cycles	Temperature	Time
Initial denaturation	1	95 °C	1 min
Denaturation	30	98 °C	15 sec
Annealing		55-62 °C	50 sec
Extension		72 °C	30 sec/kb
Final extension	1	72 °C	7 min

3.2.12.2 Quantitative real-time PCR (qPCR)

This method was used both for gene expression analysis and for evaluating the amount of immunoprecipitated chromatin in ChIP experiments.

Reactions were set up as follows:

1 µl cDNA (see 3.2.11)

7 µl SYBRGreen Mix (Thermo Scientific)

1 µl forward + revers primer mix (10 µM Stock)

up to 20 µl nuclease-free water

The reaction was performed in a quantitative RT-PCR machine as follows,

Segment	Cycles	Temperature	Time
Initial denaturation	1	50 °C	2 min
		95 °C	2 min
Denaturation	40	95 °C	3 sec
Annealing/ Extension		60 °C	30 sec
Melting curve	1	95 °C	15 sec
		60 °C	1 min
		95 °C	15 sec

Each sample was analyzed in technical triplicate. Raw data were expressed as Ct (threshold cycle), i.e. the cycle in which the fluorescence is above the background.

For qPCR experiments, *β2-MICROGLOBULIN* (*b2M*) was used as housekeeping gene for internal normalization.

qPCR data were analyzed according to the double Delta Ct method, i.e. the fold induction relative to a control was calculated.

First, the average Ct value and the standard deviation (SD) of each technical triplicate was calculated.

The difference of Ct average between the *b2M* and the target gene was calculated per each condition (ΔCt).

The SD of the ΔCt was calculated: SD ΔCt = √ (SD $_{\text{target gene}}$^2+SD $_{\text{b2M}}$^2)

The difference of ΔCt between the control and the treated sample was calculated (ΔΔCT).

The relative expression (RE) per each condition was calculated (relative expression = 2^- ΔΔCT).

The SD of the relative expression was calculated:

SD RE = √ ((RE $_{\text{control}}$ * ln (2))^2*SD $_{\text{control}}$^2);

or SD RE = √ ((RE $_{\text{treated}}$ * ln (2))^2*SD $_{\text{treated}}$^2)

ChIP data were analyzed according to the Percent input method, i.e. the enrichment of the immune-precipitated sample over the amount of chromatin. Typically, 1% chromatin was used as input sample.

First, the average Ct value of the input sample was calculated.

Using this value, the percentage input subtracted was calculated per each immune-precipitated sample (nonspecific adjustment): Ct_{ChIP} - Average Ct_{input}

The percentage of input was calculated per each immune-precipitated sample:

0.5^ percentage input subtracted.

The average and the standard deviation of the triplicate values (percentage of input) per each immune-precipitated sample were calculated.

3.3 Biochemical methods

3.3.1 Preparation of whole cell protein extracts

Cells were washed with ice cold PBS, harvest by scraping with ice cold PBS (1 ml/10 cm tissue culture dish) and collected into a 1.5 ml tube. Cells were centrifuged at 1,500 rpm, for 5 min, at 4°C. Samples were kept on ice for the whole procedure. The cell pellet was resuspended in RIPA lysis buffer, containing proteinase and phosphatase inhibitors, using a 10:1 ratio (e.g. 1 ml RIPA buffer for 100 µl pellet). Samples were incubated in ice for 30 min. Afterwards, samples were centrifuged at 14,000 rpm, for 15 min, at 4°C and cleared lysates were transferred to a new pre-chilled 1.5 ml tube.

Protein concentration was determined with the Bradford assay (see 3.3.2). Samples were diluted typically to a final concentration of 1 µg/µl, or to the lowest sample concentration. Lysates were flash frozen in liquid nitrogen and stored at -80°C. Alternatively, samples were directly prepared for SDS-PAGE (see 3.3.6).

3.3.2 Total protein quantification by colorimetric Bradford assay

Protein lysates were quantified according to the Bradford method (Bradford, 1976). The appropriate amount of Bradford reagent (900 µl/sample + blank sample +2) was

calculated and diluted with 150 mM NaCl (1:10 ratio; i.e. 100 µl NaCl + 900 µl Bradford reagent/sample). One ml diluted Bradford reagent was pipetted into cuvettes and 2 µl protein lysate was added followed by 900 µl Bradford reagent. The reaction was manually mixed and absorbance was measured at 595nm. The blank tube contained 2 µl lysis buffer and was used to set up the absorbance to 0. Protein concentration was determined according to the absorbance of a pre-calculated standard curve.

3.3.3 SDS Polyacrylamide gel electrophoresis (SDS-PAGE)

The appropriate amount of sample buffer 6x was added to the protein lysates, samples were boiled at 95°C for 5 min and spun down. An equal amount of proteins was loaded into the gel pockets using a 50 µl glass syringe (Hamilton). The PageRuler Pre-Stained Protein Ladder (Fermentas) was used as a molecular weight marker. Bis-Tris polyacrylamide gels were used for separating the proteins according to their molecular weight. The electrophoresis was performed using SDS-PAGE chambers (Biorad) filled with 1x MOPS running buffer at 80-120 V.

3.3.4 Immunoblot

After separating protein lysates by SDS-PAGE, proteins were transferred onto a PVDF membrane. The PVDF membrane was activated by incubation in methanol for 30 sec, followed by 2 min in H_2O. The membrane was equilibrated in the transfer buffer 1x before proceeding to the immunoblot assembly. The immunoblot sandwitch was assembled in transfer buffer as follows: starting from the black side of the cassette (i.e. towards the negative charged site of the immunoblot chamber), 1 sponge layer, 2 Whatman filter paper layers, the gel, the membrane, 2 Whatman filter paper layers, 1 sponge layer, ending with the red site of the cassette (i.e. towards the positive charged site of the immunoblot chamber). During the preparation, the immunoblot sandwich was inspected for the absence of air bubbles. The cassette was placed into the tank, which was filled with transfer buffer 1x. The transfer was carried out at 4°C, at 300 mA for 2 h. Afterwards, the membrane was briefly washed in TBS-T and incubated in blocking

solution for 1 h at RT under constant shaking. BSA blocking solution was used only for subsequent detection of phosphorylated proteins. After blocking, the membrane was incubated with the primary antibody at 4°C over night. On the next day, the membrane was washed 5 times for 10 min with 1x TBS-T and incubated for 1 h with the secondary antibody (diluted 1:5000 in blocking solution) followed by additional 5 washing steps of 5 min each with TBS-T. Antibodies were visualized by chemiluminescence using the Immobilon Western Substrate (Millipore) according to manufacturers' protocol and detected with the LAS-4000 imager (Fujifilm Global). Protein signals were quantified relative to the loading control using the software Multi Gauge.

3.3.5 Stripping of PVDF membranes

Membranes were stripped after detection of a phosphorylated protein, in order to detect the total, non-phosphorylated form. Membranes were incubated with stripping solution for 1 h at RT under constant shaking. Afterwards, membranes were washed 3 times in PBS-T, blocked and incubated with the primary antibody. The antibody detection was performed as above described.

3.3.6 Cycloheximide decay assay

Cells were treated with 100 µg/ml of freshly prepared CHX, dissolved in EtOH, and harvested at different time points. MYC levels were analyzed by immunoblot and quantified.

3.3.7 Pulse labeling and immunoprecipitation

Cells were treated according to the experimental setup, e.g starved for glutamine, or supplemented with glutamine and adenosine after starvation. In the last hour of treatment, cells were starved in methionine-free medium (containing glutamine or adenosine, according to each experimental condition) for 15 minutes at 37°C and then incubated with 500 mCi ^{35}S-labeled methionine (Hartmann Analytic) for 60 minutes at

37°C. The experiment was carried out in a laboratory equipped for isotope work. Cells were washed twice with ice cold PBS, harvested by scraping and collected by centrifugation. The cell pellet was lysed (see 3.3.1) and total protein concentration was determined (see 3.3.2). An equal amount of protein, typically 2 mg, was immunoprecipitated using a rabbit monoclonal MYC antibody or an isotype-control antibody (1 µg antibody/mg protein lysate). Samples were incubated for 3 h at 4°C on a rotating shaker. At the end of the incubation time, magnetic protein G dynabeads (Invitrogen) were washed 3 times with 1 ml lysis buffer. The amount of dynabeads used was 7.5 µl * µg antibody * number of samples. All washing steps of dynabeads were performed using a magnetic rack for 1.5 ml reaction tubes (Promega). After the last washing step, the beads were resuspended in lysis buffer (100 µl * 7.5 µl beads). One hundred µl of dynabeads were added to each tube containing the immunoprecipitated mix and tubes were incubated overnight at 4°C on a rotating shaker. On the next day the mix was washed 3 times with 1 ml lysis buffer, resuspended in 40 µl sample buffer 1x and boiled for 5 min at 95°C. Samples were spun down and kept on the magnetic rack in order separate the immunoprecipitated mix from the beads. Twenty µl of each sample were loaded on a 8% bis-tris polyacrylamide gel and SDS-page was performed as in 3.3.3, without letting the bromophenol blue indicator line going out of the gel. The gel was fixed for 10 min in a fixing solution and briefly washed in H_2O. Afterwards, the gel was placed onto a piece of Whatman paper and covered with a plastic wrap. The gel was dried for 2 h using a gel dryer, then transferred into a Storage Phosphor Screen BAS-IP (GE Healthcare) for 72 h. The data were acquired using a Typhoon FLA 7000 scanner (GE Healthcare). To allow bands visualization, contrast was uniformly enhanced using Adobe Photoshop CS5.

3.3.8 Chromatin immunoprecipitation (ChIP)

Seven million cells per were plated in 15 cm dishes per each condition. The starvation was performed on the next day for 3.5 or 5 h. Afterwards cells were processed for ChIP.

Protein-DNA cross-linking

Formaldehyde was directly added to the medium at 1% final concentration (405 µl/15 ml medium) and plates were incubated for 10 min at RT, slowly shaking. Afterwards, 750 µl glycine were added to inhibit the crosslinking reaction and plates were incubated for 5 min at RT, slowly shaking.

Cell harvesting and lysis

Medium was removed and cells were washed twice with ice cold PBS. Cells were harvested by scraping with 1 ml ice-cold PBS containing protease and phosphatase inhibitors. Scraping was repeated a second time and cells were collected into 15 ml tubes. Cells were centrifuged at 1200 rpm for 5 min at 4°C. Cell pellets were lysed in 3 ml ChIP swelling buffer containing protease and phosphatase inhibitors and incubated 20 min in ice. The mix was centrifuged at 1200 rpm for 5 min at 4°C. The nuclear pellet was resuspended in 2 ml RIPA buffer containing protease and phosphatase inhibitors and incubated 10 min in ice.

DNA fragmentation and size check

The nuclear lysates were sonicated using the following conditions, tested for HCT116 cells:

10 sec pulse

30 sec pause

20% amplitude

25 min time

Samples were kept in ice at 4°C until the fragment size was verified.

In order to check the DNA fragment size, 25 µl of sonicated chromatin were transferred to a 1.5 ml reaction tube. The volume was brought to 500 µl with TE buffer. In order to revert the cross-linking and degrade the RNA, 16.87 µl NaCl 5 M and 2 µl RNAse A 20 µg/ml were added to each sample and the tubes were incubated for 1 h at 37°C, followed by overnight incubation at 65°C on a thermo shaker. On the next day 5 µl EDTA 0.5 M and 2 µl Proteinase K 200 µg/ml were added to each sample and the tubes

were incubated for 2 h at 45°C on a thermo shaker. DNA was isolated by phenol-chloroform purification (see 3.2.10.4) and the pellet was resuspended in 25 µl TE. DNA loading buffer was added to each sample and DNA separation was performed on a 2% agarose gel. Once verified that the chromatin size was below 500 bp, the sonicated chromatine stored at 4°C was transferred to 1.5 ml reaction tubes and cleared by at least 3 centrifugations at 14000 rpm for 15 min at 4°C.

ChIP

The primary antibody was first coupled with Protein A Dynabeads. The beads were aliquotted (30 µl) according to the number of samples and the number of IP to perform. The beads were washed 3 times with 1 ml 0.5% BSA-PBS. All washing steps of dynabeads were performed using a magnetic rack for 1.5 ml reaction tubes (Promega). After the last washing step, 1 ml 0.5% BSA-PBS and 3 µg antibody were added to the beads and the tubes were incubated overnight at 4°C on a rotating shaker. On the next day, the beads were washed 3 times with 0.5% BSA-PBS and resuspended in 30 µl 0.5% BSA-PBS. The cleared sonicated chromatin was distributed into each tube containing the different antibodies and 1 % input was stored at 4°C. The mix was incubated overnight at 4°C on a rotating shaker. Afterwards, the mix was washed 3 times with 1 ml ChIP washing buffer I; 3 times with 1 ml ChIP washing buffer II and 3 times with 1 ml ChIP washing buffer III. The last washing steps were performed incubating the tubes for 5 min at 4°C on a rotating shaker. The samples were washed once with 1 ml TE buffer and transferred to a new 1.5 ml reaction tube. The immunoprecipitated chromatin was eluted 2 times from the beads using 250 µl freshly prepared elution buffer and incubating each time the samples for 15 min at RT on a rotating shaker. The eluates were merged and 500 µl elution buffer was added to the input samples. The chromatin decrosslinking was performed as described above. The DNA was purified using phenol-chloroform. The DNA pellet was resuspended in 500 µl ddH_2O and 10 µl were used for quantitative real-time PCR (see 3.2.12.2).

3.4 Next-generation sequencing

3.4.1 miRNA-sequencing (miRNA-seq)

3.4.1.1 Library preparation

The experiment was performed in triplicate per each condition. RNA for miRNA-seq was extracted using the miRNeasy Mini kit, in order not to exclude small size RNAs during the purification procedure. The RNA was eluted using 40 µl RNAase-free H_2O. The RNA concentration was measured using a standard sense chip for Bioanalyzer (see 3.2.9.3). One µg/µl RNA per each condition was used for library preparation. The library was prepared using the NEBNext Small RNA Library Prep Set for Illumina and the NEBNext Multiplex Oligos for Illumina (Index Primer 1-12), according to the manufacturer´s instructions. H_2O was used as negative control to check the purity of the preparation. The amplification by PCR was performed for 12 cycles and the PCR products were purified using the QIAQuick PCR purification kit. The quality of the eluted DNA was verified on the Bioanalyzer (see 3.2.9.3). Size selection was performed loading the samples on a 6% TBE polyacrylamide gel and running the gel for 4.5 h at 180 V. The gel was stained for 1 h using a Sybr Gold (Thermo) solution (1: 7000 in TBE 1x buffer) and visualized on a UV transluminator. A 140-nucleotide band, corresponding to the miRNAs ligated to the adapters, was isolated from the gel by cutting it. The DNA was eluted from the gel following the instruction provided by the NEBNext Small RNA Library Prep Set for Illumina. For gel filtration, Corning Costar Spin-X centrifuge tube filters (Sigma) were used. The quality of the purified samples was verified using the Bioanalyzer before performing the sequencing, using the Illumina GAIIx sequencer. All samples were mixed at equimolar concentration of 8 nM.

3.4.1.2 Sequencing data analysis

miRNA-seq data analysis was performed by Carsten Ade. The main steps are described. A Bowtie reference file containing all human annotated mature miRNAs was generated, in order to align the sequencing reads to a more specific dataset, rather than to a genome-wide one. The miRBase database version 21 was used. It contains 2,565 annotated miRNAs. The raw sequencing data were converted into FASTQ files, in order to be analyzed. Since the sequences generated were 33 bases long, they contained also the adaptor sequences at the 3´end. In order to allow the alignment of the sequenced miRNA sequences to the generated dsataset, the adaptor sequences were trimmed using the Cutadapt program. Sequences long 16 bases were obtained, aligned to the Bowtie dataset and alignment files were generated (SAM files). A raw count table was generated using the program Samtools and converted into an Excel table. A criterion of selection was applied in order to exclude miRNAs having too low counts (sum of counts in three replicates lower than the number of replicates, according to Anders et al, 2013). The differential expression of miRNAs between two different conditions was calculated using the program edgeR in R and MA-plots were generated.

3.4.2 RNA-sequencing (RNA-seq)

3.4.2.1 Library preparation

The experiment was performed in triplicate per each condition. RNA for RNA-seq was extracted using the RNeasy Mini kit. The RNA was eluted using 40 µl RNAase-free H_2O. The samples were kept in ice and the RNA concentration was measured using a standard sense chip for Bioanalyzer (see 3.2.9.3). One µg/µl RNA per each condition was used for library preparation. The library was prepared using the NEBNext Ultra RNA library prep kit for Illumina and the NEBNext Multiplex Oligos for Illumina (Dual Index Primers Set 1), according to the manufacturer´s instructions. H_2O was used as negative control to check the purity of the preparation. The amplification by PCR was performed for 13 cycles and the PCR products were purified using the Agencourt

AMPure XP beads. The quality of the purified DNA was verified on the Bioanalyzer (see 3.2.9.3) before performing the sequencing, using the NextSeq 500 (Illumina) sequencer. All samples were mixed at equimolar concentration of 50 nM.

3.4.2.2 Sequencing data analysis

RNA-seq data analysis was performed by Susanne Walz. The main steps are described. Base calling was performed with Illumina's CASAVA software and overall sequencing quality was tested using the FastQC script. Reads were mapped to hg19 with TopHat2 and Bowtie v1.1.2 with default settings. Reads per gene were counted using the countOverlaps function from the R package GenomicRanges, weakly expressed genes were removed (mean count over all samples <1.5) and differentially expressed genes were called using EdgeR. GSE analyses were performed with signal2noise metric, 1000 permutations and the C2 gene set collection of MSigDB.

3.4.3 ChIP-sequencing (ChIP-seq)

3.4.3.1 Library preparation

The chromatin was prepared following the same protocol used for ChIP (see 3.3.8), but increasing the number of cells and the amount of reagents of 3 times. Before proceeding with the library preparation, the quality of the immunoprecipitation was verified by quantitative RT-PCR (enrichment over the input sample or a negative control region). The DNA was quantified using the PicoGreen assay (see 3.2.9.2). Three ng of DNA per each condition were used for library preparation. The library was prepared using the NEBNext ChIP-Seq Library Prep Master Mix Set for Illumina, NEBNext Poly (A) mRNA Magnetic Isolation Module and the NEBNext Multiplex Oligos for Illumina (Dual Index Primers Set 1), according to the manufacturer´s instructions. H_2O was used as negative control to check the purity of the preparation. The DNA purification between each step was performed using the QIAquick PCR purification kit and the MinElute PCR purification kit, according to the manufacturer´s instructions. After adaptor ligation, a size selection step was performed by running the samples on a 2%

agarose gel and cutting the band corresponding to 200 bp, in order to exclude adaptor dimers of 120-150 bp. The DNA was purified from the gel using the QIAquick gel extraction kit, according to the manufacturer´s instructions. The amplification by PCR was performed for 18 cycles and the PCR products were MinElute PCR purification kit, according to the manufacturer´s instructions. The quality of the purified DNA was verified on the Bioanalyzer (see 3.2.9.3) before performing the sequencing, using the NextSeq 500 (Illumina) sequencer. All samples were mixed at equimolar concentration of 40 nM.

3.4.3.2 Sequencing data analysis

ChIP-seq data analysis was performed by Susanne Walz. The main steps are described. Base calling was performed with Illumina's CASAVA software and overall sequencing quality was tested using the FastQC script. Overall sequencing quality was verified with the fastQC script and reads were mapped to the human genome (assembly hg19) with Bowtie v1.1.2 with default settings. All samples were normalized to the sample with the smallest number of mapped reads. RNAPII-and/or MYC-bound genes are defined as having a RNAPII and/or MYC peak in a region +/-1kb around the TSS. Peaks were called with MACS v1.4.2 with a p-value cut-off of $1.0x10^{-6}$ (RNAPII) and $1.0x10^{-7}$ (MYC) and accepting at most five duplicated reads per genomic position. BedGraph files were generated using BedTools v2.26 "genomeCoverageBed" function and individual genomic loci were visualized with the Integrated Genome Browser. Heat maps are generated with SeqMiner v1.3.3 in a window of +/-5kb with a resolution of 50bp and visualized using TreeView v1.1.6. Meta gene analyses were conducted with ngs.plot v2.61 using all annotated Ensembl genes and default settings. For calculation of the RNAPII traveling ratio, RNAPII reads were counted with coverageBed in TSS (defined as -30bp to +300bp relative to the annotated TSS), gene body (TSS+300bp to annotated TES) and TES (TES to TES+1kb) with a minimum overlap of 51% to exclude double-counting of reads. To avoid dividing by 0 one pseudocount per kb was added and counts were subsequently normalized to region length. The traveling ratio was then calculated by dividing normalized counts in TSS regions by normalized counts in gene bodies. For binned data, genes were sorted based on the number of reads in the

strongest MYC peak in the promoter and grouped in equally sized bins with 200 genes each. Occupancies of each bin were calculated using the arithmetic mean. 2D kernel density estimates are drawn with the smoothScatter function in R with a fixed bandwidth.

4 Results

4.1 Comparison between effects mediated by glutamine and glucose

4.1.1 Glutamine, not glucose, availability regulates MYC protein levels

In order to evaluate whether the availability of glucose and glutamine has an effect on MYC protein levels, a medium lacking both metabolites was used. Since HCT116 cells are cultured in DMEM, a powder formulation of the same medium was used and reconstituted with 2.5 g/l glucose (Glc), 2 mM glutamine (Q) and dialyzed serum, in which, therefore, all molecules bigger than 10 kDa were excluded. Working concentrations of glucose and glutamine were determined both by titration experiments, using as read-out the highest MYC leves on immuno blot (Fig. 4.1A, B), and by comparing with previous studies (Qing et al, 2012; Yuneva et al, 2007).

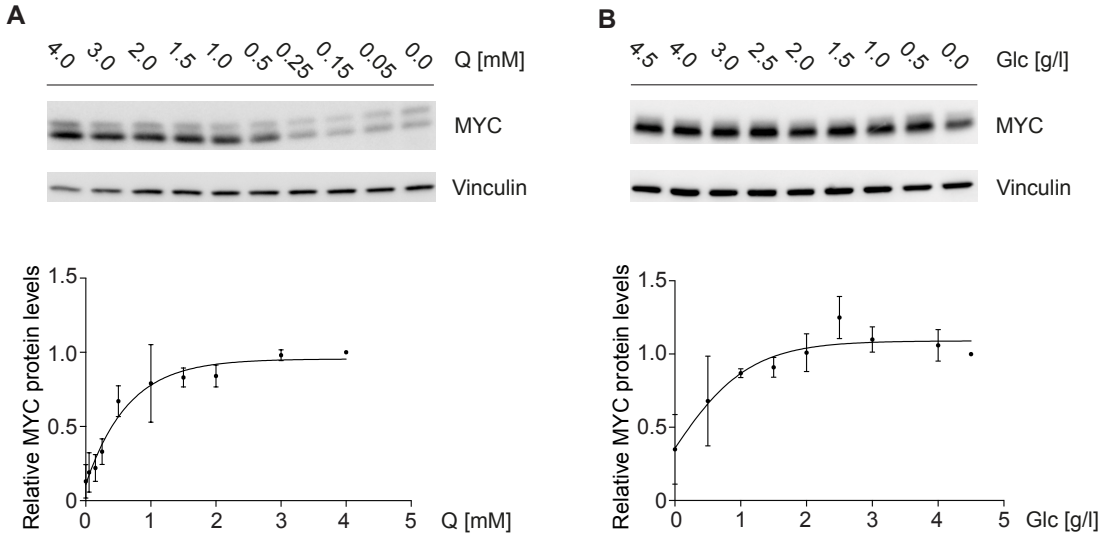

Figure 4.1: Glutamine rather than glucose starvation decreases MYC protein levels

A) IB showing MYC levels in HCT116 cells cultured in medium containing the indicated amounts of Q for 24 h. Below: Quantification of the results of three independent experiments. MYC levels are normalized to Vinculin levels. Each point represents mean ± standard deviation (SD). Curve fitting was performed using a sigmoidal dose-response equation.
B) Same as in (A), using the indicated amount of Glc.

The concentrations of the two metabolites whose combination resulted in the highest MYC protein levels were lower than those found in the commercially available DMEM (4.5 g/l and 4 mM, respectively for glucose and glutamine). Titration experiments for each metabolite showed that MYC protein levels undergo a strong downregulation when glutamine concentration was equal or below 0.25 mM, while they were mainly unaffected by decreasing the amount of glucose in the medium (Fig. 4.1A, B). To note that sodium pyruvate, normally present in the commercial DMEM, was not used in the reconstituted medium, being pyruvate (Pyr) in between the metabolism of glucose and glutamine and therefore possible cause of interference (see Fig. 1.4). As shown in Fig. 4.2, lack of pyruvate had no effect on MYC levels, either in full medium (+ Q) or in medium lacking glutamine (- Q). Cell proliferation was also not affected, as noticed by microscopic observation.

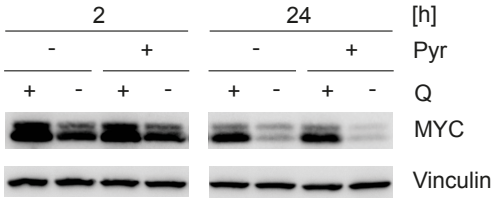

Figure 4.2: Pyruvate is a dispensable component of the reconstituted DMEM

Cells were cultured for 2 or 24 h in medium containing Pyr and Q, as indicated. The concentration of glucose in all conditions was 2.5 g/l. MYC protein levels were determined by IB. Vinculin was used as loading control.

Kinetic experiments confirmed the specificity of this regulation. MYC was strongly downregulated after 15 hours of glutamine starvation, and upregulated in a very rapid manner (i.e. after 30 minutes) when glutamine was re-added to the medium (Fig. 4.3, left part). This effect was not observed following glucose starvation and re-stimulation (Fig. 4.3, right part).

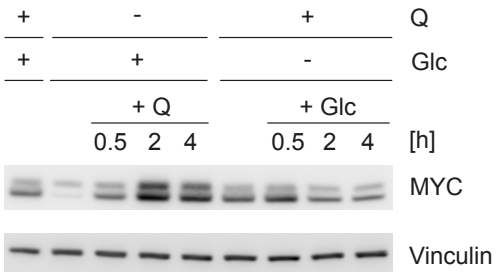

Figure 4.3: Re-addition of glutamine rapidly restores MYC levels

Cells were starved for Q or Glc. After 15 h, Q (2mM) or Glc (2.5 g/l) were re-added for the indicated time points. MYC levels were determined by IB (n=3).

Thus, two experimental conditions were used as read-out of the glutamine effect on MYC in the majority of the experiments showed in the next sections: complete starvation for 15 hours, i.e. MYC downregulation, and glutamine re-addition for 2 hours after starvation, i.e. MYC upregulation. However, MYC downregulation occurred also in a rapid manner, i.e. within one hour after glutamine withdrawal (Fig. 4.2 shows MYC downregulation after 2 hours of glutamine withdrawal). Short starvation was also used as experimental read-out in order to analyze effects occurring within a short time frame.

4.1.2 Glucose or glutamine starvation has distinct effects on cell viability

Cells viability was used as a second parameter to evaluate the effects of glucose or glutamine starvation. A crystal violet staining, performed after 36 hours of starvation, showed that HCT116 cells were more sensitive to glucose, rather than to glutamine starvation (Fig. 4.4A).

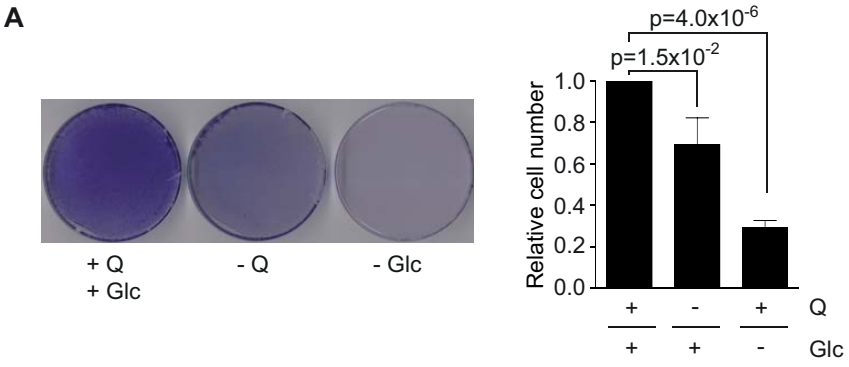

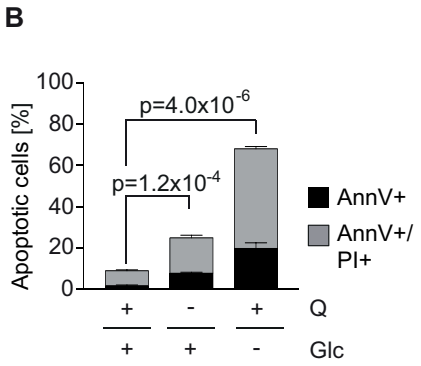

Figure 4.4: Glutamine and glucose starvation reduce cell number, but only deprivation of glucose increases apoptosis

A) Left: crystal violet staining of cells Q- or Glc-starved for 36 h. Right: quantification of 3 biological replicates. Bars show mean + SD. P-values were calculated using a two-tailed Student´s t-test.
B) FACS analysis showing the percentage of early (Ann V^+; Ann V: Annexin V) and late (Ann V^+/ PI^+; PI: Propidium Iodide) apoptotic cells after 36 h of starvation. Results represent mean + SD of biological triplicates. P-values were calculated considering the sum of apoptotic cells and using a two-tailed Student´s t-test.

Measurement of apoptosis by FACS analysis revealed that the observed decrease in cells number following glucose starvation was due to increased percentage of apoptotic cells (Fig. 4.4B). Although glutamine starvation does not considerably induce apoptosis, a decrease in cell number was observed when compared with cells grown in complete medium (Fig. 4.4A).

In order to assess effects due to glutamine starvation, BrdU/PI FACS analysis of cell cycle was performed. This technique allows both to distinguish the cell cycle phases, according to the DNA content, which is proportional to the PI staining, and to kinetically visualize the progression of cells through the cycle, according to the incorporation of BrdU, a thymine analogue, into newly or recently synthetized DNA (Cecchini et al, 2012). This experiment revealed that HCT116 cells are not able to enter S-phase after 15 hours of glutamine starvation, as shown by the decreased BrdU incorporation, and undergo arrest in G1/S-phase (Fig. 4.5A and 4.5B).

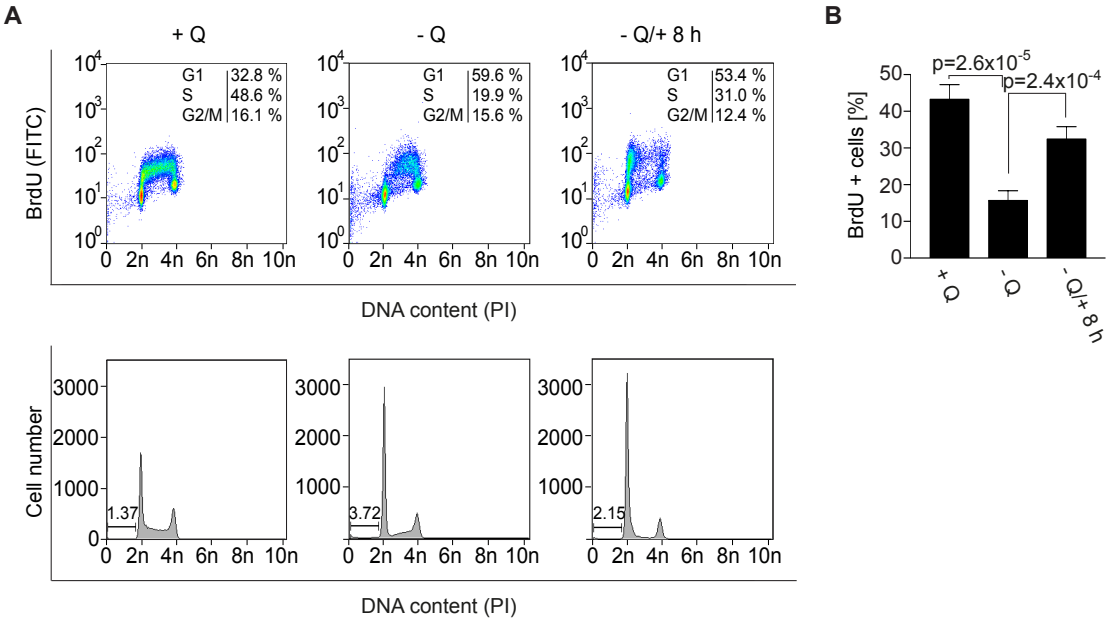

Figure 4.5: Glutamine deprivation results in cell cycle arrest

A) Cells were grown in complete medium or medium without Q for 15 h. Where indicated, Q was re-added for 8 h. Cells were labelled with BrdU for 1 h, harvested and analysed by BrdU/PI FACS. Upper panel: dot plot showing distribution of cells in G1, S and G2/M phase, according to BrdU incorporation and PI content. The percentage of cells in each phase is indicated in each box. Lower panel: histogram showing the cell distribution through the cell cycle, according to the PI content. The number of cells in Sub-G1 phase is shown as percentage of total.
B) Quantification of BrdU positive cells. Results represent mean + SD of four independent experiments. P-values were calculated using a two-tailed Student´s t-test.

The PI profile also showed a small increase in the Sub-G1 population indicating apoptotic cells (Fig. 4.5A, lower part). Conversely, re-addition of glutamine after starvation allows cells to re-enter S-phase, as assessed by increased BrdU incorporation (Fig. 4.5A, upper part, and Fig. 4.5B). This effect was clearly observed 8 hours after glutamine re-addition, while MYC upregulation occurs at earlier time points.

4.2 Identification of mechanisms responsible for the glutamine-mediated regulation of MYC

Due to the striking response of MYC to glutamine starvation and re-addition after withdrawal, potential mechanisms accounting for this regulation were investigated.

4.2.1 *MYC* mRNA levels do not parallel MYC protein levels in response to glutamine

A transcriptional mechanism of regulation was firstly evaluated, since the observed effect on MYC protein levels could reflect changes in the amount of mRNA. Steady-state *MYC* transcript levels were measured by qRT-PCR and normalized to the levels of *B2M*, a commonly used housekeeping gene, whose expression was unchanged following glutamine starvation.

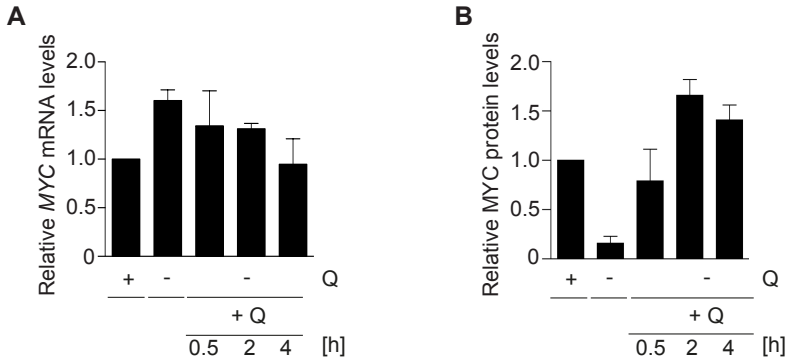

Figure 4.6 *MYC* mRNA levels do not parallel MYC protein levels

A) qRT-PCR showing levels of *MYC* mRNA in the indicated conditions. Glutamine starvation was performed for 15 hrs. Glutamine was re-added after starvation, as indicated. mRNA levels are shown relative to + Q. Bars represent mean + SD (n=3, each biological replicate in technical triplicate).
B) Quantification of MYC protein levels under the same conditions as in (A). Protein levels are shown relative to + Q. Bars represent mean + SD (n=4). A representative experiment is shown in Fig. 4.3.

Moderately increased *MYC* mRNA levels were observed after 15 hours of starvation, compared to those relative to cells grown in complete medium and used as reference for normalization. When glutamine was re-added after starvation, *MYC* mRNA levels were kept higher than control for the first 2 hours, while they decreased to control levels after 4 hours (Fig. 4.6A). This trend was therefore not comparable to the one observed for MYC protein levels (Fig. 4.6B).

4.2.2 Increased degradation does not account for glutamine-mediated MYC downregulation

MYC protein levels are controlled by degradation mechanisms, reported to be activated under stress conditions, e.g. glucose starvation and low oxygen tension (Okuyama et al., 2010; Wong et al., 2013; see 1.3.3). In a similar manner, glutamine starvation could increase the activity of E3 ubiquitin ligases, which would be conversely inhibited in the presence of glutamine. Experiments to assess MYC stability under starvation were therefore performed, aiming to test such model and the resulting possibility to perform a screening for identifying molecular players (e.g. kinases or ubiquitin ligases) involved in this regulation. Since increased degradation of MYC would correspond to decreased protein stability, a cycloheximide (CHX) assay was performed. CHX is an inhibitor of protein translation, which acts by blocking the elongation step (Schneider-Poetsch et al., 2010). This allows for the estimation of the half-life of a protein, i.e. its stability, in a time-course experiment. MYC stability was determined in cells cultured for 24 hours in medium containing high (2 mM) or low (0.5 mM) glutamine, treated in the last hour with CHX and harvested at 6 different time points. Low glutamine concentration was used to reliably detect MYC protein levels, which are too low following complete starvation. This experiment showed no significant differences in MYC stability between the two conditions (Fig. 4.7A). An average half-life of 29 and 26 min was calculated in the, presence of high or low glutamine, respectively. Levels of other short-lived proteins (c-Jun, MCL-1, Cyclin E) were then checked in order to verify the existence of a shared mechanism of regulation, being these proteins also recognized by Fbw7, one of the main ubiquitin ligases targeting MYC (Welcker and Clurman, 2008). While MYC was downregulated already after 1 hour of starvation, other proteins were unaffected (Fig. 4.7B). Finally, the involvement of a proteasomal-dependent mechanism of degradation was evaluated using the inhibitor MG132, which blocks the proteolitic function of the proteasome (Kisselev and Goldberg, 2001). In the presence of glutamine, MG132 treatment resulted in increased MYC levels, due to blocked MYC degradation. Conversely, MYC levels were not rescued by MG132 in absence of glutamine (Fig.

4.7C). Thus, also increased proteasomal degradation could be excluded as possible reason for the observed decrease in MYC levels.

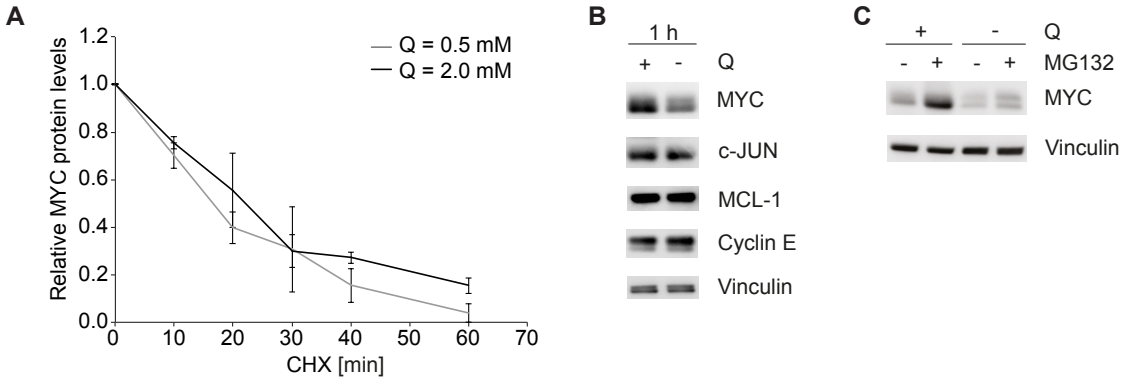

Figure 4.7: Increased degradation does not account for glutamine-mediated MYC downregulation

A) CHX assay was performed in cells cultured in the presence of high (2 mM) or low (0.5 mM) Q for 24 h and harvested at the indicated time points after CHX addition. IBs for MYC were quantified and normalized to Vinculin. Each point represents the mean of three biological replicates ± SD.
B) Cells were starved for 1 h and IB performed to detect the indicated proteins.
C) Cells were culture for 15 h in medium containing or lacking Q and treated for the last 6 hrs with the proteasomal inhibitor MG132. MYC levels were detected by IB.

4.2.3 Glutamine-induced changes in mTOR activity do not directly correspond to changes in MYC levels

Changes in MYC levels could be the direct consequence of modulating the activity of the mTOR Complex1 (mTORC1), the master regulator of protein translation, which is in turn controlled by glutamine availability (Nicklin et al, 2009; Duran et al, 2012). MYC response to glutamine was therefore checked following rapamycin-induced inhibition of mTORC1 kinase activity (Ballou and Lin, 2008). In order to consider only glutamine contribution, mTORC1 activity was blocked before starving the cells, by pretreating with the inhibitor for 2 hours. The phosphorylation status of the two best-characterized mTORC1 targets, p70S6K and 4EBP1, was used as read-out of rapamycin efficacy. The treatment did not induce evident changes in cell morphology, as detected by microscopic observation. After starvation, a decreased phosphorylation of both p70S6K and 4EBP1 was observed, indicating, as expected, a dependency of mTORC1 kinase activity on glutamine supply. Overnight rapamycin treatment led to a slight

increase of MYC in the presence of glutamine, while starvation induced MYC downregulation in both control and treated cells. Re-addition of glutamine after starvation restored mTORC1 activity. Interestingly, MYC upregulation was observed in both the absence and the presence of rapamycin, even though on a lower extent in the latter case (Fig. 4.8A).

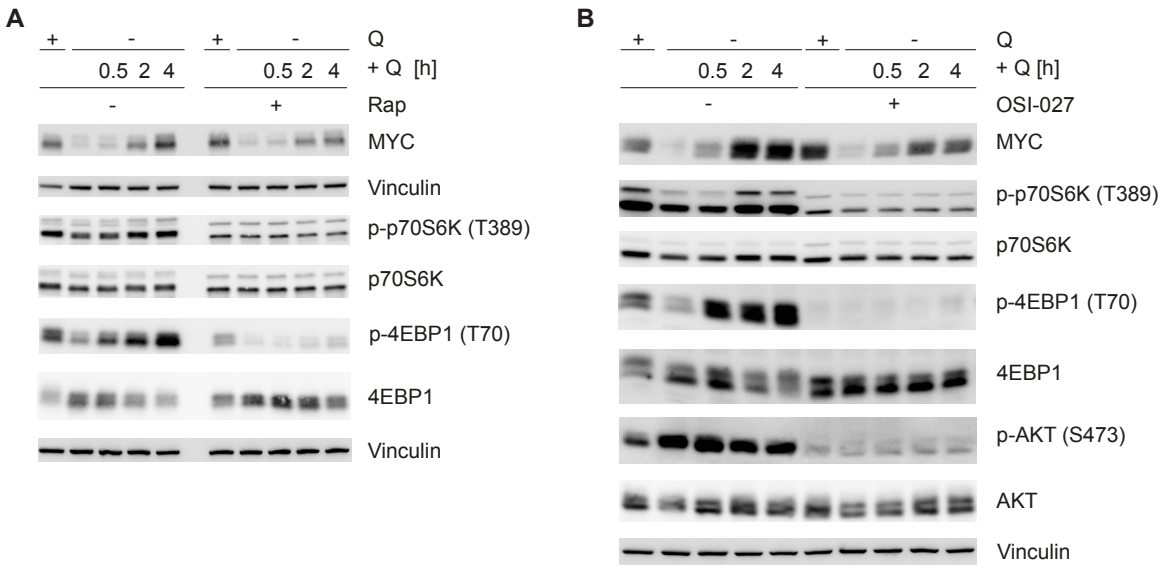

Figure 4.8: mTOR inhibition does not block the glutamine-mediated regulation of MYC

A) Cells were pre-treated with Rapamycin (Rap) or DMSO for 2 h. Afterwards, starvation was performed for 15 h in presence of the inhibitor. Glutamine was re-added after starvation for the indicated time points and the total or phosphorylated forms of the indicated proteins were detected by IB. A representative result is shown (n=2).
B) The experiment was performed as described in A) using the inhibitor OSI-027.

The same experiment was repeated using the compound OSI-027, a dual mTORC1 and mTORC2 inhibitor (Bhagwat et al, 2011). Increased phosphorylation of AKT was observed following glutamine starvation. As expected, OSI-027 treatment resulted in decreased phosphorylation of mTORC1 and mTORC2 targets, p70S6K, 4EBP1 and AKT, respectively. Consistently with the previous result, MYC downregulation occurred either with or without OSI-027 and MYC upregulation was observed in both control and treated cells after glutamine re-addition (Fig. 4.8B).

The effect of other amino acids was then checked in order to further evaluate if a correspondence between MYC levels and mTOR activity exists. Specifically, two

essential amino acids were selected, methionine and leucine, that are able to activate mTORC1 signaling (Nicklin et al, 2009; Sutter et al, 2013).

As expected, mTORC1 activity was affected by each amino acid, as assessed by the phosphorylated status of the mTOR target p70S6K. The overnight deprivation of glutamine, methionine or leucine resulted in the inhibition of mTORC1 activity, while re-addition after starvation stimulated it. Decreased MYC levels were observed in all three cases. Interestingly, MYC upregulation was observed only after re-addition of glutamine, but not of methionine or leucine. This result provided indications for a specific glutamine-mediated effect on MYC, which is not only due to modulation of mTOR activity.

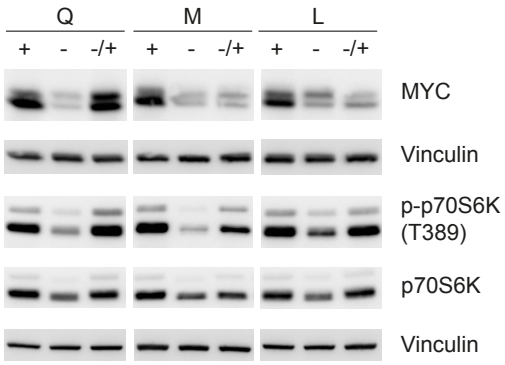

Figure 4.9: Effect of glutamine, methionine and leucine starvation and re-addition on MYC levels

Cells were starved for Q, M or L for 15 h. Each amino acid was re-added for 2 h after starvation (-/+) and MYC levels were determined by IB (n=3).

4.2.4 Glutamine regulates MYC through its 3´-UTR

Although the availability of glutamine did not directly influence MYC levels through mTOR, a translational control could occur over *MYC* mRNA, whose levels are not decreased under starvation, as assessed by steady-state measurement by qPCR (Fig. 4.6A). In order to test this hypothesis, changes in MYC translation were checked by pulse-labeling immunoprecipitation. This technique allows for the evaluation of the amount of newly synthetized proteins by labeling the cells with a radioactively-labeled form of methionine, which is incorporated during protein synthesis and which signal can be detected by autoradiography. Specific protein detection is obtained by MYC

immunoprecipitation after labeling. As shown in Fig. 4.10, radiolabeled MYC, i.e. the protein translated during the pulsing time (1 h), was detected when cells were cultured in presence of glutamine, indicating that *MYC* translation works properly under these conditions. Conversely, glutamine starvation led to decreased levels of MYC synthesis, both when the deprivation occurred for a short (2 h) or a longer time point (15 h), while re-addition of glutamine after starvation restored MYC synthesis. Thus, this result directed the investigation towards mechanisms of post-transcriptional and translational control. The glutamine-mediated control of MYC translation could be the result of mechanisms impinging on *MYC* UTRs. In general, the 5′UTR and the 3′UTR are elements involved in controlling translation due to their interaction with translation molecular players, e.g. initiating factors. Specifically, the 3′-UTR of *MYC* is known to be the target of different pathways, which can be potentially activated under stress conditions (Cannel et al, 2010; Kress et al, 2011; Masui et al, 2013, see 1.1.2.2). Translational regulation of *MYC* can also be regulated by internal ribosomal entry sites (IRES) in its 5′-UTR (Stoneley et al, 2000; Wiegering et al, 2015, see 1.1.2.2).

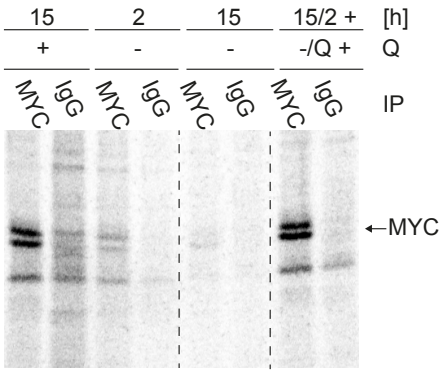

Figure 4.10: Effect of glutamine on MYC protein synthesis

Cells were starved for 2 or 15 h. Glutamine was re-added after long starvation for 2 h. In the last h of treatment, cells were deprived of endogenous methionine and pulsed with ^{35}S-Methionine. MYC was immunoprecipitated using a α-MYC or a control antibody. Levels of newly synthetized MYC protein were detected by autoradiography, after 72 h of exposure. The arrow indicates the MYC specific band. Dashed lines indicate that part of the original picture is not included (see Fig. 4.22A); (n=2).

In order to evaluate a possible involvement of these regulatory sequences, four different exogenous *MYC* constructs were expressed in HCT116 cells and their regulation

checked under glutamine starvation (Fig. 4.11A). The constructs comprised only the *MYC* coding sequence (CDS), starting from the canonical AUG site (i.e. like the majority of *MYC* transgenes described in literature) or the coding sequence plus each UTR or both. These transgenes were expressed using a doxycycline (dox)-inducible vector (pInducer21). All of them were C-terminally-HA-tagged. The tag helped to discriminate between the endogenous and exogenous form of MYC, since HCT116 cells have high levels of endogenous MYC and the exogenous constructs were lowly overexpressed (Fig.4.11B).

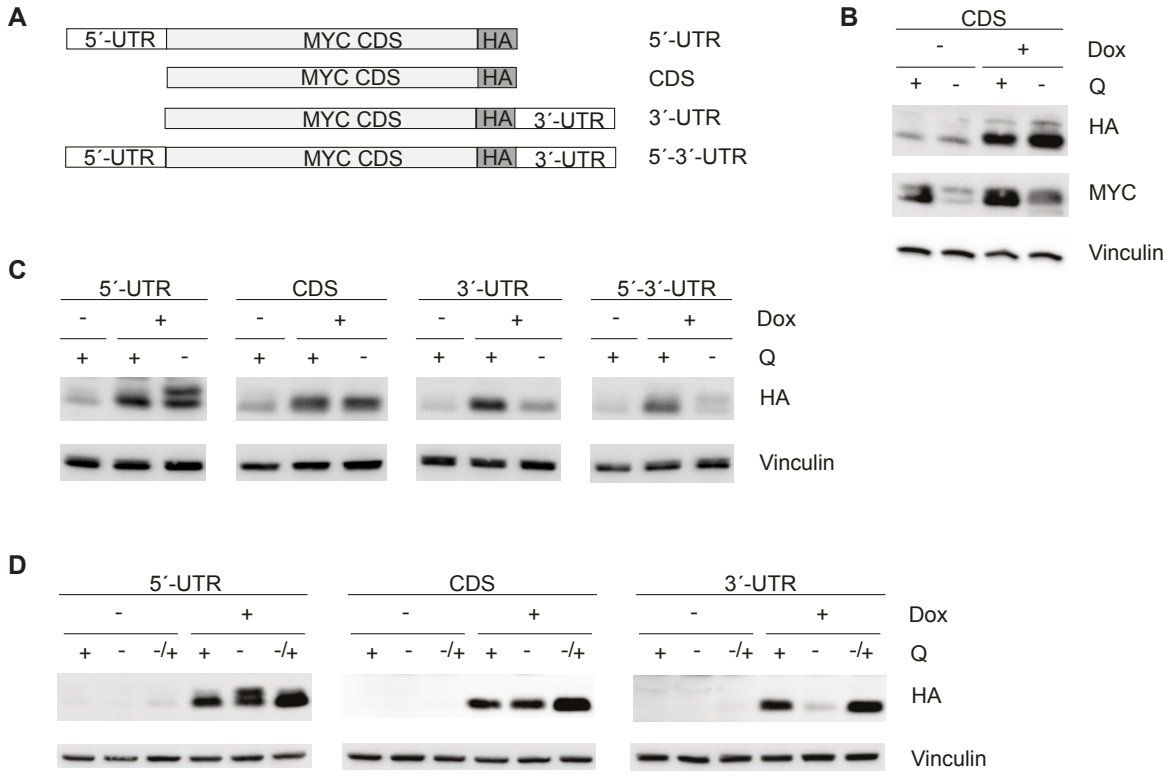

Figure 4.11: The 3´-UTR of *MYC* mediates its response to glutamine

A) Scheme of the dox-inducible *MYC* constructs used for lentiviral infection of HCT116 cells.
B) IB showing levels of exogenous and total MYC in GFP-sorted cells expressing the CDS construct. Cells were dox-induced for 2 h before undergoing starvation for 15 h.
C) The experiment was performed as in (B), using cells expressing the indicated constructs (n=3).
D) Unsorted cells expressing the indicated constructs were dox-induced for 2 h. Starvation was performed for 15 h and, where indicated, Q was re-added for 2 h. Exogenous MYC levels were detected by IB, using an anti-HA antibody.

Interestingly, detection of HA-tagged MYC after 15 hours of glutamine starvation revealed that only the constructs carrying the 3´-UTR were downregulated, while those lacking this sequence (CDS and 5´UTR) were stable (Fig. 4.11C and Fig. 4.11D). Glutamine re-addition after starvation resulted in MYC upregulation independently of the presence of the 3´-UTR (Fig. 4.11D). This result did not exclude the involvement of the 3´UTR in MYC upregulation, although pointed out the potential existence of additional mechanisms.

The appearance of a second band of higher molecular weight was detected following starvation only when the 5´-UTR and, on a lower extent, the 5´-3´-UTR constructs were expressed. The first exon of *MYC* contains a non-canonical start codon (CUG) located 45 nucleotides upstream the AUG start codon (Hann et al, 1988; see 1.1.2.2). The CUG codon is not present in standard *MYC* transgenes described in literature, which all start from the AUG in the second exon; it is instead present in the transgenes containing the 5´-UTR, being downstream this sequence. Mutating the CUG (Leu) in a UAG (Stop) codon, confirmed that the higher band is the longer isoform of MYC (MYC1), since it did not appear after induction of the mutated construct under starvation (Fig. 4.12). A decrease in MYC1 levels under starvation when the 5´-3´-UTR transgene was expressed indicates that its translation can still be regulated through *MYC* 3´-UTR (Fig. 4.11C, right).

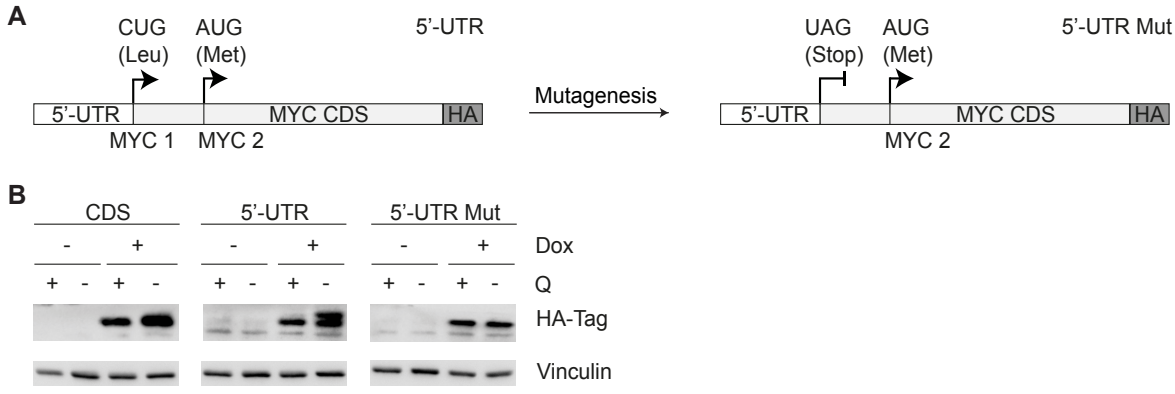

Figure 4.12: MYC1 is upregulated following glutamine starvation

A) Scheme of the mutagenesis performed on the 5´-UTR construct to allow only MYC2 expression.
B) IB from unsorted cells expressing the indicated MYC constructs and treated as in Fig. 4.11B.

Quantification of exogenous MYC levels confirmed a significant decrease in presence of the 3′-UTR (Fig. 4.13A). Levels of exogenous transcripts were determined after starvation. A decrease in HA-tagged *MYC* mRNA was observed in presence of the 3′-UTR, indicating decreased mRNA stability (Fig. 4.13B).

Finally, a luciferase assay was performed to verify the specificity of the glutamine-mediated effect on *MYC* 3′-UTR. Renilla luciferase luminescence was assessed in cells transfected with an empty vector control or a vector in which the *MYC* 3′-UTR was cloned downstream of the luciferase gene. Therefore, in the latter case the luciferase activity, is dependent upon the translational control over the 3′-UTR. Luminescence decreased following glutamine starvation in a 3′-UTR-dependent manner, although the difference with the control was not significant (Fig. 4.14).

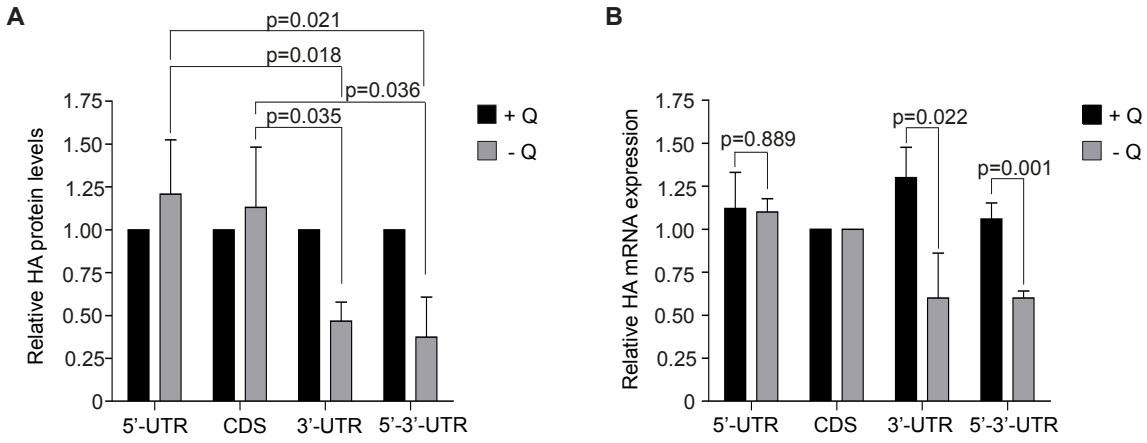

Figure 4.13: Glutamine starvation moderately decreases levels of exogenous *MYC* transcripts, when carrying the 3′UTR

A) Quantification of exogenous MYC protein levels from three independent experiments carried out as the representative one shown in Fig. 4.11C (both upper and lower bands were considered for the constructs containing the 5′UTR). The mean values of each construct + Q was set to 1 and used to normalize the corresponding mean values – Q (shown + SD). P-values were calculated using a two-tailed Student′s t-test.

B) qRT-PCR showing levels of HA-tagged *MYC* mRNA in dox-induced cells treated as in Fig. 4.10C. Each series was normalized to CDS values (+ or – Q). Results represent mean + SD of three independent experiments, each measured in technical triplicate. P-values were calculated using a two-tailed Student's t-test.

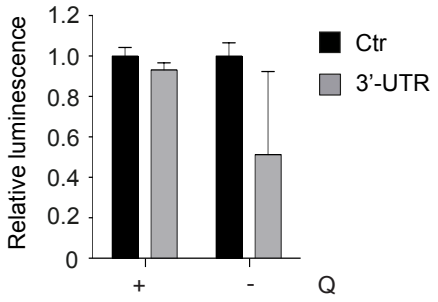

Figure 4.14: Luciferase assay confirms the glutamine-mediated regulation of *MYC* through its 3´-UTR

Cells were transfected with a double luciferase reporter vector containing the 3´-UTR of *MYC* (3´-UTR) or empty (Ctr). Forty-eight h post transfection, cells were starved for 6 h and luciferase activity was measured. The activity of renilla luciferase measured the glutamine effect on the 3´-UTR, while firefly luciferase activity was used as internal normalization control. The mean values of each construct + Q was set to 1 and used to normalize the corresponding mean values – Q. Results represent mean + SD of technical triplicates.

4.3 Investigation of post-transcriptional mechanisms of MYC regulation

4.3.1 p53 is not involved in regulating MYC

P53 is a central regulator of stress response and can be activated by different types of stimuli, including DNA damage or metabolic stress (Berkers et al, 2013). Depending on the stimulus and the extent of the damage, activation of p53 results in different outcomes, such as cell cycle arrest or apoptosis, possibly consistent with the response observed in HCT116 following glutamine starvation. Glutamine starvation has been shown to be an activating metabolic stimulus, able to induce p53 phosphorylation on Ser15 and stabilization, events required for allowing cell survival under stress conditions (Reid et al, 2013). P53, in turn, can trigger the activation of stress responsive pathways, which can potentially target *MYC* 3´-UTR (Sachdeva et al, 2009; Cannell et al, 2010; Lezina et al, 2013).

In order to check if p53 is involved in the glutamine-mediated regulation of MYC, protein levels were determined in both wild-type ($p53^{+/+}$) and *p53*-null ($p53^{-/-}$) HCT116

cells (Bunz et al, 1998). P53 was not detected by immuno blot in HCT116 *p53*$^{-/-}$, confirming the absence of the full-length protein in these cells. Phosphorylation on Ser15 was barely detected in wild-type cells and did not further increase following starvation (Fig. 4.15A). MYC was downregulated to the same extent in both cell types. Increased mTORC1 activity, as shown by increased phosphorylation of p70S6K and 4EBP1, was observed in *p53*-null cells, compared to wild-type cells, following decreased glutamine concentration (Fig. 4.15B).

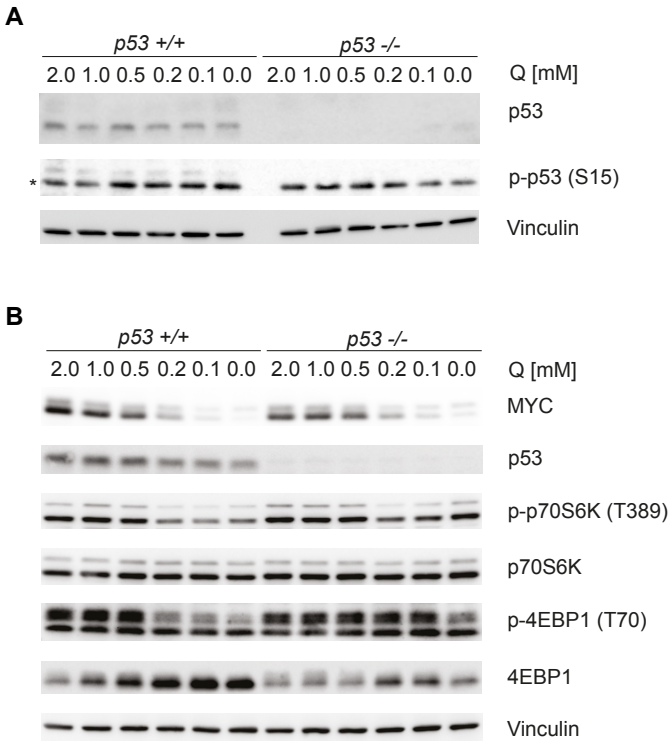

Figure 4.15: p53 is not involved in regulating MYC under glutamine starvation

A) IB showing levels of total and phosphorylated p53 in wild type (*p53*$^{+/+}$) or *p53* deficient (*p53*$^{-/-}$) cells cultured for 15 h in medium containing the indicated amounts of Q. Asterisk (*) indicates an unspecific band.
B) IB performed as in (A), showing levels of MYC and mTORC1 targets (n=2).

4.3.2 miRNAs do not play a major role in regulating MYC levels under glutamine starvation

Generally, the 3´-UTR is the preferential target of miRNAs, whose binding results in translational inhibition, due to interference of the miRNA-RISC complex with the

translational machinery. miRNAs are small non-coding RNAs which are often part of stress responsive circuits (Leung and Sharp, 2010).

Although the experiments shown in section 4.3.1 did not highlight an involvement of p53, which controls the expression of many miRNAs (Feng et al, 2011), other molecular pathways activated by glutamine starvation could be engaged. In order to evaluate the miRNA expression profile in HCT116 cells and if levels of specific miRNAs are changed following glutamine starvation, a miRNA-sequencing was performed. Specifically, miRNAs expressed in glutamine-starved cells (-Q) were compared with those expressed in control cells (+Q), aiming to find upregulated miRNA(s) which could account for the observed reduction in MYC protein levels. The starvation was performed for 2 hours, being MYC already downregulated at this time point (Fig. 4.16A). Three biological replicates per each condition were used. The results were analyzed by Carsten Ade, at the University of Wuerzburg. Between 36% and 52% of sequences were aligned to the available miRNA database miRbase 21 (Kozomara and Griffiths-Jones, 2014), which contained 2565 annotated miRNAs. After removal of lowly expressed miRNAs, a list of 886 miRNAs expressed in HCT116 was obtained. The correlation of biological replicates was assesed using scatter plots and Pearson's correlation coefficents. Replicates are highly correlated if they express a similar amount of transcripts. The Pearson´s correlation coefficient provides a measure of how well two samples are correlated. The higher is the correlation, the closer to one the Pearson´s coefficient is. The coefficient was higher than 0.99 in all cases, indicating high linear correlation of the replicates and reproducibility of the results (Fig. 4.16B). Around 72% of miRNAs was expressed between 0.4 and 5 $\log_2$ count per million (CPM). Among them miR-34-a and mir-34-b were found. Their expression was used as positive control, since already reported in literature in the same cell line (Kress et al, 2011) (Fig. 4.16C). The remaining 28% of miRNAs was expressed at higher levels (more than 5 $\log_2$ CPM). The most expressed miRNA was miR-21-5p, already shown to be upregulated in colorectal cancer and involved in promoting proliferation and metastasis (Kulda et al, 2010). miRNAs shown to define a colorectal cancer signature and to be upregulated in colorectal cancer compared to normal tissues were also expressed, e.g. miR-18a; miR-19a; miR-101; miR-106b; miR135b; miR200c (Wu et al, 2010). Differential expression

analysis revealed that levels of the majority of miRNAs were unchanged following starvation. None of the expressed miRNAs satisfied the criteria of statistical significance (q-value < 0.05). Twenty-five miRNAs were significantly regulated whit a p-value cut-off of 0.05 (red dots in Fig. 4.16C). A list of these miRNAs is presented in table 4.1. None of such miRNAs has been previously validated as targeting *MYC* (source: miRTarBase, Hsu et al, 2014; Chou et al, 2016), or found to be involved in metabolic processes. Thus, validation of this subset of miRNAs was not carried on.

A second criterion of selection was then applied, focusing on known miRNAs targeting *MYC*, independently of glutamine-induced changes in their levels. In order to obtain a limited list of miRNAs for performing further validation, only highly expressed miRNAs were selected, in order to increase the likelihood to find true candidates. Eleven miRNAs were selected, including miR-34a, which was used as positive control, although expressed at lower levels (Table 4.2).

Table 4.1: List of miRNAs selected according to significant changes +/- Q (p <0.05)

Annotated name (*)	Average log_2 CPM	-/+ Q Fold change [log_2]	p-value
hsa-miR-450a-2-3p&hsa-mir-450a-2	0.96	4.3	0.02
hsa-miR-1180-5p&hsa-mir-1180	0.90	4.1	0.03
hsa-miR-4435&hsa-mir-4435-1, hsa-miR-4435&hsa-mir-4435-2	2.14	1.47	0.02
hsa-miR-26a-2-3p&hsa-mir-26a-2	2.91	1.45	0.002
hsa-miR-6089&hsa-mir-6089-2, hsa-miR-6089&hsa-mir-6089-1	4.45	1.12	0.0006
hsa-miR-5100&hsa-mir-5100	4.44	0.67	0.038
hsa-miR-32-3p&hsa-mir-32	5.62	0.59	0.03
hsa-miR-22-3p&hsa-mir-22	11.4	0.6	0.01

* Annotated names from miRbase dataset.
Meaning of the complete miRNA identifier (example: hsa-miR-450a-2-3p):
hsa = organism (homo sapiens)
miR-450 = mature miRNA name, sequentially assigned according to the identification time
a-2 = distinct precursor sequences and genomic loci that express identical mature sequences. Lettered suffixes denote closely related mature sequences
3p (or 5p) = antisense (or sense) arm of the precursor from which the miRNA originates. (Ambros et al, RNA, 2003)

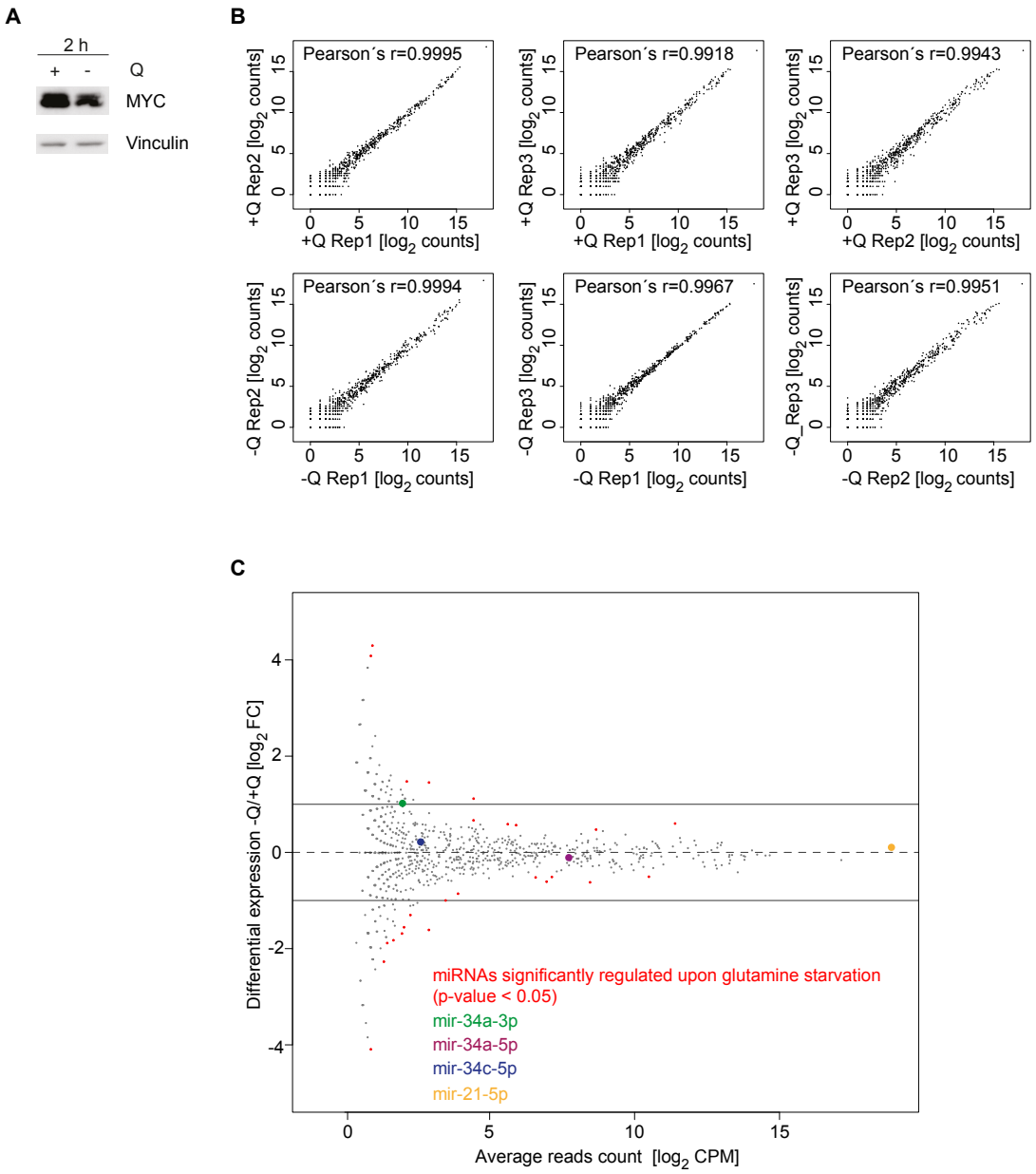

Figure 4.16: Expression levels of miRNAs do not change following glutamine starvation

A) IB showing MYC levels under the conditions used to perform the miRNA-sequencing.
B) Plots showing the read count correlation between replicates (n=3) in each experimental condition (upper panel = +Q; lower panel = -Q). The Pearson's coefficient is indicated in each plot.
C) MA-plot showing expression levels and differential expression of miRNAs between two experimental conditions (-Q *versus* +Q). Each dot represents a miRNA. Colored dots are described in the legend.

The involvement of selected miRNAs in regulating MYC levels following starvation was evaluated by using anti-miRs, i.e. oligonucleotides complementary to each miRNA and able to inhibit their function. The possible rescue of MYC levels following short starvation was checked in cells transfected with each anti-miR (Fig. 4.17). All the selected miRNAs were able to target *MYC* 3´-UTR, as shown by increased MYC protein levels in presence of glutamine in the transfected cells, compared to a negative control, i.e. cells transfected with a non-targeting sequence from *C. elegans*. However, glutamine starvation reduced MYC levels even in presence of the anti-miRs. Thus, this experiment did not provide hints that helped to identify a specific miRNA involved in the glutamine-mediated regulation of MYC, at least based on the criteria used for selecting candidate miRNAs.

Table 4.2: List of miRNAs targeting *MYC* selected according to the highest expression levels

miRNA	Sequence	Predicted miR site in *MYC* 3´-UTR	Normalized read count	-/+ Q Fold change [log_2]	adjusted P-value
let-7a-5p	UGAGGUAGUAGGUUGUAUAGUU	2017-2038	32381	-0.06	1
let-7f-5p	UGAGGUAGUAGAUUGUAUAGUU	2017-2038	39819	-0.07	1
let-7g-5p	UGAGGUAGUAGUUUGUACAGUU	2015-2038	32381	-0.05	1
miR-20a-5p	UAAAGUGCUUAUAGUGCAGGUAG	N.A.	24570		1
miR-21-5p	UAGCUUAUCAGACUGAUGUUGA	N.A.	742576	-0.09	1
miR-24-3p	UGGCUCAGUUCAGCAGGAACAG	2337-2358	1190	0.37	1
miR-26a-5p	UUCAAGUAAUCCAGGAUAGGCU	N.A.	11588	0.19	1
miR-34a-5p	UGGCAGUGUCUUAGCUGGUUGU	2015-2036	358	-0.11	1
miR-98-5p	UGAGGUAGUAAGUUGUAUUGUU	2020-2038	2215	0.07	1
miR-148a-3p	UCAGUGCACUACAGAACUUUGU	N.A.	17623	-0.16	1
miR-429	UAAUACUGUCUGGUAAAACCGU	2222-2244	4509	0.30	1

N.A. = not available

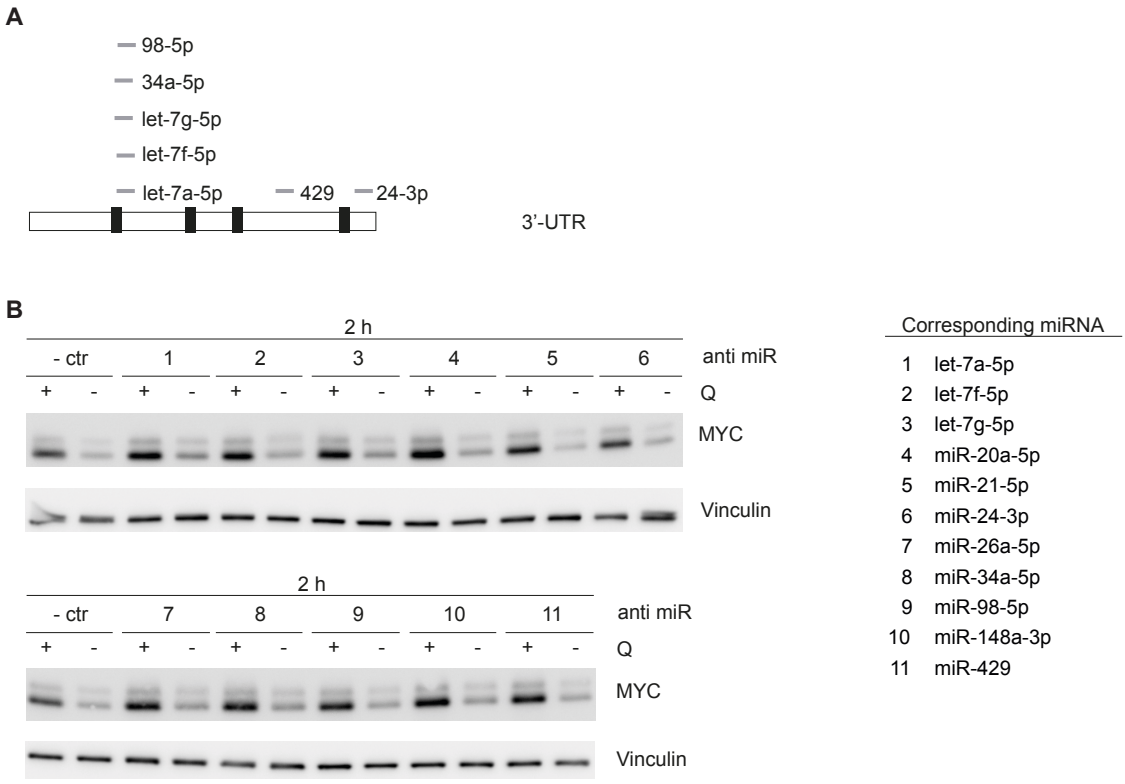

Figure 4.17: Interfering with the activity of selected miRNAs does not rescue MYC levels under starvation

A) Schematic view of *MYC* 3´-UTR. Black boxes represent the AU-rich elements; gray dashes indicate the miRNAs used in (B) and their binding position. Binding sites were predicted using www.microRNA.org (Betel et al, 2008).
B) HCT116 cells were transfected with the indicated anti-miRs and a negative control. Seventy-two h post transfection cells were starved for 2 h and MYC levels detected by IB (n=3).

4.3.3 Identification of the glutamine-responsive sequence in the 3´-UTR

Although a specific molecular player involved in regulating *MYC* translation could not be established, another approach used to gain mechanistic indications consisted in identifying the element responsible for the glutamine-mediated regulation of MYC within its 3´-UTR. A series of deletions of the MYC 3´-UTR was created by successively deleting around 100 nucleotides from the end of the sequence. Four constructs were obtained, each comprising the *MYC* coding sequence and a deleted 3´-UTR. Each deletion progressively lacked one to four AU-rich elements (Fig. 4.18A).

The same inducible system presented in Fig. 4.11 was used and the response of each construct to glutamine starvation was tested. As expected, the exogenous MYC comprising only the CDS was stable following starvation, while the exogenous protein including the entire 3´-UTR was downregulated. Interestingly, only the exogenous MYC carrying the shortest deletion in the 3´-UTR (Δ 2262-2366) was downregulated following starvation, while the levels of those carrying the next three deletions were unaffected (Fig. 4.18B). Thus, this experiment allowed for the mapping of a specific region within MYC 3´-UTR responsible for its glutamine-mediated downregulation. This region lies between the nucleotides 2127 and 2262 of *MYC* mRNA (dashed lines in Fig. 4.18A).

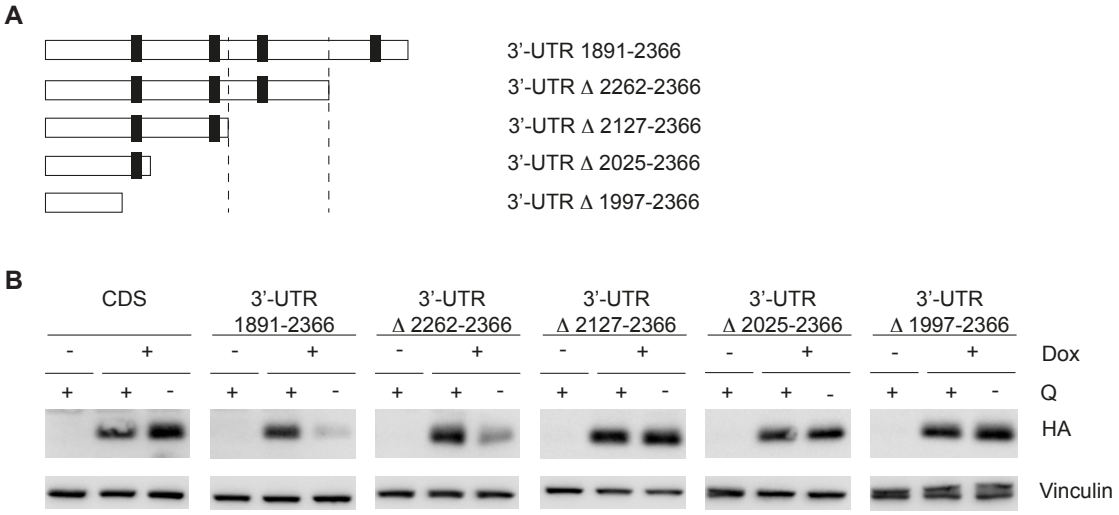

Figure 4.18: A specific region of *MYC* 3´-UTR mediates its response to glutamine

A) Scheme depicting the deleted constructs used in (B). Numbers refer to the annotated *MYC* sequence NM_002467.4. Vertical dashed lines indicate the region responsible for MYC regulation. Black boxes indicate the position of the AU-rich elements (AUUUA sequences) present in *MYC* 3´-UTR.
B) IB showing levels of exogenous MYC in GFP-sorted cells expressing the indicated construct. Cells were dox-induced for 2 h before undergoing starvation for 15 h (n=2).

4.4 Dissection of the glutamine-derived stimulus sensed by the 3´-UTR

Glutamine provides both carbons and nitrogen group for the biosynthesis of many metabolites (see Fig. 1.4). Consistently, starving cells for 15 hours increased the levels of reactive oxygen species (ROS), likely as consequence of decreased glutathione

(GSH) production. Figure 4.19A shows a right shift in the FACS-detected fluorescent signal, indicating ROS levels, in glutamine-starved cells. Appropriate positive (H_2O_2 treated cells) and negative (unstained cells) controls were used to define the percentage of fluorescent positive cells (Fig. 4.19B).

Moreover, glutamine starvation decreased the concentration of TCA cycle intermediates, polyamine and nucleotides. Metabolite concentrations were determined by gas-chromatography mass-spectrometry (GC-MS) and direct infusion MS. Those measurements were performed by Nadine Royla and Stefan Kempa, at the Institute for medical system biology in Berlin and results are presented in Dejure et al, 2017 (submitted).

Hence, the 3´-UTR of *MYC* could sense decreased levels of one or more glutamine-derived substrate(s), rather than of glutamine itself. Accordingly, the candidate substrate should be able to counteract the glutamine-induced downregulation of MYC, or mimic its upregulation observed following the re-addition of glutamine after starvation. MYC rescue was therefore used as read-out to test this hypothesis.

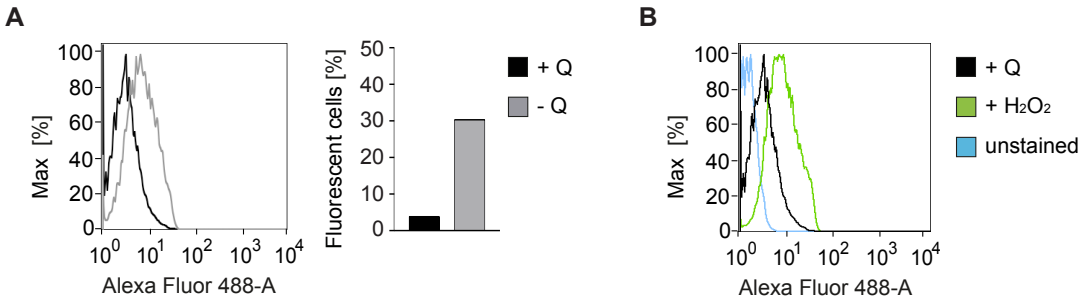

Figure 4.19: Glutamine starvation increases oxidative stress

A) Cells were starved for 15 h, stained with 2',7'-dichlorofluorescin diacetate (DCFDA) and the intensity of fluorescence, proportional to the level of ROS, was measured by FACS. The right panel shows the quantification of a representative experiment (n=2).
B) Plot showing the intensity of fluorescence in the controls used in the experiment.

4.4.1 Supplementing nucleosides rescues MYC under starvation

Substrates belonging to three major glutamine-dependent pathways (TCA cycle, nucleotides biosynthesis and glutathione biosynthesis) were used to check MYC rescue. Dimethyl-α-ketoglutarate and dimethyl-succinate are cell permeable forms of α-

ketoglutarate and succinate, two intermediates of the TCA cycle. Sodium pyruvate and glutamate can also enter the TCA cycle, as acetyl-CoA and α-ketoglutarate, respectively. Transporters for pyruvate (SLC16A1; SLC16A7) and glutamate (SLC1A1; SLC1A3) are expressed in HCT116 cells, as assessed from the transcriptomic profile (see 4.7). A mix of four ribonucleosides (adenosine, guanosine, uridine and cytidine) and one deoxynucleoside (thymidine) was used as analogue of nucleotides. Lack of phosphate groups allows for the entrance of nucleosides inside the cell, a process facilitated also by specific transporters (e.g. SLC28A2; SLC28A3; SLC43A3), which are expressed in HCT116. Finally, a cell-permeable form of glutathione and the antioxidant N-acetyl cysteine, which mimic the ROS scavenger effects of glutathione, were used.

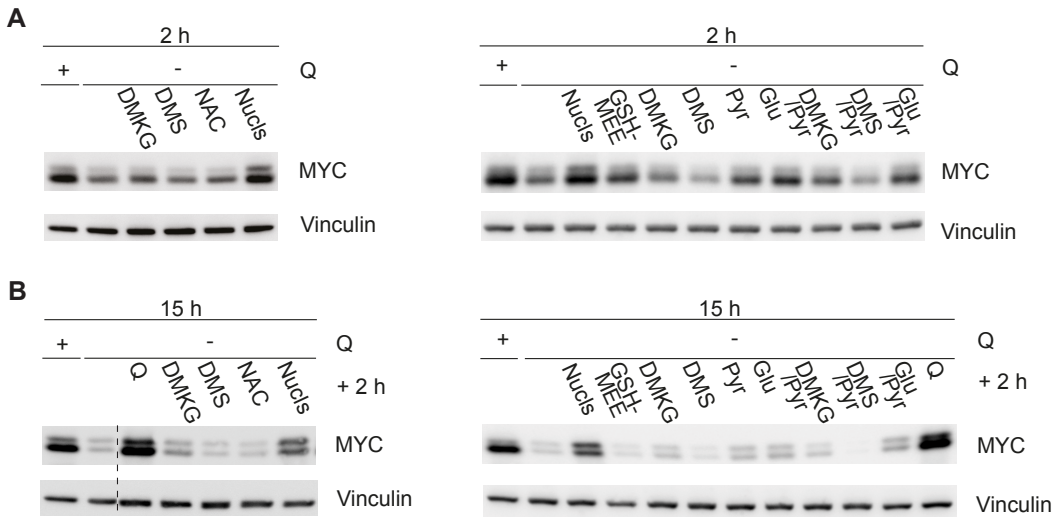

Figure 4.20: Re-addition of nucleosides restores MYC levels

A) Cells were starved for 2 h in presence of the indicated substrates. Left panel: DMKG (Dimethyl-α-ketoglutarate), DMS (dimethyl-succinate), NAC (N-Acetyl-Cysteine), Nucls (nucleoside mix), a representative result is shown (n=2); Right panel: GSH-MEE (glutathione reduced ethyl ester); Pyr (sodium pyruvate); Glu (glutamate); Q, alone or in combination.
B) Cells were starved for 15 h and, where indicated, substrates were added after starvation for 2 h, alone (left panel, a representative result is shown (n=2)) or in combination (right panel).

As expected, MYC was downregulated following short glutamine starvation. Only supplementation of nucleosides, and not of any other substrate, rescued MYC protein levels (Fig.4.20A). The result was confirmed using a different experimental setup. As

shown in Fig. 4.20B, MYC was upregulated only when nucleosides were added after starvation. The extent of the rescue effect mediated by the nucleosides was lower than the upregulation observed following glutamine re-addition, indicating the co-existence of minor potential additional mechanisms of regulation.

4.4.2 Adenosine is the specific stimulus sensed by the 3´-UTR of *MYC*

As a nucleoside mixture clearly rescued MYC protein levels, such experiment was repeated using single ribo- and deoxynucleosides, in order to further disentangle the stimulus behind this regulation. Among all nucleosides, a purine mix of adenosine and guanosine or adenosine alone rescued MYC, both under short glutamine starvation (Fig. 4.21A) and addition after starvation (Fig. 4.21B).

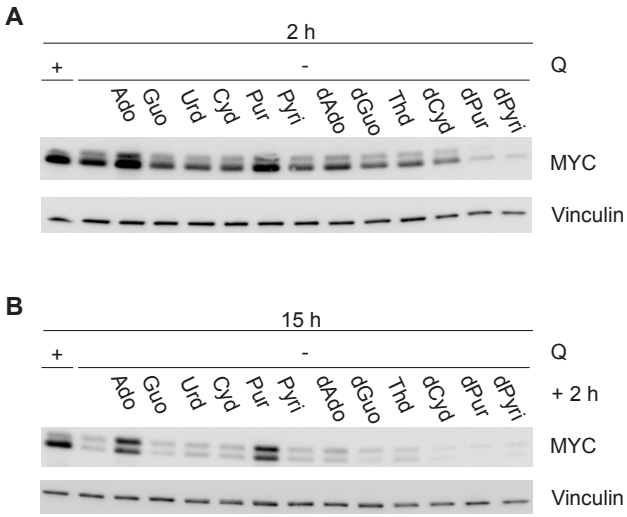

Figure 4.21: MYC levels are rescued by adenosine

A) Cells were starved for 2 h in presence of the indicated substrates: Adenosine (Ado); Guanosine (Guo); Uridine (Urd); Cytidine (Cyt); Purine mix (Pur); Pyrimidine mix (Pyri); deoxyadenosine (dAdo); deoxyguanosine (dGuo); Thymidine (Thd); deoxycytidine (dCyd); deoxypurine mix (dPur); deoxypyrimidine mix (dPyri). A representative result is shown (n=3).
B) Cells were starved for 15 h and, where indicated, single nucleosides were added after starvation for 2 h. A representative result is shown (n=2).

In order to proof that adenosine is the specific stimulus that mediates MYC regulation according to the availability of glutamine, the effect of adenosine on MYC translation was checked. Pulse labeling and immunoprecipitation experiments, performed as shown

in Fig. 4.10, confirmed that the presence of adenosine in medium lacking glutamine restored MYC translation (Fig. 4.22A).

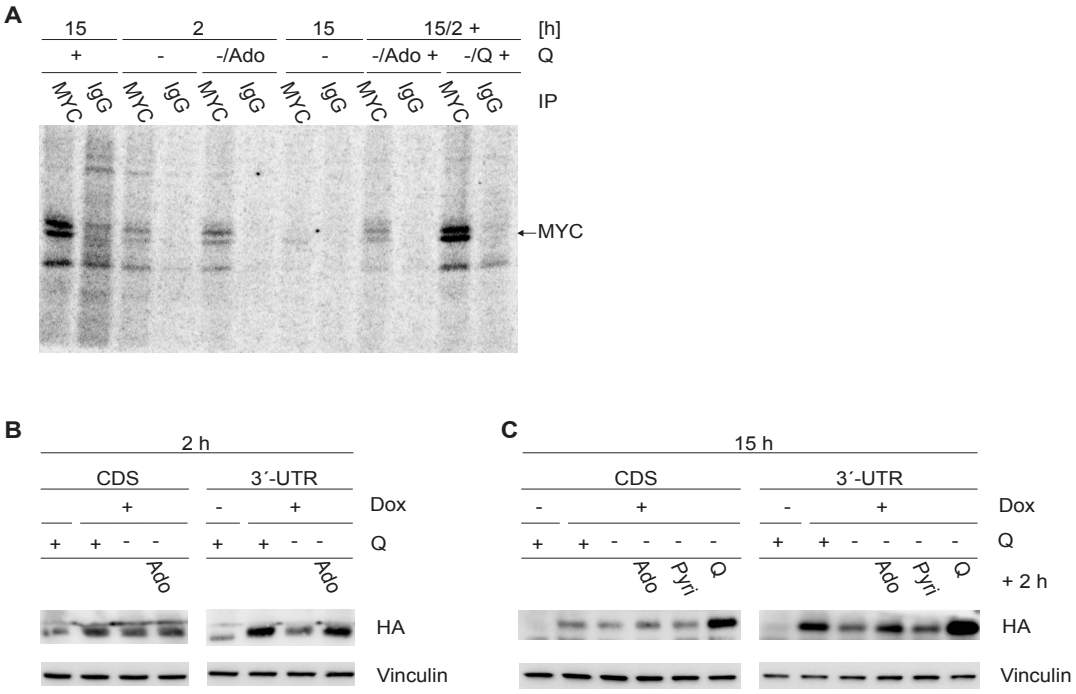

Figure 4.22: Adenosine rescues MYC translation in a 3´UTR-dependent manner

A) Effect of adenosine on MYC protein synthesis, assessed after pulse with ^{35}S-Methionine (experimental details as described in Fig. 4.10). Two additional conditions are shown: cells were starved for 2 hrs in the presence of Ado and Ado was added to the medium for 2 h after 15 h of glutamine starvation (n=2).
B) GFP-sorted HCT116 cells expressing the indicated constructs were dox-induced for 2 hrs. Starvation was performed for 2 h in the presence of Ado, as indicated. Exogenous MYC levels were detected using an anti-HA antibody. A representative result is shown (n=3).
C) Cells were dox-induced as in (A), starved for 15 h and, where indicated, Ado, Pyri or Q were added for 2 h after starvation. A representative result is shown (n=2).

Moreover, the rescue effectively depended on the presence of the 3´-UTR of *MYC*, as assessed by checking the effect of adenosine on two inducible constructs presented in Fig. 4.11A (CDS and 3´-UTR). Supplementing adenosine to glutamine-starved cells rescued exogenous MYC only in the presence of the 3´-UTR (Fig. 4.22B). Similarly, addition of adenosine, but not a pyrimidine mixture (cytidine and uridine), increased MYC levels after starvation only when the 3´-UTR construct was used. Re-addition of

glutamine raised exogenous MYC levels independently of the presence of the 3´-UTR (Fig. 4.22C).

4.5 Evaluation of biological downstream MYC downregulation

The mechanism of glutamine-mediated regulation of MYC is dependent upon its 3´UTR. Although this element is well recognized to influence *MYC* mRNA stability (see 1.1.2.2), ectopically expressed constructs usually described in the literature do not include it, potentially uncoupling the stress-induced effects on MYC from cellular responses.

4.5.1 Presence of the 3´-UTR rescues cell viability under starvation when MYC-ER is expressed

In order to analyze differences due to the presence of the 3´-UTR in exogenous *MYC* transgenes, a MYC-ER construct, containing or not the 3´-UTR, was expressed in HCT116 cells. In order to avoid any underestimation or loss of effect due to low expression levels of the *MYC* transgenes (as observed for the dox-inducible ones, see Fig. 4.11B), a spleen focus-forming virus promoter (SFFV)-driven vector (pRRL) was used to express high levels of MYC (Wiese et al, 2015). HCT116 cells were infected with MYC-ER, MYC-ER-3´-UTR and empty vector (EV) as control. MYC-ER is constitutively expressed, but only activated following treatment with 4-hydroxytamoxifen (OHT), which induces a conformational change in the ER, allowing the fused protein to function (Eilers et al, 1989). As expected, while the endogenous MYC was downregulated following glutamine starvation, MYC-ER levels were affected only when the 3´-UTR was present (Fig. 4.23A), consistently with previous results (Fig. 4.11C). Independently of glutamine, levels of endogenous MYC were lower when MYC-ER (both with or without 3´UTR) was activated, compared to those observed in control cells. This is an expected effect due to negative auto-regulation of MYC, i.e. decrease of endogenous form when an exogenous one is expressed (Penn et al, 1990), and commonly used as read-out of MYC-ER activation. A decreased number

of viable cells was observed when starved for glutamine in presence of activated MYC-ER. This result is consistent with previous reports showing MYC-dependent sensitization to apoptosis induced by stress stimuli (see 1.1.1.3). Strikingly, the presence of the 3´-UTR could significantly revert this effect, prolonging cell survival over time (Fig. 4.23B, 4.23C). This effect was largely due to decreased apoptosis, as assessed by PI FACS analysis (Fig. 4.23D).

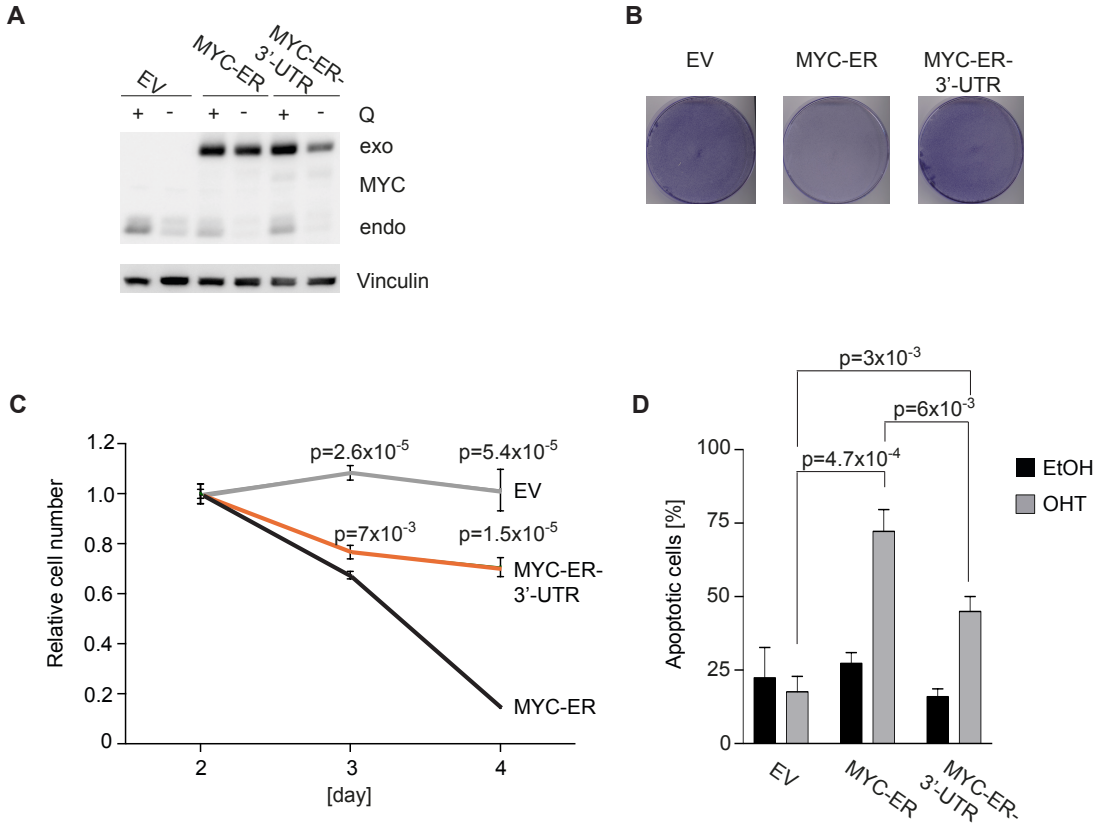

Figure 4.23: The presence of the 3´-UTR reduces starvation-induced apoptosis in cells expressing MYC-ER

A) IB of HCT116 cells stably expressing the indicated MYC-ER constructs or empty vector (EV) as control. MYC-ER activity was induced overnight with 20 nM OHT, followed by 24 h Q starvation, in presence of OHT. The upper band indicates exogenous (exo) and the lower band endogenous (endo) MYC. A representative result is shown (n=4).
B) Cells were cultured as in (A) in Q-depleted medium. Crystal violet staining was performed after 48 h of starvation.
C) Cells were cultured as in (A). At the indicated time points cells were fixed, stained with crystal violet and quantified. Each sample was normalized to the value obtained after 48 h of starvation. Each point represents the mean ± SD of three biological replicates. P-values were calculated using a two-tailed Student´s t-test, comparing EV or MYC-ER-3´-UTR to MYC-ER at each time point.
D) PI FACS of HCT116 cells Q starved for 72 h. Results represent mean + SD of biological triplicates. P-values were calculated using a two-tailed Student´s t-test.

4.6 Transcriptional consequences associated with the glutamine-mediated regulation of MYC: evaluation of gene expression

The biological outcome associated with deregulated MYC activity is mainly due to MYC-induced transcriptional changes. Thus, the aim of this research section was to identify genome-wide transcriptional effects driven by glutamine starvation and, among them, those directly linked with MYC activity. MYC-ER expressing cells provide a suitable system to evaluate MYC-mediated effects under glutamine starvation. On one side, keeping MYC levels high during starvation is expected to revert effects associated with MYC downregulation, on the other side, elucidating why MYC levels are dependent upon the glutamine supply can help understanding how overexpressed MYC sensitizes cells to apoptosis.

4.6.1 MYC-ER increases expression of S-phase related genes, independently of glutamine

Glutamine-induced changes in steady-state mRNAs levels, through modulation of MYC levels, were evaluated. mRNA-sequencing was performed in order to obtain a comprehensive view of transcriptional profiles under different conditions. Six experimental conditions were chosen and performed in biological triplicates. A representative blot for replicate #2 is shown in Fig. 4.24.

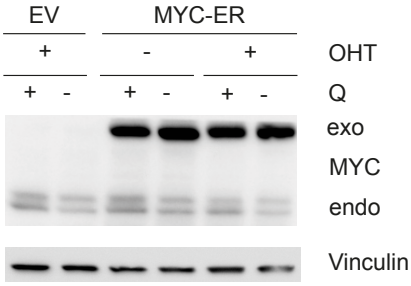

Figure 4.24: Experimental conditions chosen for performing RNA-seq

EV or MYC-ER expressing cells were treated overnight with 100 nM OHT or EtOH as control. Cells were starved for 24 hrs in medium containing OHT or EtOH, as indicated. At the end of the starvation time, cells were harvested and split into two aliquots: one was used to check MYC levels on IB, the other one was used for extracting RNA and performing mRNA-sequencing.

HCT116 cells, expressing a control EV or MYC-ER, were starved for 24 hours. This time point was selected both for detecting transcriptional changes, possibly not evident at shorter time points, and, at the same time, to avoid side effects due to prolonged starvation, such as MYC-ER-induced apoptosis. EtOH- treated MYC-ER expressing cells were used as control, in order to rule out transcriptional changes purely due to the leakiness of the construct, i.e. activation in absence of OHT, rather than to a real MYC-mediated effect.

Sequencing results were analyzed by Susanne Walz, at the bioinformatics core unit of the Comprehensive Cancer Center Mainfranken.

The analysis showed that 18,912 genes are expressed in HCT116 cells. A paired comparison of the biological replicates was performed in order to verify their correlation. The Spearman´s coefficient was higher than 0.99 for all replicates, indicating good monotonic correlation, as exemplary shown in Fig. 4.25A. Differential expression analysis was then performed to look for distinctive transcriptional regulations between two conditions. To analyze if the MYC-ER construct is leaky or if OHT treatment has an effect on gene expression several pairwise comparisons of gene expression changes were performed: regulation of MYC-ER OHT *versus* MYC-ER EtOH was plotted against regulation of MYC-ER OHT *versus* EV OHT (Q starvation: Fig 4.25B left, non-starved Fig 4.25B middle) as well as the effect of glutamine starvation in MYC-ER EtOH and EV OHT HCT116 cells (Fig 4.25B right). All comparisons show strong correlations suggesting low levels of leakiness of the MYC-ER construct and negligible off-target effects of OHT treatment. Therefore, for further analyses the EV OHT condition is used as control.

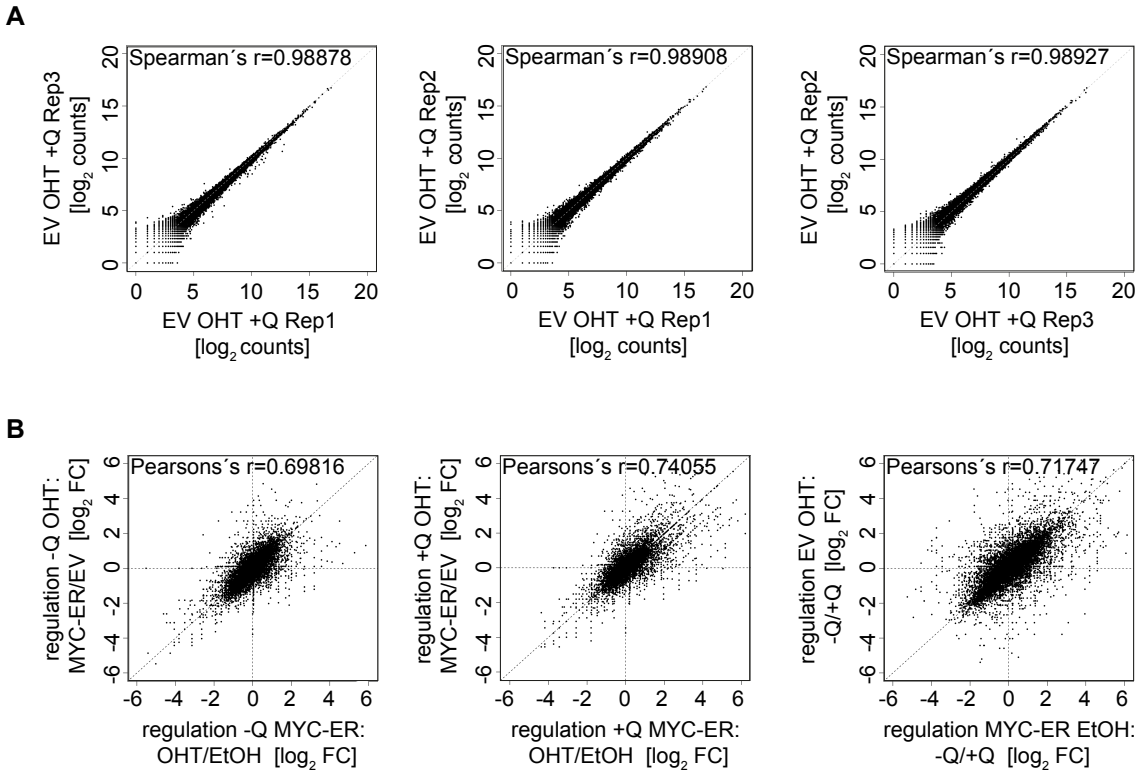

Figure 4.25: Biological replicates used for RNA-sequencing show a strong transcriptional correlation between each other

A) Scatterplots showing positive correlation of normalized counts (log_2) between three biological replicate (experimental condition: EV OHT +Q). Spearman´s correlation coefficient is shown in each plot.
B) Scatterplots showing correlation of differential regulations (log_2 FC) between the indicated conditions. Pearson´s correlation coefficient is shown in each plot.

Differentially expressed genes were visualized using MA-plots, which compare gene expression and regulation between two conditions. All expressed genes are represented by a black dot, while significantly regulated genes are depicted in red. Statistical significance was defined by a q-value lower than 0.05 (Fig. 4.26). Glutamine starvation induces deep transcriptional changes. Around 47% of all expressed genes were significantly up or downregulated in glutamine-starved samples, either in the control (EV) or in MYC-ER expressing cells, as compared to their glutamine-containing counterparts (red dots in Fig. 4.26A and B).

Overexpressing MYC in presence of glutamine, i.e. with high levels of endogenous MYC, differentially regulated around 15% of all genes, while maintaining high levels of

MYC under glutamine starvation, i.e. with activated MYC-ER, significantly regulates around 21% of all genes, as compared to each EV situation (Fig. 4.26C and D).

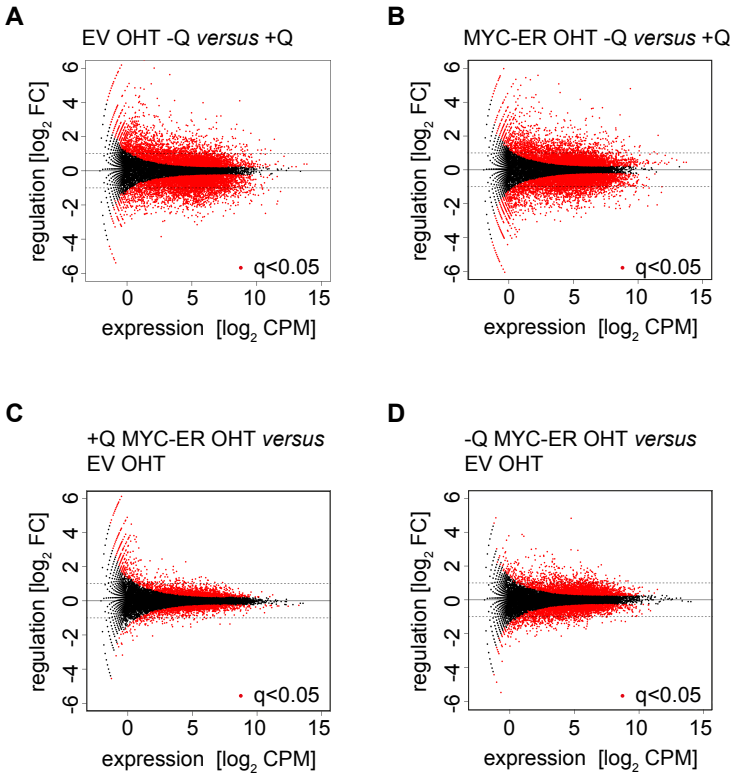

Figure 4.26: Glutamine and MYC-induced differential transcriptional regulation

A) - D) MA-plots showing differentially expressed genes in the indicated conditions. Each expressed gene is represented by a black dot. Significantly up- or down-regulated genes are shown in red (see legend in the lower right part).

Gene sets enrichment analyses (GSEA) were performed in order to better understand the biological pathways regulated in the different conditions. Briefly, GSEA ranks a gene list by comparing gene expression of two conditions of interest and finds previously defined gene sets that are enriched at both ends of the ranked list. Specifically, the molecular signature database C2 (curated gene sets) was used for the analysis; such signature database contains 4,729 gene sets, mainly from publications or online pathway databases (Subramanian et al, 2005). Two parameters were considered to define significantly enriched gene sets: the normalized enrichment score (NES) and the false discovery rate (FDR) q-value. The NES expresses the ranking of a certain gene

set in the whole ranked gene list. The higher the absolute NES value, the more genes belonging to a certain gene set are upregulated (negative NES, in this analysis) or downregulated (positive NES) in the experimentally-derived dataset, from comparison of two conditions (e.g. +Q *versus* –Q). Gene sets with a multiple-testing corrected p-value (FDR q-value, Benjamini-Höchberg procedure) lower than 0.25 are significantly enriched.

Table 4.3: Gene sets significantly regulated (FDR q-value <25%)

A) Compared conditions: EV OHT -Q *versus* EV OHT +Q
(Evaluation of glutamine-mediated effect in presence of endogenous MYC)

Regulation	Representative gene sets		
	Name (rank position)	NES	q-value
Up -Q	Krige: Amino acid deprivation (1)	-2.67	<0.001
	Gargalovic: Response to oxidized phospholipids turquoise up (22)	-2.20	0.001
	Reactome: Unfolded protein response (193)	-1.52	0.139
Down -Q	Reactome: S phase (42)	2.65	<0.001
	KEGG: Pyrimidine metabolism (215)	2.10	<0.001
	Reactome: Pyruvate metabolism and citric acid tca cycle (276)	2.00	<0.001

B) Compared conditions: MYC-ER OHT -Q *versus* MYC-ER OHT +Q
(Evaluation of glutamine-mediated effect in presence of exogenous MYC)

Regulation	Representative gene sets		
	Name (rank position)	NES	q-value
Up -Q	Krige: Amino acid deprivation (6)	-2.57	<0.001
	Gargalovic: Response to oxidized phospholipids turquoise up (40)	-2.06	0.003
	Reactome: Unfolded protein response (54)	-1.95	0.011
Down -Q	Reactome: S phase (44)	2.65	<0.001
	KEGG: Pyrimidine metabolism (468)	1.66	0.030
	Reactome: Pyruvate metabolism and citric acid tca cycle (317)	1.85	0.005

C) Compared conditions: MYC-ER OHT +Q *versus* EV OHT +Q
(Evaluation of MYC-mediated effects in presence of glutamine)

Regulation	Representative gene sets		
	Name (rank position)	NES	q-value
Up +MYC-ER	Schuhmacher: MYC targets up (3)	-2.93	0.000
	Coller: MYC targets up (10)	-1.94	0.038
	Kim: MYC amplification targets up (20)	-1.69	0.102
Down +MYC-ER	PID: Integrin1 pathway (5)	2.19	0.000
	Wu: Cell migration (19)	2.01	0.002
	Kegg: Focal adhesion (209)	1.70	0.028

D) Compared conditions: MYC-ER OHT -Q *versus* EV OHT -Q
(Evaluation of MYC-mediated effects in absence of glutamine)

Regulation	Representative gene sets		
	Name (rank position)	NES	q-value
Up +MYC-ER	Schuhmacher: MYC targets up (2)	-3.34	<0.001
	KEGG: DNA replication (11)	-2.52	<0.001
	KEGG: Pyrimidine metabolism (44)	-2.17	0.001
Down +MYC-ER	PID: Integrin1 pathway (97)	1.88	0.008
	Wu: Cell migration (31)	2.03	0.003
	KEGG: Focal adhesion (44)	1.98	0.004

Predictably, glutamine starvation upregulated genes mainly belonging to stress-associated signatures, e.g. unfolded proteins response, transport of metabolites, and downregulated genes involved in biosynthetic processes. Table 4.3A provides examples of differentially regulated gene sets in this condition. A comparable number and type of gene sets were regulated in the same way also following MYC-ER induction, as presented in table 4.3B (+Q *versus* –Q: 292 up and 952 down (EV OHT), 331 up and 990 down (MYC-ER OHT)). The same gene sets shown in table 4.3A are reported in order to highlight similar ranking positions. Signatures usually associated with MYC overexpression were regulated also in this experimental system, in the presence of glutamine (EV OHT *versus* MYC-ER OHT: 52 up and 1377 down, table 4.3C). Finally, gene sets differentially regulated under starvation, in the presence or absence of ectopically expressed MYC, were compared, in order to better evaluate the contribution of MYC in this condition and possibly explaining why cells need to downregulate it. Ectopic MYC expression led to a significant downregulation of the same gene sets both in the presence or absence of glutamine (1377 and 1166, respectively, table 4.3D). A higher number of gene sets was found to be significantly upregulated by MYC following starvation (342), rather than in presence of glutamine (52). In addition to signatures associated with MYC overexpression, gene sets linked to metabolic processes (e.g. nucleotides or amino acids metabolism) or regulation of cell cycle (e.g. G1/S transcription; E2F-mediated regulation of replication) were found to be significantly upregulated. Taken together, these data highlight transcriptional changes possibly consequences of the glutamine-induced changes in MYC protein levels

4.6.2 Transcriptional changes linked with MYC-ER activation under starvation do not directly correspond to changes in the cell cycle profile

Signatures associated with genes expressed in S-phase, including those related to metabolic processes, were upregulated when MYC was ectopically expressed. In order to verify whether these transcriptional changes underline differences in the cell cycle profile, a BrdU PI FACS analysis was performed in cells expressing MYC-ER under glutamine starvation. Consistent with previous results, HCT116 cells (expressing EV) arrested in G1/S phase when deprived of glutamine. Around 20% of cells underwent apoptosis after two days of starvation, as assessed by the percentage of cells in sub-G1, but this number did not significantly increase after six days of starvation. Activation of MYC-ER under starvation did not further push cells to enter S-phase, as detected by BrdU incorporation, but rather shifted over time the cell population towards the sub-G1 cloud, i.e. PI content lower than 2n (Fig. 4.27). Thus, although ectopic MYC activity drives expression of S-phase related genes, this experiment did not show evidence of changes in the cell cycle phases.

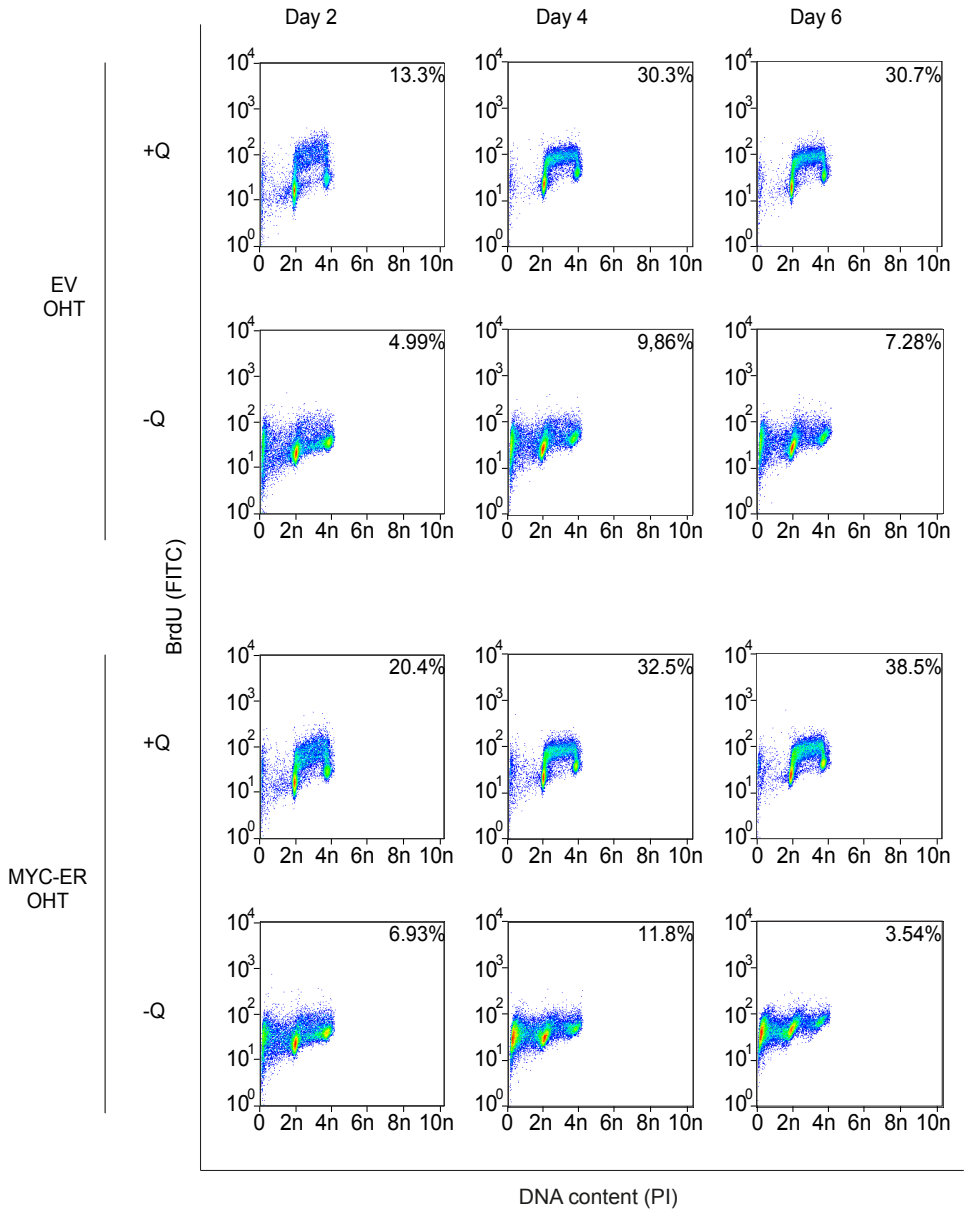

Figure 4.27: MYC-ER activation does increase S-phase entry of glutamine-starved cells

EV or MYC-ER expressing cells were treated with 100 nM OHT for 24 h. Starvation was performed for the indicated time points in the presence of OHT. Cells cultured in medium containing Q were split after two days to avoid becoming too confluent. One h before the end of each time point, cells were labeled with BrdU for subsequent analysis by FACS. Numbers inside each square indicate the percentage of BrdU positive cells.

4.6.2 Ectopic MYC expression does not affect main metabolic pathways involving glutamine

Gene sets relative to metabolic processes, such as TCA cycle of nucleotide biosynthesis, were also upregulated by MYC-ER following starvation. Glutamine starvation induces a general decrease of glutamine-derived metabolite concentrations and an increase of ROS levels (see 4.4). Since the expression of enzymes involved in these processes is controlled by MYC, MYC downregulation can contribute to altering metabolite levels. Conversely, ectopic MYC activity pushes expression of these genes, which could induce a critical depletion of metabolites.

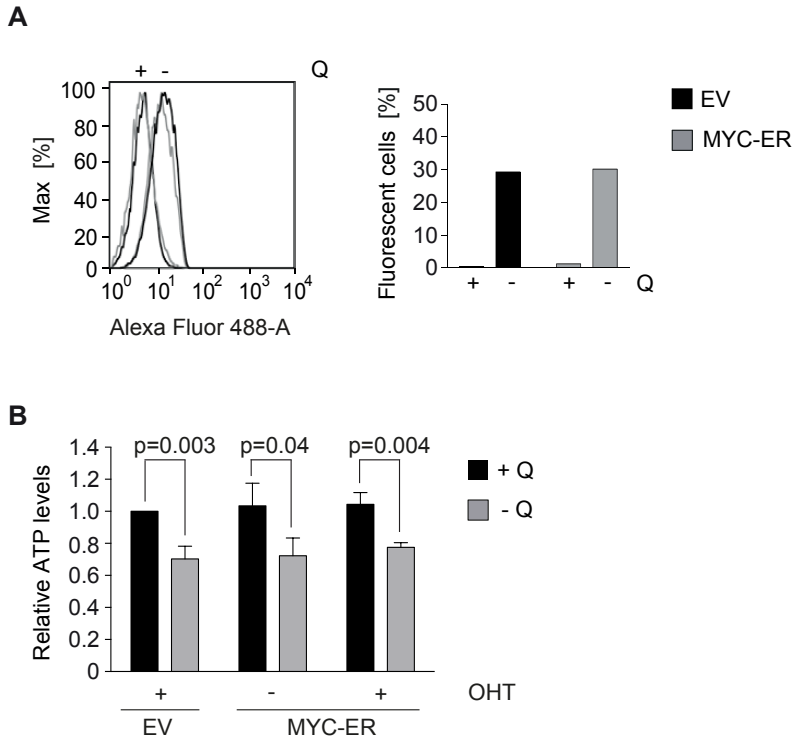

Figure 4.28: MYC activation following starvation does not further change ROS or ATP levels

A) EV- or MYC-ER-expressing cells were treated overnight with 100 nM OHT and starved for 24 h, keeping OHT in the medium. At the end of the starvation time, cells were stained with DCFDA and the intensity of fluorescence measured by FACS. The right panel shows the quantification of a representative experiment (n=2).

B) Cells were treated as in (A). After 24 h, ATP levels were determined by a luminometric assay. Values are shown relative to EV +Q condition. Results represent mean + SD of three independent experiments, each measured in technical triplicate. P-values were calculated using a two-tailed Student´s t-test.

Differences in the levels of ROS, indicator of the redox cellular state, and of ATP, indicator of the energetic cellular state, were therefore checked. Consistent with data shown in Fig. 4.19, ROS levels, as indicated by the percentage of fluorescence measured by FACS, were increased in cells starved for 24 hours, compared to non-starved control cells. However, no difference was detected between control cells (EV) and MYC-ER expressing cells, both treated with OHT (Fig. 4.28A). Since MYC can push energy-demanding biosynthetic processes, high MYC levels under starvation could lead to an unsustainable depletion of ATP. Thus, steady-state ATP levels after 24 hours of glutamine starvation were measured. Glutamine starvation led to a reduction in ATP levels of around 20%. The decrease was not further emphasized by MYC-ER activation (+ OHT), compared to control cells or EtOH-treated MYC-ER expressing cells (Fig. 4.28B).

4.6.3 Ectopic MYC expression does not activate AMPK

The steady-state ATP measurement shown in Fig. 4.28B could not exclude more dynamic changes in the ATP/AMP ratio. Since increased AMP levels activate AMPK (Hardie, 2007), the phosphorylated status of this homeostatic sensor was checked. Empty vector or MYC-ER expressing cells were glutamine starved for 24 or 72 hours. As expected, exogenous MYC levels were maintained high following glutamine starvation and MYC-ER activation worked, as estimated by repression of the endogenous form. Basal activation of AMPK was detected even in presence of glutamine, but was not further increased either by starvation or by MYC-ER activation, at both time points. Glucose starvation was used as positive control. Increased AMPK phosphorylation only occurs following glucose depletion for 48 hours (Fig. 4.29).

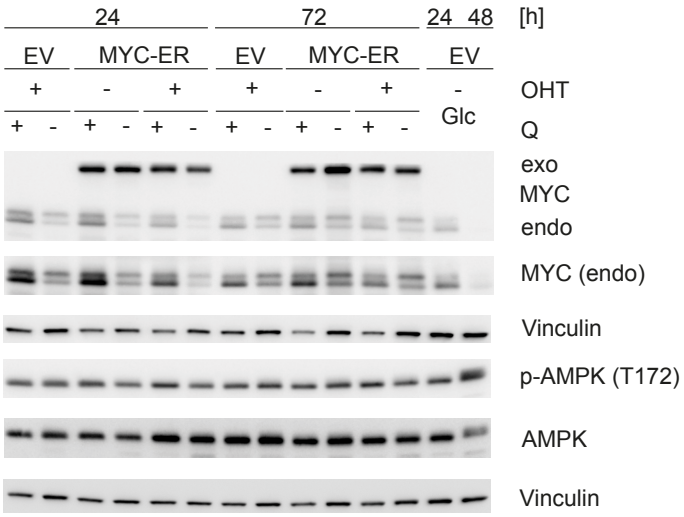

Figure 4.29: AMPK is not activated in response to high MYC levels under glutamine starvation

Cells were treated overnight with 100 nM OHT or EtOH as control and starved for Q or Glc for the indicated time points. When starved for 72 h, medium was changed after 48 h.
Note that a higher number of cells was plated when glucose starvation was performed, in order to account for cell loss due to increased cell death. The indicated proteins were detected by IB. A representative result is shown (n=3).

4.7 Transcriptional consequences associated with the glutamine-mediated regulation of MYC: evaluation of RNA Polymerase II function

MYC-mediated transcriptional regulation can occur at different steps. Depending on the studied cell system, MYC has been shown to promote both the loading of RNA Polymerase II (RNAPII) at promoter regions (Walz et al, 2014) and the elongation step (Rahl et al, 2010; Lin et al, 2012).
The rapid change in MYC levels, dictated by glutamine availability, could therefore modulate key transcriptional steps.

4.7.1 Glutamine starvation affects RNA Polymerase II function in a MYC-dependent manner

In order to test if changes in MYC levels modify RNAPII activity, chromatin immune precipitation (ChIP) was performed to visualize RNAPII binding and elongation both at specific loci or genome-wide (ChIP-sequencing). Specifically, two different antibodies recognizing RNAPII were used: the first one binds to the N-terminal domain and is an indicator of total RNAPII; the second antibody recognizes the phosphorylated serine 2, in the C-terminal domain (pSer2RNAPII). This modification is a specific indicator of elongating RNAPII (Jonkers and Lis, 2015).
Also in this case, MYC-ER expressing cells were used to evaluate the specific contribution of MYC under starvation and compared with control cells, expressing only the endogenous MYC. Starvation was performed for five hours. This short time point was chosen in order to better identify transcriptional effects associated with the fast regulation of MYC. As expected, endogenous MYC was downregulated within five hours of glutamine starvation. High levels of MYC-ER without 3´-UTR were instead detected under the same conditions and endogenous levels of MYC were further downregulated, proofing activation of the ectopic protein. Under these conditions, total

and phosphorylated RNAPII steady-state levels were not changed, as assessed by immunoblot (Fig. 4.30).

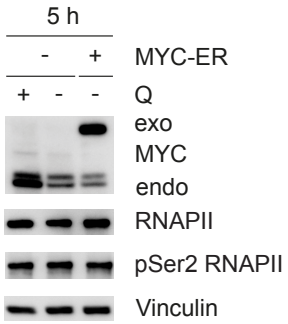

Figure 4.30: Experimental conditions chosen for ChIP and ChIP-sequencing

EV or MYC-ER expressing cells were treated overnight with 100 nM OHT. Starvation was performed for 5 h, in presence of OHT. The indicated proteins were detected by IB.

Individual loci were first examined by ChIP. Two known MYC-bound genes were selected: *ACTB* (encoding β-actin) and *NCL* (encoding nucleolin) and RNAPII binding was checked both at the transcription start site (TSS) and the transcription end site (TES). In all cases, binding to these loci was at least four folds enriched over an IgG control antibody or an intergenic control region, indicating experimental reliability (Fig. 4.31). In general, total RNAPII binding was higher at the TSS, while binding of elongating RNAPII increased at the TES, consistently with data from literature (Rahl et al, 2010; Jaenicke et al, 2015). A decreased RNAPII binding to the TSS and pSer2 RNAPII binding to the TES was observed following starvation at both loci. Interestingly, this effect was reverted when MYC-ER was activated in absence of glutamine, at both the TSS and the TES.

Since adenosine rescues MYC levels under starvation, RNAPII binding to the TSS was assessed following adenosine treatment, in order to further verify that it depends on MYC levels. Analysis of three different loci (*ACTB*, *NCL* and *GNL3* (encoding G protein nucleolar 3)) confirmed that RNAPII binding increased under glutamine starvation in a MYC-dependent manner (Fig. 4.32). This experiment indicated that the reduced association of RNAPII to the TSS depends on MYC levels, which are in turn controlled by glutamine-derived adenosine availability.

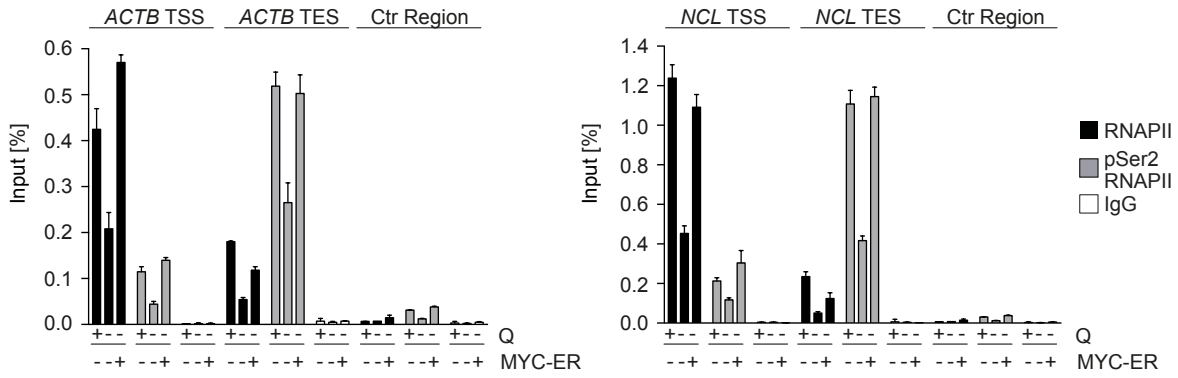

Figure 4.31: MYC-ER rescues RNAPII binding at TSS and TES on selected loci under starvation

ChIP showing RNAPII binding to the TSS and to the TES of the *ACTB* (left) and *NCL* (right) genes and to an intergenic control region (same for both targets). Bars represent mean + SD of technical triplicates. Experimental conditions are described in Fig. 4.30.

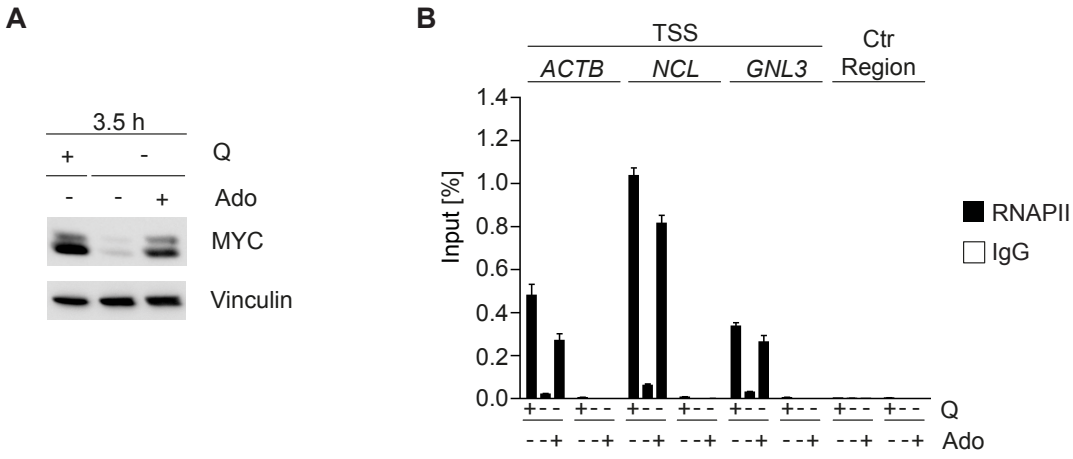

Figure 4.32: RNAPII binding at TSS depends on MYC levels

A) Cells were cultured in the presence or absence of glutamine for 3.5 h. Where indicated, adenosine was added to the medium. IB documents adenosine-mediated rescue of MYC in the cells used for performing the ChIP experiment.
B) ChIP showing RNAPII binding to the *ACTB*, *NCL* and *GNL3* genes and to an intergenic control region (same for all targets) under the indicated conditions. Bars represent mean + SD of technical triplicates.

4.7.1.1 Evaluation of global effects on RNAPII function

In order to obtain a more comprehensive picture, ChIP-seq was performed under the same experimental conditions used for ChIP. Data were analyzed by Susanne Walz. This independent experiment confirmed previous results, as assessed by looking at individual genome browser tracks. An identical trend in the binding of RNAPII (total and phosphorylated) was observed when two different loci, *PTMA* (encoding prothymosin alpha) and *LDHA* (lactate dehydrogenase A) were examined (Fig. 4.33A). A global analysis was then performed and results visualized either by heatmaps (Fig. 4.33B) or by metagene plots (Fig. 4.33C). Only genes having a RNAPII peak at the TSS (+/- 1kb) were considered for the analysis (n=9,796). The heat maps showed that the effects observed on single loci were also evident on all RNAPII-bound genes (Fig. 4.33B). Total or pSer2 RNAPII binding was visualized at the TSS or TES (+/- 5kb), respectively, of all RNAPII-bound genes.

A metagene analysis provided also a global overview of effects on RNAPII and has the advantage that the length of all analyzed genes is normalized in order to better compare effects at TSS, gene body and TES. Glutamine starvation had a global effect in decreasing RNAPII loading at promoter regions, while keeping MYC levels high under these conditions could partially restore the binding (Fig. 4.33C, left panel). Similarly, elongation was overall decreased by glutamine withdrawal and partly recovered by MYC-ER (Fig. 4.33C, right panel).

In order to obtain a more detailed view, total or pSer2 RNAPII occupancy at the promoter, gene body and TES was compared between the three conditions, as shown by the 2D Kernel density plots in Fig. 4.34A. The results further confirmed a strong effect of glutamine starvation on the promoter and a partial rescue by MYC-ER, as assessed by the linear shift of the cloud away from the dashed line in both the upper and the lower panel (RNAPII plots). Moreover, this analysis highlighted no strong differences in RNAPII occupancy in the gene body and at the TES (pSer2 RNAPII) dictated by glutamine availability or MYC levels, as shown by the centering of the density cloud around the dashed line in the corresponding plots. Additionally, the RNAPII traveling ratio was calculated in order to better characterize RNAPII behavior. The traveling ratio

is a parameter that gives a global indication of RNAPII loading and pause-release and is defined by the ratio of total RNAPII at the promoter to total RNAPII in the gene body (Rahl et al, 2010). The traveling ratio was decreased following starvation, compared to non-starved condition (Fig. 4.34B, black and grey lines). Consistently with the partial recovery of RNAPII loading driven by MYC-ER activation under starvation, the traveling ratio was increased in this condition, compared to the starvation situation (Fig. 4.34B, orange line). A decreased traveling ratio is an indicator of either increased RNAPII in the gene body compared to TSS, and therefore increased elongating speed, or decreased RNAPII at promoter region relative to RNAPII present in the gene body, as markedly observed in starved condition. Thus, these data argued for a global regulation of RNAPII binding mediated by MYC levels, which are in turn determined by glutamine, in presence of the 3´-UTR.

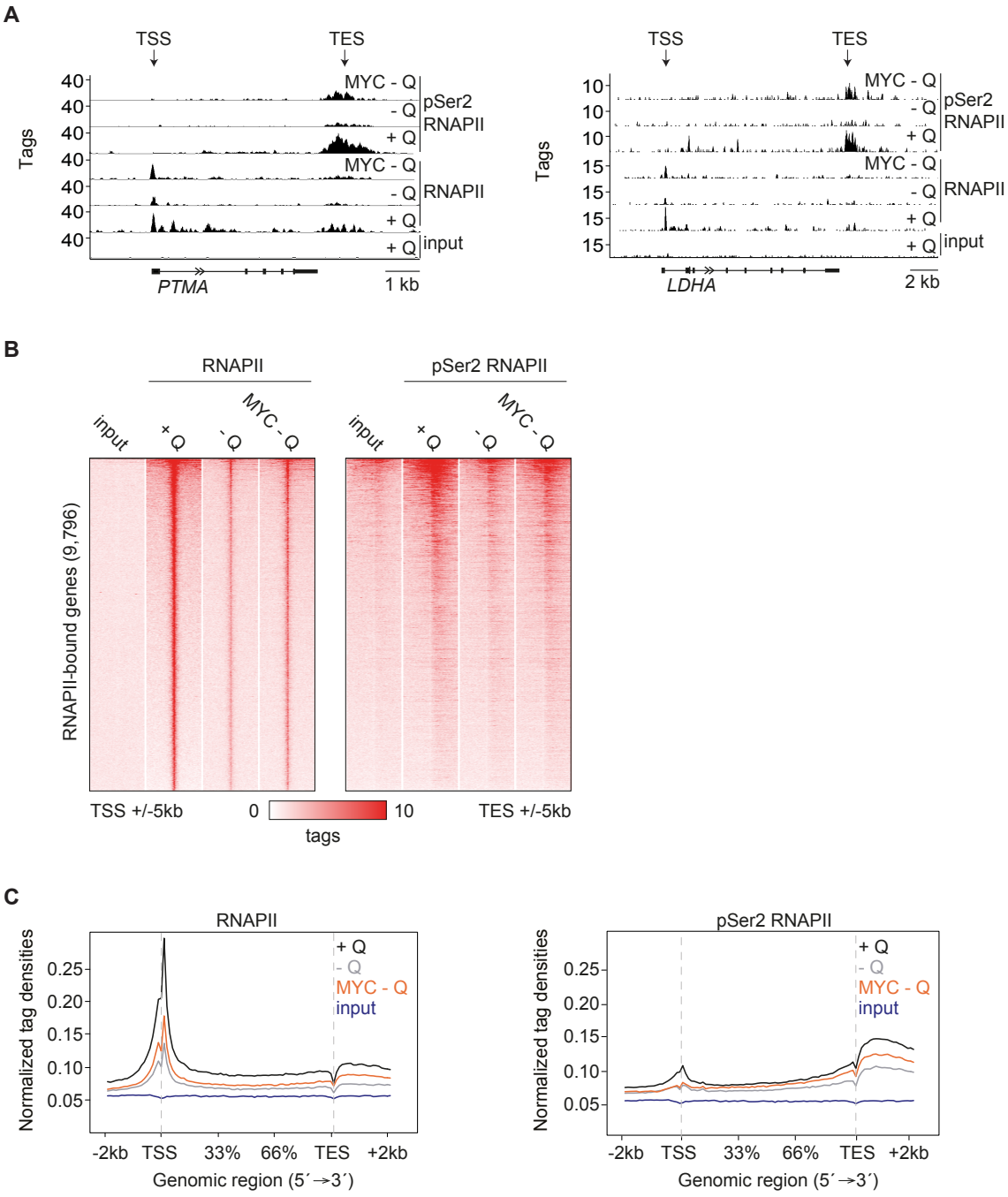

Figure 4.33: Glutamine-dictated changes in MYC levels globally affect RNAPII function

A) Exemplar of genome browser tracks from ChIP-seq analysis. The arrows highlight the TSS and TES.
B) Heat maps showing binding of RNAPII at the TSS (+/- 5 kb) and of pSer2 RNAPII at the TES (+/- 5 kb) for all genes with detectable RNAPII binding, under the indicated conditions. Genes were sorted according to the RNAPII binding in the +Q situation.
C) Metagene plots of RNAPII (left) or pSer2 RNAPII (right) for all genes with detectable RNAPII binding under the indicated conditions.

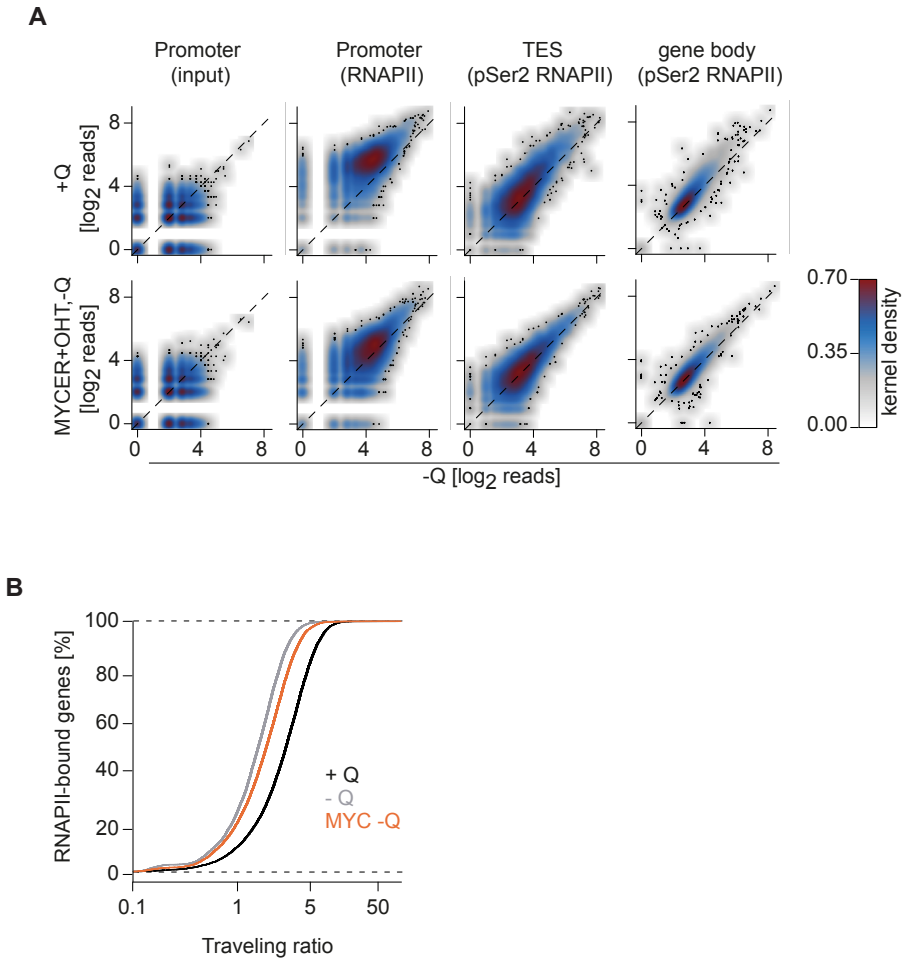

Figure 4.34: Glutamine starvation mainly alters RNAPII binding at promoter regions

A) 2D Kernel density plots comparing RNAPII occupancy at promoter region and pSer2 RNAPII occupancy at gene body and TES for all genes with detectable RNAPII binding under the indicated conditions. Black dots are outliers and dashed lines indicate lines of origin with a slope of 1.
B) Distribution of RNAPII traveling ratio for all genes with detectable RNAPII binding under the indicated conditions.

4.7.1.2 Genome-wide MYC binding correlates with RNAPII binding

In order to proof this hypothesis, global MYC binding was analyzed performing ChIP-seq in HCT116 cells, cultured in presence of glutamine, in the same reconstituted medium used for RNAPII ChIP-seq. Firstly, all RNAPII-bound genes were sorted according to the strength of MYC binding (Fig. 4.35). This analysis provided evidence that MYC binding paralleled RNAPII binding.

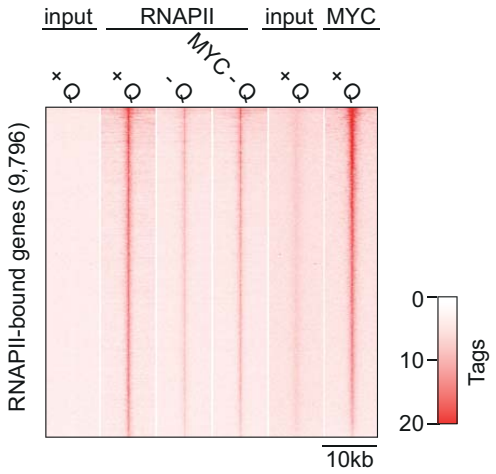

Figure 4.35: MYC binding parallels RNAPII binding at promoter regions

Heatmap showing RNAPII and MYC occupancy at all promoters (n=9,796) with detectable RNAPII binding. Gene are sorted according to the MYC binding in the +Q situation.

A direct correlation between RNAPII and MYC binding was further evaluated. Peak calling revealed 9,623 MYC peaks genome-wide. Of those, 5,220 were found in promoters (+/- 1kb). This number was much lower than the number of RNAPII peaks detected in promoters (9,796). This difference is attributable to parameters defined in the peak calling process, which ensure to analyze the most reliable positive peaks. This step allows for the determination of the genomic site (peak) enriched for binding of a protein of interest, represented by the number of sequenced reads mapped on the genome. Many parameters can influence the discrimination of real positive signals from background, e.g. efficiency of the antibodies, resulting therefore in different number of peaks detected for each specific protein (Bailey et al, 2013). Nevertheless, RNAPII binding was detected on almost 90% of MYC peaks in promoter region, corresponding to 4,615 genes (Fig. 4.36A).

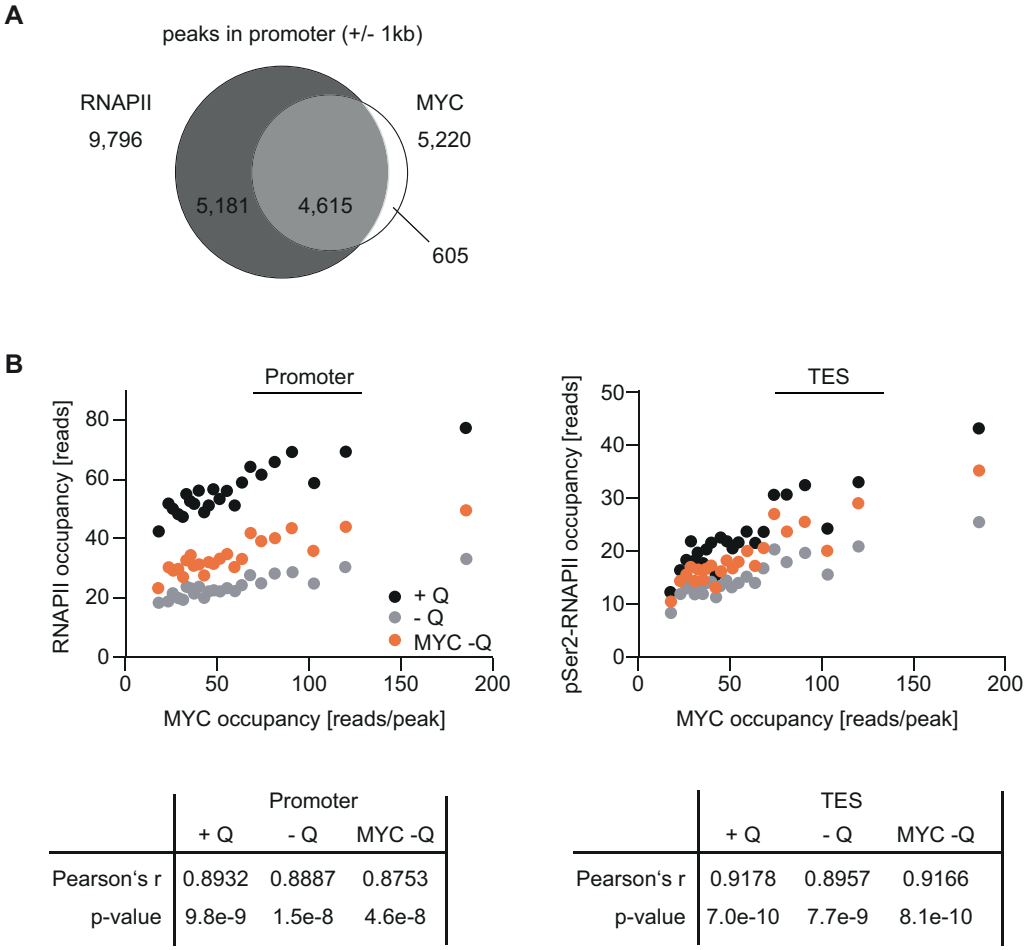

	Promoter		
	+ Q	- Q	MYC -Q
Pearson's r	0.8932	0.8887	0.8753
p-value	9.8e-9	1.5e-8	4.6e-8

	TES		
	+ Q	- Q	MYC -Q
Pearson's r	0.9178	0.8957	0.9166
p-value	7.0e-10	7.7e-9	8.1e-10

Figure 4.36: RNAPII occupancy correlates with MYC occupancy

A) Venn diagram showing peaks that were called for RNAPII and MYC and their overlap.
B) Plots showing the correlation of MYC occupancy with RNAPII occupancy at promoter and TES, under the indicated conditions. Measurement of the correlation strength is provided by the Pearson´s coefficient, while p-value indicates statistical significance, as shown in the tables below each graph.

MYC occupancy on these promoters was compared to RNAPII occupancy in the promoter (total) or TES (Ser2 phosphorylated) of the same MYC-bound genes (Fig. 4.36B). Correlations were visualized as bin plot in which each bin corresponds to 200 genes. RNAPII binding positively correlated with MYC occupancy in the promoter regions and at the TES (black dots). This correlation was direct since the same experimental conditions (+Q) were compared. RNAPII occupancy under starvation and MYC-ER activation was also plotted *versus* MYC occupancy (grey and orange dots).

Although this correlation was not direct, because the conditions compared were different, it showed the same trend of previous results: high MYC levels under starvation partially rescued RNAPII binding, especially at the promoter.

4.7.2 MYC downregulation under starvation prevents RNAPII stalling

According to previous results, differential loading of RNAPII at promoters seemed to proportionally dictate the resulting elongation rate. An open issue was therefore represented by understanding why cells need to decrease RNAPII elongation rate following the withdrawal of glutamine and why keeping MYC levels high can be potentially deleterious for them. In order to further investigate if MYC-ER can cause a distinct effect on RNAPII elongation, changes to the basal condition (+Q) were evaluated. Specifically, RNAPII occupancies at promoter and gene body were compared, considering not the single conditions, but the difference between the control (+Q) and starvation (in presence of endogenous, downregulated MYC or with activated MYC-ER), as shown in Fig. 4.37. The left plot shows the difference of RNAPII occupancy between starved and control cells (EV condition). The density cloud is almost completely shifted towards negative values on the y-axis, indicating a strong decrease in RNAPII occupancy at the promoter. Corresponding to the lower RNAPII loading, decreased binding in the gene body was observed following starvation (cloud shifted towards the left), although less pronounced than at promoters. These results confirmed those obtained with the previous analysis. The right plot shows instead the differential RNAPII occupancy between cells starved in presence of ectopic MYC and control cells.

MYC-ER is able to restore RNAPII occupancy, visible by a more symmetric distribution of the density cloud, compared to the left plot, indicating less pronounced differences between the two conditions. Being the rescue partial, the majority of genes were still found in the double-negative square (lower, left), indicating higher RNAPII binding in presence of glutamine at both promoter and gene body.

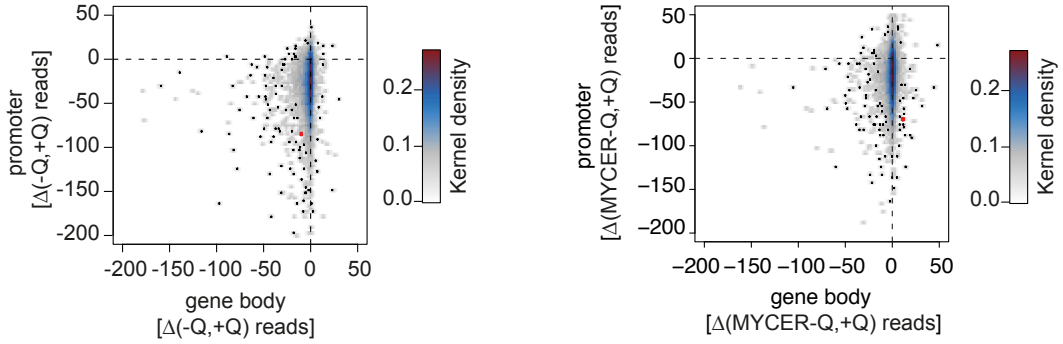

Figure 4.37: High levels of MYC lead to RNAPII stalling on certain genes under starvation

2D Kernel density plots comparing the difference in RNAPII occupancy between two indicated conditions at promoter (-30 to +300 bases) and gene body (+300 to TSS) for all RNAPII-bound genes. Outliers are shown in black. *TKT* is highlighted in red.

An interesting subset of genes was represented by those found in the lower, right square, corresponding to those genes in which RNAPII binding was lower at the promoter but higher in the gene body in starved compared to control cells. This result indicated that high MYC levels under starvation caused RNAPII stalling in the gene body of a subgroup of genes. Specifically, this category comprised 256 genes. *TKT* was the gene with the highest accumulation of RNAPII in the gene body (Fig. 4.38A) and was used for further validation by ChIP. Since from the ChIP-seq track the increased RNAPII signal was detected between exon four and eight of the *TKT* gene, primers falling in this region were used in addition to those recognizing the TSS and the TES (indicated by triangles in Fig. 4.38A).

qPCR using these specific primers confirmed the ChIP-seq result: decreased enrichment of RNAPII following starvation and partial rescue in presence of activated MYC-ER. An enrichment of RNAPII in the gene body was observed after MYC-ER activation, particularly evident when the pSer2 RNAPII antibody was used (Fig. 4.38B). This result confirmed the observed accumulation of RNAPII, at specific loci, when high levels of MYC are maintained under stress due to glutamine starvation.

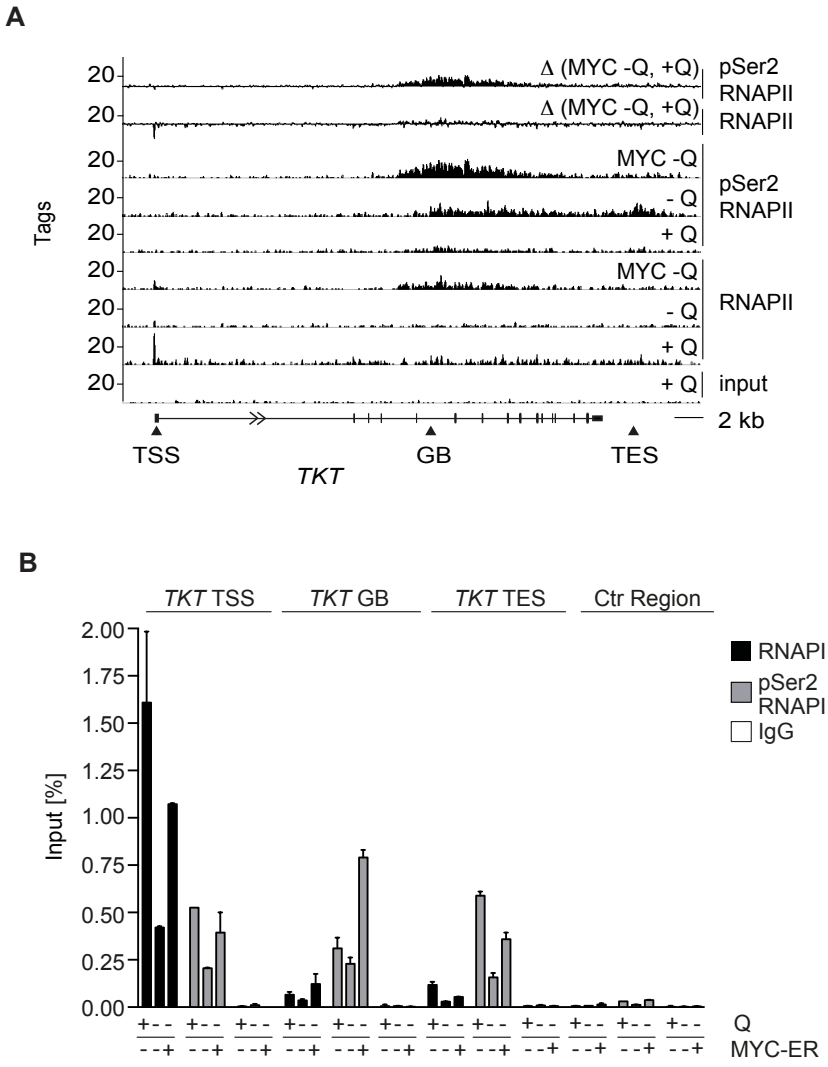

Figure 4.38: RNAPII accumulates within the *TKT* gene body when high levels of MYC are kept under starvation

A) *TKT* genome browser track highlighting MYC-ER-mediated RNAPII accumulation in the gene body. The two upper rows show the difference of RNAPII or pSer2 RNAPII tags density between MYC-ER –Q and +Q conditions. Triangles indicate the position of primers used in Fig. 4.38B

B) ChIP confirming the result showed in Fig. 4.38A. Bars represent mean + SD of technical triplicates (n=2).

5 Discussion

Cancer cells rely on two major energetic fuels, glucose and glutamine, to sustain their growth and proliferation. MYC plays a central role in rewiring cancer cell metabolism. This effect is mainly attributed to transcriptional changes induced by deregulated MYC activity. MYC directly regulates both glucose and glutamine metabolism, specifically glycolysis, glutaminolysis and other interconnected pathways (see 1.3).
In contrast to the majority of studies, which focus on how MYC regulates metabolism, this research aimed to understand if MYC itself is regulated by the availability of metabolites and any possible molecular consequences of this regulation.

5.1 MYC is regulated in a glutamine-dependent way

Titration of both metabolites in the culture medium established unequivocally that glutamine regulates MYC protein levels. MYC was rapidly and strongly downregulated following glutamine starvation, while its levels rapidly increased when glutamine was re-added to the medium (Fig. 4.1 and Fig. 4.3). This kinetics was conserved at both short and long time points of starvation and re-addition. Conversely, changing the glucose concentrations in the medium did not affect MYC protein levels. Thus, this result directed the research towards the investigation of the glutamine-mediated regulation of MYC. Importantly, even after prolonged glutamine starvation, e.g. 72 hours, cells did not relevantly undergo apoptosis. The opposite effect occurred when cells where deprived of glucose and complete cell death was observed within 36 hours (Fig. 4.4). HCT116 cells are derived from an adenocarcinoma, i.e. an advanced stage of colon cancer (Brattain et al, 1981). These cells have been widely characterized and used as an experimental system in many studies. In addition to a mutation in the gene encoding beta-catenin, which results in high levels of *MYC* expression, the oncogenes *K-RAS* and *PIK3CA* are also mutated in these cells (Ahmed et al, 2013). Deregulated oncogene activity promotes a glycolytic phenotype, since K-RAS, PI3K and its downstream effector AKT drive an increased uptake and utilization of glucose (Elstrom et al, 2004; Foster et al, 2012; Ying et al, 2012). The contribution of three potent

oncogenes, such as MYC, K-RAS and PI3K, can therefore explain the sensitivity of these cells to the deprivation of glucose. The fact that these cells have additional mutations adds, on one side, more complexity to the system, but, on the other side, reflects a more realistic situation, due to the highly heterogeneous nature of tumors, especially in an advanced stage.

The sensitivity of cancer cells to glutamine deprivation has been shown to be highly variable, with some cell types being able to proliferate regardless the presence of this amino acid (van den Heuvel et al, 2012; Timmerman et al, 2013; Yang et al, 2014). This phenomenon has been linked with the capability of tumors to synthetize glutamine from glutamate and ammonia, a reaction catalyzed by the enzyme glutamine synthetase (Kung et al, 2011). Although HCT116 cells do not significantly undergo apoptosis following glutamine deprivation, they are nevertheless sensitive to glutamine and are not able to proliferate in the absence of this metabolite. Glutamine starvation induces cell cycle arrest, which can be reversed by supplementing glutamine back to the medium (Fig. 4.5). The clearest advantage of this response is the ability to perform experiments in living cells, also over longer time points, avoiding biological variables connected to a prominent induction of apoptosis. Importantly, the downregulation of MYC following starvation and the subsequent upregulation of MYC after glutamine re-addition occurred earlier than the changes in the cell cycle, excluding therefore indirect effects on MYC due to cell cycle arrest or restored cell proliferation.

5.1.1 The pleiotropic effects of glutamine

Glutamine is the most abundant circulating amino acid. Its plasma concentration lies between 0.5 and 0.7 mM (Felig et al, 1970). Glutamine is defined as a conditionally essential amino acid. Although it can be synthetized from glutamate by glutamine synthetase, it becomes essential under certain conditions, for example during infections, after injury (Newsholme, 2001) and in cancer cells (Hensley et al, 2013). Under conditions requiring rapid growth and proliferation the demand for glutamine can exceed its supply and glutamine availability can become limiting. This, together with the fact that tumors usually display an irregular vasculature, can expose different tumor areas to regional starvation. *In vivo* studies have provided evidence that, in comparison

to all amino acids, glutamine is the most consumed one. Accordingly, core tumor areas show a deficiency of glutamine (Kamphorst et al, 2015; Pan et al, 2016). This concept is of interest for the present study since the glutamine starvation performed on two-dimensional cultured cells may reflect a situation that tumors experience *in vivo*. The importance of glutamine lies in its ability to enter several metabolic pathways, providing them both carbons and nitrogen groups (see 1.2.2.2 and Fig. 1.4). Moreover, glutamine is able to activate mTOR both directly, through glutaminolysis and indirectly, through the promotion of leucine uptake, another direct mTOR activator (Nicklin et al 2009; Duran et al, 2012). Consistent with such knowledge, metabolomics analysis confirmed that glutamine is needed to fuel major metabolic pathways, such as the TCA cycle or the nucleotide biosynthesis (Dejure et al, 2017), further corroborating the fact that HCT116 cells need glutamine to support their biosynthetic needs.

Normal proliferating cells also use these pathways, although they are differentially regulated and enhanced in a tumor context. Intestinal cells, for example, are particularly sensitive to glutamine, which is needed for supporting the high rates of intestinal mucosa proliferation (Reeds and Burrin, 2001). Interestingly, MYC downregulation was observed when the concentration of glutamine in the medium was below 0.25 mM, i.e. below the physiological plasma concentration. Thus, one could speculate that the glutamine-dependent regulation of MYC could be a mechanism conserved in cancer cells in order to allow for their survival under starvation.

5.1.2 Links between MYC and glutamine: the concept of glutamine addiction

Although the central role of glutamine in cancer metabolism has long been recognized (Souba, 1993), much more recently a link between glutamine metabolism and oncogenes has emerged. Particularly, the role of oncogenic MYC has been highlighted in three works, published between 2007 and 2009, which provided a big step forward in the field of cancer metabolism (Yuneva et al, 2007; Wise et al, 2008; Gao et al, 2009). These studies provided evidence that MYC controls the metabolism of glutamine and analyzed this event from different perspectives, using different systems. Wise *et al* and Gao *et al* mainly focused on the transcriptional aspect, showing that, in a cancer

context, MYC upregulates the expression of key genes whose products are involved in the metabolism of glutamine. The main targets are represented by *ASCT2*, which encodes for a glutamine transporter, and by *GLS*, which encodes for the enzyme glutaminase. *GLS* expression can be upregulated by MYC either directly or indirectly, through MYC-mediated inhibition of miR-23 expression, which in turn suppresses *GLS* (Gao et al, 2009). *GLS* overexpression, which has been found in several types of cancer, causes an increased flux of glutamine into the TCA cycle and provides anaplerotic substrates (Wang et al, 2010). Increased use of the TCA cycle for biosynthetic, rather than energetic purpose, is a hallmark of cancer and glutamine plays a key role in sustaining this process (DeBerardinis et al, 2007).

Yuneva *et al*, instead, showed that cells overexpressing MYC become dependent upon the availability of glutamine and die when glutamine, but not glucose, is depleted from the culture medium. This phenomenon is termed "glutamine addiction" and has been specifically linked to deregulated MYC activity. Taken together, these studies demonstrated for the first time that MYC drives a transcriptional program which leads transformed cells to avidly uptake and metabolize glutamine, mainly through the TCA cycle. Establishing such a program, in turn, makes cancer cells addicted to glutamine.

In contrast to data shown in previous works, HCT116 cells were able to survive following glutamine starvation. Since withdrawal of this essential metabolite rapidly downregulates MYC and MYC, in turn, is the major regulator of glutamine metabolism, one could speculate that cells are not able to maintain MYC-induced glutamine addiction when MYC itself is downregulated. Subsequent research aimed therefore to understand the molecular basis of the glutamine-mediated regulation of MYC and the resulting biological effects.

5.2 Glutamine regulates MYC protein levels through the 3´-UTR

Different mechanisms were considered in order to elucidate how glutamine supply regulates MYC, Although MYC levels can be potentially regulated at every single step, from gene expression to protein modification, selected mechanisms were considered, based upon their known link with metabolism and metabolic stress.

5.2.1 Candidate glutamine-regulated mechanisms do not affect MYC protein levels

A transcriptional response was first evaluated since glutamine can regulate gene expression in both a positive or negative way (Brasse-Lagnel et al, 2009). Measuring steady-state transcript levels by qPCR showed an increase in *MYC* mRNA following glutamine starvation; thus, displaying an opposite trend than the one observed at protein levels (Fig. 4.6). A previous study reported increased *MYC* mRNA levels following amino acids deprivation in rat hepatocytes (Yokota et al, 1995). These observed effects are likely the result of feedback mechanisms acting on the *MYC* promoter, through which *MYC* transcript levels change in an inversely proportional way to the protein levels (Penn et al, 1990). Nevertheless, the employment of a vector expressing exogenous *MYC* mRNA levels under a tetracycline responsive element promoter (TRE), not subject to negative auto-regulation, allowed ruling out the response due to the effects on MYC promoter. A reduction of approximately 50% in *MYC* transcript levels was observed following glutamine starvation when the 3′-UTR was present in the exogenous transcript (Fig. 4.13). This specific effect is consistent both with the presence of destabilizing elements in the *MYC* 3′-UTR, such as AU-rich elements (see 1.1.2.2), and with putative mechanisms of MYC regulation mediated by its 3′-UTR (see 5.3.2).

Degradation pathways were the second candidate mechanism considered for explaining the glutamine-mediated regulation of MYC. Two papers reported that MYC is downregulated following metabolic stress conditions induced by glucose and oxygen deprivation, due to increased mechanisms of degradation (Okuyama et al, 2010; Wong et al 2013). Although a similar response was observed following glutamine starvation, experimental results highlighted the involvement of a different mechanism of regulation. While in both cases the authors showed changes in MYC stability and rescue of MYC protein levels mediated by proteasomal inhibition, these results were not observed when repeating the same experiments under glutamine starvation (Fig. 4.7). In contrast to such studies, MYC levels were found not to be sensitive to glucose deprivation (Fig. 4.1), even employing the same tumor model (i.e., HCT116 cells). The

most evident explanation of this is represented by the fact that the present study focused on the evaluation of MYC response towards a specific stimulus and did not take into account the contribution of hypoxia. However, also these previous works underlined that MYC downregulation under hypoxia and low glucose supply accounts for increased cell survival. Taken together, these findings contribute to the conclusion that MYC is a stress-responsive protein and that different stimulus-dependent mechanisms of regulation impact cell survival under unfavorable metabolic conditions.

Changes in the activity of the mTOR pathway were also evaluated. In fact, multiple mechanisms link mTOR activity either to glutamine availability or to MYC protein levels, making therefore further investigations into the mTOR involvement necessary (see 1.3.2). The mTOR kinase is a central regulator of growth and it is able to respond to changes in the cellular metabolic status to support anabolic or catabolic processes accordingly. It can form the complex 1 (mTORC1), which is mainly involved in promoting protein synthesis, and the complex 2 (mTORC2), which mainly controls cell polarity, proliferation and differentiation. Both mTORC1 and mTORC2 activity are nutrient sensitive, although the mechanisms of sensing of mTORC1 are much better characterized than those of mTORC2 (Laplante and Sabatini, 2012). In addition to the direct involvement of mTORC1 and mTORC2 in controlling MYC translation (Csibi et al, 2014; Mausui et al, 2013), a cross talk between the two complexes also exists (Laplante and Sabatini, 2012). Thus, feedback mechanisms can potentially affect MYC protein levels in a glutamine-dependent manner. In order to evaluate the contribution of mTORC1 and mTORC2 to the glutamine-mediated regulation of MYC, MYC protein levels were evaluated in the presence of either an mTORC1 inhibitor (rapamycin) or a dual mTORC1 and mTORC2 inhibitor (OSI-027). Their efficacy was assessed by checking the phosphorylation status of targets of mTORC1 (p706K and 4EBP1) and mTORC2 (AKT). The additional employment of OSI-027 allowed for the discrimination between direct and indirect effects. For example, consistent with a recent report (Moloughney et al, 2016), glutamine starvation increases mTORC2 activity, as assessed by increased AKT phosphorylation (Fig. 4.8 B, left part). Activated AKT can subsequently stimulate mTORC1 activity. Moreover, rapamycin-mediated mTORC1 inhibition is known to induce feedback mechanisms activating mTORC2. For example,

the decreased activity of p70S6K results in the dephosphorylation of insulin receptor substrates (IRSs) and in the consequent relieve of a negative regulation. IRSs stimulate PI3K activity and PI3K, in turn, activates both mTORC2 and RAS (Xie and Proud, 2013). Both pathways can increase or stabilize MYC (see 1.1.2.3 and 1.3.3); thus, explaining the observed increase in MYC protein levels following rapamycin treatment in the presence of glutamine (Fig. 4.8). However, mTORC2 inhibition also increases MYC protein levels, likely due to activation of the FOXO/MAPK axis, which leads to the upregulation of *MYC* transcription (Wiegering et al, 2015). However, in spite of the existence of feedback mechanisms affecting MYC, glutamine availability was still able to regulate MYC in both the presence and the absence of inhibitors. The role of mTORC1, which specifically controls the global protein translation, was further evaluated. The effect of glutamine on MYC and mTORC1 was compared with the effect of two essential amino acids, methionine and leucine, in order to obtain indications regarding the specificity of the response. All tested amino acids regulate mTORC1 activity, as shown by the changes in p70S6K phosphorylation. MYC levels were also downregulated when each amino acid was depleted. Since decreased mTORC1 activity can result in decreased MYC levels, this setup did not allow for discrimination between the contribution of the amino acid-regulated mTOR activity and the exclusive effect of amino acids on MYC. However, while re-addition of all amino acids positively regulates mTORC1 activity, only glutamine upregulated MYC (Fig. 4.9). Finally, another experiment showed that MYC is downregulated even when mTORC1 activity is maintained high, as observed in p53 deficient cells (Fig 4.15B). Collectively, these experiments indicated the existence of further mechanisms of control of MYC levels in addition to a more global regulation of translation mediated by the effect of glutamine on mTORC1. MYC and mTOR are two major nodes that control growth and proliferation and a tight crosstalk exists between the two proteins, since each protein regulates the activity of the other (see 1.3.2). Moreover, both proteins converge on translation regulation (Pourdehnad et al, 2013) and biosynthesis of nucleotides (Ben-Sahra et al, 2013; Ben-Sahra et al, 2016) and these functions promote growth and progression through the cell cycle (Fingar et al, 2004). Thus, a coordinated decrease in MYC levels and mTOR activity under glutamine starvation may also explain the observed cell cycle arrest. Multiple and parallel mechanisms affecting both

MYC and mTOR under stress conditions can co-exist. This fits with the fact that cells have to ensure for a proper control on the activity of two master regulators of energy-driving processes, so that loss of control over one arm can be compensated by another one.

5.2.2 The 3′-UTR of *MYC* is an indispensable element that allows for the glutamine-mediated regulation of MYC

Since MYC decrease following starvation was observed only at the protein and not at the mRNA level, post-transcriptional mechanisms of regulation were investigated. Post-transcriptional regulation may occur at several steps and affects protein translation. A pulse-labeling experiment allowed for the verification that MYC translation is effectively controlled by glutamine availability, since the levels of newly synthetized MYC protein responded to starvation and re-addition in the same way as for total MYC protein levels (Fig. 4.10). Thus, glutamine exerts a control on MYC translation. The process of translation can be influenced by several factors. mTOR is the major upstream pathway controlling cap-dependent translation, i.e. translation which starts by recognizing the cap element at the 5′-UTR, but a direct involvement of mTOR in controlling MYC translation was excluded. When translation is initiated, the mRNA adoptes a circular conformation, with the 5′- and 3′-ends in close proximity, facilitated by the interaction between proteins binding the mRNA cap at the 5′-end and the poly-A tail at the 3′-end. This conformation improves translation efficiency and allows for the fast recycling of the ribosomes after each cycle of translation. At the same time, the circular structure allows for the inhibition of translation when the 3′-UTR is targeted, since it interferes with the recruitment of initiation factors at the 5′-end (Van Der Kelen et al, 2009). The employment of exogenous constructs comprising the coding sequence only or the coding sequence with one or both UTRs allowed for the evaluation of the contribution of each element in regulating MYC translation (Fig. 4.11). Such inducible constructs were expressed at low levels to maintain total MYC protein levels similar to the endogenous ones and not to interfere with the levels of molecular effectors possibly involved in the regulation of MYC. The 3′-UTR contained poly-A signals, which are normally provided by the vector. Although the presence of poly-A signals lowered the

viral titer, due to the interference with viral genomic sequences, it ensured for the proper termination of transcription of the 3′-UTR, without including any viral sequence. Strikingly, downregulation of exogenous MYC protein under glutamine starvation occurred only in the presence of the 3′-UTR. Thus, mechanisms impinging on the *MYC* 3′-UTR are involved in the glutamine-mediated regulation of MYC. Re-addition of glutamine following starvation upregulated all exogenous constructs. This observation implies a less specific effect of glutamine during the upregulating response, although it does not exclude the possibility that the same mechanism controls MYC levels in both directions in a 3′-UTR-dependent way (see 5.4). Moreover, this result further proved that mTOR is not directly involved in the glutamine-mediated regulation of MYC. In fact, in the absence of the 3′-UTR, MYC protein levels are maintained even after starvation, i.e. in a condition in which mTORC1 activity is decreased. The most likely scenario is that, although globally reduced, the translation machinery can still account for MYC synthesis in the absence of additional mechanisms of negative regulation. In general, the downregulation effect was stronger on the endogenous than on the exogenous MYC, possibly indicating the existence of additional mechanisms impinging on elements absent in the exogenous construct, for example on the *MYC* promoter. Reporter assays are usually employed for validating repressive effects on the 3′-UTR. However, a luciferase assay provided only weak indications regarding a specific glutamine-mediated response over the 3′-UTR (Fig. 4.14), which was instead further corroborated using a different viral system (Fig. 4.23A). A likely explanation is that high levels of the reporter construct titrated out molecular players involved in the regulation, due to transfection, while controlled expression through stable genomic integration allowed this regulation to occur.

As established by many studies, MYC can control the metabolism of glutamine, making cells addicted to such metabolite. This result provides evidence that glutamine itself acts a regulator of MYC protein levels and that the 3′-UTR of *MYC* is the critical element subjected to this regulation. The impact and the implications of glutamine-driven mechanism of regulation are further discussed in section 5.4.

5.2.3 Examples of regulatory mechanisms impinging on MYC 3′-UTR and potentially linked with the cellular metabolic status

This study reports for the first time that a metabolic stress-induced stimulus has an impact on the 3′-UTR of *MYC*. Accordingly, other stress-induced mechanisms have been shown to regulate MYC through its 3′-UTR. In addition to the role of the FOXO/miR-34 axis, described in 1.3.3, DNA damage has been extensively investigated as a stress stimulus able to reduce MYC levels. It can activate either degradation pathways or miRNAs-dependent mechanisms (Britton et al, 2008; Popov et al, 2007; Cannell et al, 2010; Li et al, 2015).

One study demonstrated that miR-34c targets MYC following UV-induced-DNA damage in order to prevent DNA replication and genomic instability under stress. Expression of miR-34c is, in this context, depends upon either p53 or p38, both of which are stress responsive proteins. Disruption of this circuitry has been proposed to have a pro-oncogenic potential and to be linked with MYC-induced replication stress (Cannell et al, 2010). Another work showed that UV irradiation leads to the miR-130a-dependent downregulation of MYC. This mechanism is mediated by the release of the ribosomal protein L11 from the nucleolus to the cytosol, where it directs the miRNA/RISC complex towards the 3′-UTR of *MYC*. Destruction of the nucleolar structure following UV-induced ribosomal stress accounts for the activation of this response (Li et al, 2015). Similarly, L11 is involved in promoting the binding of miR-24 to the 3′-UTR of *MYC* following the drug-induced inhibition of ribosomal RNA (rRNA) biosynthesis and processing (Challagundla et al, 2011). In general, stress stimuli interfering with the biogenesis of ribosomes lead to induction of ribosomal or nucleolar stress, which is mainly triggered by p53 (Zhou et al, 2015). Since the rate of ribosomal biogenesis is also regulated by the availability of nutrients, the mechanisms described above can potentially link the metabolic status of the cell with the regulation of MYC levels by post-transcriptional mechanisms. Interestingly, MYC is also involved in regulating ribosome biogenesis (see 1.3.2). Heterozygous deletion of the ribosomal protein L23 negatively impacts the progression of a MYC-driven lymphoma model, demonstrating that proper ribosome assembly and hence translation are determinants of

the oncogenic properties of MYC (Barna et al, 2008). One speculation is that the downregulation of MYC following ribosomal stress aims to decrease the otherwise wasteful synthesis of ribosomal components. This would represent a feedback loop similar to the one proposed to exist between MYC and glutamine.

5.2.4 The 5′-UTR of *MYC* does not contribute to the glutamine-mediated regulation, but MYC1 is sensitive to glutamine starvation

Evaluation of the role of single elements of MYC mRNA highlighted two interesting observations. Firstly, glutamine availability does not affect MYC protein levels in a 5′-UTR-dependent way. The 5′-UTR of *MYC* is characterized by the presence of an IRES (see 1.2.2.2), which allows for cap-independent *MYC* translation, occurring under circumstances in which cap-dependent translation is blocked, such as under stress or during apoptosis. *MYC* translation, for example, is increased in a cervical cancer cell line (HeLa) undergoing TRAIL (tumor necrosis factor-related apoptosis-inducing ligand)-induced apoptosis, since high MYC levels are required to drive this process (Stoneley et al, 2000). Direct mTOR inhibition can also lead to IRES-driven MYC upregulation (Shi et al, 2013; Wiegering et al, 2015). Finally, MYC protein levels increase in multiple myeloma following ER (endothelium reticulum)-stress, a condition in which the accumulation of unfolded proteins prevents cap-dependent translation (Shi et al, 2016). Thus, although multiple stress stimuli can upregulate MYC in an IRES-dependent way, glutamine starvation does not mediate such a response. Experiments employing a MYC construct encompassing also its 5′-UTR showed that MYC levels are stable and not upregulated following starvation; moreover, no compensatory effect was observed when both UTRs were present.

A second intriguing observation was that MYC1 – the isoform translated from a Leu start codon instead of the canonical Met codon (see 1.1.2.2) – responded to glutamine-induced stress. This effect was particularly clear when the construct with the single 5′-UTR was tested: under such setting, an upregulation of the upper MYC form was observed (Fig. 4.11). Mutating the Leu codon to a stop codon confirmed that glutamine starvation regulates MYC1, since the lower mobility band visible on the immunoblot disappeared following glutamine withdrawal (Fig. 4.12). MYC1 upregulation could

occur through an IRES-dependent mechanism, although this should lead also to the upregulation of MYC2 8i.e., the canonical isoform). Alternatively, the decreased rate of translation could promote an increased pausing of ribosome scanning on the Leu codon and could allow for pairing of the Met-tRNA to this site; a bond that is otherwise too weak under normal translation conditions. The physiological role of MYC1 is much less characterized than that of MYC2. Early studies have demonstrated that the expression of MYC1 is disrupted in some Burkitt´s lymphomas, suggesting a potential role of this isoform in the negative regulation of MYC2 and in preventing tumorigenesis (Hann et al, 1988). Consistent with the presented results, depletion of essential amino acids, and particularly of methionine, was found to increase MYC1 levels (Hann et al, 1992). Although these works suggested a role of MYC1 in the cellular stress response, the exact biological meaning of this regulation was not elucidated and no follow up studies were performed. Altogether, these results encourage further investigation of the role of MYC1 under these conditions.

However, although using different exogenous constructs helps to distinguish the contribution of single elements in the response to stress, both MYC1 and MYC2 are subjected to a 3´-UTR-mediated regulation, as shown by decreased levels of both exogenous forms when the 5´-UTR and the 3´-UTR are present. Thus, under glutamine starvation, the 3´-UTR-mediated regulation overcomes additional mechanisms.

5.3 Molecular players involved in the glutamine-mediated regulation of MYC: current investigations and future directions

The 3´-UTR of *MYC* is targeted by miRNAs or RNA binding proteins (RBPs) that can potentially belong to stress-responsive circuitries.

Therefore, these mechanisms could restrain MYC protein levels, acting in a fail-safe way to prevent further damage or cell transformation. Components belonging to these pathways are often lost during cancer progression, resulting in the consequent loss of feedback mechanisms able to control MYC levels (see 1.3.3). Glutamine starvation downregulates MYC in a cancer cell line, thus suggesting that the putative pathway responsible for this regulation is conserved, rather than inactivated, in cancer and that

activation of this pathway is relevant for allowing cell survival under glutamine-induced stress.

5.3.1 Role of miRNAs in the glutamine-mediated regulation of MYC

Activation of stress responsive pathways implies the involvement of many molecular players, for example an activated protein, such as p53, and downstream effectors. Experimental evidence has excluded a major contribution of p53 in regulating MYC protein levels in a glutamine dependent way (Fig. 4.15), although the involvement of other candidates, such as p38 or FOXO, has not yet been evaluated. This research aimed rather to find the most downstream regulator of MYC, i.e., the one directly impinging on 3´-UTR. The focus was therefore directed towards miRNAs. miRNA-mediated post-transcriptional regulation can occur by a subtle decrease in the levels of several targets or by a more specific repression of mRNAs involved in key cellular processes, such as MYC (Cannell and Bushell, 2010). Regulation by miRNAs represents an elaborated process. As previously mentioned, miRNAs are part of complex circuits that establish negative or positive feedback loops. MYC itself regulates a plethora of miRNAs and is itself subjected to miRNAs regulation (Tao et al, 2014). Although the understanding regarding the mechanisms of miRNA-mediated repression has increased over the last years, much conflicting data has been reported; thus, making it difficult to acquire a unifying view of the exact process (Wilczynska and Bushell, 2015). However, one possibility is that during stress responses, the ratio between miRNA and target mRNA increases; thus, leading to the repression of translation. Changes in the expression levels of miRNAs following glutamine starvation were evaluated by performing miRNA-sequencing. This experiment hypothesized that the rapid effect exerted by glutamine on MYC levels could be reflected by rapid changes in the miRNA expression levels. Such swift regulation has been previously reported to occur during inflammation (Perry et al, 2008), although in general miRNAs are stably associated with the RISC protein complex and are subjected to a slow turnover (Tang et al, 2008).

Evaluation of multiple parameters allowed for assessment of the technical success of the miRNA-sequencing, which was established for the first time within the research group.

The analysis demonstrated that HCT116 cells express miRNAs that are expected to be expressed in colon carcinoma. Moreover, miRNAs belonging to the miR-34 family were expressed at very low levels, consistent with their downregulation during tumor progression (Wu et al, 2010; Toyota et al, 2008; Fig. 4.16). However, glutamine-mediated changes in the miRNAs abundance could be excluded. Stress conditions can potentially induce changes in the conformation of the target mRNA, mediated for example by interaction with RBPs, which can expose a previously hidden miRNA binding site; thus, allowing for the repression of translation without altering the levels of miRNAs (Kim et al, 2007). The sequencing results were used to select miRNAs known to target MYC and which were expressed at high levels in order to ensure a proper miRNA/mRNA ratio. Inhibiting the function of the selected miRNAs using anti-miRs increased MYC levels under basal conditions; thus, proving that MYC is a physiological target of these miRNAs. However, MYC protein levels could not be rescued in the absence of glutamine (Fig. 4.17). A miRNA (miR-429) targeting the 3´-UTR within the element found to be responsible for the glutamine-mediated regulation of MYC also failed to rescue MYC. On one side, these results contradict the involvement of miRNAs in regulating MYC translation under these conditions; on the other side, the wide range of possibilities, i.e. cooperation between multiple miRNAs, make the experimental outcome inconclusive for excluding this kind of regulation.

5.3.2 Searching for molecular players: next research directions

Despite several tested hypotheses, the mechanism of glutamine-mediated regulation of MYC has not been yet deciphered. As mentioned above, multiple possibilities exist which involve one or more miRNAs, RBPs or both kinds of molecular players (van Kouwenhove et al, 2011). Therefore, global approaches aiming to detect *MYC*-interacting factors in an unbiased way need to be considered. One possibility is represented by mass-spectrometry analysis or miRNA sequencing of proteins or miRNAs bound to the 3´-UTR of *MYC*, which can be pulled-down using specific labeled probes (Marin-Bejar and Huarte, 2015). Such approaches can provide information regarding molecular interaction with *MYC* both in the presence and absence of glutamine, adding valuable information to the existent literature (see 1.1.1.2).

Although some *MYC* RBPs have already been characterized (see Table 1.1), it became evident over the past years that the spectrum of proteins able to bind target mRNAs and influence their translation is not restricted to a specific class of proteins, but involves virtually the whole proteome (Castello et al, 2013). Such knowledge makes the use of unbiased techniques, such as sequencing or mass-spectrometry, more advisable rather than examining single candidates. The employment of exogenous MYC constructs can help to obtain more specific information, for example excluding factors interacting with *MYC* elements other than the 3´-UTR or by precisely localizing the binding within the region found to be glutamine sensitive (Fig. 4.18).

A deeper investigation of the molecular mechanism can also imply the evaluation of the shifts in the intracellular localization of *MYC* mRNA following glutamine starvation. Many conditions, such as osmotic stress or heat shock, lead to the formation of stress granules. These structures are cytoplasmic aggregates of proteins in which mRNAs can be sequestered until the restoration of translation. Repression complexes mediated by both miRNAs and RBPs can be found within stress granules (Buchan and Parker, 2009). Thus, it would be interesting to investigate whether *MYC* mRNA localization is affected by glutamine starvation and whether sequestration into stress granules accounts for its downregulation.

These models assume that *MYC* mRNA levels are not affected by glutamine availability and that only changes in translation determine the decrease in MYC protein levels. However, decreased levels of exogenous *MYC* mRNA were observed following the introduction of the 3´-UTR (Fig. 4.13B). Since miRNAs can induce deadenylation-dependent mRNA decay (Wilczynska and Bushell, 2015) and RBPs can destabilize *MYC* mRNA (Barreau et al, 2005), this effect is still consistent with the involvement of these molecules and does not argue against the demonstrated effect on translation of pulse-labeling experiments (Fig. 4.10).

5.4 The 3´-UTR of *MYC* responds to glutamine-derived adenosine

The involvement of glutamine in several metabolic pathways makes it challenging to full understand how glutamine regulates MYC (Fig. 1.4). Consequently, glutamine starvation can determine broad changes in the concentrations of downstream

metabolites and in the activation of different stress responsive signaling pathways. These changes occur also in HCT116 cells, as assessed by measuring the levels of multiple metabolites, which confirmed that these cells need glutamine to fuel biosynthetic pathways (Dejure et al, 2017). Levels of reactive oxygen species (ROS) increased under glutamine starvation, likely due to decreased glutamine-derived glutathione or NADPH, which provides reducing power (Fig. 4.19). Although harmful at very high concentrations, ROS act as signaling molecules at moderate levels and assume a pro-oncogenic role for cancer cells (Panieri and Santoro, 2016). In this view, they could be a stimulus candidate able to mediate the observed decrease in MYC protein levels following starvation. Since this concept can be applied to every glutamine-derived metabolite, changes in MYC levels were evaluated accordingly to the effect of different cell-permeable substrates supplemented to starved cells. Two experimental conditions were selected as read-out, in line with previous experiments: a short starvation (2 hours) in the presence of single or combined cell-permeable substrates or a longer starvation (15 hours) followed by the addition of the same substrates for 2 hours. The selected substrates belonged to three major glutamine-controlled pathways: TCA cycle, redox and antioxidant power and nucleotides biosynthesis. These experiments established that the nucleosides are the metabolites specifically able to rescue MYC protein levels in the absence of glutamine, or to mimic the up-regulative effect of glutamine when re-added following starvation (Fig. 4.20). A deeper evaluation of the contribution of single nucleosides revealed that adenosine alone was necessary and sufficient to restore MYC levels (Fig. 4.21). Experiments performed using the exogenous MYC constructs confirmed that adenosine is the specific glutamine-derived stimulus sensed by the 3′-UTR, due to the fact that it only rescues MYC proteins when the 3′-UTR is present (Fig. 4.22B). Previous experiments demonstrated that the re-addition of glutamine following starvation led to an unspecific upregulation of MYC, since this effect was observed in all tested exogenous constructs (Fig. 4.11D). Comparing the effect of adenosine and glutamine allowed for the discrimination of the specific contribution of the latter metabolite on the 3′-UTR-mediated regulation on MYC. While glutamine upregulated the exogenous MYC both in the presence or the absence of the 3′-UTR, the adenosine-mediated effect occurred only in the presence of the 3′-UTR (Fig. 4.22B).

Adenosine can enter the purine salvage pathways either through the direct conversion to AMP or through the inosine-mediated formation of IMP (Fig. 5.1).

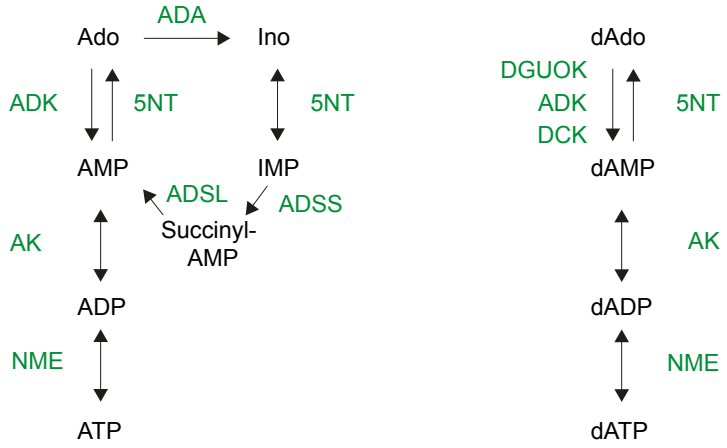

Figure 5.1 Metabolism of adenosine and deoxyadenosine

Schematic depicting the route through which adenosine and deoxyadenosine are converted into nucleotides. All enzymes are expressed in HCT116 cells, as assessed by the transcriptomic data.
5NT (5´nucleotidase); ADK (adenylate kinase); ADSL (adenylosuccinate lyase); ADSS (adenylosuccinate synthetase); ADA (adenosine deaminase); AK (adenosine kinase); DCK (deoxycytidine kinase); DGUOK (deoxyguanosine kinase); NME (nucleoside diphosphate kinase). Adapted from Hatse et al, 1999.

Notably, levels of the adenosine-derived nucleotides AMP, ADT and ATP are strongly affected by glutamine starvation and are restored by adenosine supplementation; thus, proving that adenosine enters the purine salvage pathway (Dejure et al, 2017). In comparison to nucleosides, the intracellular uptake of nucleotides is challenged by the presence of negatively charged groups. Since MYC can be rescued by adenosine and adenosine, in turn, contributes to the pool of AMP, ADP and ATP, it becomes clear that the 3´-UTR of *MYC* responds to the levels of those nucleotides, rather than to glutamine directly. Interestingly, deoxyadenosine, which is converted into dAMP (but not into adenosine (Fig. 5.1)) is not able to rescue MYC protein levels. This observation suggests a specific role of ribo-, rather than deoxyribonucleotides, in regulating MYC (Fig. 4.21).

5.4.1 Adenosine regulates *MYC* translation: molecular implications

Per the observed effect of adenosine in rescuing MYC protein levels under glutamine starvation, it can be concluded that decreased levels of adenosine-derived nucleotides are sensed by the 3´-UTR of *MYC* and this mechanism account for the regulation of MYC protein levels. Two observations clarified this model; firstly, the levels of adenosine-derived nucleotides are rapidly, i.e. within 2 hours, decreased following glutamine starvation (Dejure et al, 2017). Thus, this event can be fast enough to precede MYC downregulation. Secondly, both the presence of adenosine in medium lacking glutamine and its supplementation after starvation restores MYC translation (Fig. 4.22A). The adenosine-mediated effect on MYC levels is lower than the glutamine-mediated one, suggesting the existence of potential additional glutamine-intrinsic mechanisms, as discussed above.

Knowing the specific stimulus regulating MYC can better help to elucidate the responsible mechanism, allowing, for example, for additional layers of control in performing global scale experiments. As mentioned in section 5.3.2, the whole proteome can virtually act as RNA binding protein and regulate translation of target mRNAs. It is an appealing possibility that many metabolic enzymes can moonlight as RBPs (Castello et al, 2015). This means that in absence of the substrate needed for catalyzing a specific reaction, the enzymatic activity is paused, but the same protein is then able to bind mRNAs. Conversely, the binding is abolished when the substrate is available and the enzymatic activity is resumed. Enzymes involved in the nucleotides biosynthesis act as RBPs, as shown in different cell systems (Baltz et al, 2012; Castello et al, 2012; Kwon et al, 2013). Some examples are provided by the adenylate kinase (ADK), which catalyzes the interconversion between ATP, ADP and AMP, and by the nucleoside diphosphate kinase A (NME1), which catalyzed the conversion between nucleotide di- and tri-phosphates. Although the activity of nucleotide biosynthetic enzymes is directly affected by nucleotide levels, many other proteins involved in different metabolic pathways are ATP-binding proteins; therefore, changes in ATP levels can impact a broad range of candidate RBPs.

Many metabolites contribute to the biosynthesis of nucleotides and their depletion can affect nucleotide levels similarly to glutamine. Among them, glucose plays an important role, since it enters the pentose phosphate pathway and allows for the production of ribose-5-phosphate, which is necessary for the synthesis of nucleotides. It is likely that glucose starvation also decreases the levels of nucleotides, although it has not been formally investigated in the present study. However, MYC is not downregulated following glucose starvation. A possible explanation lies in the fact that only changes in the glutamine-dependent steps of the purine biosynthesis activate molecular players acting on MYC. According to the results of the rescue experiments, one could also conclude that only changes in the ATP levels occurring through the nucleotide biosynthetic pathway, but not through the TCA cycle, can mediate the response of MYC. Yet, TCA cycle intermediates were not able to rescue MYC levels. This observation provided additional suggestions about the specificity of the stimulus triggering the involved mechanism. Help in disentangling these complex pathways could come either through the evaluation of large scale analysis on molecules bound to the *MYC* 3′-UTR and through metabolomics flux analysis, which can allow the intracellular destiny of different substrates to be followed.

5.5 Links between the 3′-UTR and MYC-induced apoptosis: unifying opposite observations

5.5.1 The concept of MYC-induced apoptosis

In addition to several established MYC functions, MYC is also able to induce apoptosis. MYC-induced apoptosis is considered a fail-safe mechanism to prevent oncogenic transformation. Many experimental systems have demonstrated that high MYC levels are required for inducing apoptosis (Murphy et al, 2008) and that the loss of mediators of the apoptotic response, such as the tumor suppressors ARF or p53, is needed for allowing tumor development and progression (Hoffman and Liebermann, 2008). Different pro-apoptotic mechanisms mediate MYC-induced apoptosis and the involvement of molecular players depends on the cell type and the triggering stimulus

(Hoffman and Liebermann, 2008). A variety of systems have been used to demonstrate MYC´s ability to induce and sensitize cells to apoptosis. The concept of MYC-mediated sensitization to apoptosis implies that, in the presence of pro-apoptotic stimuli, cells expressing high levels of MYC are more prone to undergo apoptosis than their wildtype counterpart. Early studies, for example, have demonstrated that MYC-ER expression in rat fibroblasts increased apoptosis in cells subjected to a variety of stimuli, such as serum deprivation or starvation of glucose or the essential amino acid isoleucine (Shim et al, 1998; Evan et al, 1992). The following works have demonstrated that MYC is able to sensitize cultured cells to a variety of pro-apoptotic stimuli, including glutamine starvation (Yuneva et al, 2007; Nieminen et al, 2013). It is important to emphasize that in these studies *MYC* expression was enforced by using transgenes, such as MYC-ER, comprising of only the coding sequence of MYC2. Yuneva *et al.*, for example used human fibroblasts overexpressing MYC-ER as a system for demonstrating MYC-induced apoptosis following glutamine deprivation. Interestingly, the authors noted no decrease in the exogenous MYC levels under this condition. The present study, in contrast, highlights that HCT116 cells do not significantly undergo apoptosis following glutamine starvation and that the 3´-UTR mediates the glutamine-induced downregulation of MYC. The classical *MYC* transgenes, lacking the 3´-UTR, do not allow MYC downregulation and promote MYC-induced apoptosis by maintaining high MYC levels under stress conditions. Thus, the 3´-UTR represents the potential unifying element between such contrasting observations.

5.5.2 The presence of the 3´-UTR relieves cells from glutamine addiction

A formal proof of the fact that MYC downregulation protects HCT116 cells from the apoptosis induced by glutamine starvation can be achieved by comparing the effect of *MYC* transgenes encompassing, or lacking the 3´-UTR.

Thus, MYC-ER or MYC-ER-3´-UTR were expressed in HCT116 cells and the biological outcome was evaluated. In order to avoid a possible underestimation of the pro-apoptotic potential of MYC, MYC-ER was expressed at higher levels than the endogenous MYC. MYC overexpression is sufficient to induce apoptosis in some cell systems, such as the osteosarcoma cell line U2OS, or the mammary epithelial cell line

MCF10 (Walz et al, 2014; Wiese et al, 2016). However, although HCT116 cells highly express endogenous MYC, a further increase in MYC levels by expression and activation of MYC-ER was well tolerated by these cells in presence of glutamine. As observed by microscopic observation and assessed by BrdU/PI FACS analysis, MYC-ER activation increased the rate of proliferation without significantly affecting the percentage of apoptotic cells (Fig. 4.29, +Q situation in EV and MYC-ER). However, activation of MYC-ER under glutamine starvation strongly increased the percentage of apoptosis compared to control cells, ultimately leading to complete cell death (Fig. 4.23). On one side this observation rules out the possibility that HCT116 cells are impaired in their ability to undergo apoptosis; on the other side, it recapitulates the result of previous studies (e.g. Yuneva et al, 2007). To explain these two distinct apoptotic outcomes, as observed in control and MYC-ER expressing cells, the 3´-UTR was introduced into the exogenous MYC construct; thus, allowing for its downregulation following glutamine starvation. Strikingly, the presence of the 3´-UTR improved cell viability and decreased the number of apoptotic cells, although the rescue effect was not complete. This is likely due to the fact that, although downregulated under glutamine starvation, the remaining levels of the endogenous MYC were still higher than the exogenous ones (Fig. 4.23).

Thus, these experiments prove that the downregulation of MYC allows for cell survival under glutamine starvation and, simultaneously, demonstrated that the 3´-UTR represent the missing link between previous works and the present study in evaluating the MYC-mediated response to glutamine starvation.

5.5.3 Including regulatory sequences of *MYC* into transgenes as a better strategy for evaluating MYC function.

As discussed above, the concept of MYC-induced apoptosis has been mainly demonstrated enforcing ectopic MYC expression in different cellular systems. This study highlights the need of using MYC transgenes susceptible to stress-induced mechanisms of regulations, i.e. mimicking mechanisms occurring in an *in vivo* setting. In fact, the absence of the 3´-UTR uncouples mechanisms otherwise involved in downregulating MYC and allowing cells to escape apoptosis. Thus, the employment of

traditional systems may lead to overestimate the pro-apoptotic potential of MYC under different stress conditions.

However, the present observations do not invalidate the demonstrated ability of MYC to induce apoptosis, as demonstrated by studies showing that the endogenous MYC is able to trigger this response (Sutherland et al, 2006; Phesse et al, 2014).

Moreover, under certain circumstances, such as chemical induction of ER-stress, MYC is upregulated in an IRES-dependent way. Thus, in such cases, high MYC levels can drive an apoptotic response. Interestingly, also glutamine starvation can induce ER-stress since glutamine is necessary for the biosynthesis of N-acetylglucosamine, which is used for post-translational modifications of proteins occurring in the ER (De Berardinis and Cheng, 2010). Besides cell type-specific responses, a likely explanation for this discrepancy is that glutamine starvation induces a stronger effect on activating stress-pathways responsive to decreased nucleotide levels, rather than to ER-stress, leading to MYC downregulation. Thus, the biological outcomes in terms of induction or evasion from apoptosis can be different according to the form and to the intensity of a stress stimulus. These apparently contrasting observations underline once more the need to consider the UTR elements of *MYC* in order to precisely evaluate the effect of specific stressors and the biological outcomes associated with MYC regulation.

Another implication of the role of *MYC* 3′-UTR concerns the impact on applied follow-up studies based on MYC-induced apoptosis following stress. Since the present study focused on the role of glutamine in regulating MYC and provides a different understanding than previous studies, it is worth mentioning that the concept of MYC-induced glutamine addiction has been exploited for therapeutic purposes. The glutamine addiction results from the establishment of a specific transcriptional program; thus, the possibility to target the enzyme GLS, and therefore the glutaminolytic pathway, has been tested as a way to target MYC-driven tumors. The importance of this approach lies in the fact that MYC is non-druggable and alternative ways to target it, for example finding metabolic liabilities, must be considered. However, studies showing the efficacy of targeting glutamine metabolism made use of *in vivo* models of tumors driven by canonical exogenous *MYC* construct, which lack the 3′-UTR (Yuneva et al, 2012; Shroff et al, 2015; Xiang et al, 2015). According to the present results, inclusion of the 3′-UTR is expected to relieve the tumor dependency on glutamine; thus, affecting the

therapeutic efficacy of these compounds. Although the *in vivo* impact of the 3´-UTR in these studies can be discussed only on a speculative basis, observations obtained from two-dimensional cell culture experiments pose the rational for further and deeper investigations.

5.6 The 3´-UTR of *MYC* as a link between the cellular metabolic status and the transcriptional output

In order to protect cells from apoptosis induced by glutamine deprivation, MYC downregulation has to impact on processes whose activity under starvation may impair cell survival. Since glutamine starvation itself can induce complex changes at different cellular levels, activation of MYC-ER in the absence of glutamine, i.e. maintaining MYC levels high, provides an appropriate control for dissecting the contribution of MYC under starvation.

5.6.1 Glutamine-mediated effects on MYC: evaluation of effects on steady-state transcription

The transcriptional activity of MYC affects all cellular processes, including metabolism. The majority of studies evaluated MYC-driven transcriptional changes in a nutrient-rich context, i.e. in the presence of glucose and glutamine. For example, Wise *et al.* focused on metabolic processes and showed that MYC-ER activation in mouse embryo fibroblasts (MEFs) increased the expression of genes whose products are involved in the metabolism of glutamine, namely the glutamine transporter ASCT2 and the enzymes GLS and LDH-A. Conversely, silencing MYC in glioblastoma cells reduced the expression of these genes (Wise et al, 2008). Such experimental setups provide a clear way to assess direct MYC effects and allowed for the establishment of a link between MYC and glutamine metabolism. In comparison, this current study aimed to understand MYC-mediated effects in a starved context, i.e. due to downregulation following glutamine withdrawal. Considering such a system adds a further layer of complexity due to the fact the glutamine starvation has itself many effects, for example it affects the activity of many signaling pathways involved in transcriptional regulation.

Therefore, RNA-sequencing was performed to obtain global information regarding transcriptional changes linked to MYC downregulation and in order to understand which elements are necessary for ensuring cell survival under glutamine starvation. In order to avoid under-estimating changes in the steady-state levels of mRNAs, a long time-point (24 hours) was considered for performing this experiment. As expected, this analysis highlighted the deep transcriptional changes associated with glutamine starvation. Half of the 18,912 expressed genes were significantly regulated in the absence of glutamine, both with and without activated MYC-ER (Fig. 4.26A and 4.26B). Interestingly, even though HCT116 cells have high levels of endogenous MYC, activation of MYC-ER in the presence of glutamine still induced transcriptional changes (Fig. 4.26C). This effect is likely due to increased occupancy of low affinity binding sites and enhancer regions not saturated by the endogenous MYC (Walz et al, 2014; Lorenzin et al, 2016). A comparison with ChIP-sequencing data, which allows for the identification of MYC binding sites, under the same experimental conditions used for performing RNA-sequencing would be necessary to definitively prove this model. Besides those compelling observations, the focus of this experiment was to evaluate transcriptional changes induced by glutamine starvation and reversed by MYC-ER activation; thus, likely to be specifically associated with MYC transcriptional activity (Fig 4.23D). Twenty-one percent of all expressed genes were significantly (q-value < 0.05) regulated when MYC-ER was activated in absence of glutamine. Since this number corresponds to around four thousand genes, the analysis was based on the evaluation of gene sets, i.e. groups of genes associated with a specific cellular process, enriched between two conditions, rather than on single genes. The evaluation of the results focused on the upregulated gene sets, since those are likely to be downregulated following glutamine starvation in a MYC-dependent way (Table 4.3D). Gene set enrichment analysis allowed for the identification of three major groups of gene sets: gene sets commonly associated with deregulated MYC expression (e.g. well-known MYC-activated target genes published by Schuhmacher (Schuhmacher et al, 2001), Acosta (Acosta et al, 2008), Kim (Kim et al, 2006) and Dang (Zeller et al, 2003)), confirming that MYC-ER is functionally active under starvation; gene sets associated with replication and cell cycle (e.g. from the Reactome Pathway Database (Reactome.org): DNA strand elongation, DNA replication, S-phase, synthesis of

DNA)) and gene sets linked to metabolic processes (e.g. Wong Mitochondria gene module (Wong et al, 2008), Reactome: TCA cycle and respiratory electron transport, KEGG: Purine metabolism, KEGG: Pyrimidine metabolism). The first group contains genes activated by MYC in different cell systems and belonging to multiple pathways; the second group and third one are tightly linked since the expression of metabolic genes is cell cycle-dependent, consistent with the increased metabolic demand upon proliferation. However, gene sets belonging to the three arbitrary-defined groups were regulated by MYC-ER irrespectively of the presence or absence of glutamine. Thus, this analysis did not provide information regarding specific pathways regulated in a MYC-dependent way, whose differential regulation may account for protecting cells from MYC-induced apoptosis.

5.6.1.1 Avoiding increased replicative stress does not account for MYC downregulation under glutamine starvation

The magnitude of gene sets, not their specific type, which were upregulated by MYC-ER following starvation represented a distinctive factor worth further examination. Follow-up experiments were performed to verify whether this difference corresponded to cellular changes in an attempt to be able to explain why MYC-downregulation protects cells from glutamine-induced apoptosis. Among the broad spectrum of effects, MYC drives cell cycle progression by increasing both DNA replication and the biosynthesis of nucleotides, through its transcriptional activity. MYC overexpression increases the entry of cells in S-phase, accelerating the replication process and inducing replicative stress, which then subsequently need to be counterbalanced by activated responsive pathways to be efficiently sustained. Nucleotide starvation represents a cause of replicative stress and induces stalling of the replication fork (Rohban and Campaner, 2015). Glutamine starvation depletes the pool of deoxynucleotides (Dejure et al, 2017) - likely the main reason of the cell cycle arrest observed in this condition (Fig. 4.5). Since MYC-ER keeps pushing the expression of S-phase-related genes following starvation, abnormal S-phase entry could enhance the replicative stress over a sustainable limit, ultimately leading to apoptosis. Cell cycle analysis performed after long starvation for several days confirmed that HCT116 cells arrested through the cell cycle. According to

the DNA content, cells were arrested in the S-phase, even though they were not able to replicate their DNA, as assessed by the negative BrdU incorporation (Fig. 4.27; EV condition). However, starved cells were still able to survive after 6 days. Albeit glutamine starvation moderately induced apoptosis, as assessed by the sub-G1 population, this effect was constant over time. Consistent with the expected effect of MYC over-expression, MYC-ER activation in the presence of glutamine increased the number of cells entering the S-phase and undergoing active DNA replication, compared to the EV condition. However, this analysis did not highlight any difference between EV- and MYC-ER-expressing cells indicative of enforced S-phase entry in the absence of glutamine (Fig.4.27, compare BrdU-positive cells). Thus, glutamine starvation represents a stress stimulus to which cells adapt by arresting proliferation in a way that does not appear to be directly dependent upon MYC.

5.6.1.2 Changes in metabolite levels do not account for MYC downregulation under glutamine starvation

Another way to evaluate the accordance between MYC-driven transcriptional effects and the outcome on cellular processes was to analyze changes in the pool of metabolites. Yuneva *et al.* reported that MYC-ER-induced apoptosis following starvation depends on an excessive depletion of TCA cycle intermediates and could be rescued by supplementing cell-permeable forms of these substrates (Yuneva et al, 2007). Similarly, ectopic MYC activity following starvation could push energy-demanding processes and dramatically deplete ATP levels. These hypotheses were tested by measuring levels of multiple metabolites and ROS. In contrast to the induction of metabolic changes following glutamine starvation likely due also to MYC downregulation (see 5.4), ectopic MYC activation did not further alter the levels of metabolites or increased ROS production (Fig. 24A; Dejure et al, 2017). A possible interpretation of these results is that MYC-driven metabolic changes depend on the availability of metabolites that, in turn, dictate MYC protein levels. Blocking this positive feedback, for example during starvation, prevents additional changes even if one arm is maintained (MYC-ER in this case). However, it has to be noted that these measurements reflect steady-state metabolic levels and not their dynamic changes.

Thus, MYC-ER could potentially increase both the metabolite consumption and the activation of mechanisms able to compensate for the loss of substrates. Autophagy is one candidate mechanism, since it allows for recycling of intracellular components under stress conditions. In addition to other catabolic processes, autophagy can be activated by AMPK (Egan et al, 2011), which is involved in the maintainance of cellular homeostasis and whose activity is in turn stimulated by decreased ATP levels or increased ROS (Hardie, 2007; Park et et, 2006). Both effects are observed following glutamine starvation. Moreover, MYC hyper-activation in several systems is a sufficient stimulus to trigger AMPK activation (see 1.3.2). Neither MYC-ER activation in the presence of glutamine nor glutamine starvation activates AMPK in HCT116 cells, as assessed by its phosphorylation status. It is likely that, even if the sensing through AMPK is functional, as assessed after glucose starvation, these stimuli are not sufficient to activate it and that these cells rely on different pathways to maintain cellular homeostasis under these conditions (Fig. 4.25). The combination of the two stimuli, i.e. MYC-ER activation in the absence of glutamine, also did not activate AMPK. Based on this observation, pushed metabolic processes resulting in an imbalanced use of metabolites was not considered as the major reason explaining why cells need to downregulate MYC.

All in all, these data endorse the positive role of MYC in promoting key cellular functions, such as proliferation, and pushing increased biosynthesis under a permissive metabolic status, i.e. in the presence of glutamine, as shown by many previous works. Even though the consequences of glutamine starvation, including reduced metabolite levels, can be associated with decreased MYC protein levels, ectopic MYC expression cannot overcome these effects. Thus, different MYC-mediated changes have to be taken into account as potential explanation of its glutamine-induced downregulation.

5.6.2 Glutamine mediated effects on MYC: evaluation of effects on RNA Polymerase II function

The previous discussion highlighted that glutamine-induced changes on MYC protein levels are rapid, dynamic and depend on the levels of adenosine-derived nucleotides.

Thus, the glutamine-mediated regulation of MYC can induce transcriptional changes that are not reflected in specific changes on steady-state levels of mRNAs.

MYC can control the process of transcription at different steps. MYC recruits several cofactors that fulfill distinct functions and whose interactions can be potentially affected by glutamine starvation. However, it exerts its main effect on RNA polymerase II (RNAPII) (see 1.1.1.1). Thus, changes in the function of RNAPII were used as a read-out for evaluating if glutamine-mediated changes in MYC protein levels influence the process of transcription.

5.6.2.1 MYC globally couples RNAPII function and ribonucleotide levels

The aim of the experiments discussed in this section was to evaluate why cells need to rapidly downregulate MYC and how fast changes in MYC protein levels may affect transcription. A candidate mechanism which could account for the rapid regulation of MYC is represented by the function of MYC in stimulating RNAPII pause-release, i.e. establishing a productive elongation. A seminal study from Rahl *et al.* confirmed the fundamental role of MYC in promoting transcriptional elongation (Rahl et al, 2010). The authors of this study demonstrated that MYC controls this process in embryonic stem cells and they demonstrated that MYC depletion reduces the ability of RNAPII to elongate without affecting the amount of total RNAPII bound to and paused at the promoter. This mechanism is considered to be responsible for the transcriptional amplification observed when MYC levels increase in both non-transformed and cancer cells (specifically, in P-493 Burkitt´s lymphoma cells), i.e. through the control of RNAPII pause-release, MYC amplifies the expression of genes which are already "marked" by pre-loaded RNAPII (Lin et al, 2012; Nie et al, 2012) (see 1.1.1.2). In order to examine if the reduced MYC protein levels observed after a short starvation time affect the elongating activity of RNAPII, the binding of total RNAPII (RNAPII), or of Serine2-phosphorylated RNAPII (pSer2 RNAPII), indicator of elongating RNAPII, were investigated by chromatin immunoprecipitation (ChIP). Contrary to the expected result, evaluation of total and pSer2 RNAPII binding on single loci demonstrated not only decreased levels of elongating RNAPII folowing starvation, as assessed by the pSer2 RNAPII binding at the transcription end site (TES), but also a reduced binding of

the total RNAPII at the transcription start site (TSS) (Fig. 4.31). Importantly, immunoblot analysis demonstrated no changes in the amount of total or pSer2 RNAPII following starvation (Fig. 4.30). These observations indicate on the one side that the decreased binding of RNAPII is not simply due to reduced protein levels following glutamine starvation; on the other side, the activity of basal transcription factors involved in both the initiation and the elongation of transcription appears not to be affected by glutamine starvation, since RNAPII can still be efficiently phosphorylated. Under this condition MYC protein levels are downregulated, in a manner dependent upon the levels of adenosine-derived ribonucleotides. Thus, these observations may suggest either that MYC affects the recruitment of RNAPII and its consequent elongation or that these changes are the secondary result of decreased levels of ribonucleotides. However, ectopic activation of MYC-ER under starvation restored the recruitment and the elongation of RNAPII at both tested loci (Fig. 4.31). This effect was direct, since, under these conditions, MYC-ER does not increase the levels of any tested metabolite, including nucleotides (see 5.6.1.2). Moreover, rescue of RNAPII binding at the TSS was observed when endogenous MYC protein levels were restored by adenosine supplementation under glutamine starvation. This last observation further demonstrates that specific role played by MYC in controlling the activity of RNAPII.

A more comprehensive evaluation of the glutamine-induced and MYC-mediated effects on the RNAPII function was obtained through the analysis of ChIP-sequencing results. This experiment confirmed that glutamine starvation decreases the RNAPII binding at both the TSS and at the TES and that MYC-ER partially restores it, as assessed by both single tracks evaluation and by genome-wide analysis of all genes with detectable RNAPII binding (Fig. 4.33). Thus, it could be first concluded that the strong effect of glutamine starvation on RNAPII loading at the TSS is reflected in changes in the RNAPII occupancy in the gene body. Since this effect is dictated by changes in MYC protein levels, one can conclude that MYC affects both the loading and the elongation of RNAPII in the cellular system studied. This observation directs to a mechanism different than the one previously ascribed to MYC, i.e. inducing RNAPII pause release. Thus, the present study suggests an additional role of MYC in affecting the loading of RNAPII at promoter regions. These observations are supported by other studies, performed using further different experimental systems, demonstrating a correlation

between MYC and RNAPII occupancy, i.e. increased total RNAPII binding at the TSS when MYC protein levels increase (Walz et al, 2014; Jaenicke et al, 2016). In order to further evaluate the direct dependency of RNAPII loading on MYC, the binding pattern of MYC binding with the TSS was correlated with that of RNAPII at the same site (Fig. 4.35; Fig. 4.36). Differences due to technical issues and to the procedure of peak calling, i.e. the definition of a ChIP-seq peak - that indicates the RNAPII binding to a specific genomic site -, did not allow for the comparison of the same number of peaks, i.e. the number of MYC peaks were lower than the one of RNAPII peaks (Fig. 4.36A). Heat-map analysis showed that MYC-binding follows RNAPII-binding on RNAPII-bound genes (Fig. 4.35). Correlation between MYC and RNAPII occupancy at promoter regions proved that the increased binding of RNAPII positively correlated with higher MYC occupancy in the presence of glutamine (Fig. 4.36B, black dots). Under glutamine starvation RNAPII occupancy decreased uniformly on all genes and was partially rescued after MYC activation (Fig. 4.36B, grey and orange dots). Although it might be that the correlation between MYC and RNAPII occupancy are not direct, since MYC binding was analyzed only in presence of glutamine, they may reflect a situation in which changes in MYC binding, due to decreased or ectopically expressed protein levels, correspond to changes in the binding of RNAPII.

The same pattern of correlation was observed at the TES, although the differences between each condition were not as evident as at the promoter, probably because of differences in the antibody binding (Fig. 4.36B, right). All in all, these data confirmed that also in HCT116 cells MYC occupancy correlates with RNAPII occupancy. Further analyses of ChIP-seq data focused on the evaluation of effects on RNAPII loading and elongation dependent on the glutamine-mediated changes in MYC levels.

Global changes in the RNAPII occupancy at transcriptional start sites (TSS), within gene bodies and at transcriptional end sites (TES) were compared either under glutamine stravation (+Q *versus* –Q) or after restoration of MYC levels in starved cells (+Q *versus* MYC-ER –Q) (Fig. 4.34A). This analysis confirmed that the glutamine-induced and MYC-mediated effect on RNAPII occurred at the transcription initiation level, as assessed by the decreased RNAPII occupancy at promoter regions that was then rescued by MYC-ER. However, this analysis also highlighted that the binding of

elongating RNAPII did not substantially differ in the absence of glutamine, as assessed by only minor changes in pSer2 RNAPII occupancy in gene bodies (Fig. 4.34A). Thus, the traveling ratio decreased following glutamine starvation and this effect could be partially reverted by activating MYC-ER (Fig. 4.34B). Consistent with previous data (Rahl et al, 2010), the traveling ratio for the majority of RNAPII-bound genes (circa 80 %) was higher than one, in both the presence and the absence of glutamine. Since this parameter results from the ratio between total RNAPII occupancy at the promoter and in the gene body, a value greater than one indicates that the RNAPII accumulates in the promoter, rather than in the gene body. The literature describes this as evidence of RNAPII pausing at promoter regions, from which the enzyme is subsequently released (Rahl et al, 2010).

A decreased traveling ratio between two different biological situations, can be either due to a decrease of RNAPII in the promoter and unchanged elongating RNAPII in the gene body or increased RNAPII binding in the gene body while initiation at the promoter is unchanged. The latter has been shown for a MYC-dependent RNAPII pause-release in a B cell lymphoma cell line (Rahl et al, 2010). In contrast, RNAPII levels at promoters are strongly decreased but RNAPII binding in gene bodies shows only a small decrease in HCT116 cells under glutamine starvation; thus, this effect leads to a decrease in the traveling ratio. A decreased traveling ratio suggests that glutamine starvation slows down RNAPII elongation or decreases pause-release from promoters. Restoration of MYC after glutamine withdrawal largely but not completely rescues this effect. Thus, in the cell system studied, MYC predominantly regulates the transcriptional initiation, so that decreased MYC protein levels following glutamine starvation result in decreased RNAPII occupancy at promoter regions, while levels of elongating RNAPII, i.e. occupancy in the gene body, are not deeply affected.

In conclusion, the emerging picture suggests that MYC protein levels are controlled by the availability of ribonucleotides and MYC, in turn, controls the function of RNAPII. Since the nucleotide-mediated control on MYC occurs through its 3´-UTR, it becomes evident that this element links the cellular metabolic requirements, in terms of ribonucleotide availability, to changes in the RNAPII activity. Thus, the glutamine-

induced MYC downregulation can be functional to modulate the rate of transcription and to adapt it to starvation-induced stress.

5.7 The glutamine-induced downregulation of MYC prevents apoptosis due to accumulation of transcriptional stress

The results obtained from analyzing transcriptional changes following glutamine starvation highlighted that the transcriptional machinery is still able to cope with starvation-induced stress. MYC downregulation is required to maintain a balance in such harmful situation. This assumption is further demonstrated by the fact that ectopic activation of MYC shifts the balance towards an apoptotic phenotype. Although previously discussed analyses helped to establish that MYC downregulation controls RNAPII function, they do not provide specific indications regarding mechanisms potentially leading to increased cell death when such regulation is lost. ChIP-seq data showed that MYC-ER boosts the loading and elongation of RNAPII in the absence of glutamine. However, transcriptomic data did not point to specific changes in the final outcome, i.e. the amount of mRNA production, which appears to be differentially regulated in both directions, likely because of the deep changes induced by glutamine. One possible explanation is that the restoration of RNAPII function following high MYC levels in the absence of glutamine does not occur as efficiently as when glutamine is present, i.e. when the transcription works properly. In order to better investigate this possibility, changes in the RNAPII occupancy at promoter and gene body regions, in each condition of starvation, i.e. in the presence of low or high MYC protein levels, were compared with the control situation, i.e. the presence of glutamine (Fig. 4.37). This kind of analysis provided a different overview of changes that occur following starvation compared to the analysis obtained by previous global evaluations, such as the metagene analysis. In fact, changes occurring on single genes were considered in this case, rather than an average over all RNAPII-bound genes. In addition to confirming previous observations, such as the pronounced effect on RNAPII loading following glutamine starvation, it demonstrated that, although on average decreased following starvation, the RNAPII occupancy on some genes is higher than control levels at either the promoter regions or in the gene body (Fig. 4.37, left plot, upper and right squares).

Increased RNAPII occupancy under starvation can be an indicator of stress or can be due to the fact that cells need to increase transcription of certain genes. These data have not been further analyzed and have not been correlated with the transcriptomic data in the present study, since they are representative of a condition that is still tolerated by the cells. On the contrary, activating MYC-ER in starved cells changes the distribution of RNAPII occupancy. On a subset of around 200 genes, RNAPII occupancy in the gene body was found to be significantly higher when MYC-ER was activated, compared to both the control situation and to the starved condition, as exemplary shown for the *TKT* gene (Fig. 4.37, compare *TKT* position between the left and the right plot). This result indicated that, although maintaining high MYC levels following glutamine starvation restores the RNAPII function, this process is not as efficient as in presence of glutamine, since it leads to the accumulation of RNAPII on a group of genes. Stalled RNAPII can be an indicator of transcriptional-associated stress and can occur, for example, in the presence of damaged DNA (Edenberg et al, 2014). Thus, one possibility is that the increased RNAPII function, due to enforced MYC activity, exacerbates the harmful effects associated with the glutamine starvation. This scenario is supported by the fact that glutamine withdrawal is a sufficient stimulus able to induce DNA damage, for example because of an increased production of ROS (Cadet and Wagner, 2013). Moreover, MYC induces DNA damage in both a ROS-dependent or -independent manner (Vafa et al, 2002; Ray et al, 2006). Although these mechanisms contribute to drive MYC-induced genomic instability, which is associated with cell transformation and tumor progression (Kuzyk and Mai, 2014), it is possible that cells still need to strike a balance between the metabolic input and the transcriptional output, i.e. by avoiding too much transcription- associated damage.

Stalled RNAPII can have different molecular consequences that are markers of transcriptional stress. One of those markers is represented by formation of R-loops. R-loops are DNA-RNA hybrid structures that can be formed during transcription, following the re-annealing of the mRNA to the transcribed DNA strand. In this way, the complementary non-transcribed DNA strand is left as a single strand, which would be more exposed to the action of damaging agents, such as ROS, leading to DNA strand breaks. Thus, these events represent a potential source of genomic instability (Aguilera and Garcia-Muse, 2012). Increased R-loops formation at the same site of RNAPII

stalling in the *TKT* gene (Fig. 4.38) occurred only in MYC-ER expressing cells after 24 hours of starvation (Dejure et al, 2017). R-loop-associated genomic instability can be attributed to the collision between the replication fork and the stalled RNAPII (Aguilera and Garcia-Muse, 2012). Replication-associated genomic instability is unlikely to occur since glutamine starvation induces cell cycle arrest and subsequent blockade of replication due to the lack of deoxynucleotides. This condition is also not altered by MYC-ER activation. However, one possible scenario is that the transcriptional damage induced by R-loop formation, e.g. single strand DNA breaks, accumulates over time until it overcomes a threshold sensed as a pro-apoptotic stimulus. A conclusive proof of such model could be obtained by overexpressing the enzyme RNase H1, which is normally involved in resolving R-loops structures (Aguilera and Garcia-Muse, 2012). Enforcing its activity is expected to revert the apoptotic phenotype associated with MYC-ER overexpression following glutamine starvation.

5.8 Glutamine-mediated regulation of MYC: revisiting old concepts in the light of new findings

The present work analyzed the link between MYC and the metabolism of glutamine from a different perspective, focusing on how glutamine regulates MYC. It provides new information compared to previous studies which were mainly focused on evaluating how MYC drives the metabolism of glutamine (Fig. 5.2).

From a mechanistic point of view, the present study demonstrates that ribonucleotides, specifically adenosine-derived nucleotides, are the critical glutamine-derived metabolites that mediate the downregulation of MYC. Previous studies established that the prominent oncogenic-associated function of glutamine is providing anaplerotic substrates through the glutaminolysis and that MYC enhances the glutamine entrance into the TCA cycle (Yuneva et al, 2007; Wise et al, 2008). The present work provides evidences that, although glutamine contributes to sustain the TCA cycle, this function is independent of the control on MYC protein levels.

This study also highlighted the role of MYC as a linker between the cellular metabolic status and the global control of the process of transcription. Changes in MYC levels that are dictated by the availability of ribonucleotides are reflected in changes in the function

of the RNAPII. In this regard, MYC controls both the recruitment and the elongation of the RNAPII. This observation discloses a further way through which MYC regulates transcription in this experimental setting and underlines the broad role of MYC in controlling the function of RNAPII at different levels following metabolic stress. Loss of control of MYC regulation following decreased ribonucleotide levels and in presence of stress stimuli enhances the RNAPII function and drives the formation of aberrant transcriptional structures, which can potentially represent a signal able to induce apoptosis.

However, a major point supported by this mechanism is represented by the fact that the glutamine-mediated regulation of MYC occurs through its 3′-UTR. The absence of regulatory sequences (5′-UTR and 3′-UTR) can potentially lead to the disruption of feedback mechanisms of regulation that are still working in cancer. Thus, this study highlights the need of including regulatory sequences into transgenes, for evaluating the response of MYC towards stress stimuli, both *in vitro* and *in vivo*. The rationale behind many pharmacological approaches targeting cancer cells, possibly in a MYC-dependent way, is based on the induction of metabolic perturbations. The establishment of tumor models that allow potential regulatory circuitry to still operate, i.e. to target or work through the UTRs, may provide a better way to evaluate the drug efficacy. As exemplarily shown in this experimental setting, the 3′-UTR-mediated regulation of MYC relieves the cells from the glutamine addiction. Thus, in general, such mechanisms may protect cells that experience metabolic stress and avoid the induction of an apoptotic response. Since this response has been observed in a tumor cell line, it is possible to speculate that such regulatory effect represents a further level of the metabolic reprogramming characteristic of cancer cells. In light of this, such mechanisms could be functional to allow for the adaptation of cancer cells towards the metabolic pressure they are often exposed to.

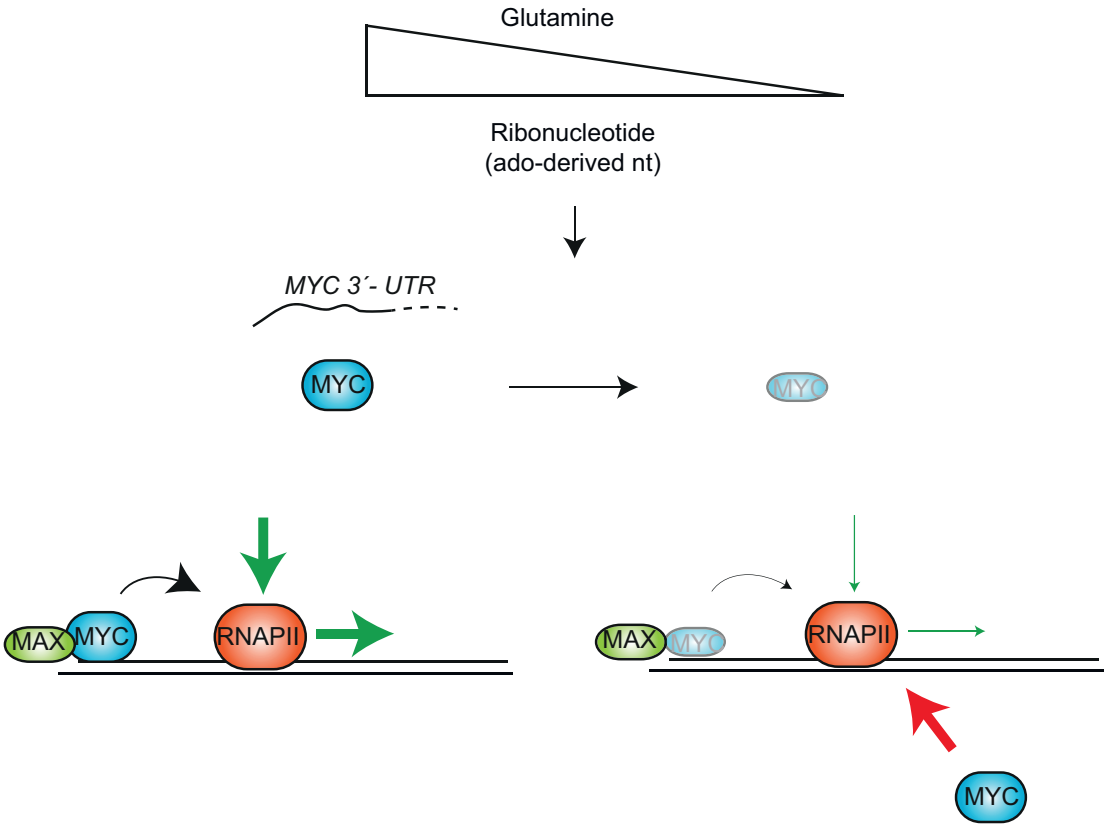

Figure 5.2 Model summarizing the findings presented in this study

6 Bibliography

Abdelhaleem, M. (2004). Over-expression of RNA helicases in cancer. Anticancer research *24*, 3951-3953.

Acosta, J.C., Ferrandiz, N., Bretones, G., Torrano, V., Blanco, R., Richard, C., O'Connell, B., Sedivy, J., Delgado, M.D., and Leon, J. (2008). Myc inhibits p27-induced erythroid differentiation of leukemia cells by repressing erythroid master genes without reversing p27-mediated cell cycle arrest. Molecular and cellular biology *28*, 7286-7295.

Adhikary, S., and Eilers, M. (2005). Transcriptional regulation and transformation by Myc proteins. Nature reviews Molecular cell biology *6*, 635-645.

Aguilera, A., and Garcia-Muse, T. (2012). R loops: from transcription byproducts to threats to genome stability. Molecular cell *46*, 115-124.

Ahmed, D., Eide, P.W., Eilertsen, I.A., Danielsen, S.A., Eknaes, M., Hektoen, M., Lind, G.E., and Lothe, R.A. (2013). Epigenetic and genetic features of 24 colon cancer cell lines. Oncogenesis *2*, e71.

Akhoondi, S., Sun, D., von der Lehr, N., Apostolidou, S., Klotz, K., Maljukova, A., Cepeda, D., Fiegl, H., Dafou, D., Marth, C.*, et al.* (2007). FBXW7/hCDC4 is a general tumor suppressor in human cancer. Cancer research *67*, 9006-9012.

Altman, B.J., Stine, Z.E., and Dang, C.V. (2016). From Krebs to clinic: glutamine metabolism to cancer therapy. Nature reviews Cancer.

Ambros, V., Bartel, B., Bartel, D.P., Burge, C.B., Carrington, J.C., Chen, X., Dreyfuss, G., Eddy, S.R., Griffiths-Jones, S., Marshall, M.*, et al.* (2003). A uniform system for microRNA annotation. RNA (New York, NY) *9*, 277-279.

Anders, S., McCarthy, D.J., Chen, Y., Okoniewski, M., Smyth, G.K., Huber, W., and Robinson, M.D. (2013). Count-based differential expression analysis of RNA sequencing data using R and Bioconductor. Nature protocols *8*, 1765-1786.

Audic, Y., and Hartley, R.S. (2004). Post-transcriptional regulation in cancer. Biology of the cell *96*, 479-498.

Bahram, F., von der Lehr, N., Cetinkaya, C., and Larsson, L.G. (2000). c-Myc hot spot mutations in lymphomas result in inefficient ubiquitination and decreased proteasome-mediated turnover. Blood *95*, 2104-2110.

Bailey, T., Krajewski, P., Ladunga, I., Lefebvre, C., Li, Q., Liu, T., Madrigal, P., Taslim, C., and Zhang, J. (2013). Practical guidelines for the comprehensive analysis of ChIP-seq data. PLoS computational biology *9*, e1003326.

Ballou, L.M., and Lin, R.Z. (2008). Rapamycin and mTOR kinase inhibitors. Journal of chemical biology *1*, 27-36.

Baltz, A.G., Munschauer, M., Schwanhausser, B., Vasile, A., Murakawa, Y., Schueler, M., Youngs, N., Penfold-Brown, D., Drew, K., Milek, M.*, et al.* (2012). The mRNA-bound proteome and its global occupancy profile on protein-coding transcripts. Molecular cell *46*, 674-690.

Barna, M., Pusic, A., Zollo, O., Costa, M., Kondrashov, N., Rego, E., Rao, P.H., and Ruggero, D. (2008). Suppression of Myc oncogenic activity by ribosomal protein haploinsufficiency. Nature *456*, 971-975.

Barrero, M.J., Boue, S., and Izpisua Belmonte, J.C. (2010). Epigenetic mechanisms that regulate cell identity. Cell stem cell *7*, 565-570.

Bartel, D.P. (2009). MicroRNAs: target recognition and regulatory functions. Cell *136*, 215-233.

Ben-Sahra, I., Howell, J.J., Asara, J.M., and Manning, B.D. (2013). Stimulation of de novo pyrimidine synthesis by growth signaling through mTOR and S6K1. Science (New York, NY) *339*, 1323-1328.

Ben-Sahra, I., Hoxhaj, G., Ricoult, S.J., Asara, J.M., and Manning, B.D. (2016). mTORC1 induces purine synthesis through control of the mitochondrial tetrahydrofolate cycle. Science (New York, NY) *351*, 728-733.

Berkers, C.R., Maddocks, O.D., Cheung, E.C., Mor, I., and Vousden, K.H. (2013). Metabolic regulation by p53 family members. Cell Metab *18*, 617-633.

Bernstein, P.L., Herrick, D.J., Prokipcak, R.D., and Ross, J. (1992). Control of c-myc mRNA half-life in vitro by a protein capable of binding to a coding region stability determinant. Genes & development *6*, 642-654.

Beroukhim, R., Mermel, C.H., Porter, D., Wei, G., Raychaudhuri, S., Donovan, J., Barretina, J., Boehm, J.S., Dobson, J., Urashima, M.*, et al.* (2010). The landscape of somatic copy-number alteration across human cancers. Nature *463*, 899-905.

Betel, D., Wilson, M., Gabow, A., Marks, D.S., and Sander, C. (2008). The microRNA.org resource: targets and expression. Nucleic acids research *36*, D149-153.

Bhagwat, S.V., Gokhale, P.C., Crew, A.P., Cooke, A., Yao, Y., Mantis, C., Kahler, J., Workman, J., Bittner, M., Dudkin, L.*, et al.* (2011). Preclinical characterization of OSI-027, a potent and selective inhibitor of mTORC1 and mTORC2: distinct from rapamycin. Molecular cancer therapeutics *10*, 1394-1406.

Blackwood, E.M., Luscher, B., and Eisenman, R.N. (1992). Myc and Max associate in vivo. Genes & development *6*, 71-80.

Bradford, M.M. (1976). A rapid and sensitive method for the quantitation of microgram quantities of protein utilizing the principle of protein-dye binding. Analytical biochemistry *72*, 248-254.

Brannan, K., and Bentley, D.L. (2012). Control of Transcriptional Elongation by RNA Polymerase II: A Retrospective. Genetics research international *2012*, 170173.

Brasse-Lagnel, C., Lavoinne, A., and Husson, A. (2009). Control of mammalian gene expression by amino acids, especially glutamine. The FEBS journal *276*, 1826-1844.

Brattain, M.G., Fine, W.D., Khaled, F.M., Thompson, J., and Brattain, D.E. (1981). Heterogeneity of malignant cells from a human colonic carcinoma. Cancer research *41*, 1751-1756.

Brewer, G. (1991). An A + U-rich element RNA-binding factor regulates c-myc mRNA stability in vitro. Molecular and cellular biology *11*, 2460-2466.

Britton, S., Salles, B., and Calsou, P. (2008). c-MYC protein is degraded in response to UV irradiation. Cell cycle (Georgetown, Tex) *7*, 63-70.

Buchan, J.R., and Parker, R. (2009). Eukaryotic stress granules: the ins and outs of translation. Molecular cell *36*, 932-941.

Bullock, M.D., Bruce, A., Sreekumar, R., Curtis, N., Cheung, T., Reading, I., Primrose, J.N., Ottensmeier, C., Packham, G.K., Thomas, G.*, et al.* (2013). FOXO3 expression during colorectal cancer progression: biomarker potential reflects a tumour suppressor role. British journal of cancer *109*, 387-394.

Bunz, F., Dutriaux, A., Lengauer, C., Waldman, T., Zhou, S., Brown, J.P., Sedivy, J.M., Kinzler, K.W., and Vogelstein, B. (1998). Requirement for p53 and p21 to sustain G2 arrest after DNA damage. Science (New York, NY) *282*, 1497-1501.

Cadet, J., and Wagner, J.R. (2013). DNA base damage by reactive oxygen species, oxidizing agents, and UV radiation. Cold Spring Harbor perspectives in biology *5*.

Cannell, I.G., and Bushell, M. (2010). Regulation of Myc by miR-34c: A mechanism to prevent genomic instability? Cell cycle (Georgetown, Tex) *9*, 2726-2730.

Cannell, I.G., Kong, Y.W., Johnston, S.J., Chen, M.L., Collins, H.M., Dobbyn, H.C., Elia, A., Kress, T.R., Dickens, M., Clemens, M.J.*, et al.* (2010). p38 MAPK/MK2-mediated induction of miR-34c following DNA damage prevents Myc-dependent DNA replication. Proceedings of the National Academy of Sciences of the United States of America *107*, 5375-5380.

Castello, A., Fischer, B., Eichelbaum, K., Horos, R., Beckmann, B.M., Strein, C., Davey, N.E., Humphreys, D.T., Preiss, T., Steinmetz, L.M.*, et al.* (2012). Insights into RNA biology from an atlas of mammalian mRNA-binding proteins. Cell *149*, 1393-1406.

Castello, A., Horos, R., Strein, C., Fischer, B., Eichelbaum, K., Steinmetz, L.M., Krijgsveld, J., and Hentze, M.W. (2013). System-wide identification of RNA-binding proteins by interactome capture. Nature protocols *8*, 491-500.

Cecchini, M.J., Amiri, M., and Dick, F.A. (2012). Analysis of cell cycle position in mammalian cells. Journal of visualized experiments : JoVE.

Challagundla, K.B., Sun, X.X., Zhang, X., DeVine, T., Zhang, Q., Sears, R.C., and Dai, M.S. (2011). Ribosomal protein L11 recruits miR-24/miRISC to repress c-Myc expression in response to ribosomal stress. Molecular and cellular biology *31*, 4007-4021.

Chappell, S.A., LeQuesne, J.P., Paulin, F.E., deSchoolmeester, M.L., Stoneley, M., Soutar, R.L., Ralston, S.H., Helfrich, M.H., and Willis, A.E. (2000). A mutation in the c-myc-IRES leads to enhanced internal ribosome entry in multiple myeloma: a novel mechanism of oncogene de-regulation. Oncogene *19*, 4437-4440.

Chaube, B., Malvi, P., Singh, S.V., Mohammad, N., Viollet, B., and Bhat, M.K. (2015). AMPK maintains energy homeostasis and survival in cancer cells via regulating p38/PGC-1alpha-mediated mitochondrial biogenesis. Cell death discovery *1*, 15063.

Chen, J.Q., and Russo, J. (2012). Dysregulation of glucose transport, glycolysis, TCA cycle and glutaminolysis by oncogenes and tumor suppressors in cancer cells. Biochimica et biophysica acta *1826*, 370-384.

Chou, C.H., Chang, N.W., Shrestha, S., Hsu, S.D., Lin, Y.L., Lee, W.H., Yang, C.D., Hong, H.C., Wei, T.Y., Tu, S.J.*, et al.* (2016). miRTarBase 2016: updates to the experimentally validated miRNA-target interactions database. Nucleic acids research *44*, D239-247.

Christoffersen, N.R., Shalgi, R., Frankel, L.B., Leucci, E., Lees, M., Klausen, M., Pilpel, Y., Nielsen, F.C., Oren, M., and Lund, A.H. (2010). p53-independent upregulation of miR-34a during oncogene-induced senescence represses MYC. Cell death and differentiation *17*, 236-245.

Comerford, S.A., Huang, Z., Du, X., Wang, Y., Cai, L., Witkiewicz, A.K., Walters, H., Tantawy, M.N., Fu, A., Manning, H.C*., et al.* (2014). Acetate dependence of tumors. Cell *159*, 1591-1602.

Conacci-Sorrell, M., Nguoenet, C., Eisenman, R.N. (2010). Myc-nick: a cytoplasmic cleavage product of Myc that promotes alpha-tubulin acetylation and cell differentiation. Cell *142*, 480-493.

Conacci-Sorrell, M., Nguoenet, C., Anderson, S., Brabletz, T., Eisenman, R.N. (2014). Stress-induced cleavage of Myc promotes cancer cell survival. Genes & development *28*, 689-707.

Csibi, A., Lee, G., Yoon, S.O., Tong, H., Ilter, D., Elia, I., Fendt, S.M., Roberts, T.M., and Blenis, J. (2014). The mTORC1/S6K1 pathway regulates glutamine metabolism through the eIF4B-dependent control of c-Myc translation. Current biology : CB *24*, 2274-2280.

Cunningham, J.T., Moreno, M.V., Lodi, A., Ronen, S.M., and Ruggero, D. (2014). Protein and nucleotide biosynthesis are coupled by a single rate-limiting enzyme, PRPS2, to drive cancer. Cell *157*, 1088-1103.

Dalla-Favera, R., Bregni, M., Erikson, J., Patterson, D., Gallo, R.C., and Croce, C.M. (1982). Human c-myc onc gene is located on the region of chromosome 8 that is translocated in Burkitt lymphoma cells. Proceedings of the National Academy of Sciences of the United States of America *79*, 7824-7827.

Dang, C.V. (2012). MYC on the path to cancer. Cell *149*, 22-35.

Dani, C., Blanchard, J.M., Piechaczyk, M., El Sabouty, S., Marty, L., and Jeanteur, P. (1984). Extreme instability of myc mRNA in normal and transformed human cells. Proceedings of the National Academy of Sciences of the United States of America *81*, 7046-7050.

David, C.J., Chen, M., Assanah, M., Canoll, P., and Manley, J.L. (2010). HnRNP proteins controlled by c-Myc deregulate pyruvate kinase mRNA splicing in cancer. Nature *463*, 364-368.

DeBerardinis, R.J., and Cheng, T. (2010). Q's next: the diverse functions of glutamine in metabolism, cell biology and cancer. Oncogene *29*, 313-324.

DeBerardinis, R.J., Lum, J.J., Hatzivassiliou, G., and Thompson, C.B. (2008). The biology of cancer: metabolic reprogramming fuels cell growth and proliferation. Cell Metab *7*, 11-20.

DeBerardinis, R.J., Mancuso, A., Daikhin, E., Nissim, I., Yudkoff, M., Wehrli, S., and Thompson, C.B. (2007). Beyond aerobic glycolysis: transformed cells can engage in glutamine metabolism that exceeds the requirement for protein and nucleotide synthesis. Proceedings of the National Academy of Sciences of the United States of America *104*, 19345-19350.

Dejure, F.R., Royla, N., Herold, S., Kalb, J., Walz, S., Ade, C.P., Mastrobuoni, G., Vanselow, J., Schlosser, A., Wolf, E., *et al.* (2017). The MYC mRNA 3´-UTR couples RNA Polymerase II function to glutamine and ribonucleotide levels. The EMBO journal *36*, 1854-1868.

Doherty, J.R., Yang, C., Scott, K.E., Cameron, M.D., Fallahi, M., Li, W., Hall, M.A., Amelio, A.L., Mishra, J.K., Li, F.*, et al.* (2014). Blocking lactate export by inhibiting the Myc target MCT1 Disables glycolysis and glutathione synthesis. Cancer research *74*, 908-920.

Doyle, G.A., Bourdeau-Heller, J.M., Coulthard, S., Meisner, L.F., and Ross, J. (2000). Amplification in human breast cancer of a gene encoding a c-myc mRNA-binding protein. Cancer research *60*, 2756-2759.

Duran, R.V., Oppliger, W., Robitaille, A.M., Heiserich, L., Skendaj, R., Gottlieb, E., and Hall, M.N. (2012). Glutaminolysis activates Rag-mTORC1 signaling. Molecular cell *47*, 349-358.

Edenberg, E.R., Downey, M., and Toczyski, D. (2014). Polymerase stalling during replication, transcription and translation. Current biology : CB *24*, R445-452.

Edmunds, L.R., Sharma, L., Wang, H., Kang, A., d'Souza, S., Lu, J., McLaughlin, M., Dolezal, J.M., Gao, X., Weintraub, S.T.*, et al.* (2015). c-Myc and AMPK Control Cellular Energy Levels by Cooperatively Regulating Mitochondrial Structure and Function. PloS one *10*, e0134049.

Eick, D., and Bornkamm, G.W. (1986). Transcriptional arrest within the first exon is a fast control mechanism in c-myc gene expression. Nucleic acids research *14*, 8331-8346.

Eijkelenboom, A., and Burgering, B.M. (2013). FOXOs: signalling integrators for homeostasis maintenance. Nature reviews Molecular cell biology *14*, 83-97.

Eilers, M., and Eisenman, R.N. (2008). Myc's broad reach. Genes & development *22*, 2755-2766.

Eilers, M., Picard, D., Yamamoto, K.R., and Bishop, J.M. (1989). Chimaeras of myc oncoprotein and steroid receptors cause hormone-dependent transformation of cells. Nature *340*, 66-68.

Elkon, R., Loayza-Puch, F., Korkmaz, G., Lopes, R., van Breugel, P.C., Bleijerveld, O.B., Altelaar, A.F., Wolf, E., Lorenzin, F., Eilers, M.*, et al.* (2015). Myc coordinates transcription and translation to enhance transformation and suppress invasiveness. EMBO reports *16*, 1723-1736.

Elstrom, R.L., Bauer, D.E., Buzzai, M., Karnauskas, R., Harris, M.H., Plas, D.R., Zhuang, H., Cinalli, R.M., Alavi, A., Rudin, C.M.*, et al.* (2004). Akt stimulates aerobic glycolysis in cancer cells. Cancer research *64*, 3892-3899.

Evan, G.I., Wyllie, A.H., Gilbert, C.S., Littlewood, T.D., Land, H., Brooks, M., Waters, C.M., Penn, L.Z., and Hancock, D.C. (1992). Induction of apoptosis in fibroblasts by c-myc protein. Cell *69*, 119-128.

Faubert, B., Boily, G., Izreig, S., Griss, T., Samborska, B., Dong, Z., Dupuy, F., Chambers, C., Fuerth, B.J., Viollet, B.*, et al.* (2013). AMPK is a negative regulator of the Warburg effect and suppresses tumor growth in vivo. Cell Metab *17*, 113-124.

Felig, P., Marliss, E., Ohman, J.L., and Cahill, C.F., Jr. (1970). Plasma amino acid levels in diabetic ketoacidosis. Diabetes *19*, 727-728.

Feng, Z., Zhang, C., Wu, R., and Hu, W. (2011). Tumor suppressor p53 meets microRNAs. Journal of molecular cell biology *3*, 44-50.

Ferber, E.C., Peck, B., Delpuech, O., Bell, G.P., East, P., and Schulze, A. (2012). FOXO3a regulates reactive oxygen metabolism by inhibiting mitochondrial gene expression. Cell death and differentiation *19*, 968-979.

Fingar, D.C., Richardson, C.J., Tee, A.R., Cheatham, L., Tsou, C., and Blenis, J. (2004). mTOR controls cell cycle progression through its cell growth effectors S6K1 and 4E-BP1/eukaryotic translation initiation factor 4E. Molecular and cellular biology *24*, 200-216.

Foster, R., Griffin, S., Grooby, S., Feltell, R., Christopherson, C., Chang, M., Sninsky, J., Kwok, S., and Torrance, C. (2012). Multiple metabolic alterations exist in mutant PI3K cancers, but only glucose is essential as a nutrient source. PloS one *7*, e45061.

Gao, P., Tchernyshyov, I., Chang, T.C., Lee, Y.S., Kita, K., Ochi, T., Zeller, K.I., De Marzo, A.M., Van Eyk, J.E., Mendell, J.T.*, et al.* (2009). c-Myc suppression of miR-23a/b enhances mitochondrial glutaminase expression and glutamine metabolism. Nature *458*, 762-765.

Gunzburg, M.J., Sivakumaran, A., Pendini, N.R., Yoon, J.H., Gorospe, M., Wilce, M.C., and Wilce, J.A. (2015). Cooperative interplay of let-7 mimic and HuR with MYC RNA. Cell cycle (Georgetown, Tex) *14*, 2729-2733.

Gutschner, T., Hammerle, M., Pazaitis, N., Bley, N., Fiskin, E., Uckelmann, H., Heim, A., Grobeta, M., Hofmann, N., Geffers, R.*, et al.* (2014). Insulin-like growth factor 2 mRNA-binding protein 1 (IGF2BP1) is an important protumorigenic factor in hepatocellular carcinoma. Hepatology (Baltimore, Md) *59*, 1900-1911.

Hanahan, D., and Weinberg, R.A. (2011). Hallmarks of cancer: the next generation. Cell *144*, 646-674.

Hann, S.R., King, M.W., Bentley, D.L., Anderson, C.W., and Eisenman, R.N. (1988). A non-AUG translational initiation in c-myc exon 1 generates an N-terminally distinct protein whose synthesis is disrupted in Burkitt's lymphomas. Cell *52*, 185-195.

Hann, S.R., Sloan-Brown, K., and Spotts, G.D. (1992). Translational activation of the non-AUG-initiated c-myc 1 protein at high cell densities due to methionine deprivation. Genes & development *6*, 1229-1240.

Hara, K., Yonezawa, K., Weng, Q.P., Kozlowski, M.T., Belham, C., and Avruch, J. (1998). Amino acid sufficiency and mTOR regulate p70 S6 kinase and eIF-4E BP1 through a common effector mechanism. The Journal of biological chemistry *273*, 14484-14494.

Hardie, D.G. (2007). AMP-activated/SNF1 protein kinases: conserved guardians of cellular energy. Nature reviews Molecular cell biology *8*, 774-785.

Hatse, S., De Clercq, E., and Balzarini, J. (1999). Role of antimetabolites of purine and pyrimidine nucleotide metabolism in tumor cell differentiation. Biochemical pharmacology *58*, 539-555.

He, L., He, X., Lim, L.P., de Stanchina, E., Xuan, Z., Liang, Y., Xue, W., Zender, L., Magnus, J., Ridzon, D.*, et al.* (2007). A microRNA component of the p53 tumour suppressor network. Nature *447*, 1130-1134.

He, T.C., Sparks, A.B., Rago, C., Hermeking, H., Zawel, L., da Costa, L.T., Morin, P.J., Vogelstein, B., and Kinzler, K.W. (1998). Identification of c-MYC as a target of the APC pathway. Science (New York, NY) *281*, 1509-1512.

Hensley, C.T., Wasti, A.T., and DeBerardinis, R.J. (2013). Glutamine and cancer: cell biology, physiology, and clinical opportunities. The Journal of clinical investigation *123*, 3678-3684.

Hermeking, H. (2010). The miR-34 family in cancer and apoptosis. Cell death and differentiation *17*, 193-199.

Hnisz, D., Abraham, B.J., Lee, T.I., Lau, A., Saint-Andre, V., Sigova, A.A., Hoke, H.A., and Young, R.A. (2013). Super-enhancers in the control of cell identity and disease. Cell *155*, 934-947.

Hoffman, B., and Liebermann, D.A. (2008). Apoptotic signaling by c-MYC. Oncogene *27*, 6462-6472.

Hsu, S.D., Tseng, Y.T., Shrestha, S., Lin, Y.L., Khaleel, A., Chou, C.H., Chu, C.F., Huang, H.Y., Lin, C.M., Ho, S.Y.*, et al.* (2014). miRTarBase update 2014: an information resource for experimentally validated miRNA-target interactions. Nucleic acids research *42*, D78-85.

Jackstadt, R., and Hermeking, H. (2015). MicroRNAs as regulators and mediators of c-MYC function. Biochimica et biophysica acta *1849*, 544-553.

Jaenicke, L.A., von Eyss, B., Carstensen, A., Wolf, E., Xu, W., Greifenberg, A.K., Geyer, M., Eilers, M., and Popov, N. (2016). Ubiquitin-Dependent Turnover of MYC Antagonizes MYC/PAF1C Complex Accumulation to Drive Transcriptional Elongation. Molecular cell *61*, 54-67.

Jager, R., Migliorini, G., Henrion, M., Kandaswamy, R., Speedy, H.E., Heindl, A., Whiffin, N., Carnicer, M.J., Broome, L., Dryden, N.*, et al.* (2015). Capture Hi-C identifies the chromatin interactome of colorectal cancer risk loci. Nature communications *6*, 6178.

Jain, M., Arvanitis, C., Chu, K., Dewey, W., Leonhardt, E., Trinh, M., Sundberg, C.D., Bishop, J.M., and Felsher, D.W. (2002). Sustained loss of a neoplastic phenotype by brief inactivation of MYC. Science (New York, NY) *297*, 102-104.

Jensen, K.S., Binderup, T., Jensen, K.T., Therkelsen, I., Borup, R., Nilsson, E., Multhaupt, H., Bouchard, C., Quistorff, B., Kjaer, A.*, et al.* (2011). FoxO3A promotes metabolic adaptation to hypoxia by antagonizing Myc function. The EMBO journal *30*, 4554-4570.

Jeon, S.M., Chandel, N.S., and Hay, N. (2012). AMPK regulates NADPH homeostasis to promote tumour cell survival during energy stress. Nature *485*, 661-665.

Jin, S., and White, E. (2007). Role of autophagy in cancer: management of metabolic stress. Autophagy *3*, 28-31.

Jonkers, I., and Lis, J.T. (2015). Getting up to speed with transcription elongation by RNA polymerase II. Nature reviews Molecular cell biology *16*, 167-177.

Kamphorst, J.J., Cross, J.R., Fan, J., de Stanchina, E., Mathew, R., White, E.P., Thompson, C.B., and Rabinowitz, J.D. (2013). Hypoxic and Ras-transformed cells support growth by scavenging unsaturated fatty acids from lysophospholipids. Proceedings of the National Academy of Sciences of the United States of America *110*, 8882-8887.

Kamphorst, J.J., Nofal, M., Commisso, C., Hackett, S.R., Lu, W., Grabocka, E., Vander Heiden, M.G., Miller, G., Drebin, J.A., Bar-Sagi, D*., et al.* (2015). Human pancreatic cancer tumors are nutrient poor and tumor cells actively scavenge extracellular protein. Cancer research *75*, 544-553.

Kaplon, J., van Dam, L., and Peeper, D. (2015). Two-way communication between the metabolic and cell cycle machineries: the molecular basis. Cell cycle (Georgetown, Tex) *14*, 2022-2032.

Kelly, K., Cochran, B.H., Stiles, C.D., and Leder, P. (1983). Cell-specific regulation of the c-myc gene by lymphocyte mitogens and platelet-derived growth factor. Cell *35*, 603-610.

Kent, W.J., Sugnet, C.W., Furey, T.S., Roskin, K.M., Pringle, T.H., Zahler, A.M., and Haussler, D. (2002). The human genome browser at UCSC. Genome research *12*, 996-1006.

Kim, H.H., Kuwano, Y., Srikantan, S., Lee, E.K., Martindale, J.L., and Gorospe, M. (2009). HuR recruits let-7/RISC to repress c-Myc expression. Genes & development *23*, 1743-1748.

Kim, J.H., Paek, K.Y., Choi, K., Kim, T.D., Hahm, B., Kim, K.T., and Jang, S.K. (2003). Heterogeneous nuclear ribonucleoprotein C modulates translation of c-myc mRNA in a cell cycle phase-dependent manner. Molecular and cellular biology *23*, 708-720.

Kim, Y.H., Girard, L., Giacomini, C.P., Wang, P., Hernandez-Boussard, T., Tibshirani, R., Minna, J.D., and Pollack, J.R. (2006). Combined microarray analysis of small cell lung cancer reveals altered apoptotic balance and distinct expression signatures of MYC family gene amplification. Oncogene *25*, 130-138.

Kisselev, A.F., and Goldberg, A.L. (2001). Proteasome inhibitors: from research tools to drug candidates. Chemistry & biology *8*, 739-758.

Koromilas, A.E., Lazaris-Karatzas, A., and Sonenberg, N. (1992). mRNAs containing extensive secondary structure in their 5' non-coding region translate efficiently in cells overexpressing initiation factor eIF-4E. The EMBO journal *11*, 4153-4158.

Kozomara, A., and Griffiths-Jones, S. (2014). miRBase: annotating high confidence microRNAs using deep sequencing data. Nucleic acids research *42*, D68-73.

Kress, T.R., Cannell, I.G., Brenkman, A.B., Samans, B., Gaestel, M., Roepman, P., Burgering, B.M., Bushell, M., Rosenwald, A., and Eilers, M. (2011). The MK5/PRAK kinase and Myc form a negative feedback loop that is disrupted during colorectal tumorigenesis. Molecular cell *41*, 445-457.

Kulda, V., Pesta, M., Topolcan, O., Liska, V., Treska, V., Sutnar, A., Rupert, K., Ludvikova, M., Babuska, V., Holubec, L., Jr*., et al.* (2010). Relevance of miR-21 and miR-143 expression in tissue samples of colorectal carcinoma and its liver metastases. Cancer genetics and cytogenetics *200*, 154-160.

Kung, H.N., Marks, J.R., and Chi, J.T. (2011). Glutamine synthetase is a genetic determinant of cell type-specific glutamine independence in breast epithelia. PLoS genetics *7*, e1002229.

Kuzyk, A., and Mai, S. (2014). c-MYC-induced genomic instability. Cold Spring Harbor perspectives in medicine *4*, a014373.

Kwon, S.C., Yi, H., Eichelbaum, K., Fohr, S., Fischer, B., You, K.T., Castello, A., Krijgsveld, J., Hentze, M.W., and Kim, V.N. (2013). The RNA-binding protein repertoire of embryonic stem cells. Nature structural & molecular biology *20*, 1122-1130.

Langmead, B., Trapnell, C., Pop, M., and Salzberg, S.L. (2009). Ultrafast and memory-efficient alignment of short DNA sequences to the human genome. Genome biology *10*, R25.

Laplante, M., and Sabatini, D.M. (2012). mTOR signaling in growth control and disease. Cell *149*, 274-293.

Laxman, S., Sutter, B.M., and Tu, B.P. (2014). Methionine is a signal of amino acid sufficiency that inhibits autophagy through the methylation of PP2A. Autophagy *10*, 386-387.

Leprivier, G., Remke, M., Rotblat, B., Dubuc, A., Mateo, A.R., Kool, M., Agnihotri, S., El-Naggar, A., Yu, B., Somasekharan, S.P., *et al.* (2013). The eEF2 kinase confers resistance to nutrient deprivation by blocking translation elongation. Cell *153*, 1064-1079.

Leung, A.K., and Sharp, P.A. (2010). MicroRNA functions in stress responses. Molecular cell *40*, 205-215.

Levens, D. (2010). You Don't Muck with MYC. Genes & cancer *1*, 547-554.

Levens, D. (2013). Cellular MYCro economics: Balancing MYC function with MYC expression. Cold Spring Harbor perspectives in medicine *3*.

Lezina, L., Purmessur, N., Antonov, A.V., Ivanova, T., Karpova, E., Krishan, K., Ivan, M., Aksenova, V., Tentler, D., Garabadgiu, A.V., *et al.* (2013). miR-16 and miR-26a target checkpoint kinases Wee1 and Chk1 in response to p53 activation by genotoxic stress. Cell death & disease *4*, e953.

Li, F., Wang, Y., Zeller, K.I., Potter, J.J., Wonsey, D.R., O'Donnell, K.A., Kim, J.W., Yustein, J.T., Lee, L.A., and Dang, C.V. (2005). Myc stimulates nuclearly encoded mitochondrial genes and mitochondrial biogenesis. Molecular and cellular biology *25*, 6225-6234.

Li, Y., Challagundla, K.B., Sun, X.X., Zhang, Q., and Dai, M.S. (2015). MicroRNA-130a associates with ribosomal protein L11 to suppress c-Myc expression in response to UV irradiation. Oncotarget *6*, 1101-1114.

Liao, B., Hu, Y., and Brewer, G. (2007). Competitive binding of AUF1 and TIAR to MYC mRNA controls its translation. Nature structural & molecular biology *14*, 511-518.

Lin, C.J., Cencic, R., Mills, J.R., Robert, F., and Pelletier, J. (2008). c-Myc and eIF4F are components of a feedforward loop that links transcription and translation. Cancer research *68*, 5326-5334.

Lin, C.Y., Loven, J., Rahl, P.B., Paranal, R.M., Burge, C.B., Bradner, J.E., Lee, T.I., and Young, R.A. (2012). Transcriptional amplification in tumor cells with elevated c-Myc. Cell *151*, 56-67.

Liu, L., Ouyang, M., Rao, J.N., Zou, T., Xiao, L., Chung, H.K., Wu, J., Donahue, J.M., Gorospe, M., and Wang, J.Y. (2015). Competition between RNA-binding proteins CELF1 and HuR modulates MYC translation and intestinal epithelium renewal. Molecular biology of the cell *26*, 1797-1810.

Liu, L., Rao, J.N., Zou, T., Xiao, L., Wang, P.Y., Turner, D.J., Gorospe, M., and Wang, J.Y. (2009). Polyamines regulate c-Myc translation through Chk2-dependent HuR phosphorylation. Molecular biology of the cell *20*, 4885-4898.

Liu, L., Ulbrich, J., Muller, J., Wustefeld, T., Aeberhard, L., Kress, T.R., Muthalagu, N., Rycak, L., Rudalska, R., Moll, R.*, et al.* (2012). Deregulated MYC expression induces dependence upon AMPK-related kinase 5. Nature *483*, 608-612.

Liu, Y.C., Li, F., Handler, J., Huang, C.R., Xiang, Y., Neretti, N., Sedivy, J.M., Zeller, K.I., and Dang, C.V. (2008). Global regulation of nucleotide biosynthetic genes by c-Myc. PloS one *3*, e2722.

Locasale, J.W., and Cantley, L.C. (2011). Metabolic flux and the regulation of mammalian cell growth. Cell Metab *14*, 443-451.

Lombardi, O., Varshney, D., Phillips, N.M., and Cowling, V.H. (2016). c-Myc deregulation induces mRNA capping enzyme dependency. Oncotarget.

Lorenzin, F., Benary, U., Baluapuri, A., Walz, S., Jung, L.A., von Eyss, B., Kisker, C., Wolf, J., Eilers, M., and Wolf, E. (2016). Different promoter affinities account for specificity in MYC-dependent gene regulation. eLife *5*.

Loven, J., Hoke, H.A., Lin, C.Y., Lau, A., Orlando, D.A., Vakoc, C.R., Bradner, J.E., Lee, T.I., and Young, R.A. (2013). Selective inhibition of tumor oncogenes by disruption of super-enhancers. Cell *153*, 320-334.

Mannava, S., Grachtchouk, V., Wheeler, L.J., Im, M., Zhuang, D., Slavina, E.G., Mathews, C.K., Shewach, D.S., and Nikiforov, M.A. (2008). Direct role of nucleotide metabolism in C-MYC-dependent proliferation of melanoma cells. Cell cycle (Georgetown, Tex) *7*, 2392-2400.

Marderosian, M., Sharma, A., Funk, A.P., Vartanian, R., Masri, J., Jo, O.D., and Gera, J.F. (2006). Tristetraprolin regulates Cyclin D1 and c-Myc mRNA stability in response to rapamycin in an Akt-dependent manner via p38 MAPK signaling. Oncogene *25*, 6277-6290.

Martinez-Outschoorn, U.E., Peiris-Pages, M., Pestell, R.G., Sotgia, F., and Lisanti, M.P. (2016). Cancer metabolism: a therapeutic perspective. Nature reviews Clinical oncology.

Masui, K., Tanaka, K., Akhavan, D., Babic, I., Gini, B., Matsutani, T., Iwanami, A., Liu, F., Villa, G.R., Gu, Y.*, et al.* (2013). mTOR complex 2 controls glycolytic metabolism in glioblastoma through FoxO acetylation and upregulation of c-Myc. Cell Metab *18*, 726-739.

Mayers, J.R., Torrence, M.E., Danai, L.V., Papagiannakopoulos, T., Davidson, S.M., Bauer, M.R., Lau, A.N., Ji, B.W., Dixit, P.D., Hosios, A.M*., et al.* (2016). Tissue of origin dictates branched-chain amino acid metabolism in mutant Kras-driven cancers. Science (New York, NY) *353*, 1161-1165.

Mazan-Mamczarz, K., Lal, A., Martindale, J.L., Kawai, T., and Gorospe, M. (2006). Translational repression by RNA-binding protein TIAR. Molecular and cellular biology *26*, 2716-2727.

Meerbrey, K.L., Hu, G., Kessler, J.D., Roarty, K., Li, M.Z., Fang, J.E., Herschkowitz, J.I., Burrows, A.E., Ciccia, A., Sun, T*., et al.* (2011). The pINDUCER lentiviral toolkit for inducible RNA interference in vitro and in vivo. Proceedings of the National Academy of Sciences of the United States of America *108*, 3665-3670.

Mendoza, O., Bourdoncle, A., Boule, J.B., Brosh, R.M., Jr., and Mergny, J.L. (2016). G-quadruplexes and helicases. Nucleic acids research *44*, 1989-2006.

Merrick, W.C. (2004). Cap-dependent and cap-independent translation in eukaryotic systems. Gene *332*, 1-11.

Miltenberger, R.J., Sukow, K.A., and Farnham, P.J. (1995). An E-box-mediated increase in cad transcription at the G1/S-phase boundary is suppressed by inhibitory c-Myc mutants. Molecular and cellular biology *15*, 2527-2535.

Moloughney, J.G., Kim, P.K., Vega-Cotto, N.M., Wu, C.C., Zhang, S., Adlam, M., Lynch, T., Chou, P.C., Rabinowitz, J.D., Werlen, G*., et al.* (2016). mTORC2 Responds to Glutamine Catabolite Levels to Modulate the Hexosamine Biosynthesis Enzyme GFAT1. Molecular cell *63*, 811-826.

Morgenstern, J.P., and Land, H. (1990). A series of mammalian expression vectors and characterisation of their expression of a reporter gene in stably and transiently transfected cells. Nucleic acids research *18*, 1068.

Murphy, T.A., Dang, C.V., Young, J.D. (2013). Isotopically nonstationary 13C flux analysis of Myc-induced metabolic reprogramming in B-cells. Metabolic engineering *15*, 206-217.

Murphy, D.J., Junttila, M.R., Pouyet, L., Karnezis, A., Shchors, K., Bui, D.A., Brown-Swigart, L., Johnson, L., Evan, G.I. (2008). Distinct tresholds govern Myc´s biological output in vivo. Cancer Cell *14*, 447-457.

Nakazawa, M.S, Keith, B., Simon, C.M. (2016). Oxygen availability and metabolic adaptation. Nature Reviews *16*, 663-673.

Newsholme, P. (2001). Why is L-glutamine metabolism important to cells of the immune system in health, postinjury, surgery or infection? The Journal of nutrition *131*, 2515S-2522S; discussion 2523S-2514S.

Nicklin, P., Bergman, P., Zhang, B., Triantafellow, E., Wang, H., Nyfeler, B., Yang, H., Hild, M., Kung, C., Wilson, C.*, et al.* (2009). Bidirectional transport of amino acids regulates mTOR and autophagy. Cell *136*, 521-534.

Nicol, J.W., Helt, G.A., Blanchard, S.G., Jr., Raja, A., and Loraine, A.E. (2009). The Integrated Genome Browser: free software for distribution and exploration of genome-scale datasets. Bioinformatics (Oxford, England) *25*, 2730-2731.

Nie, Z., Hu, G., Wei, G., Cui, K., Yamane, A., Resch, W., Wang, R., Green, D.R., Tessarollo, L., Casellas, R.*, et al.* (2012). c-Myc is a universal amplifier of expressed genes in lymphocytes and embryonic stem cells. Cell *151*, 68-79.

Okuyama, H., Endo, H., Akashika, T., Kato, K., and Inoue, M. (2010). Downregulation of c-MYC protein levels contributes to cancer cell survival under dual deficiency of oxygen and glucose. Cancer research *70*, 10213-10223.

Osthus, R.C., Shim, H., Kim, S., Li, Q., Reddy, R., Mukherjee, M., Xu, Y., Wonsey, D., Lee, L.A., and Dang, C.V. (2000). Deregulation of glucose transporter 1 and glycolytic gene expression by c-Myc. The Journal of biological chemistry *275*, 21797-21800.

Pan, M., Reid, M.A., Lowman, X.H., Kulkarni, R.P., Tran, T.Q., Liu, X., Yang, Y., Hernandez-Davies, J.E., Rosales, K.K., Li, H.*, et al.* (2016). Regional glutamine deficiency in tumours promotes dedifferentiation through inhibition of histone demethylation. Nature cell biology *18*, 1090-1101.

Panieri, E., and Santoro, M.M. (2016). ROS homeostasis and metabolism: a dangerous liason in cancer cells. Cell death & disease *7*, e2253.

Park, I.J., Hwang, J.T., Kim, Y.M., Ha, J., and Park, O.J. (2006). Differential modulation of AMPK signaling pathways by low or high levels of exogenous reactive oxygen species in colon cancer cells. Annals of the New York Academy of Sciences *1091*, 102-109.

Pavlova, Natalya N., and Thompson, Craig B. The Emerging Hallmarks of Cancer Metabolism. Cell Metabolism *23*, 27-47.

Pelletier, J., Graff, J., Ruggero, D., and Sonenberg, N. (2015). Targeting the eIF4F translation initiation complex: a critical nexus for cancer development. Cancer research *75*, 250-263.

Penn, L.J., Brooks, M.W., Laufer, E.M., and Land, H. (1990). Negative autoregulation of c-myc transcription. The EMBO journal *9*, 1113-1121.

Perry, M.M., Moschos, S.A., Williams, A.E., Shepherd, N.J., Larner-Svensson, H.M., and Lindsay, M.A. (2008). Rapid changes in microRNA-146a expression negatively regulate the IL-1beta-induced inflammatory response in human lung alveolar epithelial cells. Journal of immunology (Baltimore, Md : 1950) *180*, 5689-5698.

Phesse, T.J., Myant, K.B., Cole, A.M., Ridgway, R.A., Pearson, H., Muncan, V., van den Brink, G.R., Vousden, K.H., Sears, R., Vassilev, L.T.*, et al.* (2014). Endogenous c-Myc is essential for p53-induced apoptosis in response to DNA damage in vivo. Cell death and differentiation *21*, 956-966.

Popov, N., Herold, S., Llamazares, M., Schulein, C., and Eilers, M. (2007). Fbw7 and Usp28 regulate myc protein stability in response to DNA damage. Cell cycle (Georgetown, Tex) *6*, 2327-2331.

Pourdehnad, M., Truitt, M.L., Siddiqi, I.N., Ducker, G.S., Shokat, K.M., and Ruggero, D. (2013). Myc and mTOR converge on a common node in protein synthesis control that confers synthetic lethality in Myc-driven cancers. Proceedings of the National Academy of Sciences of the United States of America *110*, 11988-11993.

Qing, G., Li, B., Vu, A., Skuli, N., Walton, Z.E., Liu, X., Mayes, P.A., Wise, D.R., Thompson, C.B., Maris, J.M.*, et al.* (2012). ATF4 regulates MYC-mediated neuroblastoma cell death upon glutamine deprivation. Cancer cell *22*, 631-644.

Qiu, B., and Simon, M.C. (2015). Oncogenes strike a balance between cellular growth and homeostasis. Seminars in cell & developmental biology *43*, 3-10.

Quinlan, A.R., and Hall, I.M. (2010). BEDTools: a flexible suite of utilities for comparing genomic features. Bioinformatics (Oxford, England) *26*, 841-842.

Rahl, P.B., Lin, C.Y., Seila, A.C., Flynn, R.A., McCuine, S., Burge, C.B., Sharp, P.A., and Young, R.A. (2010). c-Myc regulates transcriptional pause release. Cell *141*, 432-445.

Ray, S., Atkuri, K.R., Deb-Basu, D., Adler, A.S., Chang, H.Y., Herzenberg, L.A., and Felsher, D.W. (2006). MYC can induce DNA breaks in vivo and in vitro independent of reactive oxygen species. Cancer research *66*, 6598-6605.

Reeds, P.J., and Burrin, D.G. (2001). Glutamine and the bowel. The Journal of nutrition *131*, 2505S-2508S; discussion 2523S-2504S.

Reid, M.A., Wang, W.I., Rosales, K.R., Welliver, M.X., Pan, M., and Kong, M. (2013). The B55alpha subunit of PP2A drives a p53-dependent metabolic adaptation to glutamine deprivation. Molecular cell *50*, 200-211.

Rennoll, S., and Yochum, G. (2015). Regulation of MYC gene expression by aberrant Wnt/beta-catenin signaling in colorectal cancer. World journal of biological chemistry *6*, 290-300.

Reya, T., and Clevers, H. (2005). Wnt signalling in stem cells and cancer. Nature *434*, 843-850.

Rohban, S., and Campaner, S. (2015). Myc induced replicative stress response: How to cope with it and exploit it. Biochimica et biophysica acta *1849*, 517-524.

Ross, J., Lemm, I., and Berberet, B. (2001). Overexpression of an mRNA-binding protein in human colorectal cancer. Oncogene *20*, 6544-6550.

Sabo, A., and Amati, B. (2014). Genome recognition by MYC. Cold Spring Harbor perspectives in medicine *4*.

Sabo, A., Kress, T.R., Pelizzola, M., de Pretis, S., Gorski, M.M., Tesi, A., Morelli, M.J., Bora, P., Doni, M., Verrecchia, A.*, et al.* (2014). Selective transcriptional regulation by Myc in cellular growth control and lymphomagenesis. Nature *511*, 488-492.

Sachdeva, M., Zhu, S., Wu, F., Wu, H., Walia, V., Kumar, S., Elble, R., Watabe, K., and Mo, Y.Y. (2009). p53 represses c-Myc through induction of the tumor suppressor miR-145. Proceedings of the National Academy of Sciences of the United States of America *106*, 3207-3212.

Schneider-Poetsch, T., Ju, J., Eyler, D.E., Dang, Y., Bhat, S., Merrick, W.C., Green, R., Shen, B., and Liu, J.O. (2010). Inhibition of eukaryotic translation elongation by cycloheximide and lactimidomycin. Nature chemical biology *6*, 209-217.

Schuhmacher, M., Kohlhuber, F., Holzel, M., Kaiser, C., Burtscher, H., Jarsch, M., Bornkamm, G.W., Laux, G., Polack, A., Weidle, U.H.*, et al.* (2001). The transcriptional program of a human B cell line in response to Myc. Nucleic acids research *29*, 397-406.

Sears, R., Nuckolls, F., Haura, E., Taya, Y., Tamai, K., and Nevins, J.R. (2000). Multiple Ras-dependent phosphorylation pathways regulate Myc protein stability. Genes & development *14*, 2501-2514.

Shen, L., Shao, N., Liu, X., and Nestler, E. (2014). ngs.plot: Quick mining and visualization of next-generation sequencing data by integrating genomic databases. BMC genomics *15*, 284.

Shi, Y., Frost, P., Hoang, B., Yang, Y., Fukunaga, R., Gera, J., and Lichtenstein, A. (2013). MNK kinases facilitate c-myc IRES activity in rapamycin-treated multiple myeloma cells. Oncogene *32*, 190-197.

Shichiri, M., Hanson, K.D., and Sedivy, J.M. (1993). Effects of c-myc expression on proliferation, quiescence, and the G0 to G1 transition in nontransformed cells. Cell growth & differentiation : the molecular biology journal of the American Association for Cancer Research *4*, 93-104.

Shim, H., Chun, Y.S., Lewis, B.C., and Dang, C.V. (1998). A unique glucose-dependent apoptotic pathway induced by c-Myc. Proceedings of the National Academy of Sciences of the United States of America *95*, 1511-1516.

Shroff, E.H., Eberlin, L.S., Dang, V.M., Gouw, A.M., Gabay, M., Adam, S.J., Bellovin, D.I., Tran, P.T., Philbrick, W.M., Garcia-Ocana, A.*, et al.* (2015). MYC oncogene overexpression drives renal cell carcinoma in a mouse model through glutamine metabolism. Proceedings of the National Academy of Sciences of the United States of America *112*, 6539-6544.

Souba, W.W. (1993). Glutamine and cancer. Annals of surgery *218*, 715-728.

Spotts, G.D., Patel, S.V., Xiao, Q., and Hann, S.R. (1997). Identification of downstream-initiated c-Myc proteins which are dominant-negative inhibitors of transactivation by full-length c-Myc proteins. Molecular and cellular biology *17*, 1459-1468.

Stine, Z.E., Walton, Z.E., Altman, B.J., Hsieh, A.L., and Dang, C.V. (2015). MYC, Metabolism, and Cancer. Cancer discovery.

Stoneley, M., Chappell, S.A., Jopling, C.L., Dickens, M., MacFarlane, M., and Willis, A.E. (2000). c-Myc protein synthesis is initiated from the internal ribosome entry segment during apoptosis. Molecular and cellular biology *20*, 1162-1169.

Subkhankulova, T., Mitchell, S.A., and Willis, A.E. (2001). Internal ribosome entry segment-mediated initiation of c-Myc protein synthesis following genotoxic stress. The Biochemical journal *359*, 183-192.

Subramanian, A., Tamayo, P., Mootha, V.K., Mukherjee, S., Ebert, B.L., Gillette, M.A., Paulovich, A., Pomeroy, S.L., Golub, T.R., Lander, E.S.*, et al.* (2005). Gene set enrichment analysis: a knowledge-based approach for interpreting genome-wide expression profiles. Proceedings of the National Academy of Sciences of the United States of America *102*, 15545-15550.

Sutherland, K.D., Vaillant, F., Alexander, W.S., Wintermantel, T.M., Forrest, N.C., Holroyd, S.L., McManus, E.J., Schutz, G., Watson, C.J., Chodosh, L.A., *et al.* (2006). c-myc as a mediator of accelerated apoptosis and involution in mammary glands lacking Socs3. The EMBO journal *25*, 5805-5815.

Svitkin, Y.V., Pause, A., Haghighat, A., Pyronnet, S., Witherell, G., Belsham, G.J., and Sonenberg, N. (2001). The requirement for eukaryotic initiation factor 4A (elF4A) in translation is in direct proportion to the degree of mRNA 5' secondary structure. RNA (New York, NY) *7*, 382-394.

Talwar, S., Jin, J., Carroll, B., Liu, A., Gillespie, M.B., and Palanisamy, V. (2011). Caspase-mediated cleavage of RNA-binding protein HuR regulates c-Myc protein expression after hypoxic stress. The Journal of biological chemistry *286*, 32333-32343.

Tao, J., Zhao, X., and Tao, J. (2014). c-MYC-miRNA circuitry: a central regulator of aggressive B-cell malignancies. Cell cycle (Georgetown, Tex) *13*, 191-198.

Timmerman, L.A., Holton, T., Yuneva, M., Louie, R.J., Padro, M., Daemen, A., Hu, M., Chan, D.A., Ethier, S.P., van 't Veer, L.J., *et al.* (2013). Glutamine sensitivity analysis identifies the xCT antiporter as a common triple-negative breast tumor therapeutic target. Cancer cell *24*, 450-465.

Tomlinson, I., Webb, E., Carvajal-Carmona, L., Broderick, P., Kemp, Z., Spain, S., Penegar, S., Chandler, I., Gorman, M., Wood, W., *et al.* (2007). A genome-wide association scan of tag SNPs identifies a susceptibility variant for colorectal cancer at 8q24.21. Nature genetics *39*, 984-988.

Toyota, M., Suzuki, H., Sasaki, Y., Maruyama, R., Imai, K., Shinomura, Y., and Tokino, T. (2008). Epigenetic silencing of microRNA-34b/c and B-cell translocation gene 4 is associated with CpG island methylation in colorectal cancer. Cancer research *68*, 4123-4132.

Truitt, M.L., and Ruggero, D. (2016). New frontiers in translational control of the cancer genome. Nature reviews Cancer *16*, 288-304.

Tuupanen, S., Turunen, M., Lehtonen, R., Hallikas, O., Vanharanta, S., Kivioja, T., Bjorklund, M., Wei, G., Yan, J., Niittymaki, I., *et al.* (2009). The common colorectal cancer predisposition SNP rs6983267 at chromosome 8q24 confers potential to enhanced Wnt signaling. Nature genetics *41*, 885-890.

Vafa, O., Wade, M., Kern, S., Beeche, M., Pandita, T.K., Hampton, G.M., and Wahl, G.M. (2002). c-Myc can induce DNA damage, increase reactive oxygen species, and mitigate p53 function: a mechanism for oncogene-induced genetic instability. Molecular cell *9*, 1031-1044.

van den Heuvel, A.P., Jing, J., Wooster, R.F., and Bachman, K.E. (2012). Analysis of glutamine dependency in non-small cell lung cancer: GLS1 splice variant GAC is essential for cancer cell growth. Cancer biology & therapy *13*, 1185-1194.

Van Der Kelen, K., Beyaert, R., Inze, D., and De Veylder, L. (2009). Translational control of eukaryotic gene expression. Critical reviews in biochemistry and molecular biology *44*, 143-168.

van Kouwenhove, M., Kedde, M., and Agami, R. (2011). MicroRNA regulation by RNA-binding proteins and its implications for cancer. Nature reviews Cancer *11*, 644-656.

van Riggelen, J., Yetil, A., and Felsher, D.W. (2010). MYC as a regulator of ribosome biogenesis and protein synthesis. Nature reviews Cancer *10*, 301-309.

Vander Heiden, M.G., Cantley, L.C., and Thompson, C.B. (2009). Understanding the Warburg effect: the metabolic requirements of cell proliferation. Science (New York, NY) *324*, 1029-1033.

Vazquez, A., Markert, E.K., and Oltvai, Z.N. (2011). Serine biosynthesis with one carbon catabolism and the glycine cleavage system represents a novel pathway for ATP generation. PloS one *6*, e25881.

Vazquez, A., Tedeschi, P.M., and Bertino, J.R. (2013). Overexpression of the mitochondrial folate and glycine-serine pathway: a new determinant of methotrexate selectivity in tumors. Cancer research *73*, 478-482.

Vervoorts, J., Luscher-Firzlaff, J., and Luscher, B. (2006). The ins and outs of MYC regulation by posttranslational mechanisms. The Journal of biological chemistry *281*, 34725-34729.

Vita, M., and Henriksson, M. (2006). The Myc oncoprotein as a therapeutic target for human cancer. Seminars in cancer biology *16*, 318-330.

von Eyss, B., Jaenicke, L.A., Kortlever, R.M., Royla, N., Wiese, K.E., Letschert, S., McDuffus, L.A., Sauer, M., Rosenwald, A., Evan, G.I.*, et al.* (2015). A MYC-Driven Change in Mitochondrial Dynamics Limits YAP/TAZ Function in Mammary Epithelial Cells and Breast Cancer. Cancer cell *28*, 743-757.

Walz, S., Lorenzin, F., Morton, J., Wiese, K.E., von Eyss, B., Herold, S., Rycak, L., Dumay-Odelot, H., Karim, S., Bartkuhn, M.*, et al.* (2014). Activation and repression by oncogenic MYC shape tumour-specific gene expression profiles. Nature *511*, 483-487.

Wang, J.B., Erickson, J.W., Fuji, R., Ramachandran, S., Gao, P., Dinavahi, R., Wilson, K.F., Ambrosio, A.L., Dias, S.M., Dang, C.V., *et al.* (2010). Targeting mitochondrial glutaminase activity inhibits oncogenic transformation. Cancer cell *18*, 207-219.

Ward, P.S., and Thompson, C.B. (2012). Metabolic reprogramming: a cancer hallmark even warburg did not anticipate. Cancer cell *21*, 297-308.

Waters, C.M., Littlewood, T.D., Hancock, D.C., Moore, J.P., and Evan, G.I. (1991). c-myc protein expression in untransformed fibroblasts. Oncogene *6*, 797-805.

Welcker, M., and Clurman, B.E. (2008). FBW7 ubiquitin ligase: a tumour suppressor at the crossroads of cell division, growth and differentiation. Nature reviews Cancer *8*, 83-93.

Welcker, M., Orian, A., Jin, J., Grim, J.E., Harper, J.W., Eisenman, R.N., and Clurman, B.E. (2004). The Fbw7 tumor suppressor regulates glycogen synthase kinase 3 phosphorylation-dependent c-Myc protein degradation. Proceedings of the National Academy of Sciences of the United States of America *101*, 9085-9090.

Wiegering, A., Uthe, F.W., Jamieson, T., Ruoss, Y., Huttenrauch, M., Kuspert, M., Pfann, C., Nixon, C., Herold, S., Walz, S., *et al.* (2015). Targeting Translation Initiation Bypasses Signaling Crosstalk Mechanisms That Maintain High MYC Levels in Colorectal Cancer. Cancer discovery *5*, 768-781.

Wiese, K.E., Haikala, H.M., von Eyss, B., Wolf, E., Esnault, C., Rosenwald, A., Treisman, R., Klefstrom, J., and Eilers, M. (2015). Repression of SRF target genes is critical for Myc-dependent apoptosis of epithelial cells. The EMBO journal *34*, 1554-1571.

Wilczynska, A., and Bushell, M. (2015). The complexity of miRNA-mediated repression. Cell death and differentiation *22*, 22-33.

Wisdom, R., and Lee, W. (1991). The protein-coding region of c-myc mRNA contains a sequence that specifies rapid mRNA turnover and induction by protein synthesis inhibitors. Genes & development *5*, 232-243.

Wise, D.R., DeBerardinis, R.J., Mancuso, A., Sayed, N., Zhang, X.Y., Pfeiffer, H.K., Nissim, I., Daikhin, E., Yudkoff, M., McMahon, S.B., *et al.* (2008). Myc regulates a transcriptional program that stimulates mitochondrial glutaminolysis and leads to glutamine addiction. Proceedings of the National Academy of Sciences of the United States of America *105*, 18782-18787.

Wolf, E., Lin, C.Y., Eilers, M., and Levens, D.L. (2015). Taming of the beast: shaping Myc-dependent amplification. Trends in cell biology *25*, 241-248.

Wolfe, A.L., Singh, K., Zhong, Y., Drewe, P., Rajasekhar, V.K., Sanghvi, V.R., Mavrakis, K.J., Jiang, M., Roderick, J.E., Van der Meulen, J.*, et al.* (2014). RNA G-quadruplexes cause eIF4A-dependent oncogene translation in cancer. Nature *513*, 65-70.

Wong, D.J., Nuyten, D.S., Regev, A., Lin, M., Adler, A.S., Segal, E., van de Vijver, M.J., and Chang, H.Y. (2008). Revealing targeted therapy for human cancer by gene module maps. Cancer research *68*, 369-378.

Wong, W.J., Qiu, B., Nakazawa, M.S., Qing, G., and Simon, M.C. (2013). MYC degradation under low O2 tension promotes survival by evading hypoxia-induced cell death. Molecular and cellular biology *33*, 3494-3504.

Wu, W.K., Law, P.T., Lee, C.W., Cho, C.H., Fan, D., Wu, K., Yu, J., and Sung, J.J. (2011). MicroRNA in colorectal cancer: from benchtop to bedside. Carcinogenesis *32*, 247-253.

Xiang, Y., Stine, Z.E., Xia, J., Lu, Y., O'Connor, R.S., Altman, B.J., Hsieh, A.L., Gouw, A.M., Thomas, A.G., Gao, P.*, et al.* (2015). Targeted inhibition of tumor-specific glutaminase diminishes cell-autonomous tumorigenesis. The Journal of clinical investigation *125*, 2293-2306.

Xie, J., and Proud, C.G. (2013). Crosstalk between mTOR complexes. Nature cell biology *15*, 1263-1265.

Yang, L., Moss, T., Mangala, L.S., Marini, J., Zhao, H., Wahlig, S., Armaiz-Pena, G., Jiang, D., Achreja, A., Win, J.*, et al.* (2014). Metabolic shifts toward glutamine regulate tumor growth, invasion and bioenergetics in ovarian cancer. Molecular systems biology *10*, 728.

Ye, T., Krebs, A.R., Choukrallah, M.A., Keime, C., Plewniak, F., Davidson, I., and Tora, L. (2011). seqMINER: an integrated ChIP-seq data interpretation platform. Nucleic acids research *39*, e35.

Ying, H., Kimmelman, A.C., Lyssiotis, C.A., Hua, S., Chu, G.C., Fletcher-Sananikone, E., Locasale, J.W., Son, J., Zhang, H., Coloff, J.L.*, et al.* (2012). Oncogenic Kras maintains pancreatic tumors through regulation of anabolic glucose metabolism. Cell *149*, 656-670.

Yochum, G.S., Cleland, R., and Goodman, R.H. (2008). A genome-wide screen for beta-catenin binding sites identifies a downstream enhancer element that controls c-Myc gene expression. Molecular and cellular biology *28*, 7368-7379.

Yochum, G.S., Sherrick, C.M., Macpartlin, M., and Goodman, R.H. (2010). A beta-catenin/TCF-coordinated chromatin loop at MYC integrates 5' and 3' Wnt responsive enhancers. Proceedings of the National Academy of Sciences of the United States of America *107*, 145-150.

Yokota, T., Kanamoto, R., and Hayashi, S. (1995). c-myc mRNA is stabilized by deprivation of amino acids in primary cultured rat hepatocytes. Journal of nutritional science and vitaminology *41*, 455-463.

Yuan, T.L., and Cantley, L.C. (2008). PI3K pathway alterations in cancer: variations on a theme. Oncogene *27*, 5497-5510.

Yuneva, M., Zamboni, N., Oefner, P., Sachidanandam, R., and Lazebnik, Y. (2007). Deficiency in glutamine but not glucose induces MYC-dependent apoptosis in human cells. The Journal of cell biology *178*, 93-105.

Yuneva, M.O., Fan, T.W., Allen, T.D., Higashi, R.M., Ferraris, D.V., Tsukamoto, T., Mates, J.M., Alonso, F.J., Wang, C., Seo, Y.*, et al.* (2012). The metabolic profile of tumors depends on both the responsible genetic lesion and tissue type. Cell Metab *15*, 157-170.

Zeller, K.I., Jegga, A.G., Aronow, B.J., O'Donnell, K.A., and Dang, C.V. (2003). An integrated database of genes responsive to the Myc oncogenic transcription factor: identification of direct genomic targets. Genome biology *4*, R69.

Zhang, Y., Liu, T., Meyer, C.A., Eeckhoute, J., Johnson, D.S., Bernstein, B.E., Nusbaum, C., Myers, R.M., Brown, M., Li, W.*, et al.* (2008). Model-based analysis of ChIP-Seq (MACS). Genome biology *9*, R137.

Zhou, X., Liao, W.J., Liao, J.M., Liao, P., and Lu, H. (2015). Ribosomal proteins: functions beyond the ribosome. Journal of molecular cell biology *7*, 92-104.

7 Appendix

7.1 Abbreviations

Prefixes

n	nano
µ	micro
c	centi
m	milli
k	kilo

Units

A	ampere
°C	degree celsius
Ci	curie
Da	daltons
g	gram
h	hour
l	liter
m	meter
min	minute
M	Mol/l
sec	second
U	unit
V	Volt
w/v	Weight per volume

Other abbreviations

α	anti
A	adenine
Ado	adenosine
ADP	adenosin-5'-diphosphate
AMP	adenosin-5'-monophosphate
Ann V	annexin V
APS	ammoniumpersulfate
ATCC	American type culture collection
ATP	adenosin-5'-triphosphate
bp	basepair
BrdU	5-bromo 2-deoxy uridine
c.ca	circa
cDNA	complementary DNA
CDS	coding sequence
ChIP	chromatin immunoprecipitation
ChIP-seq	chromatin immunoprecipitation followed by next generation sequencing
CHX	cycloheximide
cpm	count per million
ctr	control
cyt	cytidine
d	deoxy
Δ or del	deletion; also difference
DCFDA	2',7'-dichlorofluorescin diacetate
ddH_2O	bidistilled water
DMEM	Dulbecco´s Modified Eagle Medium
DMKG	dimethyl-α-ketoglutarate

DMS	dimethyl-succinate
DMSO	dimethylsulfoxide
DNA	deoxyribonucleic acid
Dox	doxycyclin
ECL	enhanced chemoluminescence
E.coli	*Escherichia coli*
EDTA	ethylendiamintetraacetate
e.g.	*exempla gratia*, for example
endo	endogenous
Eμ	immunoglobulin heavy chain enhancer
ER	estrogen receptor
etc	et cetera
EtOH	ethanol
EV	empty vector
exo	exogenous
FACS	fluorescence-activated cell sorting
FBS	fetal bovine serum
FC	fold change
FDR	false discovery rate
Fig.	figure
FITC	fluorescein
GB	gene body
GFP	green fluorescent protein
Glc	glucose
Glu	glutammate
GSH-MEE	glutathione reduced ethyl ester
Guo	guanosine
HA	hemagglutinin

HRP	horseradish peroxidase
i.e.	*id est*, that means
IB	immunoblot
IgG	immunoglubulin
IP	immunoprecipitation
IRES	internal ribosomal entry site
LB	Luria-Bertani
Leu/L	Leucine
Met/M	Methione
miRNA	micro RNA
mRNA	messenger RNA
Mut	mutated
n	number of biological replicate
NA	not available
NAC	N-Acetyl-Cysteine
NES	normalized enrichment score
nt	nucleotide
nucls	nucleoside mixture
OHT	4-O-hydroxytamoxyfen
p	phospho
PAGE	polyacrylamide-gelelectrophoresis
PBS	phosphate-buffered saline
PCR	polymerase chain reaction
PEI	polyethylenimin
PI	propidium iodide
PMSF	phenylmethylsulfonyl fluoride
PP	primer pair
Pur	purine mixture

Pyr	sodium pyruvate
Pyri	pyrimidine mixture
Q	glutamine
qPCR	quantitative PCR
Rap	rapamycin
RBP	RNA binding protein
RIPA	radioimmunoprecipitation assay buffer
RNA	ribonucleic acid
RNAPII	RNA polymerase II
RNase	ribonuclease
ROS	reactive oxygen species
rpm	revolutions per minute
RT	room temperature
SD	standard deviation
SDS	sodium dodecyl sulfate
seq	sequencing
Ser	serine
SFFV	spleen focus forming virus
siRNA	small interfering RNA
S-phase	synthesis-phase
$t_{1/2}$	half-life
TBE	Tris-borate EDTA buffer
TBS	Tris-buffered saline
TBS-T	Tris-buffered saline with tween-20
TCA	tricarboxylic acid cycle or Krebs cycle
TE	Tris-EDTA buffer
TEMED	N,N,N’,N’-tetramethylethylendiamine
TES	transcription end site

THF	tetrahydrofolate
Thr	threonine
Tris	Tris-(hydroxymethyl)-aminomethan
TSS	transcription start site
U	uracil
urd	uridine
UTR	untranslated region
UV	ultraviolet light

7.2 Acknowledgments

I would like to express first of all my gratitude to Prof. Dr. Martin Eilers who followed my path as a PhD student and guided me through it. Thanks for the big opportunity I had working in your group and learning from you. Thanks for the challenges you offered me, which made me a stronger person and a better scientist.

I would also like to thank the members of my thesis committee, Prof. Dr. Thomas Rudel and Prof. Dr. Antje Gohla, for supporting my scientific development during these years and for the kindness you demonstrated me.

Thanks to the Graduate School of Life Science (GSLS) for founding part of my PhD as fellow student and for giving me the opportunity to know many interesting people and to exchange ideas with them.

Completing this long pathway would have not been possible without the great help and support of all present and past members of the Chair of Biochemistry and Molecular Biology. I would like to thank especially Steffi Herold, who helped me to develop this project, trusted in my skills and always demonstrated positivity towards my work. Thanks to all those colleagues who became friends during these years and with whom I shared many nice moments both inside and outside the lab. Particularly, I would like to thank Anne C., Eva, Fra L. and Jiajia.

Thanks to Katrin and Markus for a lot of help when I really needed. Thanks to Anne von Thun for always finding time for listening to me and answering my questions.

Thanks to the "thesis-correction team" Giacomo, Suse and Steffi.

I would also like to thank all people I knew in Würzburg during these years and the good friends I found outside the lab. Thanks to the fantastic group of Italian-Latin American friends. You always made my day! Special thanks to Linda, Giulia and Silvia. And I do not need to explain you why. Thanks to Volker and Krischan, you were much more than flat-mates. Endless thanks to my family for giving me always the strength to go on.

Thanks to all those people who let me smile when I could not find good reasons to do it, but, especially, thanks to all friends who rejoiced with me when I was happy.

7.3 Publications

Dejure, F.R.*, Royla, N.*, Herold, S., Kalb, J., Walz, S., Ade, C.P., Mastrobuoni, G., Vanselow, J., Schlosser, A., Wolf, E., *et al.* (2017). The MYC mRNA 3´-UTR couples RNA Polymerase II function to glutamine and ribonucleotide levels.
The EMBO journal, *36*, 1854-1868.
* Authors contributed equally

7.4 Curriculum Vitae

7.5 Affidavit

I hereby confirm that my thesis entitled “Investigation of the role of Myc as a stress responsive protein” is the result of my own work. I did not receive any help or support from commercial consultants. All sources and/or materials are listed and specified in the thesis.

Furthermore, I confirm that this thesis has not yet been submitted as part of another examination process neither in identical nor in similar form.

Place, Date	Signature

Eidesstattliche Erklärung

Hiermit erkläre ich an Eides statt, die Dissertation “Untersuchung der Rolle von Myc als stress-reguliertes Protein” eigenständig, d.h. insbesondere selbständig und ohne Hilfe eines kommerziellen Promotionsberaters, angefertigt und keine anderen als die von mir angegebenen Quellen und Hilfsmittel verwendet zu haben.

Ich erkläre außerdem, dass die Dissertation weder in gleicher noch in ähnlicher Form bereits in einem anderen Prüfungsverfahren vorgelegen hat.

Ort, Datum	Unterschrift